INTERSTELLAR SPACE –

THE ASTROCHEMIST'S LABORATORY

Thesis by

Mark Andrew Allen

In Partial Fulfillment of the Requirements

for the Degree of

Doctor of Philosophy

California Institute of Technology

Pasadena, California

1976

(Submitted May 25, 1976)

ACKNOWLEDGEMENTS

In addition to the beneficent attributes usually ascribed to one's research advisor, I would like to thank Professor G. Wilse Robinson for his encouragement to explore the various aspects of astrochemistry. Not all of the effort was productive (in the sense of being publishable), but all of it was very educational. I gratefully acknowledge the assistance I have received from many Caltech graduate students, faculty, and staff of several different divisions and the staff of the various observatories around the country at which I have observed. Also I am very appreciative of the financial assistance received from the National Science Foundation, State of California, E. I. du Pont de Nemours and Company, Inc., Owens Valley Radio Observatory, and National Radio Astronomy Observatory.

ABSTRACT

In the first part of this thesis, a mechanism for the formation of molecules on small (radius $\lesssim 0.04\ \mu$) interstellar grains is proposed. It is suggested that the energy liberated when a chemical bond is formed between two atoms on a grain is transferred to the lattice vibrations of the grain, heating up the grain. The "hot" grain, during the time that it is radiatively recooling, may then liberate its adsorbed volatiles. The timescales for molecular desorption from a grain are calculated for OH and CO for four different grain compositions.

A simplified H_2 formation model is then presented that utilizes this surface reaction mechanism. The resulting value for the formation rate constant R is $\lesssim 2 \times 10^{-18}\ cm^{-3}s^{-1}$ for dark clouds at 10°K. The nascent H_2 molecules are ejected in excited states in qualitative agreement with Copernicus observations. With the synthesis of H_2 as the dominant process, a time-dependent treatment of the chemical evolution of a dark cloud with little or no ionizing radiation ($\zeta_H \lesssim 10^{-18}\ s^{-1}$) shows that the clouds require more than 10^7 years to achieve chemical equilibrium. It is also suggested that the observed residual atomic hydrogen in several dark clouds indicates that the clouds are 10^6-10^7 years old.

This approach is further developed into an ab initio chemical model for dense interstellar clouds that incorporates 598 grain surface reactions, with small grains again providing the key reaction area.

Gas-phase molecules are depleted through collisions with grains. The abundances of 372 chemical species are calculated as a function of time and are found to be of sufficient magnitude to explain most observations. Peak abundances are achieved on timescales on the order of 10^5-10^6 years, depending on cloud density and kinetic temperature. The reaction rates for ion-molecule chemistry are approximately the same, therefore indicating that surface and gas-phase chemistry may be coupled in certain regions. The composition of grain mantles is shown to be a function of grain radius. In certain grain size ranges, large molecules containing two or more heavy atoms are more predominant than lighter "ices"--H_2O, NH_3, and CH_4. It is possible that absorption due to these large molecules in the mantles may contribute to the observed 3μ band in astronomical spectra.

The second part of this thesis is an account of a radio astronomy observational program to detect new transitions of both previously observed and yet undetected interstellar molecules. The negative results yield order of magnitude upper limits to the column densities of the lower transition states of the various molecules. One special project was the search for the Λ- doublet transitions of the $^2\Pi_{3/2}$, $J = 3/2$ state of OD. The resulting upper limit for the OD/OH column density ratio towards the galactic center is 1/400 and is discussed with reference to theories about deuterium enrichment in interstellar molecules.

TABLE OF CONTENTS

Introduction

A THEORETICAL AND OBSERVATIONAL STUDY OF INTERSTELLAR CLOUDS-- AN OVERVIEW

Forty different chemical species (see table 1) have been detected in interstellar space. Microwave transitions of all but CH^+ and H_2 have been observed; visible and/or ultraviolet spectral lines of CH, CH^+, CN, CO, H_2, and OH have been seen. Besides the common isotopic versions, molecules have been observed with one or more of the rarer isotopes -- ^2H, ^{13}C, ^{17}O, ^{18}O, ^{15}N, ^{33}S, and ^{34}S. The discovery of the richness of interstellar chemistry raises questions as to its extent and detail, thus the burgeoning field of astrochemistry. Some of the more recent reviews of the work in this area are Aannestad and Purcell (1973), Herbig (1974), Winnewisser, Mezger, and Breuer (1974), Turner (1974a,b), Zuckerman and Palmer (1974), and Penzias (1975). [Unless specifically noted, the following material will be drawn from these sources without further attribution.]

The more complicated molecules generally tend to be seen in a limited type of interstellar region. The molecule clouds often correspond to areas in the sky which have a diminished number of visible stars. It is generally believed that these darkened areas are regions of high "dust" density; the light from background stars is absorbed or scattered out of the line of sight and not detected. Observations indicate that the molecule and dust clouds seen in a given direction are basically coextensive. Compared to H II regions (where hydrogen, the cosmically most abundant element, exists

TABLE 1

INTERSTELLAR MOLECULES REPORTED AS OF 1 APRIL 1976

CH	SiS	SO_2	CH_3OH
CH^+	HCN	HNCO	CH_3CN
CN	HNC	H_2CO	CH_3NH_2
CO	HCO	H_2CS	CH_3CHO
CS	HCO^+	NH_3	CH_2CHCN
H_2	OCS	HCO_2H	CH_3C_2H
OH	C_2H	NH_2CN	HC_2C_2CN
NS	N_2H^+	CH_2NH	CH_3OCHO
SO	H_2O	HC_2CN	CH_3OCH_3
SiO	H_2S	NH_2CHO	CH_3CH_2OH

primarily in its ionized atomic state) and HI regions (where hydrogen exists primarily as neutral atoms), the dense dust clouds (often called "dark" or "black" clouds) have a unique combination of conditions (see table 2) propitious for molecule survival in an otherwise seemingly hostile environment. Especially important, the various forms of high energy radiation (ultraviolet light, X-rays, and cosmic rays) that can destroy a molecule through ionization or dissociation and which permeate the general interstellar medium may be significantly attenuated by the large dust column densities associated with molecular clouds. Then these clouds would be a place where molecules could be formed more rapidly than they are being destroyed.

From the point of view of molecule survival, the physical conditions of dense dust clouds make these appropriate regions for the accumulation of large amounts of complex molecules. However, the question of molecule formation is still unclear. Assuming the molecules are synthesized near where they are observed (other suggestions have also been presented), the low temperatures and extremely low densities (by terrestial laboratory standards) suggest that an unusual chemical system is at work. The physical conditions of these clouds restrict the available kinetic pathways to spontaneous, zero-activation-energy reaction steps involving a collision of no more than two bodies. The various reaction schemes proposed have been recently summarized by Winnewisser, Mezger, and Breuer (1974), Turner (1974a, b), and Watson (1975). Various gas-phase reaction mechanisms involving radiative association and ion-

TABLE 2

INTERSTELLAR PHYSICAL CONDITIONS

	Density (cm^{-3})	Temperature (°K)
H II region	10^4	10^4
H I region	10^{-1} - 1	10^2 - 10^4
Dense dust cloud	10^2 - 10^6	10 - 10^2

molecule exchange reactions have been suggested. The ubiquitous dust also may play a role in chemical synthesis, the big problem being to what extent the generally assumed low dust temperatures initially inhibit surface reactions from occurring and/or result in the retention of the newly-formed molecules on the surface.

It is this last point -- the role of the grains in molecule formation -- that the theoretical research presented in Part I of this thesis considers. A reaction dynamics model is proposed that suggests that the energy released in molecular bond formation is transmitted to the grain phonon modes and results in the grain substrate heating up. The probability that the nascent molecule will desorb during the "hot" lifetime of the grain may be high, depending on the size of the grain and the adsorption energy of the molecule. The low ambient grain temperatures are therefore not as great a hindrance to molecule formation and ejection from the grains as has been previously thought. This ejection mechanism is then applied to calculating the formation rates for H_2 and a large number of other molecules. Since the theoretically-calculated abundances compare favorably with observations, surface reactions seem to be efficient in the dense cloud environment and may play a significant role in the chemistry of interstellar molecular clouds. A novel and integral part of this kinetics model is the treatment of the abundances as time-dependent quantities. The introduction of cloud age suggests a way of interpreting presently observed variations in the relative abundances of molecules. In turn, observations may be able to yield information about the physical development of molecule clouds.

The formation model presented in Part I proposes that complicated molecules are produced in a series of radical recombination reactions on grain surfaces. One consequence of this approach is the prediction that a large number of exotic, and heretofore undetected, free radicals and non-radical molecules exist in the interstellar molecular clouds. The extensively developed formation models of others predict the existence of some of the same and some different species. Even when the same molecules are predicted, relative abundances often differ from model to model.

In order to expand the available observational data base by which molecule synthesis theories can be tested, a series of molecule searches were conducted. From a qualitative point of view, establishing the very existence of a particular species through the detection of a few transitions is important in setting general bounds on the nature of the chemistry. For example, the observation of HCO^+ and N_2H^+ confirmed the speculation that ion-molecule reactions play an important role in interstellar processes. Since the observed molecules are usually not in thermal equilibrium, abundances cannot be easily derived from observation of a limited number of transitions. The populations of different rotational levels are often coupled to the physical environment of the molecule and/or the formation pathway. To achieve a quantitative picture of the chemical composition of molecule clouds, observations of a large number of transitions of a given species are needed for comparison with non-equilibrium excitation calculations. Therefore, detections of new transitions of new or previously-discovered molecules are

important and the molecules searched for in my observing program were chosen accordingly. Although no detections were made, the upper limits to the molecule column densities are still very useful when included with other data and are reported in Chapter 4 of this thesis.

The observation of one minor isotopic form of HCN generated a lot of excitement in astrophysical circles. The detection of DCN and the subsequent determination that the DCN/HCN abundance ratio was significantly greater than the generally assumed cosmic D/H abundance ratio led to speculation about a possibly anomalous cosmic D/H ratio or possible chemical processes that could result in an enrichment of deuterium in the molecule. To explore some of the suggestions, observations of OD were performed and the results (unsuccessful) and their consequences are discussed in Chapter 5.

As can be seen, theoretical and observational studies of interstellar clouds are closely intertwined. Theories must be developed to rationalize the observations. In turn, theories suggest new observations to be performed. This interdependence is a classic example of the scientific method operating in its pure form to elucidate the details of an unusual chemical system. Because the interstellar molecule formation processes and the nature of the molecules' continuing existence are intricately connected with the past, present, and future evolution of the dust clouds in which they are observed, astrochemical research is additionally interesting due to its involvement with wider questions of concern to astrophysicists.

REFERENCES

Aannestad, P. A., and Purcell, E. M. 1973, Ann. Rev. Astr. and Ap., 11, 309.

Herbig, G. H. 1974, Amer. Sci., 62, 200.

Penzias, A. A. 1975, in Atomic and Molecular Physics and the Interstellar Matter, ed. R. Balian, P. Encrenaz, and J. Lequeux (Amsterdam: North-Holland), p. 373.

Turner, B. E. 1974a, R.A.S.C. Jour., 68, 55.

_____. 1974b, in Galactic and Extra-Galactic Radio Astronomy, ed. G. L. Verschuur and K. I. Kellerman (New York: Springer-Verlag), p. 199.

Watson, W. D. 1975, in Atomic and Molecular Physics and the Interstellar Matter, ed. R. Balian, P. Encrenaz, and J. Lequeux (Amsterdam: North-Holland), p. 177.

Winnewisser, G., Mezger, P. G., and Breuer, H.-D. 1974, Topics in Current Chemistry, 44, 1.

Zuckerman, B., and Palmer, P. 1974, Ann. Rev. Astr. and Ap., 12, 279.

PART I

INTERSTELLAR SURFACE CHEMISTRY MODEL

Chapter 1

FORMATION OF MOLECULES ON SMALL INTERSTELLAR GRAINS*

MARK ALLEN AND G. WILSE ROBINSON
Arthur Amos Noyes Laboratory of Chemical Physics,†
California Institute of Technology

*The Astrophysical Journal, 195, 81 (1975).

†Contribution No. 4859.

I. INTRODUCTION

In the past few years, a large number of molecules have been discovered to exist in interstellar space, a region whose conditions were at one time thought not to be conducive to the formation of molecules. The question of how these molecules are formed is of increasing interest to chemists and astrophysicists. In a recent paper, Sagan (1972) discusses the various mechanisms proposed for the synthesis of molecules seen in interstellar regions. One method that seems to provide a feasible way for molecules to form in interstellar clouds is the recombination of atoms on interstellar grains. Watson and Salpeter (1972) examined this process, giving much consideration to the pathway by which the newly-formed molecules leave the grain surface. If the grains are too cool, the molecules will not evaporate. Watson and Salpeter use primarily photodesorption to eject molecules from the grain surfaces. Duley (1973) suggests that small grains, due to the absorption of single photons, experience large temperature fluctuations, facilitating molecule desorption. However, both mechanisms have a low probability in the interior of dense interstellar clouds.

In this paper, we propose a mechanism for the ejection of molecules formed on very small interstellar grains (radius $\lesssim 0.04\ \mu$). Energy need not be provided through interaction of these grains with any radiation field, but rather is supplied by the chemical heat of reaction upon bond formation. Such a process would be effective in

the depths of the darkest clouds. Even though similar suggestions have appeared in the previous literature (Solomon and Wickramasinghe 1969; Brecker and Arrhenius 1971; Watson and Salpeter 1972), the development in this paper should yield a new view of this mechanism.

The existence of small grains has been theoretically postulated for many years, but experimental evidence has been sparse. From theoretical considerations on grain growth and destruction, Oort and van de Hulst (1946) (see also Greenberg 1968) derived a steady state size distribution for grains in an interstellar dust cloud,

$$n(r) = \exp[-X(r/Y)^3] , \qquad (1)$$

where n(r) is the normalized number density of grains with radius r, and X and Y are constants. Such a distribution predicts an increase in the number density as the grain size decreases. This and other similar monotonically decreasing size distributions have been shown, with the appropriate choice of constants, to predict in a reasonable way the interstellar extinction curve in the visible spectral region (Wickramasinghe and Nandy 1972). Recent observations in the ultraviolet region taken with Orbiting Astronomical Observatories 2 and 3 conclusively show a rapid increase in the interstellar extinction with decreasing wavelength (Bless and Savage 1972; York et al. 1973). Attempts to explain these results have focused attention on smaller grain sizes for fitting the extinction curves (Gilra 1971; Bless and Savage 1972; Greenberg 1973; York et al. 1973).

Small grains may be formed in the atmospheres of stars and blown into space--graphite grains (radius $\lesssim 0.1\ \mu$) from carbon stars (Hoyle and Wickramasinghe 1962) and silicate grains (radius $\simeq 0.01\ \mu$) from M-type giants (Kamijo and de Jong 1973). These small particles, which can serve as the condensation nuclei for larger grains, probably survive in the interstellar environment, especially in a dense cloud where the interior is most likely shielded from grain-destroying low-energy cosmic rays (de Jong and Kamijo 1973). On the other hand, Carrasco, Strom, and Strom (1973) suggest that the mean grain size increases in denser interstellar clouds, but they do not give a quantitative size distribution for grains in these clouds. The motivation for our paper is that there may be enough small grains to play an important role in molecule formation.

II. FORMATION AND VAPORIZATION OF MOLECULES ON SMALL GRAINS

In this paper the following model for the formation and subsequent ejection of diatomic molecules from small interstellar grains is proposed. The model can be readily generalized to include polyatomic molecules. A small grain situated in the background radiation field is at temperature T', determined by the radiant properties of the grain material and the nature of the radiation field. Since the temperature of grains is very low in dark interstellar clouds, atoms stick to the grain upon collision (Watson and Salpeter 1972). Adsorbed atoms may diffuse through or over the surface of the small grain. Atoms sufficiently near each other will form a chemical bond if there is little or no activation energy for the process.

When a chemical bond is formed, the liberated bond energy is transmitted to the vibrational lattice modes (phonon modes) of the grain by a vibrational relaxation process, thus heating the grain. This is somewhat analogous to the situation of atoms or molecules adsorbing onto a surface, in which case most of the energy released is transferred to the phonon modes of the substrate (McCarroll 1969). In experimental beam studies of accommodation coefficients, the atom (or molecule) impinging on a surface must transfer much of the adsorption energy to the substrate within one vibrational period if it is to stick. In the present case the atoms are already adsorbed on the grain, permitting the energy transfer process to occur over

the course of several vibrational periods of the adsorbed reaction complex.

The Watson and Salpeter (1972) model for molecule ejection during the formation of the molecular bond differs from the one here in that they expect the energy gained from bond formation to be partly transformed into localized translational motion of the molecule across the grain surface. This could lead to molecule desorption from the grain, but would require that coupling of the molecule with a very particular translational mode is important even in the face of an undoubtedly rapid vibrational relaxation process involving all the vibrational degrees of freedom of the grain. Even in this model, energy is transferred to the grain phonon modes when the hopping molecule recollides with surface atoms. Eventually most of the energy released upon bond formation is transferred to the grain if the newly-formed molecule is not ejected on one of its hops, thus achieving the grain-molecule energy thermalization postulated in this paper.

In the present paper the temperature of the grain is assumed to peak "instantaneously" (rise time $\lesssim 10^{-11}$ s) upon formation of the bond. This assumption seems realistic considering the small size of the grains under study, and the fact that phonons travel through solids at the speed of sound ($\sim 10^5$ cm s^{-1}). The rapid transmission of vibrational energy through a solid has been confirmed by one-dimensional dynamics calculations using classical interparticle interactions (Zwanzig 1960; McCarroll and Ehrlich 1963; McCarroll 1963). These treatments show that surface disturbances are

transmitted through the whole crystal on a time scale approximately equal to the vibrational period of the surface disturbance if the interparticle vibrations are strongly coupled. Thus it is reasonable to believe that: (a) the grain will be heated approximately uniformly to its maximum temperature on a time scale much shorter than the adsorbed lifetime of the newly-formed molecule, and therefore (b) local heating of the crystal near the site of the molecule formation would not occur to a sufficient degree to allow the molecule to desorb instantaneously.

The hot grain may actually disintegrate if it is small enough, or the grain-molecule system may simply get sufficiently hot that any weakly adsorbed molecules (including the molecule formed) have a high probability of being vaporized. Our calculations will show circumstances under which these various processes occur.

We have taken the structure of very small grains (radius $\lesssim$ 0.001 μ) to be the classical "equilibrium" clusters of McGinty (1971) composed of roughly spherical atomic or molecular components. Intermolecular potentials between the particles in the cluster are approximated by the Lennard-Jones "6-12" potential. We shall choose the force constants of the intermolecular potentials to simulate various molecules and atoms which have been suggested for the composition of interstellar grains. Internal vibrational modes of molecular components, except for the molecule being formed (see below), are ignored.

McGinty (1971) has calculated in reduced units the lattice phonon spectrum and the average potential energy V(N) per particle

for equilibrium clusters with N particles [where $V(N) < 0$]. Phonon spectra resulting from a similar type of calculation have also been published by Burton (1972). One must multiply McGinty's phonon frequency spectrum for a cluster of size N by a scaling factor $\underline{F}$ to convert the frequencies from reduced units to units of radians second^{-1}. $\underline{F}$ depends on the nature of the grain material:

$$F = (\epsilon k/m)^{\frac{1}{2}} \sigma^{-1} , \tag{2}$$

where ϵ (°K) and σ (centimeters) are the corresponding Lennard-Jones force constants, and $\underline{m}$ (grams) is the mass of the individual atoms or molecules of which the cluster is composed; $\underline{k}$ is Boltzmann's constant. To convert to units of ergs per particle, $V(N)$ must be multiplied by $[\epsilon k]$.

Neglecting zero-point energy and using the harmonic oscillator approximation for the 3N-6 phonon modes ω_i, the energy of a cluster of N particles in thermal equilibrium at a temperature $\underline{T}$ (excluding the translational energy of the center of mass of the grain and bulk rotation around the center of mass) is

$$E(N,T) = NV(N)\epsilon k + \sum_{i=1}^{3N-6} n_i(T)\hbar\omega_i , \tag{3}$$

where

$$n_i(T) = [\exp(\hbar\omega_i/kT) - 1]^{-1} . \tag{4}$$

If the temperature is sufficiently high, then

$$E(N, T) \geq 0 , \tag{5}$$

and the cluster will disintegrate.

The potentials describing the interaction of the two atoms on the grain and the interaction of the newly formed molecule and the grain are both taken for simplicity to be truncated harmonic oscillators (see fig. 1). Use of a truncated harmonic oscillator to describe the intramolecular potential in thermal dissociation studies has been shown to give results in good agreement with the more exact Morse potential (Johnston and Birks 1972). Each potential well may then be described by two unique parameters, E_d and ω, where $\omega (= 2\pi\nu)$ is the fundamental vibrational frequency in radians s^{-1} and E_d is the dissociation energy. In the case of the molecule being formed, E_d is the bond energy. In the case of the molecule-grain bond, E_d is the adsorption energy at 0°K. Assuming that the adsorption is non-activated, E_d would be the heat of adsorption.

The two atoms adsorbed on the grain surface contribute six extra modes due to their own vibrational motion. To calculate the energy of a "McGinty grain" before the molecule is formed, equation (3) is evaluated at T′, with the sum over 3N modes. Since the calculations are not too sensitive to the precise form of the phonon frequency spectrum, it is assumed for simplicity that the extra modes have the same frequency as the lowest frequency mode of the basic grain. (McGinty's data are too coarsely distributed to allow a

Fig. 1. - Truncated harmonic oscillator interaction potential. Interaction potential energy V is a function of the separation X of the two interacting particles. The system is at equilibrium when the particles are separated by a distance x_e. The system disintegrates when the separation distance increases beyond x_d.

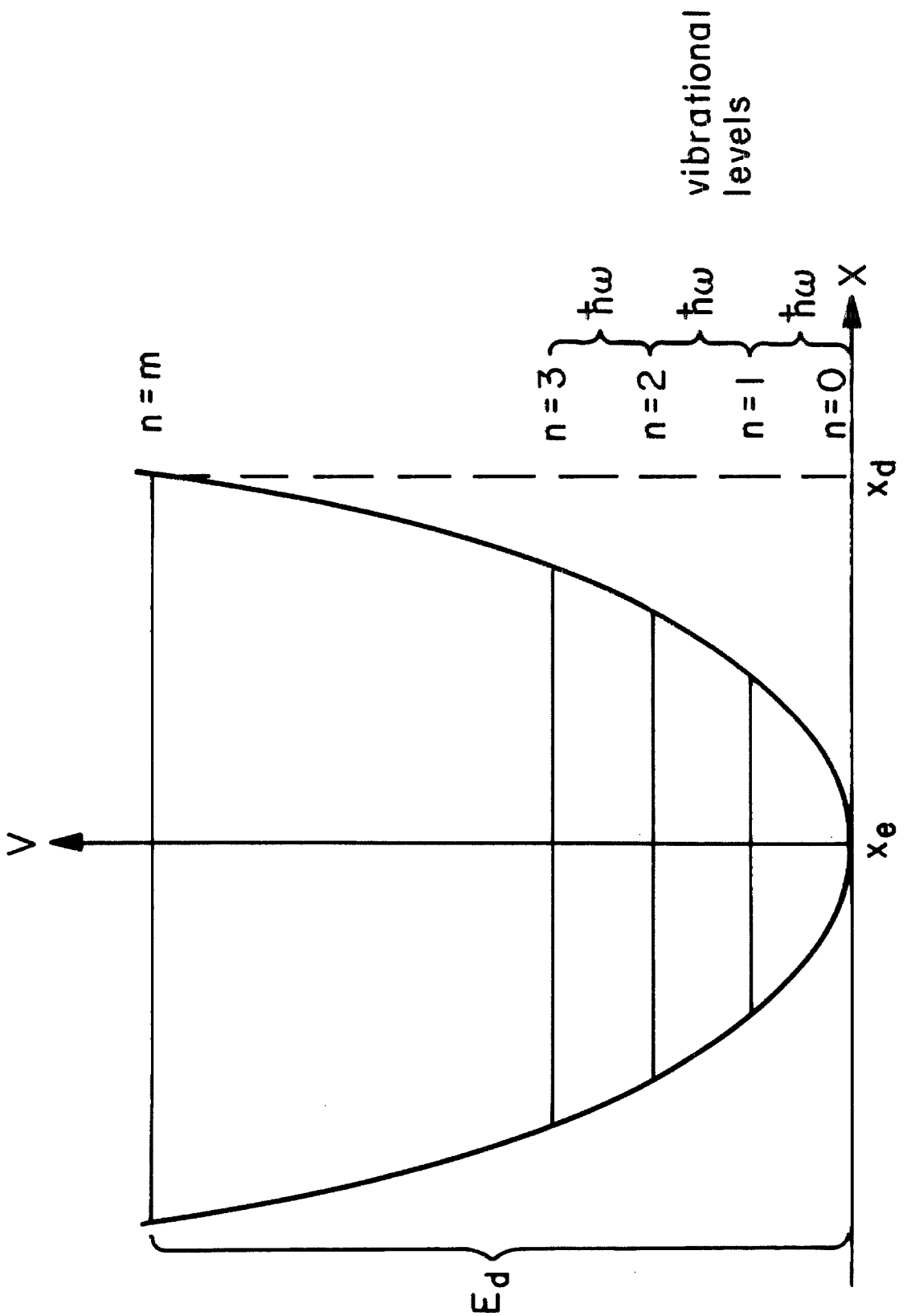
vibrational
levels
n=m
n=3
n=2
n=1
n=0
ħω
ħω
ħω
X
V
x_d
x_e
E_d

more accurate procedure.)

The grain, except for the molecule that is formed, is treated as if composed of "structureless particles." One is then relieved of having to be concerned with the partition of energy into internal modes of any other molecular constituents of the grain. Upon molecule formation the grain/molecule system reaches thermal equilibrium "instantaneously", and the energy distribution among the phonon modes and the energy distributions in the molecular mode and the grain-molecule modes can be described by a temperature T_0. Even for the smallest grains, kT_0 is usually much smaller than the typical spacing between internal molecular vibrational levels, thus confirming the use of the "structureless particle" approximation.

Therefore, before the molecule is formed, the vibrational energy of the McGinty grain/molecule system is

$$E(T') = \sum_{j=1}^{3N} n_j(T')\hbar\omega_j \ . \tag{6}$$

Immediately after the molecule is formed a new temperature T_0 is reached such that

$$E(T') + E_{bond} = n_m(T_0)\hbar\omega_m + n_{gm}(T_0)\hbar\omega_{gm} + \sum_{j=1}^{3N-2} n_j(T_0)\hbar\omega_j \ . \tag{7}$$

Here E_{bond} is the bond energy of the new molecule and the subscripts m and gm refer to the molecular bond and the grain-molecule bond, respectively. The grain/molecule system is viewed here in the center-of-mass frame of reference. This equation assumes that the

vibrational modes of the system are not coupled to the center-of-mass motions of the entire grain. The motion of the molecule on the grain has six degrees of freedom. There are three vibrational modes where the entire molecule is moving relative to the grain surface, two torsional (quasi-rotational modes), and one internal molecular vibrational mode. The mode perpendicular to the grain surface is the vibration of the grain-molecule bond. The other two vibrational modes and the two torsional modes are again taken to be equal to the lowest frequency phonon mode of the basic grain.

Grains with radii $\gtrsim 0.003\ \mu$ approach the limiting behavior of the bulk material. At low temperatures, the molar heat capacity C_v^m of a material at temperature $\underline{T}$ is (Debye 1912; Blackman 1955)

$$C_v^m(T) = \frac{12\pi^4}{5} R\left(\frac{T}{\theta_D}\right)^3 , \tag{8}$$

where R is the molar gas constant and θ_D is the Debye temperature of the material. The error in this approximation for C_v^m is less than 12 percent for $(T/\theta_D) < \frac{1}{2}$ and less than 1 percent for $(T/\theta_D) < 1/12$. The heat capacity C_v of a spherical grain of radius $\underline{r}$ is

$$C_v(T) = C_v^m(T)\ \frac{4}{3}\ \pi r^3 d/M, \tag{9}$$

where $\underline{d}$ is the mass density and $\underline{M}$ is the mole weight of the grain material. T_0 is calculated by the relation

$$E_{bond} = \int_{T'}^{T_0} C_v(T)dT . \tag{10}$$

If T_0 is sufficiently high, the grain will tend to disintegrate. T_0 might not be so high that the original grain would actually disappear, but the adsorbed volatiles and some of the grain constituents might vaporize.

According to the model proposed here, the grain temperature after reaching T_0 decreases with time due to cooling by evaporation and by emission of radiation. One can integrate the desorption probability over the grain cooling curve to calculate the adsorbed lifetime of the molecule on the grain. The following calculations assume that the grain cools solely through the emission of radiation at wavelengths much larger than the size of the grain. The amount of radiant energy emitted in an increment of time dt by a spherical grain of radius r at a constant temperature T is (Greenberg and de Jong 1969)

$$(dE/dt) = 4\pi r^2 \sigma \epsilon(T) T^4 , \qquad (11)$$

where σ is the Stefan-Boltzmann constant and $\epsilon(T)$ is an efficiency factor averaged over all the emitted radiation frequencies. All quantities are expressed in cgs units. In the ideal case of a perfect blackbody sphere, $\epsilon(T) = 1$. For the situation where the radiation wavelength λ is much larger than r, Greenberg and de Jong derive from Mie scattering theory a maximum wavelength-dependent efficiency factor

$$\epsilon(\lambda) = 4\pi r/\lambda . \qquad (12)$$

Averaging $\epsilon(\lambda)$ over all frequencies gives

$$\epsilon(T) = 33.3 r T \, . \tag{13}$$

Such a radiation-emission efficiency factor is expected to be an upper limit to interstellar grain cooling rates. The decrease in temperature due to the decrease of the internal energy of the grain/molecule system can be found by differentiating equation (7):

$$(dT/dE) = k^{-1} \left\{ \frac{(\hbar\omega_m/kT)^2 \exp(\hbar\omega_m/kT)}{[\exp(\hbar\omega_m/kT) - 1]^2} + \frac{(\hbar\omega_{gm}/kT)^2 \exp(\hbar\omega_{gm}/kT)}{[\exp(\hbar\omega_{gm}/kT) - 1]^2} + \sum_{i=1}^{3N-2} \frac{(\hbar\omega_i/kT)^2 \exp(\hbar\omega_i/kT)}{[\exp(\hbar\omega_i/kT) - 1]^2} \right\}^{-1} . \tag{14}$$

Note that this is the inverse heat capacity of this system. For grains with radii $\gtrsim 0.003\ \mu$,

$$(dT/dE) = C_v^{-1}(T) \, , \tag{14a}$$

where $C_v(T)$ is defined in equation (9). The rate of decrease in grain temperature is found by combining equation (11) with (14) or (14a). Representative plots of the cooling behavior of grains are shown in figure 2.

Based on the truncated harmonic oscillator model for the grain-molecule interaction, the probability p(T) at temperature T of the

Fig. 2. - Cooling of quartz grains heated by CO formation: (a) 10 Å radius, $T_0 = 584\,^{\circ}K$, and (b) 100 Å radius, $T_0 = 42\,^{\circ}K$.

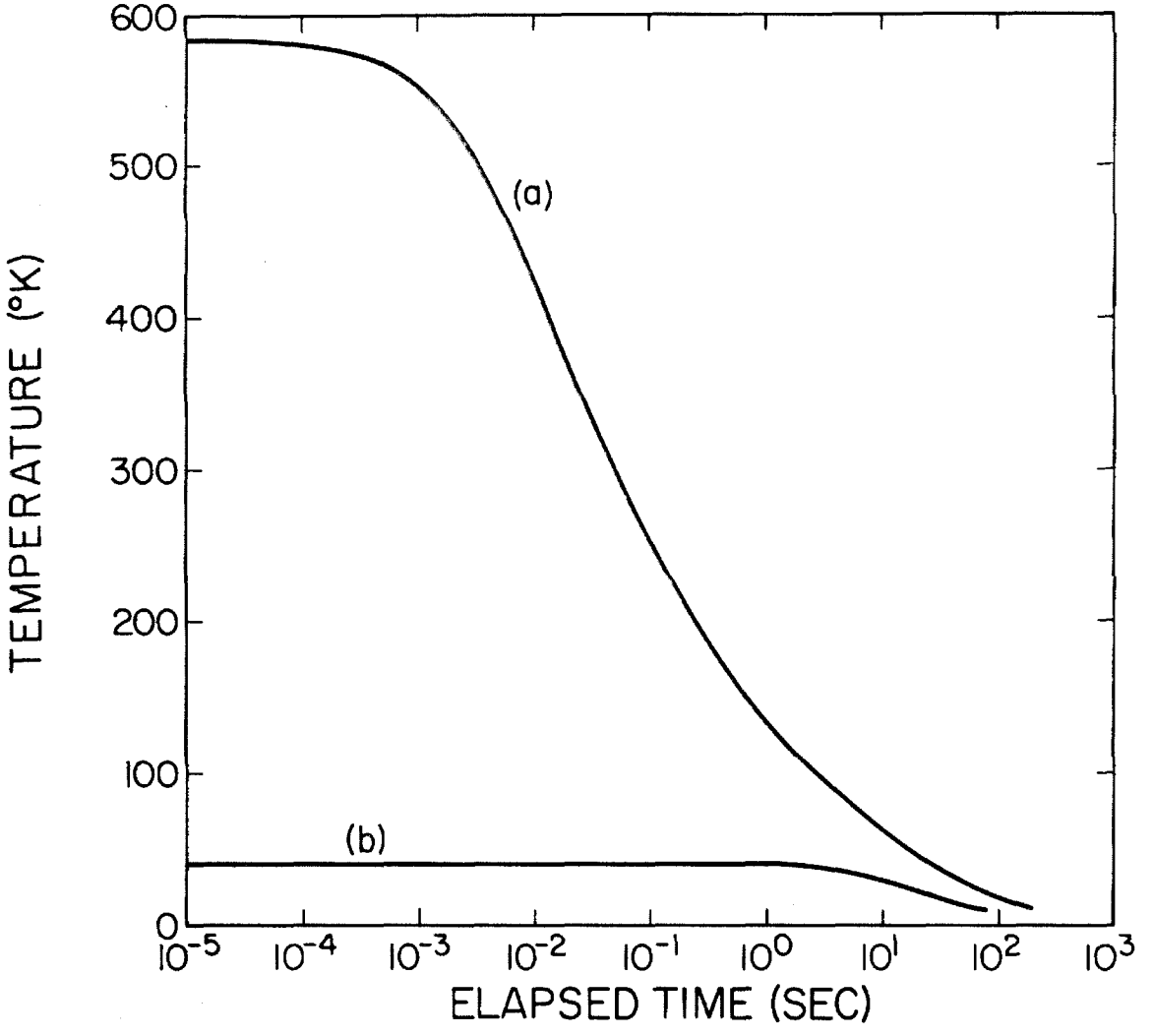
600
500
400
300
200
100
0
TEMPERATURE (°K)
(a)
(b)
10^{-5}
10^{-4}
10^{-3}
10^{-2}
10^{-1}
10^{0}
10^{1}
10^{2}
10^{3}
ELAPSED TIME (SEC)

molecule desorbing from the grain during one period of the grain - molecule vibration is

$$p(T) = \sum_{n=m}^{\infty} \exp(-n\hbar\omega_{gm}/kT)/Q(T) \ , \tag{15}$$

where the partition function Q(T) for a harmonic oscillator of fundamental frequency ω_{gm} is (Davidson 1962)

$$Q(T) = \sum_{n=0}^{\infty} \exp(-n\hbar\omega_{gm}/kT) \ . \tag{16}$$

The index m is determined by the relation

$$m\hbar\omega_{gm} = E_d \ . \tag{17}$$

In other words, the probability of desorption is the probability that one of the dissociative vibrational levels of the grain-molecule bond is populated, with the assumption that the population of the vibrational levels can be given by the Boltzmann formula. The probability that the molecule does not desorb during a given vibrational period is 1-p(T). If the temperature, and therefore the desorption probability per vibrational period, remains constant, the total probability P'(T) of not desorbing after v vibrational periods is

$$P'(T) = [1 - p(T)]^{v} \ , \tag{18}$$

and the total probability of desorbing is 1 - P′ (T). For a time interval of 1 s, when p(T) ≪ 1 and kT ≫ $\hbar\omega_{gm}$, 1 - P′ (T) reduces to the expression generally used in the literature to calculate desorption rates (Moelwyn-Hughes 1961),

$$\text{desorption rate} = \nu \exp(-E_d/kT) \tag{19}$$

where $\underline{v}$ is replaced by the vibrational frequency ν. We will not use equation (19) in our calculations.

To calculate a total desorption probability over time as the grain undergoes radiative cooling, one can divide the time elapsed after the grain reaches T_0 into intervals of v_j vibrational periods, the temperature T_j remaining essentially the same during each interval. $P'(T_j)$ is then calculated for each interval. In this paper, the adsorbed lifetime of the molecule on the grain is taken to be the elapsed time necessary for a 99 percent desorption probability. Thus

$$\prod_{j=1}^{f} P'(T_j) = 10^{-2} \tag{20}$$

and

$$\text{adsorbed lifetime} = \sum_{j=1}^{f} v_j \tau, \tag{21}$$

and τ is the vibrational period (in seconds) of the grain-molecule system.

III. CALCULATIONS

As already stated, the parameters describing the nature of the clusters were chosen to simulate the grain composition suggested by observations. Therefore, calculations were carried out with C atoms (graphite), SiO_2 (quartz), and H_2O (ice) as the material from which the model grains are composed. Solid N_2 is examined to illustrate another range of behavior. The parameters for the different grains are listed in table 1. Except for those referenced to Hirschfelder, Curtiss, and Bird (1954), the listed values of the parameters are estimates. The phonon spectrum scaling factor $\underline{F}$ for a given substance (eq. [2]) is directly proportional to the Debye temperature θ_D for that material. If one knows or can estimate $\underline{m}$ and σ for some material X, the ϵ for that material may be computed from the relation

$$F(X) = F(Ar) \left[\theta_D(X) / \theta_D(Ar) \right] , \qquad (22)$$

where F(Ar) can be determined from the mass and the Lennard-Jones parameters of argon (Hirschfelder, Curtiss, and Bird 1954). The Debye temperatures are found in the literature [in the case of θ_D(Ar), see Hollis Hallett 1961] and also are reported in table 1. The estimates for σ are derived from density data. Assuming that the clusters are roughly spherical, the radius of a cluster of N particles can also be calculated from these data.

TABLE 1

GRAIN COMPOSITION INPUT PARAMETERS

Grain Material	ϵ(°K)	θ_D(°K)	σ(Å)	Density (10^{22} molecules cm^{-3})
N_2(solid)	95.05*	79†	3.968*	2.21
H_2O(ice)	304.02	224‡	2.846	3.07
C(graphite)	294.57	420§	1.830	11.54
SiO_2(quartz)	6560.32	542‖	2.990	2.65

* Hirschfelder, Curtiss, and Bird 1954.

† Bezuglyi, Tarasenko, and Ivanov 1968.

‡ Proctor 1966.

§ Gray 1963.

‖ Natarajan 1967.

The parameters describing the intramolecular potential functions for the molecules OH and CO are listed in table 2. The parameters describing the potential function for the various grain-molecule bonds are listed in table 3. For each pairing of molecule and grain, E_d and ω_{gm} are given, with reference to the source of data for E_d. The value of ω_{gm} (converted to wave numbers) was estimated to be 100 cm^{-1} if the molecule is physically adsorbed or 1000 cm^{-1} if chemisorbed.

Calculations were carried out on an IBM 370/158 computer. Theoretical values for the steady-state grain temperature (T′) have been reported in the literature and range between 2.7°K and 30°K, depending on the composition of the grains (Wickramasinghe and Nandy 1972). For each pairing of molecule and grain, the grain temperature T_0 and the total grain energy at T_0 were computed for 15 McGinty clusters having different sizes (ranging between 5 and 100 molecular [or atomic] entities per cluster) and six different initial temperatures T′ between 5 and 30°K. For the case where T′ is 10°K, T_0 was determined for grains of larger size ($0.003 \leq$ radii $\leq 0.015\ \mu$, at $0.001\ \mu$ intervals). The adsorbed lifetimes A(r) then calculated were fit to an empirical function of the form,

$$\log A(r) = -\log[\nu_{gm} A(\infty)]\ \exp[-a(\log r)^b] + \log A(\infty)\ , \qquad (23)$$

where $\underline{r}$ is the grain radius in angstroms, and $\underline{a}$ and $\underline{b}$ are the parameters varied in the least squares fitting procedure. $A(\infty)$ is the adsorbed lifetime of the molecule on an infinitely large grain,

TABLE 2

PARAMETERS OF INTRAMOLECULAR POTENTIAL FUNCTIONS

Molecule	E_d(kcal mole^{-1})*	$\bar{\nu}_m$(cm^{-1})†‡
OH	102.4	3735.2
CO	256.7	2170.21

* Weast 1968.

† $\omega_m = 2\pi\bar{\nu}_m c$, where $\underline{c}$ is the speed of light in cm s^{-1}.

‡ Herzberg 1950.

TABLE 3

PARAMETERS OF GRAIN-MOLECULE INTERACTION POTENTIAL*

	Molecule					
	OH			CO		
Grain		E_d(kcal mole^{-1})	$\bar{\nu}_{gm}$(cm^{-1})†		E_d(kcal mole^{-1})	$\bar{\nu}_{gm}$(cm^{-1})†
N_2	I	1.5‡	100	II	0.8‡	100
Ice	III	7.0§	1000	IV	2.3‖	100
Graphite	V	50.0#**	1000	VIII	2.4††	1000
	VI	17.0#‡‡	1000			
	VII	2.7§§	100			
Quartz	IX	2.7§§	100	X	2.0‖‖	100

* Each set of grain-molecule interaction potential parameters is assigned a Roman numeral to identify the results of the calculations presented in table 4 and figure 3.

† $\omega_{gm} = 2\pi\bar{\nu}_{gm}c$, where c is the speed of light in cm s^{-1}.

‡ $E_d = 4\epsilon$ (Hollenbach and Salpeter 1970), where ϵ is calculated from the "combining rule" using values for N_2, HCl for OH (both molecules are of similar size and dipole moment), and CO, respectively (Hirschfelder, Curtiss, and Bird 1954).

§ Strength of hydrogen bond (Castellan 1964).

‖ Experimental value (Nair and Adamson 1970).

Heats of chemisorption of NO on graphite, with the assumption that NO and OH chemisorption is about the same due to the unpaired electron. For the NO chemisorption values, see Zarif'yants 1964.

** Chemisorption on edges of basal plane.

†† Heat of adsorption on graphitized carbon black (Smith and Ford 1965).

‡‡ Chemisorption on face of basal plane.

§§ Experimental value (Brown and Hall 1973).

‖ ‖ Heat of sublimation of CO (Brunauer 1945).

in which case the temperature never deviates from 10°K; ν_{gm} is the vibrational frequency of the grain-molecule bond. For example, in the case of CO formed on solid N_2, $\nu_{gm} = 3 \times 10^{12} s^{-1}$, $A(\infty) = 8.6 \times 10^{6}$ s, a = 0.049, and b = 5.5.

The results of the calculations are presented in table 4 and figure 3. In table 4 we list for each grain-molecule interaction potential (T′ = 10°K) the calculated T_0 for several grain sizes. Figure 3 presents the calculated and extrapolated values of the adsorbed lifetimes for each grain-molecule interaction potential. Note that the desorption times are much longer than the cooling times. This is because integration over the tail of the cooling curve significantly contributes to the desorption probability. Under the criterion of equation (5), the calculations of total grain energy at T_0 (for T′ = 10°K) show that the heat of formation of OH disrupts solid N_2 grains with radii $\lesssim$ 10Å and the heat of formation of CO disrupts grains with radii $\lesssim$ 15Å. But for grains with $\theta_D > 200$°K, even the formation of CO will disrupt grains no larger than 8 Å in radius.

The dependence of the results on the errors introduced in estimating the input parameters will now be considered. The thermal history of the grain has a direct bearing on the adsorbed lifetimes. In the case of the larger grains, an increase in T′ noticeably decreases the calculated adsorbed lifetimes. An increase in $\theta_D(X)$ will produce higher calculated T_0's, a correlation easily seen upon comparing tables 1 and 4. Therefore, the adsorbed lifetimes may be too short if our choice of $\theta_D(X)$ is too high. However, if

TABLE 4

CALCULATED T_0(°K) FOR THE VARIOUS GRAIN-MOLECULE INTERACTION POTENTIALS (T' = 10°K)*

	Molecule									
	OH					CO				
	Particles per cluster					Particles per cluster				
Grain		10	10^2	10^4	10^5		10	10^2	10^4	10^5
N_2	I	1786	196	15	11	II	4370	456	18	12
Ice	III	1836	236	32	18	IV	4400	499	40	22
Graphite	V	1876	282	51	28	VIII	4441	552	64	35
	VI	1876	282	51	28					
	VII	1857	281	51	28					
Quartz	IX	1882	308	61	34	X	4446	584	77	44

* Roman numerals identify the grain-molecule interaction potential used in the calculations (cf. table 3).

Fig. 3.- Adsorbed lifetimes of OH (open symbols) and CO (solid symbols) on (a) solid N_2, (b) ice, (c) graphite, and (d) quartz grains. The symbols are the results of calculations using discrete grain sizes and the solid lines are nonlinear least squares fits of the data. The Roman numeral associated with each curve correlates the results with the input parameters for the grain-molecule interaction potential (cf. table 3).

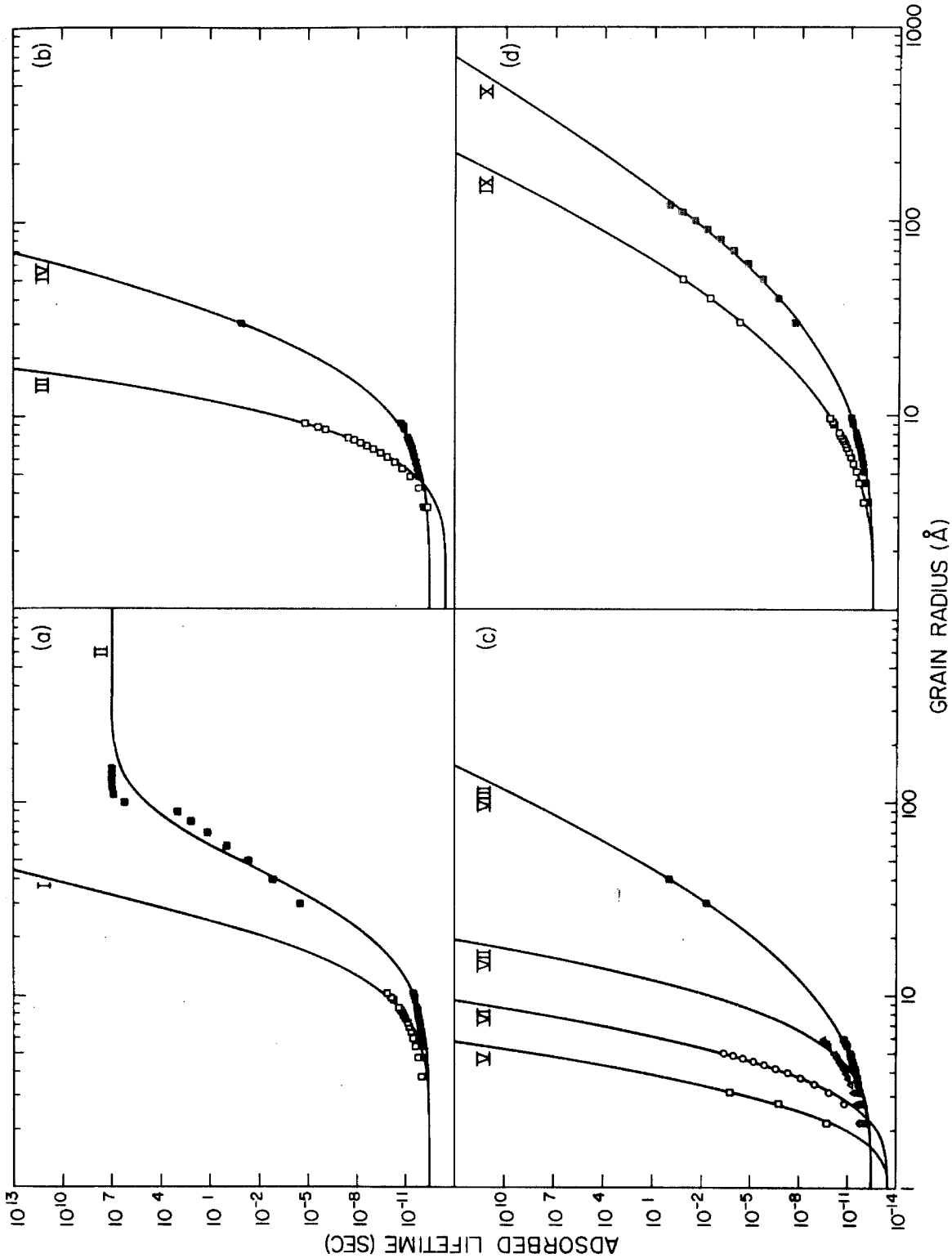
(a)
(b)
(c)
(d)
I
II
III
IV
V
VI
VII
VIII
IX
X
ADSORBED LIFETIME (SEC)
GRAIN RADIUS (Å)
10^13
10^10
10^7
10^4
10^1
10^-2
10^-5
10^-8
10^-11
10^-14
1
10
100
1000

$\theta_D(X)$ is too high, the "hot" lifetime of the grain will be shorter, partially canceling the previous effect. On the other hand, the approximation that equated the frequencies of the extra grain-molecule vibrational and torsional modes with the lowest-frequency grain-phonon mode would tend to lower the calculated T_0. The fact that equation (11) gives an upper limit to grain radiative cooling rates tends to lengthen the adsorbed lifetimes.

The calculation of $p(T_j)$ is affected by several other parameters besides temperature. If the adsorption energy E_d is too large, the adsorbed lifetimes will be too long (see eqs. [15] and [17]). McGinty (1973) has shown that the densities of small clusters are lower than the density of bulk material of the same composition. Since the interaction between a molecule and a grain is a function of the density of particles in the grain, it is to be expected that the heats of adsorption we used, which were reported in the literature for bulk material, are larger than the real heats of adsorption for molecules on small grains. Moreover, using the bulk density of the material gives too small a grain radius, which will affect the extrapolation derived from a least squares fit using the adsorbed lifetimes of McGinty grains. The choice of the fundamental frequency of the grain-molecule bond ω_{gm} also affects the calculated desorption probabilities. When the grains are small and the T_j's are so high that $kT_j \gg \hbar\omega_{gm}$, errors in the estimated ω_{gm} produce very little change in the calculated desorption probabilities. But when $kT_j < \hbar\omega_{gm}$, too low a value of ω_{gm} would increase the desorption probability.

In general, when there was a question about the estimates, we chose values which would tend to maximize the calculated adsorbed lifetimes. Thus we feel that the calculations do show the reasonableness of the idea that the chemical heat of reaction can lead to grain heating and efficient molecule release from grains having radii $\lesssim 0.04\ \mu$.

IV. CONCLUSIONS

In the depths of dense interstellar dust clouds, where the normal interstellar radiation field is highly attenuated, even the smallest dust grains may be expected to cool down to the average grain temperature calculated for larger sizes. The results presented in this paper were done for $T' = 10\,^{\circ}K$ and bear out the main points of the proposed molecule ejection mechanism--the energy released upon molecule formation heats up the grain, causing the grain partially to vaporize and/or weakly adsorbed molecules to desorb.

If the molecule is still adsorbed on the grain when another atom or molecule collides with and, in most cases, sticks to the grain, the originally adsorbed molecule may desorb due to a later chemical reaction on the grain or may react with the newly-adsorbed species to form a new molecule. Given a time scale for successive collisions of gas-phase atoms or molecules with the grain, one may use the adsorbed lifetimes charted in figure 3 to determine the sizes of grains that will be the most efficient sites for the formation and release of molecules. The proposed mechanism can take place on grains having radii $\lesssim 0.04\ \mu$, the upper limit being reached for non-volatile grains in an environment where the time scale for successive collisions is $\sim 10^8$ s. The temperature dependence of the results is such that for $T' > 10\,^{\circ}K$ even larger grains would eject newly-formed molecules.

The comparison of adsorbed lifetime with gra. gas collision time yields the δ (fraction of molecules formed that do not leave the surface in the formation process) of Watson and Salpeter (1972) and the α (defined the same way as δ) of Aannestad (1973). These are important parameters in kinetics calculations. One should remember that the situations used for the calculations were chosen for the purpose of illustration and that real interstellar grains are probably mixtures of these and other materials, requiring some averaging of the different curves of figure 3 in more realistic models.

Several conclusions may be drawn from these results. (1) Free radicals will desorb more slowly than molecules without unpaired electrons, since the free radicals are expected to be adsorbed more securely on most grain surfaces. (2) The stronger the molecular bond formed, the more readily the new molecule will desorb, since the grain is heated to higher temperatures. Both of these conclusions would predict that in the gas phase in the depths of the dark clouds, where photodestruction is not significant, CO would be more abundant relative to OH than one would expect from considerations of the cosmic abundances of the C, O, and H atoms. Indeed, a calculation based on elemental cosmic abundances from Aller (1961) and observed molecular column densities from Rank, Townes, and Welch (1971) shows the ratio $(OH/CO)_{observed}/(OH/CO)_{expected}$ to be $\sim 2 \times 10^{-6}$ (assuming that the OH and CO clouds observed in the direction of Sgr B2 are coextensive). Conclusion (1) may also explain why observations have revealed the existence of only a few free radicals and these only in abundances lower than expected from the

cosmic abundances of the constituent elements (Rank, Townes, and Welch 1971). Watson and Salpeter (1972) provide a similar explanation for the low observed abundances of free radicals. The next stage of this project is to study rates of molecule formation using the calculated probabilities for ejection from different grain sizes, to determine whether sufficient numbers of molecules will be formed and released to the gas phase to be consistent with the number densities reported from astronomical observations.

It is interesting to note that recent experimental work (Lorents, Olson, and Conklin 1973) has shown that ions may be much more strongly attracted to neutral molecules than the classical charge-induced dipole force would suggest. Thus charged molecules may be strongly adsorbed onto the grain and could therefore be released only at extremely high temperatures. Moreover, the grain/charged-molecule system probably quickly scavenges a particle of opposite charge, leading to a neutralization of the adsorbed charged species. For both reasons it seems that grains are not favorable sites for efficient production of gaseous molecular ions in the interstellar medium.

The calculations show that very small quartz grains may be heated sufficiently to result in at least a partial disintegration of the grain. This may be a source of interstellar SiO in various vibrational states (Davis et al. 1974). The general ejection of adsorbed volatiles during the hot lifetime of a grain may be the way that molecules, having previously collided with and stuck to the grain, return to the gas phase. The temperature may even be high enough to promote

further surface reactions between adsorbed molecules or to promote molecular rearrangements, including isotopic exchange reactions. Many such processes are probably fast enough to take place rather efficiently during the early high temperature stages of the grain.

The calculations also suggest that small interstellar grains (radius $\lesssim 0.04\ \mu$) may be of a different composition than the larger grains. Since the small grains are heated to the extent that all weakly adsorbed molecules evaporate, these grains are expected to be primarily made up of nonvolatile material. Molecules formed on large grains will not be readily liberated from the surface by the heating effect. Many volatile molecules may form on the grain surface before the grains are sufficiently perturbed by external forces to cause molecule evaporation. Therefore, large grains may have a core of nonvolatile material and a mantle partially composed of volatile material. Under these circumstances, it would be reasonable to try to fit the interstellar extinction curve by a mixture of particles of different composition in different size ranges as has been attempted by some investigators (Wickramasinghe and Nandy 1972). It is interesting to note that Greenberg and Hong (1973) suggest that physical causes, like large temperature fluctuations, would result in a similar bimodal size distribution for interstellar grains. In addition, our calculations indicate that the rate of mantle growth in the work of Aannestad (1973) is directly related to the size of the grain.

We thank W. Weinberg and M. Werner for their very helpful comments during the preparation of this paper and the referee for his constructive criticism of the originally submitted manuscript. This work was supported by a National Science Foundation grant (No. GP-32438). In addition, M. A. was partially supported by a California State Graduate Fellowship and a DuPont Summer Fellowship.

REFERENCES

Aannestad, P. A. 1973, Ap. J. Suppl., 25, 205.

Aller, L. H. 1961, The Abundance of the Elements (New York: Interscience).

Bezuglyi, P. A., Tarasenko, L. M., and Ivanov, Yu. S. 1968, Fiz. Tverd. Tela., 10, 2119.

Blackman, M. 1955, in Handbuch der Physik, ed. S. Flügge (Berlin: Springer), Vol. 7, Part I, p. 325.

Bless, R. C., and Savage, B. 1972, Ap. J., 171, 293.

Brecher, A., and Arrhenius, G. 1971, Nature Phys. Sci., 230, 107.

Brown, C. E., and Hall, P. G. 1973, J. Colloid Interface Sci., 42, 334.

Brunauer, S. 1945, The Adsorption of Gases and Vapors.I. Physical Adsorption (Princeton: Princeton University Press), p. 193.

Burton, J. J. 1972, J. Chem. Phys., 56, 3133.

Carrasco, L., Strom, S. E., and Strom, K. M. 1973, Ap. J., 182, 95.

Castellan, G. W. 1964, Physical Chemistry (Reading, Mass.: Addison-Wesley), p. 484.

Davidson, N. 1962, Statistical Mechanics (New York: McGraw-Hill), p. 115.

Davis, J. H., Blair, G. N., Van Till, H., and Thaddeus, P. 1974, Ap. J. (Letters), 190, L117.

Debye, P. 1912, Ann. Phys. (Leipzig), 39, 789.

de Jong, T., and Kamijo, F. 1973, Astr. and Ap., 25, 363.

Duley, W. W. 1973, Ap. and Space Sci., 23, 43.

Gilra, D. P. 1971, Nature, 229, 237.

Gray, D. E., ed. 1963, American Institute of Physics Handbook (2d ed.; New York: McGraw-Hill), p. 4-60.

Greenberg, J. M. 1968, in Nebulae and Interstellar Matter, ed. B. M. Middlehurst and L. H. Aller (Chicago: University of Chicago Press), p. 221.

_____. 1973, in Molecules in the Galactic Environment, ed. M. A. Gordon and L. E. Snyder (New York: Wiley-Interscience), p. 93.

Greenberg, J. M., and Hong, Seung-Soo. 1973, Bull. AAS, 5, 380.

Greenberg, J. M., and de Jong, T. 1969, Nature, 224, 251.

Herzberg, G. 1950, Molecular Spectra and Molecular Structure. I. Spectra of Diatomic Molecules (2d ed.; New York: Van Nostrand Reinhold).

Hirschfelder, J. O., Curtiss, C. F., and Bird, R. B. 1954, Molecular Theory of Gases and Liquids (New York: Wiley).

Hollenbach, D., and Salpeter, E. E. 1970, J. Chem. Phys., 53, 79.

Hollis Hallet, A. C. 1961, in Argon, Helium, and the Rare Gases, Vol. 1, ed. G. A. Cook (New York: Interscience), p. 340.

Hoyle, F., and Wickramasinghe, N. C. 1962, M. N. R. A. S., 124, 417.

Johnston, H., and Birks, J. 1972, Accts. Chem. Res., 5, 327.

Kamijo, F., and de Jong, T. 1973, Astr. and Ap., 25, 371.

Lorents, D. C., Olson, R. E., and Conklin, G. M. 1973, Chem. Phys. Letters, 20, 589.

McCarroll, B. 1963, J. Chem. Phys., 39, 1317.

_____. 1969, J. Chem. Phys., 50, 4758.

McCarroll, B., and Ehrlich, G. 1963, J. Chem. Phys., 38, 523.

McGinty, D. J. 1971, J. Chem. Phys., 55, 580.

_____. 1973, J. Chem. Phys., 58, 4733.

Moelwyn-Hughes, E. A. 1961, Physical Chemistry (2d ed.; Oxford: Pergamon), p. 952.

Nair, N. K., and Adamson, A. W. 1970, J. Phys. Chem., 74, 2229

Natarajan, N. S. 1967, Indian J. Pure Appl. Phys., 5, 372.

Oort, J. H., and van de Hulst, H. C. 1946, B. A. N., 10, No. 376, 187.

Proctor, T. M. 1966, J. Acoust. Soc. Am., 39, 972.

Rank, D. M., Townes, C. H., and Welch, W. J. 1971, Science, 174, 1083.

Sagan, C. 1972, Nature, 238, 77.

Smith, W. R., and Ford, D. G. 1965, J. Phys. Chem., 69, 3587.

Solomon, P. M., and Wickramasinghe, N. C. 1969, Ap. J., 158, 449.

Watson, W. D., and Salpeter, E. E. 1972, Ap. J., 174, 321.

Weast, R. C., ed. 1968, Handbook of Chemistry and Physics (49th ed.; Cleveland: Chemical Rubber), p. F-158.

Wickramasinghe, N. C., and Nandy, K. 1972, Rep. Prog. Phys., 35, 157.

York, D. G., Drake, J. F., Jenkins, E. B., Morton, D. C., Rogerson, J. B., and Spitzer, L. 1973, Ap. J. (Letters), 182, L1.

Zarif'yants, Yu. A. 1964, Zh. Fiz. Khim., 38, 2655.

Zwanzig, R. W. 1960, J. Chem. Phys., 32, 1173.

Chapter 2

MOLECULAR HYDROGEN IN INTERSTELLAR DARK CLOUDS*

MARK ALLEN

Arthur Amos Noyes Laboratory of Chemical Physics,†

California Institute of Technology

G. WILSE ROBINSON

Department of Physical Chemistry, University of Melbourne

and Arthur Amos Noyes Laboratory of Chemical Physics,

California Institute of Technology

* The Astrophysical Journal, 207, August 1, 1976.

† Contribution No. 5220.

I. INTRODUCTION

Interstellar molecules are observed in a variety of environments (Zuckerman and Palmer 1974), which can be generally grouped into three categories: the "standard" H I cloud (Spitzer 1968) with total gas density $[H + 2H_2] \approx 10\ cm^{-3}$, visual extinction $A_V \approx 0.1$ mag, and gas kinetic temperature $T_k \approx 70\,°K$; "dark" clouds (Scoville 1972) with $[H + 2H_2] \approx 10^3 - 10^4\ cm^{-3}$, $A_V \approx 1 - 10$ mag, $T_k \approx 10\,°K$, and "black" clouds (Scoville 1972) with $[H + 2H_2] \gtrsim 10^4\ cm^{-3}$, $A_V > 10$ mag, and $T_k > 20\,°K$. The latter regions are associated with H II regions and/or strong infrared sources and are therefore felt to be the sites of recent and/or current star formation. Turner (1974) suggests that the chemistry varies from region to region. In the standard cloud, where the galactic ultraviolet radiation field is only weakly attenuated, photodestruction of molecules strongly affects the observed abundances. On the other hand, the physical conditions under which molecule synthesis is occurring in black clouds are unclear due to uncertainty about the spatial relationship of the molecular cloud vis-a-vis the neighboring H II regions and/or infrared sources [a good example is the speculation about the Orion Nebula (Zuckerman 1973)]. Although compact H II regions (Gilmore, Brown, and Zuckerman 1975) and small infrared sources (Strom et al. 1975) recently have been detected in the direction of some dark clouds, in general the internal radiation field of dark clouds is basically the 3° cosmic background radiation field, since

the high visual extinction restricts high energy galactic radiation to the peripheral cloud regions. The limited radiation field and low temperatures confine, but also simplify, the cloud chemistry. Therefore, this paper focuses on dark cloud chemistry in the hope that it is possible to develop "complete" chemical models for these regions.

The element hydrogen is the primary chemical component of the universe. Solomon and Wickramasinghe (1969) and Hollenbach, Werner, and Salpeter (1971) suggest that molecular hydrogen will be the predominant species in dust clouds with $A_V \gtrsim 1$ mag. Indeed, recent ultraviolet observations of H_2 in standard clouds made by the Orbiting Astronomical Observatory 3 (Copernicus) generally follow the theoretical predictions (Spitzer et al. 1973). On the other hand, direct observation of H_2 in dark clouds is not presently possible, but high H_2 abundances are inferred from several types of observations: (1) The general correlation of the observed atomic hydrogen column density N_H with interstellar reddening E_{B-V} breaks down for high values of E_{B-V} (Heiles 1971). (2) A survey of 21-cm HI absorption in the dark clouds (Knapp 1974a) finds a significant underabundance of atomic hydrogen if the general interstellar value for N_H/E_{B-V} is also valid for dark clouds. (3) The gas densities derived from observation of the excitation of molecules in dark clouds are too large to be ascribed to anything but H_2 (Zuckerman and Palmer 1974; Turner 1974). It seems that the most important chemistry occurring in dark clouds involves the formation and destruction of H_2; thus the direction of this paper.

The most recent study of H_2 chemistry in dark clouds is by de Jong (1972). He considers both gas phase and surface formation processes, but finds that surface recombination is the predominant mechanism, especially under dark cloud conditions of high density and low radiative destruction. The details of hydrogen recombination on surfaces are presented by Hollenbach and Salpeter (1971; hereinafter referred to as HS). At dark cloud temperatures (~ 10 °K), HS predict the formation of thin H_2 mantles on the grains. This will not hinder surface recombination providing that some surface sites exist at which hydrogen atoms bind more strongly than hydrogen molecules and to which atoms impinging on the grain can tunnel through the mantle. In that case a newly adsorbed atom would be able to remain on the grain until another adsorbs and recombines. As an alternative to the HS hopping ejection mechanism, an earlier paper by the authors (Allen and Robinson 1975; hereinafter referred to as Paper I) suggests that nascent molecules rapidly equilibrate with the grain substrate resulting in desorption from the smaller, hotter grains. Mantle growth is hindered on smaller grains. Thus the need for a special kind of grain adsorption site to allow effective H_2 formation in dark clouds is eliminated.

With the H_2 recombination rate constants calculated with the proposed mechanism, this paper will study the evolution of molecular hydrogen as a dark cloud ages. The problem with earlier equilibrium calculations (for example, de Jong 1972) is that H_2 radiative destruction is necessary to maintain a reasonable fraction of atomic hydrogen to match dark cloud observations (e. g., Knapp 1974). However,

H_2 ionization by cosmic rays (seemingly the only available destruction route in the cloud interior) is observed to be very low (Brown 1973) and could be negligible if residual internal magnetic fields are of sufficient strength to screen out the cosmic rays (Nakano and Tademaru 1972). However, Shu (1973) finds that a non-equilibrium collapsing cloud model can result in significant amounts of residual atomic hydrogen at certain ratios of cloud collapse rate to H_2 formation rate. Here the problem is that the nature and degree of collapse that various dark clouds are actually undergoing is highly uncertain. The low-radiation, static cloud nonequilibrium model proposed in the present paper can account for the observed N_H/A_V dark cloud ratios in terms of cloud density and age without invoking very special or restrictive conditions.

II. H_2 SURFACE RECOMBINATION MECHANISM

The basic details of the mechanism for hydrogen recombination on the surfaces of interstellar grains are presented by HS. Two hydrogen atoms which have previously collided with and stuck to the grain migrate from adsorption site to adsorption site, since the energy barrier between sites is sufficiently low to allow quantum mechanical tunneling readily. If the atoms approach closely enough, a molecular bond is formed, energy is released, and, under certain conditions, the nascent molecule is ejected from the surface. No H_2 will form on a grain whose mean temperature is so high that the length of time an atom sticks to the grain is less than the timescale for successive collisions of the grain with gas-phase atoms. Grains that are sufficiently cold will be coated with several layers of molecular hydrogen and, in the absence of special adsorption sites, the length of time an atom sticks to the grain becomes less than the timescale for successive grain/gas-phase atom collisions. Again the recombination process is inhibited. Dark cloud grain temperatures are such that it is the latter inhibitory process with which this paper is concerned. Paper I suggests that the energy released upon molecular bond formation heats up the whole grain and, in the case of small grains (radii less than a few hundred angstroms), the grain becomes sufficiently hot to eject the nascent molecule and other weakly adsorbed species. Recently Barlow and Silk (1975) considered the case of H_2 formation on grains on which H atoms are

strongly chemisorbed and H_2 only weakly physically adsorbed and conclude that only a minimal amount of the newly released bond energy is transferred to the substrate. However, the experimental data they quote to support this viewpoint are derived from high temperature experiments. This fact along with the special potential surface used in this reaction scheme (upon recombination H_2 is repelled from the surface) suggests that their conclusions are inapplicable to the present situation. Indeed thermal energy accommodation is known to be highly efficient at low temperatures (Hobson 1967). Experiments which measure the accommodation of large amounts of vibrational energy at various beam and surface temperatures would help to clarify the dynamics of the formation process.

For present purposes, bare silicate (actually quartz) grains will comprise the substrate in the recombination process. Augason (1970) finds that the adsorption energies of H_2 on silicates and ice are 0.93 and 0.92 kcal $mole^{-1}$, respectively, and, assuming that the electronic polarizability of H is ~ 81% that of H_2 and that adsorption energies scale with polarizability, the adsorption energies for H are 0.78 and 0.77 kcal $mole^{-1}$, respectively. More extensive calculations by HS give a value of 1.09 kcal $mole^{-1}$ for the H_2-ice adsorption energy (claimed to be within 10% of an experimental value). However, other experimental work (Lee 1972) reports a value of 1.71 kcal $mole^{-1}$ for this adsorption energy. The ambiguity in the H_2-ice number makes the choice of a H_2-silicate value difficult. The Augason value will be used (he claims that experimental results confirm his calculations) but will be scaled by a factor 1.09/0.92 to

be on a more conservative footing. There are $\sim 10^{14}$ adsorption sites cm^{-2} (HS) at which the H_2 and H physical adsorption energies will be taken to be 1.11 and 0.93 kcal $mole^{-1}$, respectively. There are undoubtedly higher adsorption energy sites due to radiation damage, for example, at which H atoms may be chemisorbed. These sites are quickly occupied at dark cloud densities, and adsorbed atoms are rendered chemically inactive due to the cold cloud temperatures. Barlow and Silk (1975) suggest the chemisorbed atoms will not be inert if the migration energy is greater than the activation energy for the reaction. At 10°K, this possibility is exceedingly unlikely. Therefore, the grains are treated as relatively smooth, chemically neutral surfaces upon which only physical adsorption occurs.

Following the details developed in Paper I, the adsorbed lifetime L(r) of the nascent hydrogen molecule as a function of grain radius r can now be calculated, all the other parameters describing the silicate grains and the molecule/grain bond retaining the values adopted in Paper I for the cases of physical adsorption on silicates [for the intramolecular H_2 bond, E_d = 104 kcal $mole^{-1}$ and ω_m = 4395 cm^{-1} (Weast 1968; Herzberg 1950)]. Calculated for an initial grain temperature of 10°K, L(r) is plotted as curve (a) in figure 1. Other timescales relevant to the formation process are also presented in figure 1. The residence times for H and H_2 (approximately the same due to a cancellation of factors) on silicate [this being the limit of L(r) for infinite r] or solid H_2 grains at 10°K are also calculated by the summation technique outlined in Paper I.

Fig. 1.- Relevant timescales for H_2 recombination on silicate grains. (a) Adsorbed lifetime L(r) of nascent H_2 molecule. (b) Residence time for H or H_2 on a silicate grain at 10°K. (c) Residence time for H or H_2 on a solid H_2 grain at 10°K. (d) Timescale $t_{H_2G}(r)$ for successive collisions of grain with gas phase H_2 where $[H_2] = 10^4\ cm^{-3}$ and $T_k = 10°K$ (timescale for collisions with H less by a factor of $\sqrt{2}$ for the same density).

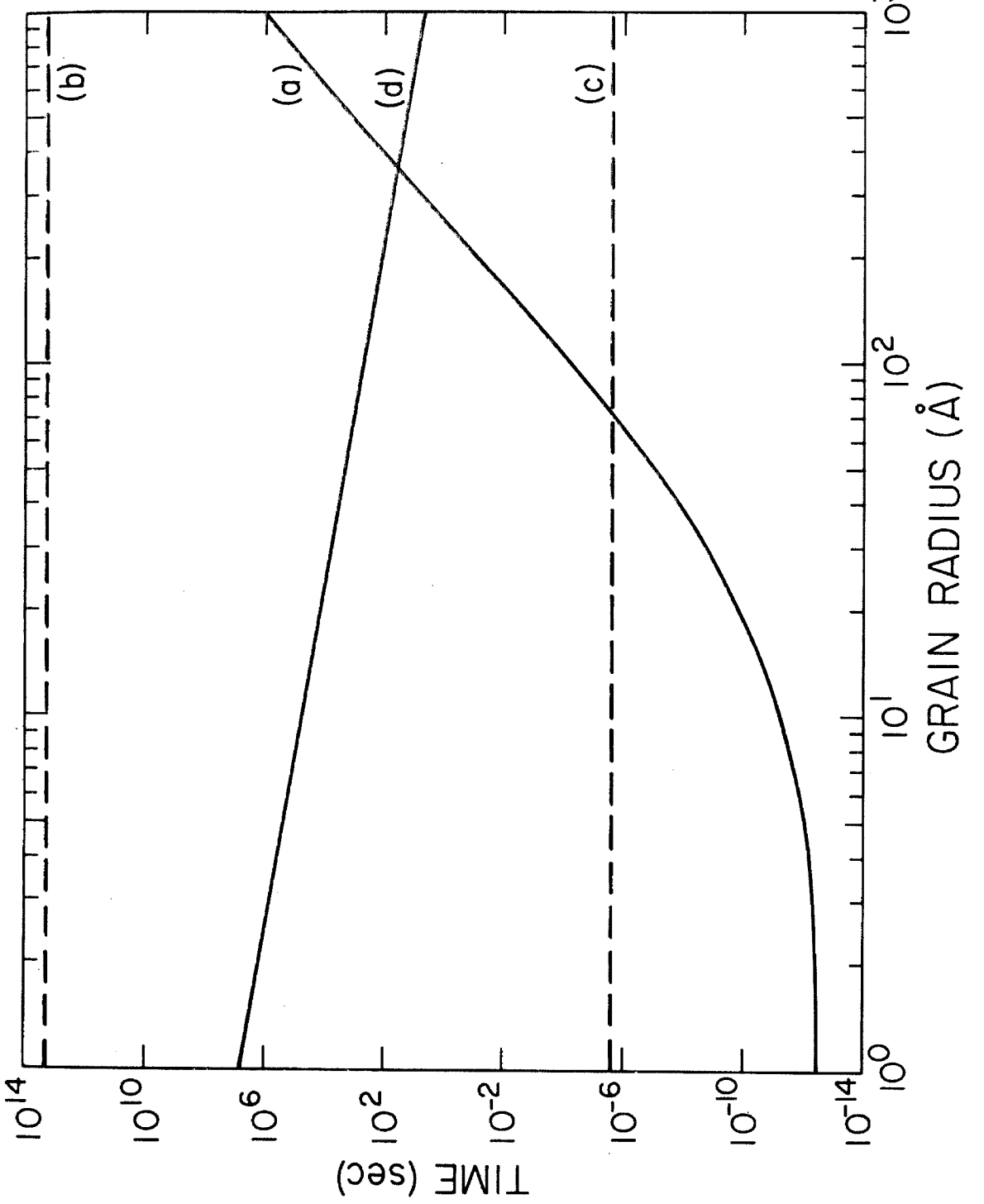
(b)
(a)
(d)
(c)
10^{14}
10^{10}
10^{6}
10^{2}
10^{-2}
10^{-6}
10^{-10}
10^{-14}
TIME (sec)
10^{0}
10^{1}
10^{2}
10^{3}
GRAIN RADIUS (Å)

The plotted grain-H_2 collision timescale $t_{H_2G}(r)$ is defined as follows:

$$t_{H_2G}(r) = 1/\pi r^2 [H_2] v_{H_2} , \quad (1)$$

where $[H_2]$ means volume density (and N_{H_2} column density) and v_{H_2} is the mean H_2 velocity such that

$$v_{H_2} = (8kT_k/\pi M_{H_2})^{\frac{1}{2}} , \quad (2)$$

where k is Boltzmann's constant, M_{H_2} is the molecular mass, and $T_k = 10\,^{\circ}K$, the dark cloud kinetic temperature adopted for the purposes of this paper. Figure 1 shows that, as discussed before, accretion of an H_2 mantle will render the grain useless as a site for H_2 formation.

For a grain to be an effective site for H_2 formation, it must be (a) large enough so that an H_2 mantle does not quickly grow sufficiently thick to drop the surface adsorption energy to the sublimation point and (b) small enough that the bond energy released heats the grain enough to destroy any accumulated H_2 mantle and to have a positive net production rate. There is a grain radius r_{min} below which five layers of H_2 will accrete before two atoms are adsorbed and form a new molecule. In that case, the H_2 (and H) adsorption energy would drop to the level of the sublimation energy of solid H_2. Then the timescale for hydrogen atom residence on a grain becomes less than the timescale for gas-grain collisions [cf. curves (c) and (d) in fig. 1] and hydrogen recombination is

inhibited. Thus

$$1/0.5[H]v_H\pi r_{min}^2 = 4\pi r_{min}^2\, 5\times 10^{14}/[H_2]v_{H_2}\pi r_{min}^2 . \qquad (3)$$

On the other hand, there is a radius r_{max} above which the nascent H_2 adsorbed lifetime is longer than the timescale for the appearance of H_2 on the grain, through either additional hydrogen recombination or H_2 adsorption; in other words,

$$L(r \geq r_{max}) \geq 1/([H_2]v_{H_2} + 0.5[H]v_H)\pi r^2 . \qquad (4)$$

These grains are useless sites for H_2 formation, since the net formation-release rate is negative. Moreover, an H_2 mantle (> 5 layers) will rapidly form, and then no hydrogen recombination is possible. Thus only grains with radii between r_{min} and r_{max} provide the effective reaction surface area.

If a hard sphere model for grain-gas collision dynamics is used, the rate of formation of gas-phase H_2 is

$$\left.\frac{d[H_2]}{dt}\right|_+ = 0.5\ a\epsilon[H]v_H\pi \int_{r_{min}}^{r_{max}} n'(r)r^2\,dr, \qquad (5)$$

where $n'(r)\,dr$ is the volume number density of grains with radii between r and r + dr. At peak efficiency, only every other H-grain collision results in an H_2 formed; thus the factor of 0.5 on the right-hand side of equation (5). Also appearing in equation (5) are the

factors a, the accommodation coefficient (the probability that the atom does not rebound from the surface after the initial collision and reaches thermal equilibrium with the surface), and ϵ, the reaction efficiency (the probability that a molecule is formed upon every second H-grain collision). For conditions of $T_k \approx T_{grain} \approx 10\,^{\circ}K$, it seems reasonable that a = 1 (Hobson 1967). Surface migration seems to be sufficiently rapid to set $\epsilon = 1$(HS). To facilitate comparison between our calculated H_2 formation rate constants and those determined from ultraviolet observations of H_2 (e. g., Jura 1975a, b), a formation rate constant R is defined:

$$R = 0.5\ a\epsilon\ v_H \pi \int_{r_{min}}^{r_{max}} n'(r) r^2\ dr / [H + 2H_2] \ . \qquad (6)$$

III. TIME EVOLUTION OF DARK CLOUD CHEMISTRY

If observations of the abundances of chemical species in a dark cloud are to be interpreted in a temporal sense, the cloud conditions at "birth" must be realistically estimated and all the important chemical processes of the aging cloud must be included in the time-dependent treatment. The simple cloud evolutionary model proposed in this paper starts with a condensed, cold, un-ionized cloud with all of the hydrogen, carbon, nitrogen, and oxygen in the form of gas-phase atoms. The various physical processes which could prepare a cloud in such a state and therefore the plausibility of this approach will be discussed.

a) Initial Cloud State

Interstellar clouds form out of the diffuse intercloud and/or interarm H I regions. These regions are hot, $\log T_k \approx 2 - 4$ (Dalgarno and McCray 1972), and the gas is composed of neutral atoms and atomic ions. To characterize the gas, this paper adopts a "cosmic" (i.e., solar system) abundance ratio for H:He:C:N:O:Si of $1:6.95 \times 10^{-2}:3.71 \times 10^{-4}:1.18 \times 10^{-4}:6.67 \times 10^{-4}:3.14 \times 10^{-5}$ (Cameron 1973).

There also exists in this medium a solid-state component composed of grains (radii $\lesssim 1\mu$). Based on attempts to fit the observed interstellar extinction curve, the suggested grain composition ranges from hydrocarbons and ices to more refractory materials

like graphite and silicates or some composite of both types (Aannestad and Purcell 1973). The high kinetic temperatures and the presence of high-energy radiation seemingly make the diffuse H I regions an inhospitable environment for nonrefractory grains (Greenberg and Hong 1973). Moreover, the birefringent properties of the interstellar medium suggest that the grains are composed of dielectric materials (Martin and Angel 1974). Thus bare silicate grains become the favored candidate for the diffuse medium grain material. This is further supported by the suggestion of Kamijo and de Jong (1973) that small silicate grains are injected into the interstellar medium from the atmospheres of M supergiant stars, the validity of the idea being enhanced by the tentative identification of the 10 μ excess in late-type stellar spectra as being due to hot condensed silicates. Also, recent infrared observations of the 3 μ ice absorption band indicate an absence of icy mantles in the direction of low extinction (Gillett et al. 1975).

Huffman and Stapp (1971) propose that, with a proper choice of grain size distribution parameters, the interstellar extinction curve might be fitted with an all-refractory and predominantly silicate grain distribution, the form of their best fit being

$$n(r) = 10^{-4}\{0.024 \exp[-(r-1400/900)^2] + \exp[-(r-600/200)^2] + 281 \exp[-(r-90/60)^2]\}, \quad (7)$$

where n(r) is the normalized number density of grains with radius r (in angstroms) per angstrom interval. Figure 2 displays a plot of

n(r) along with the fractional area function F(r):

$$F(r) = \int_0^r n(r)r^2dr \Big/ \int_0^\infty n(r)r^2dr \ . \qquad (8)$$

The average radius in this size distribution is 100 Å, much smaller than is generally used for an all-silicate distribution (Greenberg 1974). This fact combined with uncertainties about the magnitude of the silicate extinction cross section as a function of wavelength and grain radius (Day, Steyer, and Huffman 1974) presents the possibility that the cosmic abundance of silicate material might be sufficient to produce the observed extinction. Thus, for computational ease, this paper adopts bare silicate grains-in particular, quartz grains-for the solid-state component of the diffuse H I regions.

To obtain an appropriate gas-to-dust ratio, a scaling factor β is calculated by making the assumption that all silicon atoms are in the quartz grains,

$$\beta = \chi_{Si}[H + 2H_2](m_{Si} + 2m_O) \Big/ 4/3\,\pi\, d_{SiO_2} \int_0^\infty n(r)r^3dr \ , \quad (9)$$

where χ_{Si} is the cosmic Si to H abundance ratio, $[H + 2H_2]$ is the total hydrogen density, and d_{SiO_2} is the density of quartz (2.64 g cm^{-3}). The grain mass to hydrogen mass density in this model is $\sim 2 \times 10^{-3}$, a factor of 6 lower than the 1.3×10^{-2} value derived from observations for a material with the density of quartz using the Kramers-Kronig relations (Aannestad and Purcell 1973) (indeed this

Fig. 2. - Characteristics of the grain distribution used in the calculations of this paper. (a) Normalized number density n(r) per angstrom radius interval (left ordinate scale). (b) Fractional area function F(r) (right ordinate scale).

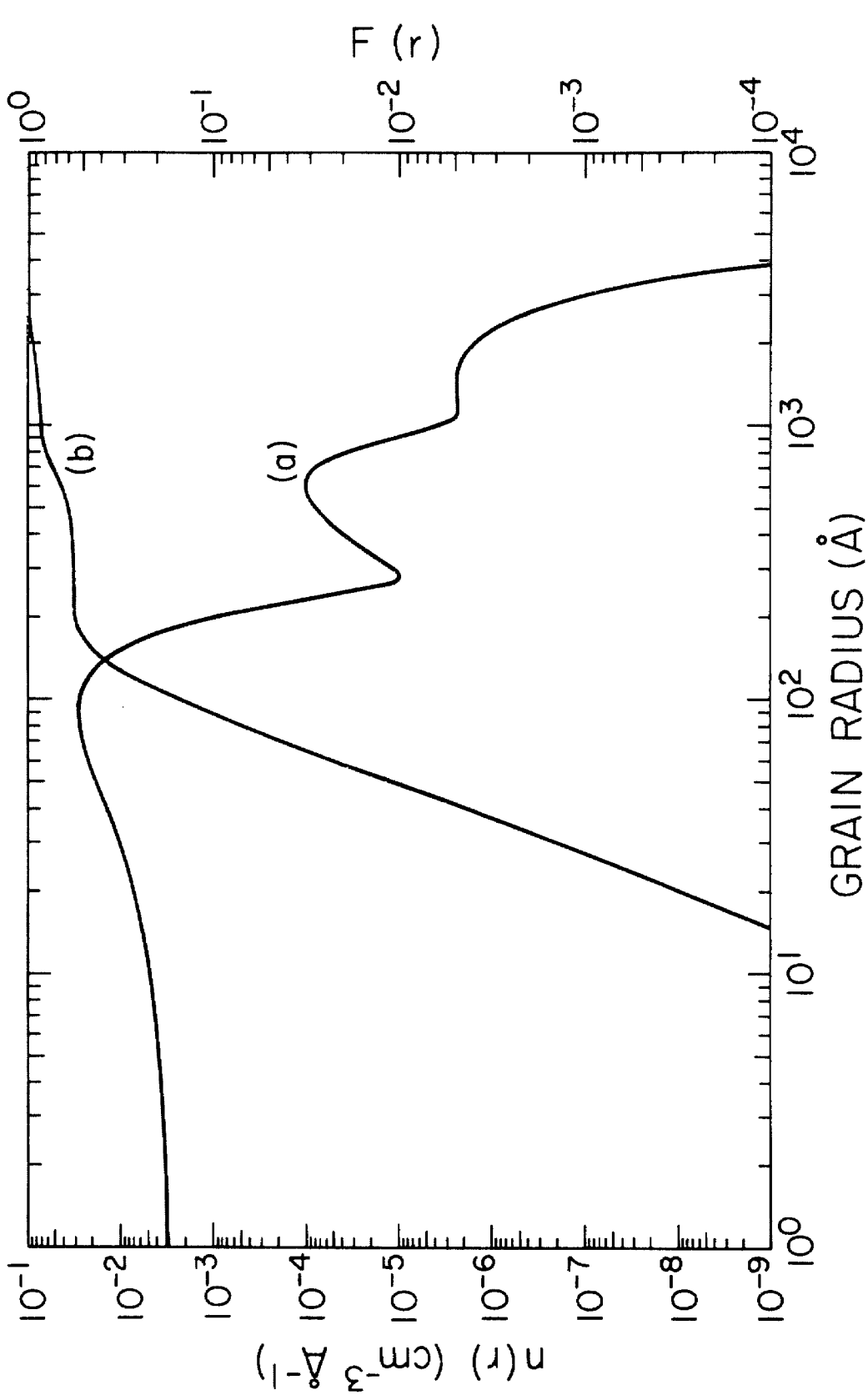
F (r)
n(r) (cm⁻³ Å⁻¹)
GRAIN RADIUS (Å)
(a)
(b)

analysis seemingly contradicts an earlier assumption that the cosmic abundance of silicon is sufficient to produce the observed extinction). However, a value of 6×10^{-3} is derived from interstellar hydrogen Lα observations, but is very grain model dependent (Jenkins and Savage 1974). On the other hand, other grain distribution characteristics like total grain surface area per hydrogen atom (6×10^{-22} cm^{-1}) and grain to hydrogen number ratio (3×10^{-11}) are similar to generally used values of $\sim 3 \times 10^{-22}$ cm^{-1} (Spitzer 1968) and 4×10^{-13} (Hollenbach, Werner, and Salpeter 1971) to 4×10^{-10} (Greenberg and Hong 1973), respectively.

The starting point for the temporal cloud chemistry calculations is the "instantaneous" condensation of the diffuse medium into a dense dark cloud. A comparison of cloud formation timescales with chemical timescales will suggest the plausibility of the desired initial state. "Cataclysmic" cloud formation theories proposing sudden cloud birth suggest that diffuse gas and/or low density clouds could be highly compressed as the interarm material falls into the compression region of a galactic shock arm (Shu et al. 1972) or when a supernova-generated shock wave sweeps through the intercloud medium (Mufson 1974). In either case, some of the medium rapidly condenses into much higher density clouds, the kinetic temperature of the gas initially rising precipitously and then rapidly decreasing (the degree of ionization of the material follows a similar pattern), resulting in a basically atomic, low ionization, low temperature, high density cloud being formed out of the diffuse interstellar medium in about 10^5 - 10^6 years. Another possibility is that thermal

instabilities in the intersteller medium suddenly heated by a pulse of electromagnetic energy would result in the formation of discrete, high density, low temperature, low ionization condensations in $\sim 10^6$ years (Schwarz, McCray, and Stein 1972). An "evolutionary" cloud formation theory suggests thermal instabilities in a hot steady-state medium would result in the formation of these dense clouds in pressure equilibrium with the lower density, higher temperature diffuse medium (Field, Goldsmith, and Habing 1969) on a timescale of $\sim 10^7$ years (Goldsmith 1970). A partly atomic, high density, cold cloud could be formed if an old molecular cloud collides with another cloud, the resultant shock wave elevating the internal temperature to such a degree that any icy mantles are destroyed by sputtering and molecules are partially dissociated (Aannestad 1973). Depending on the nature of the cooling processes, the relaxation time for return to a cold, dense medium is $\sim 10^4$ years. Since the timescales for most chemical processes (molecule formation and grain mantle growth) occurring in dense clouds are $\sim 10^5$-10^7 years (vide infra) and the suggested timescales for cloud formation are somewhat shorter, it seems reasonable to adopt a model in which the physical and chemical cloud development are decoupled.

b) Temporal Evolution of Dark Cloud Chemistry

The basic time-dependent chemical processes to be studied in this paper are the recombination of atomic hydrogen to form molecular hydrogen and the depletion of heavy elements (i.e., carbon, nitrogen, and oxygen) onto grains, the latter process setting an upper

limit to the rate of formation of icy mantles and heavy molecules (assuming no gas-phase chemistry exists for heavy elements).

Molecular hydrogen is formed at the time-dependent rate

$$\frac{d[H_2(t)]}{dt} = R(t)[H(t)][H + 2H_2] - k_{diss}(H_2)[H_2(t)] , \qquad (10)$$

where $k_{diss}(H_2)$ is the time-independent H_2 radiative dissociation rate constant. The complementary expression for atomic hydrogen is

$$\frac{d[H(t)]}{dt} = -2 \frac{d[H_2(t)]}{dt} . \qquad (11)$$

As presented here, all of the hydrogen is in the gas phase, in either atomic or molecular form, at any point in time. Thus the factor $[H + 2H_2]$ is the time-independent elemental hydrogen density. R(t) is time-dependent because r_{min} approaches r_{max} as the cloud ages (cf. eq. [6]). Depletion of the heavy elements (hereinafter referred to as CNO) is governed by the expression

$$\frac{d[CNO(t)]}{dt} = - [CNO(t)] v_{CNO} \beta \pi \int_0^\infty n(r) r^2 dr , \qquad (12)$$

where

$$v_{CNO} = \frac{\chi_C v_C + \chi_N v_N + \chi_O v_O}{\chi_C + \chi_N + \chi_O} . \qquad (13)$$

The calculations of Hollenbach, Werner, and Salpeter (1971) show that H_2 photodissociation by ultraviolet radiation incident upon the exterior of a dark cloud is significant only very close to the cloud surface where the optical depth in the ultraviolet is $\lesssim 1$. They also find that the Habing interstellar radiation field produces an atomic hydrogen column density of $8.5 \times 10^{22}/[H + 2H_2]$ cm^{-2} independent of cloud mass. This is often no more than a small fraction of the observed HI (cf. table 1). In the case of dark clouds with $A_V > 4$, only cosmic rays (energy $\gtrsim$ 2 MeV) might penetrate the cloud sufficiently to produce appreciable atomic hydrogen ionization and molecular hydrogen dissociation in the cloud interior (Solomon and Werner 1971). For medium density dust clouds, O'Donnell and Watson (1974) set an upper limit to the atomic hydrogen ionization rate constant ζ_H of $\sim 10^{-17}$- 10^{-16} s^{-1}. For dark clouds, the atomic recombination line observations of Brown (1973) set an upper limit to ζ_H of 3×10^{-16}s^{-1} assuming a normal gas/extinction ratio. Such a low value is consistent with the H_2CO excitation model of Evans et al. (1975). If the observed ionization of the diffuse interstellar medium is not caused by cosmic rays or x-rays (Spitzer and Jenkins 1975), then ζ_H for dark clouds would be even lower than the upper limits that have been set. Moreover, for clouds with diameters $\gtrsim$ 1 pc and densities $[H + 2H_2] \gtrsim 5 \times 10^3$cm^{-3}, 2 MeV protons are restricted to a thin outer shell (Glassgold and Langer 1973b). Higher energy cosmic rays will be able to penetrate further into the clouds, but their effectiveness may be significantly reduced because the hydrogen ionization cross section and the

interstellar cosmic ray spectrum are decreasing functions of energy (Nakano and Tademaru 1972). These authors also point out that small internal magnetic fields may prevent cosmic rays from penetrating the clouds. Therefore, for dense dark clouds, a value for ζ_H of $\lesssim 10^{-18} s^{-1}$ for most of the cloud interior is not unreasonable. In turn, $k_{diss}(H_2) \approx \zeta_H$ (Solomon and Werner 1971; Glassgold and Langer 1973a).

The temporal development of the cloud chemistry was calculated by a time-dependent numerical solution of the rate equations. The initial conditions for the various runs were $[H_2(0)] = 0$ and, for $k_{diss}(H_2) = 0\ s^{-1}$, various values between 1×10^3 and $2 \times 10^4 cm^{-3}$ for $[H(0)]$, for $k_{diss}(H_2) = 10^{-18} s^{-1}$, $[H(0)] = 1 \times 10^3$ or $1 \times 10^4 cm^{-3}$. The results of the 1×10^3 and $1 \times 10^4\ cm^{-3}$ runs for both values of $k_{diss}(H_2)$ are displayed in figure 3-5. Plotted in figures 3 and 4 are fractional abundances $f_x(t)$ where

$$f_H(t) = [H(t)]/[H + 2H_2] \quad (14)$$

$$f_{H_2}(t) = 2[H_2(t)]/[H + 2H_2] \quad (15)$$

and

$$f_{CNO}(t) = [CNO(t)]/[CNO(0)] \ . \quad (16)$$

The values of $r_{min}(t)$, $r_{max}(t)$, and $R(t)$ for these runs are presented in figure 5.

Fig. 3.- Temporal evolution of f_H, f_{H_2}, and f_{CNO} for initial conditions of $[H_2] = 0$ and $[H] = 10^3$ cm^{-3} (solid lines) or 10^4 cm^{-3} (dashed lines). When the curves for runs with different $k_{diss}(H_2)$ differ, the branches are marked with the appropriate value of $k_{diss}(H_2)$.

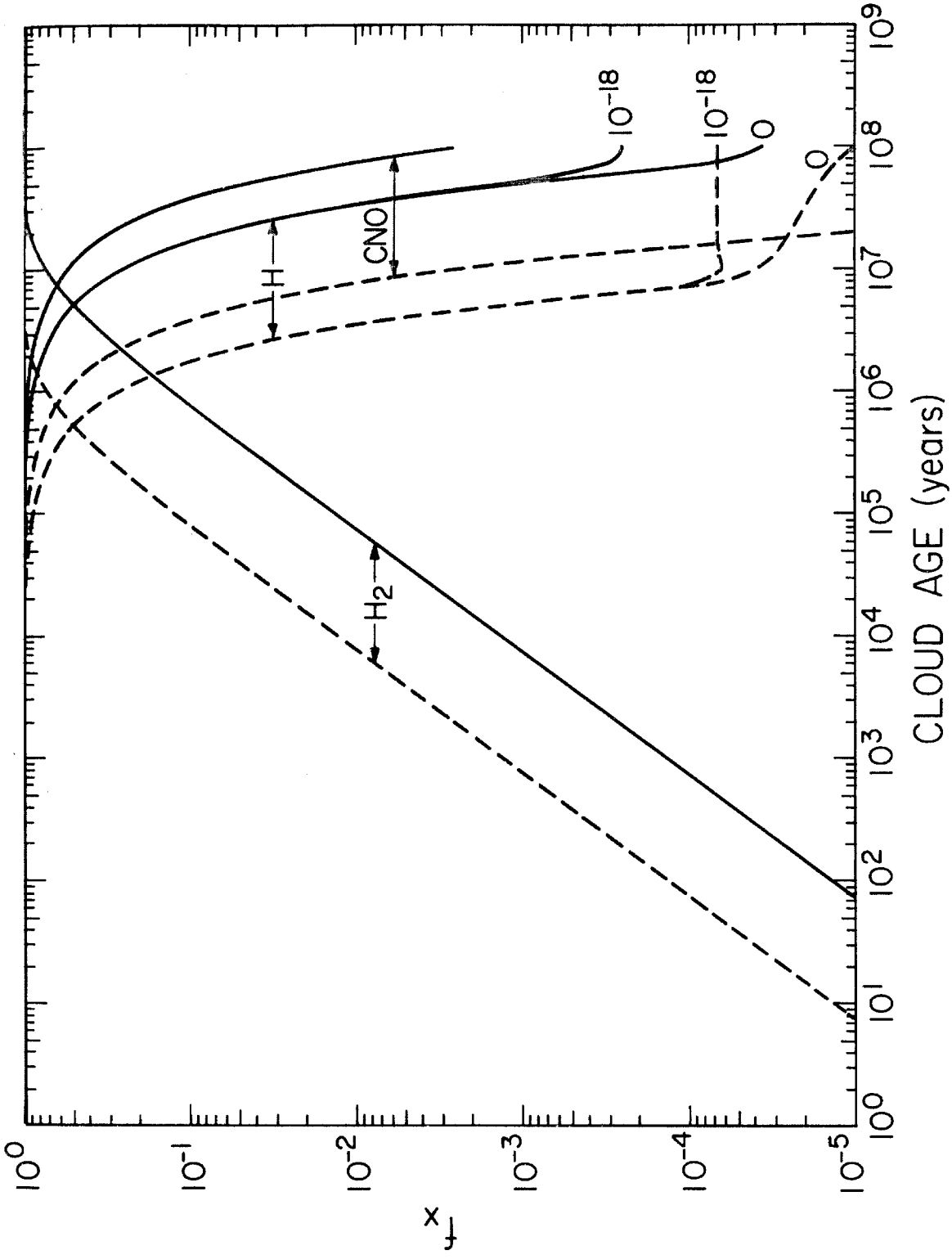
10^{0}
10^{-1}
10^{-2}
10^{-3}
10^{-4}
10^{-5}
f_x
10^{0}
10^{1}
10^{2}
10^{3}
10^{4}
10^{5}
10^{6}
10^{7}
10^{8}
10^{9}
CLOUD AGE (years)
10^{-18}
10^{-18}
O
O
CNO
H
H_2

Fig. 4. - Same as fig. 3 but scale expanded to emphasize the period between 10^6 and 10^7 years.

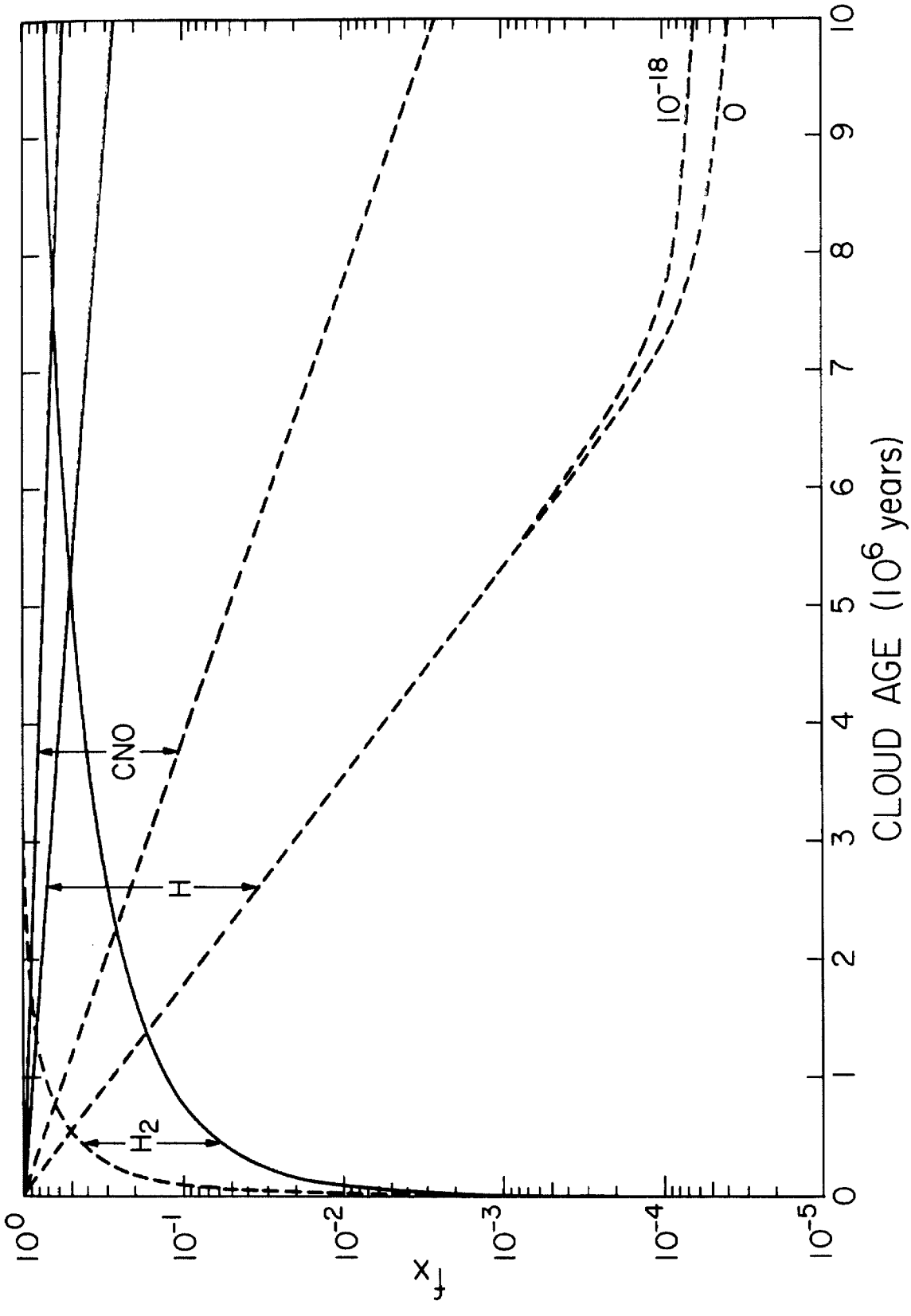
10^{0}
10^{-1}
10^{-2}
10^{-3}
10^{-4}
10^{-5}
x_f
0
1
2
3
4
5
6
7
8
9
10
CLOUD AGE (10^6 years)
CNO
H
H_2
10^{-18}
O

Fig. 5. - Temporal evolution of R(left ordinate scale) and the effective grain radii limits, r_{min} and r_{max} (right ordinate scale). Initial conditions are $[H_2] = 0$ and $[H] = 10^3\ cm^{-3}$ (solid lines) or $10^4\ cm^{-3}$ (dashed lines). When the curves for runs with different $k_{diss}(H_2)$ differ, the branches are marked with the appropriate value of $k_{diss}(H_2)$.

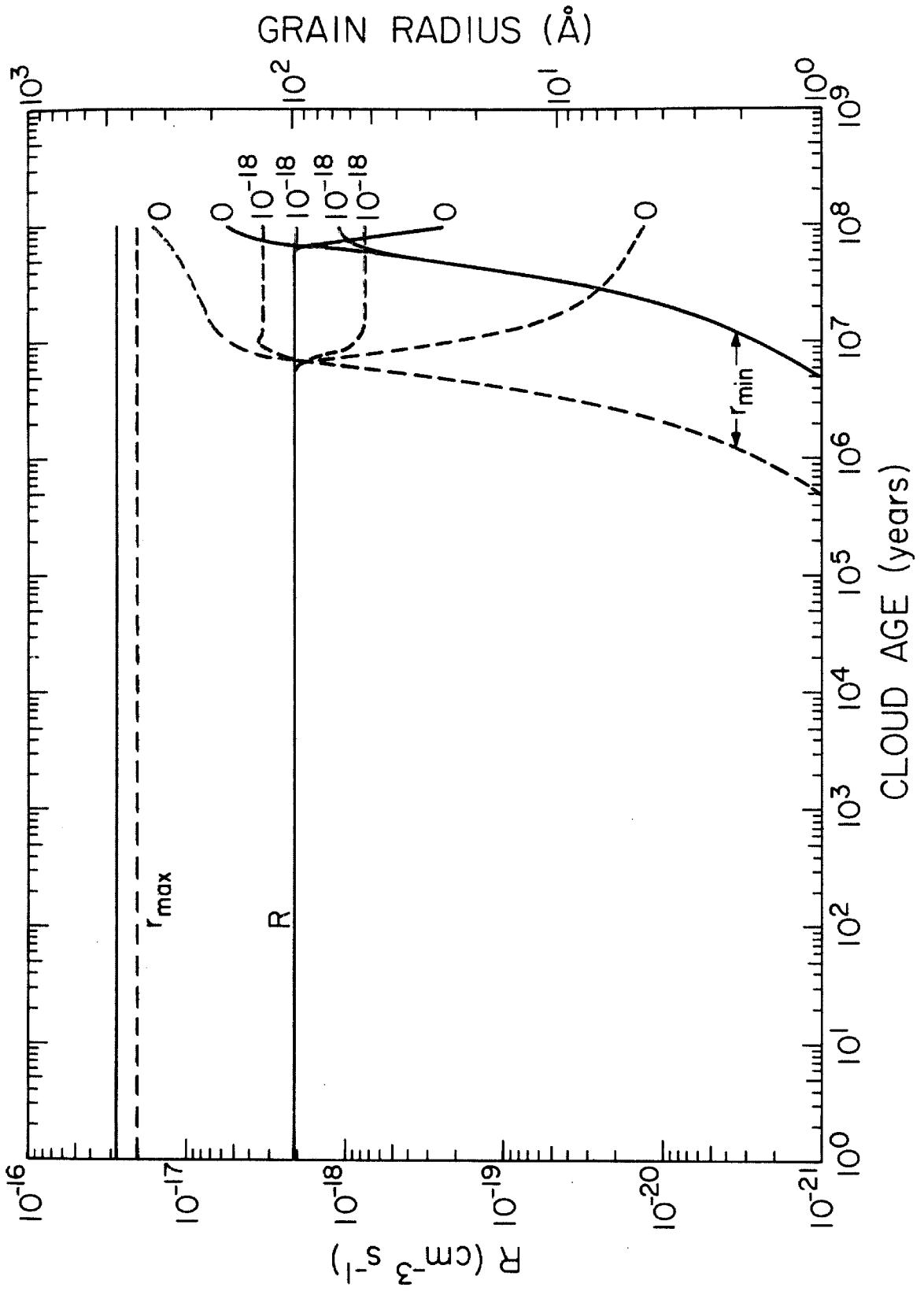
GRAIN RADIUS (Å)
CLOUD AGE (years)
R (cm⁻³ s⁻¹)
r_max
R
r_min
0
10⁻¹⁸

c) Model Assumptions

Many assumptions were made in formulating the model and executing the calculations. These will now be discussed as a way of suggesting uncertainty limits on the reported results.

The physical development of the cloud is decoupled from the chemical development at two different stages of the model. First, the assumption that the timescale for cloud "formation" is much shorter than for cloud chemistry (see §IIIa) strongly affects the ability to interpret observed $f_x(t)$'s in terms of real cloud age. If the cloud reaches physical steady-state more slowly than has been assumed or if the pre-cloud material is partly molecular, one can adjust the timescales in figures 3-5 for the appropriate value of $f_H(0)$. Second, the assumption that the cloud physically remains in steady-state (temperature, ionization, and mass density not varying with time) affects the reliability of the calculated temporal development of the chemistry. After the initial formation stimulus, there are several other forces that may keep the cloud in an evolving physical state. If the gravitational binding energy of a cloud is greater than its thermal kinetic energy, the cloud tends to collapse with a free-fall time $\sim 10^5$ years, the time being an inverse function of density (Larson 1973). The collapse will be resisted by internal cloud magnetic fields, centrifugal force generated by any cloud rotation, and internal cloud turbulence. If the cloud is initially at pressure equilibrium with the surrounding diffuse medium (Field, Goldsmith, and Habing 1969), the conversion of atomic hydrogen into molecules may result in a drop in the internal cloud pressure,

possibly resulting in an instability leading to cloud collapse (Reddish 1975). Alternatively, Glassgold and Langer (1976) suggest that ion-molecule reactions could trigger cloud collapse. On the other hand, if cloud cooling agents are depleted onto the grains as the mantles grow, in the absence of change in other forces, the cloud would heat up, resulting in an increase in internal pressure, cloud expansion, and possibly the dissipation of the cloud [the timescale for this process is $> 10^7$ yr (Mészáros 1972)]. The steady-state cloud model is suggested to be a reasonable compromise of all these conflicting trends.

The temporal variation of f_H and f_{H_2} depends on the time-dependent function R(t) which is formation model-dependent. In the case of the model proposed in § II of this paper, the time variation in R(t) reflects temporal changes in the effective reaction surface area. Small changes in L(r) as derived from the proposed nascent molecule ejection mechanism result in minimal changes in r_{max} for given values of [H] and $[H_2]$. But the most crucial factor is n(r). The particular size distribution used in this paper is actually the result of an attempt to show that the interstellar extinction curve could be explained with almost any material, given enough varying parameters (D. Huffman, private communication). However, many different size distributions have basically the same fractional area function and, if the grain properties are similar to that of the silicates, the resulting values of R will be little changed for a given pair of r_{min} and r_{max}. As is also seen, f_H and f_{H_2} are pretty insensitive to the value of $k_{diss}(H_2)$ used, radiative destruction

having a significant rate only after $\sim 8 \times 10^6$ years at the highest densities and $\sim 5 \times 10^7$ years at the lower densities.

The hydrogen mass balance approach of the rate equations assumes that all the elemental hydrogen of the cloud remains in the gas phase, either in atomic or molecular form. Indeed, if all the grains were coated with five layers of solid hydrogen only $2 \times 5 \times 10^{14} \times 6 \times 10^{-22}$ $(= 6 \times 10^{-7})$ of the hydrogen would be depleted. This negligible loss confirms the validity of this assumption.

Finally, the larger grains (radii $\gtrsim$ 350 Å) are probably growing icy mantles as the heavy elements accrete, but the increase in cross-sectional area involved in the rate of depletion is not taken into account. Since a "large" ice grain distribution with all the heavy atoms incorporated into the grains does not have a total cross-sectional area much larger than that of this model (see § IIIa), it is expected that the growth of mantles on the larger grains in the present case will not result in a significant increase in surface area.

IV. DISCUSSION

The analysis of the molecular hydrogen content of interstellar dark clouds is treated in two stages: (1) The nascent molecule ejection mechanism developed in Paper I is employed to calculate the rate constant R for the H_2 formation process. (2) The temporal evolution of a dark cloud from a basically atomic to a mainly molecular system is computed using the R's derived according to the formulation of step (1). However, a similar analysis could be done with R's derived from any given H_2 formation model.

a) H_2 Formation Process

Since H_2 should also be formed in less dense clouds predominantly by the proposed mechanism, ultraviolet observations of H_2 should not contradict the consequences peculiar to this model. That there are enough small grains to furnish a sufficient reaction cross-sectional surface area is shown by the calculated values of the H_2 formation rate constant R, $\sim 2 \times 10^{-18}$ cm^{-3} s^{-1} (fairly independent of the total gas density, falling off only in the older more dense clouds), which is only a factor of 5-10 smaller than the usual theoretical estimate (HS) and the value derived from observations of standard clouds (Jura 1975a, b). In low density clouds, higher values of R would result from (a) higher kinetic temperatures ($\sim 100\,^{\circ}K$) and (b) the existence of physical processes which could destroy accumulated H_2 mantles [photodestruction of the mantles

by ultraviolet radiation or cosmic rays (Watson and Salpeter 1972) being one possibility], thus creating in effect a larger cross-sectional reaction surface area. The values for $R[H + 2H_2]$ derived from observations (Jura 1975b) suggest within the uncertainty limits of the calculations, a possible inverse relationship between the two variables, which would result if mantle destruction affected R (the attenuation of the sputtering radiation increasing as the gas density increases).

Ultraviolet observations of interstellar H_2 reveal that a significant fraction of the molecules exist in excited rotational states in the ground electronic and vibrational state (Spitzer and Cochran 1973). In the HS H_2 formation model, molecules are produced in excited vibrational and rotational states; this is suggested by Spitzer and Zweibel (1974) to be one of the mechanisms for producing the observed excitation. In the case of the H_2 ejection process developed in this paper, the adsorbed lifetime of a nascent molecule is much less than the H_2 residence time on a silicate grain at 10 °K (fig. 1), indicating that the desorption is from a hyperthermal surface and that the molecule is leaving in some excited energy state. The formation of an H_2 bond heats a 5 Å-radius grain to ~ 1300 °K, a 10 Å-radius grain to ~ 300 °K, a 30 Å-radius grain to ~ 83 °K, and a 100 Å-radius grain to ~ 34 °K. Thus rotationally excited, but not vibrationally excited, molecules may be produced by the proposed ejection pathway. Since the radiative lifetime of a given vibrational state is $\lesssim 10^7$ s (Field, Somerville, and Dressler 1966) and is much less than the timescale for H_2

formation, the observed absence of vibrationally excited species (Spitzer, Cochran, and Hirshfeld 1974) cannot be used to decide between the different ejection mechanisms. These authors also report that, in the direction of several stars, there is an increase in the Doppler-broadened line widths with increasing state of rotational excitation, which is not inconsistent with the fact that smaller, hotter grains produce molecules in higher rotational and translational energy states. Moreover, Spitzer and Cochran (1973) report an observed decrease in molecular excitation with increasing N_{H_2}. This might result from the proposed nascent molecule ejection mechanism since, with increasing cloud density, r_{min} increases more rapidly with time (fig. 5), a correlation that would be enhanced if photodestruction of mantles is important. Thus, for a given cloud age, the probability that smaller grains, which produce the more highly excited molecules, are ineffective H_2 formation sites increases as cloud column and volume density increase. It should be noted that F (30 Å) is only ~ 0.001 for the grain size distribution used in this paper. Unless the size distribution in low density regions is much more heavily weighted with very small (radius $\lesssim$ 30 Å) grains, the agreement between the consequences of the H_2 production model of this paper and the Copernicus observations is merely qualitative. Other phenomena have to be invoked to explain the actual observations (Spitzer and Zweibel 1974; Joshi and Tarafdar 1975).

The ratio of total to selective extinction $\mathcal{R}_V$ ($= A_V/E_{B-V}$) increases as the mean grain size increases (Spitzer 1968). Figures 3 and 4 show that as the cloud ages, grain mantles accumulate, on

the larger grains, in particular. $\mathcal{R}_V$ will increase as a result. At the same time, R is decreasing due to a loss of effective reactive cross-sectional surface area, thus suggesting an inverse relationship between these two parameters. A variation in the nature of the initial grain size distribution-specifically, a change in F(r)-would also result in the suggested inverse relationship of $\mathcal{R}_V$ and R. An observational program to measure both $\mathcal{R}_V$ and R for a range of cloud types would be an important test of the proposed grain ejection mechanism.

Through the process of gas-phase collisional deexcitation of highly energetic nascent H_2, the heat of formation of H_2 may contribute to the heating of the gas. It has been suggested that as much as 50% of the bond energy released may be transferred to the gas (Spitzer and Cochran 1973; Glassgold and Langer 1974b; Barlow and Silk 1975). Such a large fraction of the energy might be available under the HS or Barlow and Silk ejection schemes. However, in the mechanism proposed in this paper, the nascent molecule is in thermal equilibrium with the substrate grain, so it leaves with only a small fraction of the bond energy released (number of grain degrees of freedom $\gg$ number of molecule degrees of freedom). Moreover, since the hot lifetime of the grain is $\sim 10^2$ s (fig. 2 in Paper I), which is usually much less than the grain-gas collision timescale, the grain will release the energy acquired as infrared radiation when a molecule is formed. Therefore, the H_2 heat of formation is a negligible cloud heat source in the context of the present ejection mechanism.

b) Dark Cloud Chemical Evolution

Equilibrium calculations of the state of hydrogen in dense clouds predict that $f_H \sim 1\text{-}5 \times 10^{-2}$ (de Jong 1972) or $\sim 10^{-4}$ - 10^{-5} (Barlow and Silk 1975), these numbers being a function of ζ_H. On the other hand, the dust cloud observations of Knapp (1974a) found values of f_H from 0 to 10^{-1}. This discrepancy between theory and observations seems to be resolved by the time-dependent treatment proposed in this paper. The calculations indicate that after a million years of cloud development $f_H \gtrsim 0.1$, even in the absence of dissociative radiation. Moreover, except at high densities ($[H + 2H_2] \gtrsim 10^4$ cm^{-3}) and/or high internal cloud radiation field ($\zeta_H \gtrsim 10^{-18}$s^{-1}), chemical equilibrium is not achieved in the course of a typical cloud lifetime of $\sim 10^7$ years [the limit being set by the estimated timescale for cloud-cloud collisions (Spitzer 1968)]. In this model, equilibrium results when all the grains are coated with a sufficient amount of H_2 to inhibit any surface recombination, and in essence the reaction is frozen out. At high densities, even before all the grains are coated, a critical $[H_2]/[H]$ ratio is reached which allows the small rate of radiative destruction of H_2 to balance the rate of H_2 formation. The equilibrium values of f_H are $\lesssim 10^{-4}$, in agreement with Barlow and Silk (1975), but this never really occurs in the average lifetime of a cloud.

That the observed range of f_H can be explained by realistic cloud models which do not incorporate radiative H_2 destruction is a significant result (Shu 1973 also offers a nonradiative explanation). Indeed, measurements of H I absorption in the direction of Kh3

(Knapp 1974b; Myers 1975) seem to show that the atomic hydrogen is well mixed with the dust and recent 21-cm aperture synthesis maps of dark clouds (Chu 1975) do not show "limb brightening." These observations conflict with the predictions of theories incorporating H_2 destruction processes initiated by radiation incident upon the cloud as significant contributors to the HI abundance.

To test the detailed temporal results of the model calculations of this paper, the 21-cm dark cloud observations of Knapp (1974a) are plotted versus cloud density in figure 6 and compared with the temporal predictions of the model. The column density N_{H+2H_2} for each cloud was calculated using the general interstellar value for N_H/A_V of $\sim 1.7 \times 10^{21}$ cm^{-2} mag^{-1} (Knapp 1974a). The total gas volume density $[H + 2H_2]$ was derived using the distances reported in Knapp (1974a) and the angular areas estimated by Lynds (1962), and adopting a spherical geometry for the cloud. Thus only clouds observed by Knapp for which all of these parameters are known are used. The input and calculated parameters of the chosen clouds are also reported in table 1. Also, those clouds are marked in which more than 20% of the observed HI column density might be due to the external ultraviolet radiation field (see §IIIb). It is noteworthy that all but two of the points fall within the boundaries set by the 1×10^6 and 1×10^7 year curves. In fact, the two errant points are for clouds whose angular extents in the sky are so large that the diameter-estimating technique employed may be invalid. In actuality the densities are most likely at least 10-15 times greater, bringing the points into good agreement with the rest of the data.

Fig. 6.- Fractional atomic hydrogen abundance f_H as a function of cloud gas density $[H + 2H_2]$ and cloud age. Theoretical points [derived from model runs in which $k_{diss}(H_2) = 0$] are marked with crosses and the lines are hand fits connecting the data for a given cloud age: (a) 1×10^6 years, (b) 3×10^6 years, (c) 6×10^6 years, and (d) 1×10^7 years. The clouds listed in table 1 are marked with solid dots. Dots grouped together by a dashed line represent clouds which appear to exist in the same part of the galaxy.

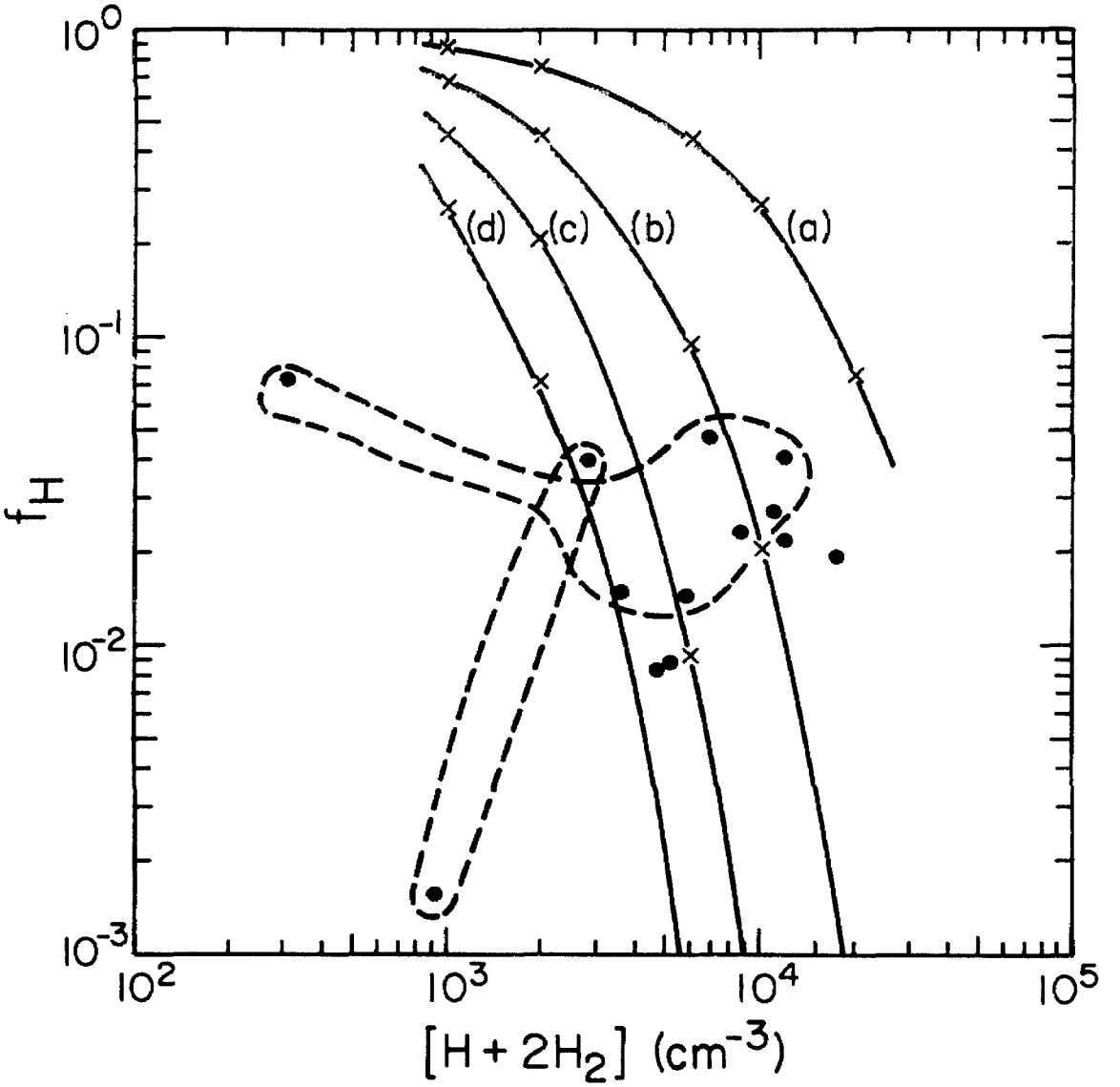
10^0
10^{-1}
10^{-2}
10^{-3}
f_H
(d)
(c)
(b)
(a)
10^2
10^3
10^4
10^5
$[H + 2H_2]$ (cm^{-3})

TABLE 1

DARK CLOUD PARAMETERS

Cloud	Distance* (pc)	Size† (degree^2)	Diameter (pc)	A_V‡ (mag)	N_H* (10^{20}cm^{-2})	$[H + 2H_2]$§ (cm^{-3})	f_H‖
L7	250	0.036	0.933	8	1.14	4.72×10^3	8.38×10^{-3}
L466	400	0.012	0.861	8	1.18	5.12×10^3	8.68×10^{-3}
L1379	250	0.002	0.221	7	2.33	1.75×10^4	1.96×10^{-2}
L1521	75	4.100	2.991	5	0.13#	9.21×10^2	1.53×10^{-3}
L1534	75	0.870	1.377	7	4.66	2.80×10^3	3.92×10^{-2}
L1552	200	0.009	0.372	8	3.00	1.18×10^4	2.21×10^{-2}
L1686	200	0.016	0.498	8	3.16	8.84×10^3	2.32×10^{-2}
L1687	200	3.170	7.012	4	4.83#	3.14×10^2	7.10×10^{-2}
L1690	200	0.020	0.557	7	5.66	6.93×10^3	4.76×10^{-2}
L1692	200	0.007	0.330	7	4.82	1.17×10^4	4.05×10^{-2}
L1696	200	0.036	0.747	8	1.94	5.90×10^3	1.43×10^{-2}

L1704	200	0.010	0.394	8	3.75	1.12×10^{4}	2.76×10^{-2}
L1709	200	0.099	1.239	8	2.01	3.56×10^{3}	1.48×10^{-2}

*Knapp 1974.

†Lynds 1962.

‡Modified values of Lynds's estimates used by Knapp.

§$[H + 2H_2] = 1.7 \times 10^{21} A_V$/cloud diameter.

‖$f_H = N_H/1.7 \times 10^{21} A_V$.

#More than 20% of the observed H I column density might be due to ultraviolet photodissociation (Hollenbach, Werner, and Salpeter 1971).

If clouds are formed in a cataclysmic process, it is probable that several clouds of varying density may form at the same time in the same general direction and estimated to be at about the same distance should lie along a single temporal curve. The only large cluster of spatially neighboring clouds in the sample plotted do not behave in this manner; instead they fall into two basic age groups. This deviation from predictions may be due to a deficiency in the model or to inaccuracies in the various observations needed to define the cloud parameters or may actually reveal a real variation in cloud ages in this part of the galaxy. The other spatially close grouping of two clouds does follow the predicted pattern if the density of the larger cloud is scaled upward by a factor of ~ 10 (as previously discussed).

The dating of the solid curves is very sensitive to the exact value of R. An increase in R will decrease the cloud age for a given f_H vs $[H + 2H_2]$ curve. However, the cloud age limits derived from the calculations are consistent with previous suggestions for cloud ages. An upper limit on cloud age of $\sim 10^7$ years is set by the cloud-cloud collision timescale (Spitzer 1968) or by the timescale for gravitational collapse (Shu 1973). From considerations of mantle growth through heavy element depletion, as revealed by an observed increase in the value of $\mathcal{R}_V$ in the higher density regions of the ρ Oph cloud, Carrasco, Strom, and Strom (1973) suggest a lower limit to the cloud age at $\sim 7 \times 10^5$ years. From a relationship between N_H and dust density derived from observations of ρ Oph and with a simple H_2 formation rate expression, Mészáros (1968) derived a cloud age

of $\sim 3 \times 10^6$ years. The regions L1692 and L1696 are the same clouds observed by Mészáros, and their calculated ages in this model are $\sim 2 \times 10^6$ and 6×10^6 years, respectively. The good consistency of results obtained from different sets of observations suggests that observed relative abundances of chemical species may be useful in the future for cloud dating and, in turn, variation of relative abundances from region to region might be able to be rationalized in terms of varying chemical age.

Figures 3 and 4 show that in the denser clouds most of the heavy atoms CNO have collided with the grains after a few million years. Paper I suggests that CNO colliding with small grains are probably converted into molecules that are returned to the gas phase; CNO colliding with large grains are incorporated into icy mantles. Such a process would result (Paper I) in the development of a bimodal grain size distribution, which has been suggested to explain the interstellar extinction curve (Greenberg and Hong 1973). If the bare-grain size distribution actually produces the observed interstellar extinction, the growth of icy mantles on the larger grains causes an increase in $\mathcal{R}_V$ and the dust-to-gas mass ratio approaches more closely the accepted value (§ IIIa). Indeed, Carrasco, Strom, and Strom (1973) report an observed increase in $\mathcal{R}_V$ in the denser parts of ρ Oph. They conclude that this is due to heavy element depletion. If most of the heavy elements are already depleted onto the grains in the more diffuse interstellar medium, this increase in $\mathcal{R}_V$ could only be accounted for by some more esoteric grain growth process, for example, grain agglomeration (Lefévre 1974). The

fact that Carrasco, Strom, and Strom find an increase in $\mathcal{R}_V$ only in the denser regions is consistent with the calculated degree of CNO depletion as a function of cloud density for cloud ages in the 10^6 year range, giving additional support to the validity of the ages derived from the model.

In the later cloud stages when heavy molecule formation becomes appreciable, $f_H(t) \ll f_{CNO}(t)$ resulting in the increase of the formation rate of non-hydrogen-containing molecules relative to the formation rate of hydrogen-containing molecules. Another consequence of this model is that molecular hydrogen composes a significant fraction of grain mantles (a partial return to some earlier speculation, for example, Solomon and Wickramasinghe 1969). A thin, pure H_2 mantle will grow rapidly on grain cores. Due to the enhanced binding interaction between heavy molecules and H_2, the later accretion of ices will enable more H_2 to stick. Since the residence time for CNO on solid H_2 is much greater than the residence time for H or H_2 on solid H_2, the formation of molecules containing hydrogen are rather specifically inhibited on H_2-dominated grain mantles. These relative abundance and mantle effects may also contribute to the observed anomalous CO/OH column density ratio (see § IV of Paper I).

V. CONCLUSIONS

In this paper, a simplified H_2 formation mechanism is suggested, which relies on the existence of small interstellar grains as the reaction sites. A silicate grain distribution is presented that has a significant fraction of the surface area contributed by small grains. For dark clouds with a kinetic temperature of 10°K, the value of the H_2 formation rate constant R calculated with this distribution is $\lesssim 2 \times 10^{-18}$, consistent with values derived from ultraviolet observations of hotter regions. The observation of rotationally excited H_2, the increase in line widths with increase in rotational excitation, and the increase in excitation with decrease in column density agrees qualitatively with the proposed ejection scheme. Contrary to other formation theories, hydrogen recombination is a negligible cloud heat source if the proposed ejection mechanism is correct.

A time-dependent, non-equilibrium model of dark cloud chemistry is proposed and is shown to be consistent with many astronomical observations. In particular, the observed variation in f_H in dense clouds can be interpreted in terms of cloud age and density. For densities calculated from observed cloud parameters, the derived cloud ages are between 10^6 and 10^7 years, a range covering previous estimates of dark cloud ages. Thus the interrelationship of the chemical abundance ratio of different species and cloud age is strongly suggested. Among other results, the observed increase in

R_V in the denser regions of ρ Oph is shown to agree with the proposed evolution of a bare grain distribution into a bimodal distribution as the cloud ages.

We thank D. Huffman, M. Jura, G. Knapp, N. Scoville, F. Shu, J. Silk, W. Weinberg, and M. Werner for their very helpful assistance during the development of this paper and the referee for his constructive criticism of the originally submitted manuscript. This work was supported by a National Science Foundation grant (MPS73-05140). In addition, M. A. was partially supported by a California State Graduate Fellowship.

REFERENCES

Aannestad, P. A. 1973, Ap. J. Suppl., 25, 223.

Aannestad, P. A., and Purcell, E. M. 1973, Ann. Rev. Astr. and Ap., 11, 309.

Allen, M., and Robinson, G. W. 1975, Ap. J., 195, 81 (Paper I; also Chapter 1 of this thesis).

Augason, G. C. 1970, Ap. J., 162, 463.

Barlow, M. J., and Silk, J. 1975, preprint.

Brown, R. L. 1973, Ap. J., 184, 693.

Cameron, A. G. W. 1973, Space Sci. Rev., 15, 121.

Carrasco, L., Strom, S. E., and Strom, K. M. 1973, Ap. J., 182, 95.

Chu, K. W. 1975, unpublished Ph.D. thesis, California Institute of Technology, Pasadena.

Dalgarno, A., and McCray, R. A. 1972, Ann. Rev. Astr. and Ap., 10, 375.

Day, K. L., Steyer, T. R., and Huffman, D. R. 1974, Ap. J., 191, 415.

de Jong, T. 1972, Astr. and Ap., 20, 263.

Evans, N. J., Zuckerman, B., Morris, G., and Sato, T. 1975, Ap. J., 196, 433.

Field, G. B., Goldsmith, D. W., and Habing, H. J. 1969, Ap. J. (Letters), 155, L149.

Field, G. B., Somerville, W. B., and Dressler, K. 1966, Ann. Rev. Astr. and Ap., 4, 207.

Gillett, F. C., Jones, T. W., Merrill, K. M., and Stein, W. A. 1975, Bull. AAS, 7, 428.

Gilmore, W., Brown, R. L., and Zuckerman, B. 1975, Bull. AAS, 7, 260.

Glassgold, A. E., and Langer, W. D. 1973a, Ap. J. (Letters), 179, L147.

_____. 1973b, Ap. J., 186, 859.

_____. 1976, Ap. J., 204, 403.

Goldsmith, D. W. 1970, Ap. J., 161, 41.

Greenberg, J. M. 1974, Ap. J. (Letters), 189, L81.

Greenberg, J. M., and Hong, S. S. 1974 in IAU Symposium, No. 60, Galactic Radio Astronomy, ed. F. J. Kerr and S. C. Simonson (Dordrecht: D. Reidel), p. 155.

Heiles, C. 1971, Ann. Rev. Astr. and Ap., 9, 293.

Herzberg, G. 1950, Molecular Spectra and Molecular Structure. I. Spectra of Diatomic Molecules (2d ed; New York: Van Nostrand Reinhold).

Hobson, J. P. 1967, in The Solid-Gas Interface, Vol. 1, ed. E. A. Flood (New York: Marcel Dekker), p. 447.

Hollenbach, D., and Salpeter, E. E. 1971, Ap. J., 163, 155 (HS).

Hollenbach, D., Werner, M. W., and Salpeter, E. E. 1971, Ap. J., 163, 165.

Huffman, D. R. and Stapp, J. L. 1971, Nature Phys. Sci., 229, 45.

Jenkins, E. B. and Savage, B. D. 1974, Ap. J., 187, 243.

Joshi, P., and Tarafdar, S. P. 1975, Ap. and Space Sci., 36, 281.

Jura, M. 1975a, Ap. J., 197, 575.

_____. 1975b, Ap. J., 197, 581.

Kamijo, F., and de Jong, T. 1973, Astr. and Ap., 25, 371.

Knapp, G. R. 1974a, A. J., 79, 527.

_____. 1974b, A. J., 79, 541.

Larson, R. B. 1973, Fund. Cosmic Phys., 1, 1.

Lee, T. J. 1972, Nature Phys. Sci., 237, 99.

Lefévre, J. 1974, Astr. and Ap., 37, 17.

Lynds, B. T. 1962, Ap. J. Suppl., 7, 1.

Martin, P. G., and Angel, J. R. P. 1974, Ap. J., 193, 343.

Mészáros, P. 1968, Ap. and Space Sci., 2, 510.

_____. 1972, Ap. J., 177, 79.

Mufson, S. L. 1974, Ap. J., 193, 561.

Myers, P. C. 1975, Ap. J., 198, 331.

Nakano, T., and Tademaru, E. 1973, Ap. J., 173, 87.

O'Donnell, E. J., and Watson, W. D. 1974, Ap. J., 191, 89.

Reddish, V. C. 1975, M.N.R.A.S., 170, 261.

Schwarz, J., McCray, R., and Stein, R. F. 1972, Ap. J., 175, 673.

Scoville, N. Z. 1972, unpublished Ph.D. thesis, Columbia University, New York.

Shu, F. H. 1973, in IAU Symposium, No. 52, Interstellar Dust and Related Topics, ed. J. M. Greenberg and H.D. van de Hulst (Dordrecht: Reidel), p. 257.

Shu, F. H., Milione, V., Gebel, W., Yuan, C., Goldsmith, D. W., and Roberts, W. W. 1972, Ap. J., 173, 557.

Solomon, P. M., and Werner, M. W. 1971, Ap. J., 165, 41.

Solomon, P. M., and Wickramasinghe, N. C. 1969, Ap. J., 158, 449.

Spitzer, L. 1968, Diffuse Matter in Space (New York: Interscience).

Spitzer, L., and Cochran, W. D. 1973, Ap. J. (Letters), 186, L23.

Spitzer, L., Cochran, W. D., and Hirshfeld, A. 1974, Ap. J. Suppl., 28, 373.

Spitzer, L., Drake, J. F., Jenkins, E. B., Morton, D. C., Rogerson, J. B., and York, D. G. 1973, Ap. J. (Letters), 181, L116.

Spitzer, L., and Jenkins, E. 1975, Ann. Rev. Astr. and Ap., 13, 133.

Spitzer, L., and Zweibel, E. G. 1974, Ap. J. (Letters), 191, L127.

Strom, K. M., Strom, S. E., Carrasco, L., and Vrba, F. J. 1975, Ap. J., 196, 489.

Turner, B. E. 1974, in Galactic and Extra-Galactic Radio Astronomy, ed. G. L. Verschuur and K. I. Kellerman (New York: Springer-Verlag), p. 199.

Watson, W. D., and Salpeter, E. E. 1972, Ap. J., 174, 321.

Weast, R. C., ed. 1968, Handbook of Chemistry and Physics (49th ed.; Cleveland: Chemical Rubber Co.), p. F-158.

Zuckerman, B. 1973, Ap. J., 183, 863.

Zuckerman, B., and Palmer, P. 1974, Ann. Rev. Astr. and Ap., 12, 279.

Chapter 3

THE MOLECULAR COMPOSITION OF DENSE INTERSTELLAR CLOUDS

MARK ALLEN
Arthur Amos Noyes Laboratory of Chemical Physics,
California Institute of Technology

G. WILSE ROBINSON
Department of Physical Chemistry, University of Melbourne
and Arthur Amos Noyes Laboratory of Chemical Physics,
California Institute of Technology

I. INTRODUCTION

The discovery of complex interstellar molecules was a great surprise to the general astronomical community (Metz 1973). By now, however, over forty different chemical species have been detected in interstellar clouds, but there is still no all-encompassing theory which explains their abundances reasonably well. The various proposals for gas-phase and grain surface molecular synthesis have been reviewed recently by Turner (1974a, b), Winnewisser, Mezger, and Breuer (1974), Brown (1974), and Watson (1975).

The most extensively developed gas-phase model involves ion-molecule reactions (Herbst and Klemperer 1973). Unfortunately, molecules with more than five atoms are not included in these calculations. The applicability of this model to chemical synthesis in dense isolated dark clouds is uncertain because of their extremely low ionization level (Allen and Robinson 1976, hereinafter referred to as Paper II). Moreover, observations of certain simple molecules [HDCO versus H_2CO (Watson, Crutcher, and Dickel 1975); HCN versus HCO^+ (Turner and Thaddeus 1976)] throw doubt on the importance of such processes in the formation of even some of the simpler molecules.

Grain surfaces are used as the reaction sites for interstellar molecule synthesis by Watson and Salpeter (1972 a, b). These authors predict the abundances of a number of complex molecules. Since in their model molecule desorption from grains is photoinduced, their results are applicable only to regions of, at most, intermediate visual extinction. Recently Iguchi (1975) has presented a detailed surface

formation model involving reactions between semi-chemisorbed species. However, only for high grain temperatures ($\sim$40-50°K) are observations close to being consistent with his predictions.

As can be seen, current molecular synthesis models may not be appropriate for cold dense dark clouds isolated from intense sources of radiation. Ironically, the restricted nature of the physical conditions of dark clouds seems to make these clouds the simplest interstellar chemical systems and most amenable to theoretical modeling. In an attempt to understand these systems, a new mechanism for molecule formation on the surfaces of cold grains has been developed (Allen and Robinson 1975, hereinafter referred to as Paper I). In this picture, energy released upon the formation of a chemical bond heats the grain substrate, resulting in small grains becoming sufficiently hot to release the nascent molecule and other adsorbed volatiles. This process is really just a simple extension of Watson and Salpeter's considerations of molecule ejection during the formation process. For, if the molecules do not desorb from the grains after a few "hops" over the surface, the liberated chemical energy must go somewhere, the grain phonon modes being the most obvious energy sink.

Applying the hot grain ejection mechanism to the formation of molecular hydrogen, Paper II models a physically-static, chemically-dynamic dark cloud and finds that a cloud does not reach steady-state in an average lifetime ($\sim 10^7$ years). This result casts doubt on the facile assumptions that underpin the previously presented steady-state models. [Aannestad (1973 a, b) does present a time-dependent model for

reactions in a quiescent low density cloud and in a cloud in the aftermath of a shock wave.]

The surface formation mechanism of Paper I and the chemically-dynamic cloud model of Paper II are expanded in this paper to explain the presence of complex interstellar chemical species (the largest molecule contains 11 atoms). This is an ab initio model in the sense that the only astronomical inputs are the physical conditions, the cosmic abundances of the elements, and the grain composition and size distribution. In no way is this model presented as the complete picture. The observation of interstellar molecular ions proves conclusively that ion-molecule reactions are occurring. However gas-phase and surface reactions are probably strongly coupled since the timescale for molecule formation via ion-molecule reactions or surface recombination is approximately the same, $\lesssim$ few $\times$ 10^6 years [cf. Paper II and Langer and Glassgold (1976); the assumption that all the hydrogen initially is in the form of H_2 and all the carbon in CO led Herbst and Klemperer (1973) to underestimate the time to achieve steady-state]. By considering a pure surface reaction model, the authors hope that the importance of such chemistry will be clearly demonstrated and that its special features compared to gas-phase reactions will be most easily apparent.

II. INTERSTELLAR SURFACE CHEMISTRY

The reaction model proposed in this paper for the synthesis of complex molecules on interstellar grains is a simple generalization of the H_2 formation process detailed in Paper II. The discussion will be divided into three parts: (a) choice of chemical species, reaction set and related parameters, (b) reaction efficiency, and (c) the detailed formation rate expressions.

a) Choice of Chemical Species, Reaction Set, and Related Parameters

Because they are the simplest of interstellar chemical systems, the reaction model will be focussed on explaining the chemistry of dark clouds, although it will be generally applicable to other interstellar regions. Dark cloud conditions of low radiation energy and intensity and low temperatures (grain temperature T_{gr} and gas kinetic temperature T_k both about 10°K) place severe constraints on the nature of possible chemical reactions. Besides the fact that only spontaneous reactions (ΔG, the change in free energy during the reaction, is negative) can be considered, an effective reaction cannot have an activation energy (kT is only $\sim 10^{-2}$ kcal mole^{-1}), i.e., there can be no energy barrier over which the reaction must proceed. Therefore endothermic reactions (ΔH, the change in heat content during the reaction, is positive) must be excluded. In addition, many exothermic reactions have activation energies and those particular reactions also cannot be expected to provide active chemical pathways.

Ion-molecule reactions generally have negligible activation energies (Herbst and Klemperer 1973). These will not be considered in this paper because of uncertainties about ion-surface interactions and the degree of ionization in dark clouds (Paper II). Reactions between neutral species generally have significant activation energies because the reactions usually require at least partial chemical bond disruption in order to proceed. However, in the special case of recombination reactions involving free radicals (species with unpaired electrons), the experimentally measured activation energies are generally negligible (Kerr 1973). For the purposes of the present model, non-free radicals are therefore chemically inert.

The basic reaction to be considered is a three-body recombination,

$$A + B + M \rightarrow AB + M \qquad (1)$$

where M catalyzes the reaction by absorbing an appreciable amount of the released energy. The third body is necessary since only in the case of a large (> 10 atoms) activated complex AB* may there be a sufficient number of vibrational modes to stabilize the complex long enough to make radiative association an efficient reaction pathway (Millar and Williams 1975). Besides having no activation energy when A and B are radicals, gas-phase three-body free radical recombination reaction rate constants often increase exponentially with decreasing temperature (Reiter, Bauer, and Coroniti 1975). In the context of this paper, the third body M will be a grain on which A and B have previously adsorbed. (Gas-phase three-body collisions are extraordinarily unlikely under

dark cloud conditions.)

Contrary to the statement made earlier in this paper about neutral-neutral reactions, there may be a small subset of radical-radical exchange reactions having negligible activation energies, namely

$$A + O_2 \rightarrow AO + O \qquad (2)$$

whenever $\Delta H \ll 0$ (W. A. Goddard III, private communication). These reactions will also be included as surface processes.

Although solid-state materials are used in industry to catalyze reactions by furnishing new kinetic pathways with lower activation energies, it should be noted that the grains are not viewed here in this manner. Instead, a more conservative approach is being taken--in the case of free radicals physically adsorbed to a grain, it is assumed that a reaction that has no activation energy in the gas phase probably will not have an activation energy on a grain surface. The grains merely serve as third bodies to bring the reactive species together and help relax the activated complex, thus allowing the reaction to proceed to conclusion.

With these ideas in mind, we tried to identify the most important reactions (i.e., those involving the generally most abundant species produced in preliminary calculations). In all, 598 reactions were chosen and are listed in table 1 with their exoergicities (E_{bond}). (Reactions are listed in order of number of constituent atoms, and then mass, of reactant 1 and, when necessary, a similar ordering for reactant 2). The choice of most of the reactions was based on simple

TABLE I
FREE RADICAL REACTIONS

$H + H \rightarrow H_2 + 104.2$
$H + C \rightarrow CH + 81.0$
$H + N \rightarrow NH + 84.1$
$H + O \rightarrow OH + 102.3$
$H + CH \rightarrow CH_2 + 102.0$
$H + NH \rightarrow NH_2 + 93.0$
$H + OH \rightarrow H_2O + 119.3$
$H + C_2 \rightarrow C_2H + 138.3$
$H + CN \rightarrow HCN + 123.8$
$H + NO \rightarrow HNO + 49.9$
$H + O_2 \rightarrow HO_2 + 56.5$
$H + CH_2 \rightarrow CH_3 + 109.4$
$H + NH_2 \rightarrow NH_3 + 103.2$
$H + C_2H \rightarrow C_2H_2 + 111.9$
$H + N_2H \rightarrow N_2H_2 + 91.2$
$H + COH \rightarrow CHOH + 100.0$
$H + HCO \rightarrow H_2CO + 76.9$
$H + NOH \rightarrow NHOH + 90.0$
$H + HO_2 \rightarrow H_2O_2 + 89.6$
$H + CCN \rightarrow CHCN + 100.0$
$H + NCN \rightarrow NHCN + 90.0$
$H + CCO \rightarrow HCCO + 110.0$
$H + NCO \rightarrow HNCO + 118.1$
$H + CNO \rightarrow HCNO + 100.0$
$H + NOO \rightarrow NOOH + 70.0$
$H + NO_2 \rightarrow HNO_2 + 78.6$
$H + CH_3 \rightarrow CH_4 + 104.8$
$H + CH_2C \rightarrow CH_2CH + 106.0$
$H + NH_2C \rightarrow NH_2CH + 100.0$
$H + CH_2N \rightarrow CH_2NH + 90.0$
$H + CHNH \rightarrow CH_2NH + 105.0$
$H + NH_2N \rightarrow NH_2NH + 90.0$
$H + CHOH \rightarrow CH_2OH + 100.0$
$H + NH_2O \rightarrow NH_2OH + 100.0$
$H + NHOH \rightarrow NH_2OH + 90.0$
$H + C_3H \rightarrow CHC_2H + 100.0$
$H + NHC_2 \rightarrow NH_2C_2 + 90.0$
$H + CHCN \rightarrow CH_2CN + 100.0$
$H + NC_2H \rightarrow NHC_2H + 90.0$
$H + CCHO \rightarrow CHCHO + 100.0$
$H + HCCO \rightarrow H_2CCO + 110.0$
$H + NHCN \rightarrow NH_2CN + 90.0$
$H + HC_2O \rightarrow HC_2OH + 100.0$
$H + C_2OH \rightarrow HC_2OH + 110.0$
$H + NCHO \rightarrow NHCHO + 90.0$
$H + N_2OH \rightarrow HN_2OH + 90.0$
$H + OCHO \rightarrow HCO_2H + 100.0$
$H + CO_2H \rightarrow HCO_2H + 90.0$
$H + COOH \rightarrow HCOOH + 100.0$
$H + NHNO \rightarrow NH_2NO + 90.0$
$H + NHOO \rightarrow NH_2OO + 90.0$
$H + NOOH \rightarrow NHOOH + 90.0$
$H + HO_3 \rightarrow H_2O_3 + 90.0$
$H + CCCO \rightarrow HCCCO + 100.0$
$H + NCCO \rightarrow HNCCO + 115.0$
$H + C_2NO \rightarrow HC_2NO + 105.0$
$H + CNO_2 \rightarrow CHNO_2 + 100.0$
$H + OOCN \rightarrow HOOCN + 100.0$
$H + NNO_2 \rightarrow NHNO_2 + 90.0$
$H + OONO \rightarrow HOONO + 100.0$
$H + NO_3 \rightarrow HNO_3 + 100.0$
$H + CH_3C \rightarrow CH_3CH + 100.0$
$H + CH_2CH \rightarrow CH_2CH_2 + 104.0$
$H + CHNH_2 \rightarrow CH_2NH_2 + 100.0$
$H + CH_2N \rightarrow CH_3NH + 90.0$
$H + NH_2NH \rightarrow N_2H_4 + 76.0$
$H + CH_3O \rightarrow CH_3OH + 102.0$
$H + CH_2OH \rightarrow CH_3OH + 92.0$
$H + CH_2C_2 \rightarrow CH_2C_2H + 125.0$
$H + CHC_2H \rightarrow CH_2C_2H + 100.0$
$H + CH_2CC \rightarrow CH_2CCH + 105.0$
$H + CH_2CN \rightarrow CH_3CN + 80.0$
$H + CCHNH \rightarrow CHCHNH + 100.0$
$H + NHC_2H \rightarrow NH_2C_2H + 90.0$
$H + NH_2C_2 \rightarrow NH_2C_2H + 125.0$
$H + CH_2NC \rightarrow CH_2NCH + 100.0$
$H + CCHOH \rightarrow CHCHOH + 105.0$
$H + CHCHO \rightarrow CH_2CHO + 100.0$
$H + NCHNH \rightarrow NHCHNH + 90.0$
$H + CHOHN \rightarrow HOCHNH + 90.0$
$H + CHNOH \rightarrow CH_2NOH + 105.0$
$H + NHCOH \rightarrow HOCHNH + 105.0$
$H + NHCHO \rightarrow NH_2CHO + 90.0$
$H + CNHOH \rightarrow CHNHOH + 100.0$
$H + OCHNH \rightarrow HOCHNH + 100.0$
$H + CH_2NO \rightarrow CH_2NOH + 100.0$
$H + NH_2CO \rightarrow NH_2CHO + 100.0$
$H + CHOOH \rightarrow CH_2OOH + 100.0$
$H + C(OH)_2 \rightarrow CH(OH)_2 + 100.0$
$H + NNHOH \rightarrow NHNHOH + 90.0$
$H + ONHOH \rightarrow NH(OH)_2 + 100.0$
$H + NH_2OO \rightarrow NH_2OOH + 100.0$
$H + NHOOH \rightarrow NH_2OOH + 90.0$
$H + N(OH)_2 \rightarrow NH(OH)_2 + 90.0$
$H + HC_2C_2 \rightarrow (HC_2)_2 + 105.0$
$H + C_2CHO \rightarrow HC_2CHO + 125.0$
$H + HCCCO \rightarrow H_2CCCO + 100.0$
$H + C_2OOH \rightarrow HC_2OOH + 105.0$
$H + HOCCO \rightarrow HOCHCO + 100.0$
$H + HC_2OO \rightarrow HC_2OOH + 100.0$
$H + CCO_2H \rightarrow CHCO_2H + 100.0$
$H + COCHO \rightarrow (HCO)_2 + 100.0$
$H + NCO_2H \rightarrow NHCO_2H + 90.0$
$H + NOCHO \rightarrow NHOCHO + 90.0$
$H + CHNO_2 \rightarrow CH_2NO_2 + 100.0$
$H + NHNO_2 \rightarrow NH_2NO_2 + 90.0$
$H + OOCHO \rightarrow HOOCHO + 100.0$
$H + HCO_3 \rightarrow H_2CO_3 + 110.0$
$H + NOHNO \rightarrow NHOHNO + 90.0$
$H + HO_4 \rightarrow (HO_2)_2 + 100.0$
$H + ONCCO \rightarrow ONCHCO + 100.0$
$H + OONO_2 \rightarrow HOONO_2 + 100.0$
$H + CH_3CH \rightarrow CH_3CH_2 + 100.0$
$H + CH_2NH_2 \rightarrow CH_3NH_2 + 100.0$
$H + CH_2NH \rightarrow CH_3NH_2 + 92.0$
$H + CH_2CCH \rightarrow CH_2CCH_2 + 105.0$
$H + CH_2CHC \rightarrow CH_2CHCH + 100.0$
$H + CH_2C_2H \rightarrow CH_3C_2H + 100.0$
$H + CH_2CHN \rightarrow CH_2CHNH + 90.0$
$H + CH_2NCH \rightarrow CH_2NCH_2 + 100.0$
$H + CCHNH_2 \rightarrow CHCHNH_2 + 105.0$
$H + CHCHNH \rightarrow CH_2CHNH + 100.0$
$H + NHCHNH \rightarrow NH_2CHNH + 90.0$
$H + CH_3OC \rightarrow CH_3OCH + 100.0$
$H + CH_2CH\text{-}O \rightarrow CH_2CHOH + 100.0$
$H + CH_2NNH \rightarrow CH_2NNH_2 + 90.0$
$H + CHCHOH \rightarrow CH_2CHOH + 105.0$
$H + NH_2CNH \rightarrow NH_2CHNH + 100.0$
$H + CCH_2OH \rightarrow CHCH_2OH + 100.0$
$H + CH_2CHO \rightarrow CH_3CHO + 100.0$
$H + CH_2COH \rightarrow CH_2CHOH + 108.0$
$H + CHNOH \rightarrow CH_2NOH + 100.0$
$H + CH_3ON \rightarrow CH_3ONH + 90.0$
$H + NCH_2OH \rightarrow NHCH_2OH + 90.0$
$H + NH_2COH \rightarrow NH_2CHOH + 100.0$
$H + NHNHOH \rightarrow NH_2NHOH + 90.0$
$H + OCH_2OH \rightarrow CH_2(OH)_2 + 100.0$
$H + NH_2NOH \rightarrow NH_2NHOH + 90.0$
$H + CH_2OO \rightarrow CH_3OOH + 100.0$
$H + CH(OH)_2 \rightarrow CH_2(OH)_2 + 100.0$
$H + CH_2OOH \rightarrow CH_3OOH + 100.0$
$H + CCHCHO \rightarrow CHCHCHO + 105.0$
$H + HC_2COH \rightarrow HC_2CHOH + 100.0$
$H + HCOCHN \rightarrow HCOCHNH + 90.0$
$H + HC_2NOH \rightarrow HC_2NHOH + 100.0$
$H + NH_2CCO \rightarrow NH_2CHCO + 100.0$
$H + CH_2CNO \rightarrow CH_2CHNO + 105.0$
$H + HCOCOH \rightarrow HOCHCHO + 100.0$
$H + CHCO_2H \rightarrow CH_2CO_2H + 100.0$
$H + CH_2NO_2 \rightarrow CH_3NO_2 + 100.0$
$H + HCONOH \rightarrow HCONHOH + 90.0$
$H + NHCO_2H \rightarrow NH_2CO_2H + 90.0$
$H + NHOCHO \rightarrow NH_2OCHO + 90.0$
$H + CH_2NOO \rightarrow CH_2NOOH + 100.0$
$H + OOCHNH \rightarrow HOOCHNH + 100.0$
$H + OOOCHO \rightarrow HOOOCHO + 100.0$
$H + HOOCOH \rightarrow HOOCHOH + 100.0$
$H + OONHOH \rightarrow HOONHOH + 90.0$
$H + HOONOH \rightarrow HOONHOH + 100.0$
$H + HC_2CCO \rightarrow HC_2CHCO + 100.0$
$H + HCOCCO \rightarrow HCOCHCO + 100.0$
$H + HOOCCO \rightarrow HOOCHCO + 100.0$
$H + OOCO_2H \rightarrow HOOCO_2H + 100.0$
$H + CH_3CH_2 \rightarrow CH_3CH_3 + 98.0$
$H + CH_2CHCH \rightarrow CH_2CHCH_2 + 100.0$
$H + CH_3CHC \rightarrow CH_3CHCH + 105.0$
$H + CH_2CHNH \rightarrow CH_2CHNH_2 + 90.0$
$H + CHCHNH_2 \rightarrow CH_2CHNH_2 + 105.0$
$H + CH_2NCH_2 \rightarrow CH_2NCH_3 + 100.0$
$H + CH_3CHN \rightarrow CH_3CHNH + 90.0$
$H + CH_2CNH_2 \rightarrow CH_2CHNH_2 + 105.0$
$H + CH_3COH \rightarrow CH_3CHOH + 100.0$
$H + CH_3OCH \rightarrow CH_3OCH_2 + 100.0$
$H + C(NH_2)_2 \rightarrow CH(NH_2)_2 + 100.0$
$H + CHCH_2OH \rightarrow CH_2CH_2OH + 100.0$
$H + NHCH_2OH \rightarrow NH_2CH_2OH + 90.0$
$H + NH_2CHOH \rightarrow NH_2CH_2OH + 100.0$
$H + CH_2NHOH \rightarrow CH_3NHOH + 100.0$
$H + CH_3NOH \rightarrow CH_3NHOH + 90.0$
$H + CH_3ONH \rightarrow CH_3ONH_2 + 90.0$
$H + CH_2CHC_2 \rightarrow CH_2CHC_2H + 105.0$
$H + CH_2CC_2H \rightarrow CH_2CHC_2H + 105.0$
$H + HC_2CNH_2 \rightarrow HC_2CHNH_2 + 100.0$
$H + HC_2CHOH \rightarrow HC_2CH_2OH + 100.0$
$H + CH_2CCHO \rightarrow CH_2CHCHO + 105.0$
$H + CHCHCHO \rightarrow CH_2CHCHO + 105.0$
$H + CH_3CCO \rightarrow CH_3CHCO + 100.0$
$H + NH_2CCHO \rightarrow NH_2CHCHO + 100.0$
$H + CH_2CHOO \rightarrow CH_2CHOOH + 100.0$
$H + CH_2COOH \rightarrow CH_2CHOOH + 105.0$
$H + CH_2CO_2H \rightarrow CH_3CO_2H + 100.0$
$H + HOCHCHO \rightarrow HOCH_2CHO + 100.0$
$H + NH_2COOH \rightarrow NH_2CHOOH + 100.0$
$H + CH_3OOO \rightarrow CH_3OOOH + 100.0$
$H + HOOCHOH \rightarrow HOOCH_2OH + 100.0$
$H + OOCH_2OH \rightarrow HOOCH_2OH + 100.0$
$H + ONCHCHO \rightarrow ONCH_2CHO + 100.0$
$H + CH_3CHCH \rightarrow CH_2CHCH_3 + 105.0$
$H + CH_2CHCH_2 \rightarrow CH_2CHCH_3 + 85.0$
$H + CH_2CCH_3 \rightarrow CH_2CHCH_3 + 105.0$
$H + CH_3CNH_2 \rightarrow CH_3CHNH_2 + 100.0$
$H + CH_2CHOH \rightarrow CH_3CH_2OH + 100.0$
$H + CH(NH_2)_2 \rightarrow CH_2(NH_2)_2 + 100.0$
$H + CH_3OCH_2 \rightarrow CH_3OCH_3 + 100.0$
$H + CH_2CH_2OH \rightarrow CH_3CH_2OH + 100.0$
$H + HC_2CHNH_2 \rightarrow HC_2CH_2NH_2 + 100.0$
$H + CH_2CHCOH \rightarrow CH_2CHCHOH + 100.0$
$H + NH_2CHCHO \rightarrow NH_2CH_2CHO + 100.0$
$H + CH_2CHNO \rightarrow CH_3CH_2NO + 100.0$
$H + NH_2CHOOH \rightarrow NH_2CH_2OOH + 100.0$
$H + HC_2CHCHO \rightarrow HC_2CH_2CHO + 100.0$
$H + CH(CHO)_2 \rightarrow CH_2(HCO)_2 + 100.0$
$H + HOOCHCHO \rightarrow HOOCH_2CHO + 100.0$
$H + CH_3CHNH_2 \rightarrow CH_3CH_2NH_2 + 100.0$
$H + CH_3CHC_2H \rightarrow CH_3CH_2C_2H + 100.0$
$H + CH_2CHCHOH \rightarrow CH_2CHCH_2OH + 100.0$
$H + CH_3CHCHO \rightarrow CH_3CH_2CHO + 100.0$
$H + CH_3CHOOH \rightarrow CH_3CH_2OOH + 100.0$
$H + CH_3CHCH_3 \rightarrow CH_3CH_2CH_3 + 100.0$
$C + C \rightarrow C_2 + 141.6$
$C + N \rightarrow CN + 179.9$
$C + O \rightarrow CO + 256.9$
$C + CH \rightarrow C_2H + 198.9$
$C + NH \rightarrow HNC + 113.0$
$C + OH \rightarrow COH + 80.0$
$C + C_2 \rightarrow C_3 + 175.1$
$C + CN \rightarrow CCN + 149.2$
$C + NO \rightarrow CNO + 100.0$
$C + O_2 \rightarrow CO + O + 135.0$
$C + CH_2 \rightarrow CH_2C + 150.0$
$C + NH_2 \rightarrow NH_2C + 75.0$
$C + C_2H \rightarrow C_3H + 140.0$
$C + COH \rightarrow C_2OH + 140.0$
$C + HCO \rightarrow CCHO + 60.0$
$C + NOH \rightarrow HONC + 140.0$
$C + HO_2 \rightarrow COOH + 85.0$
$C + CCO \rightarrow CCCO + 140.0$
$C + NO_2 \rightarrow CNO_2 + 75.0$
$C + CH_3 \rightarrow CH_3C + 80.0$
$C + CH_2C \rightarrow CH_2CC + 140.0$
$C + NH_2C \rightarrow NH_2C_2 + 190.0$
$C + CH_2N \rightarrow CH_2NC + 70.0$
$C + CHNH \rightarrow CCHNH + 80.0$
$C + CHOH \rightarrow CCHOH + 140.0$
$C + NHOH \rightarrow CNHOH + 70.0$
$C + OCHO \rightarrow COCHO + 85.0$
$C + CO_2H \rightarrow CCO_2H + 80.0$
$C + CH_2CH \rightarrow CH_2CHC + 80.0$
$C + CHNH_2 \rightarrow CCHNH_2 + 140.0$
$C + CH_3O \rightarrow CH_3OC + 85.0$
$C + CH_2OH \rightarrow CCH_2OH + 80.0$
$C + CHCHO \rightarrow CCHCHO + 140.0$
$C + CH_3CH \rightarrow CH_3CHC + 140.0$
$N + N \rightarrow N_2 + 226.0$
$N + O \rightarrow NO + 151.0$
$N + CH \rightarrow HCN + 222.7$
$N + NH \rightarrow N_2H + 122.0$
$N + OH \rightarrow NOH + 80.0$
$N + C_2 \rightarrow CCN + 187.5$
$N + CN \rightarrow NCN + 114.2$
$N + NO \rightarrow N_2O + 115.0$
$N + O_2 \rightarrow NOO + 50.0$
$N + CH_2 \rightarrow CH_2N + 150.0$
$N + NH_2 \rightarrow NH_2N + 40.0$
$N + C_2H \rightarrow NC_2H + 70.0$
$N + COH \rightarrow HOCN + 200.0$
$N + HCO \rightarrow NCHO + 70.0$
$N + NOH \rightarrow N_2OH + 100.0$
$N + HO_2 \rightarrow NOOH + 50.0$
$N + CCO \rightarrow NCCO + 145.0$
$N + NO_2 \rightarrow NNO_2 + 50.0$
$N + CH_3 \rightarrow CH_3N + 70.0$
$N + CH_2C \rightarrow CH_2CN + 145.0$
$N + NH_2C \rightarrow NH_2CN + 210.0$
$N + CH_2N \rightarrow CH_2N_2 + 100.0$
$N + CHNH \rightarrow NCHNH + 70.0$
$N + CHOH \rightarrow CHOHN + 145.0$
$N + NHOH \rightarrow NNHOH + 40.0$
$N + OCHO \rightarrow NOCHO + 50.0$
$N + CO_2H \rightarrow NCO_2H + 70.0$
$N + CH_2CH \rightarrow CH_2CHN + 70.0$
$N + CHNH_2 \rightarrow NH_2CHN + 145.0$
$N + CH_3O \rightarrow CH_3ON + 50.0$
$N + CH_2OH \rightarrow NCH_2OH + 70.0$
$N + CHCHO \rightarrow HCOCHN + 145.0$
$N + CH_3CH \rightarrow CH_3CHN + 145.0$
$O + O \rightarrow O_2 + 119.2$
$O + CH \rightarrow HCO + 204.5$
$O + NH \rightarrow HNO + 116.8$
$O + OH \rightarrow HO_2 + 64.0$
$O + C_2 \rightarrow CCO + 191.3$
$O + CN \rightarrow NCO + 125.5$
$O + NO \rightarrow NO_2 + 73.3$
$O + O_2 \rightarrow O_3 + 25.5$
$O + CH_2 \rightarrow H_2CO + 166.0$
$O + NH_2 \rightarrow NH_2O + 50.0$
$O + C_2H \rightarrow HC_2O + 85.0$
$O + COH \rightarrow CO_2H + 175.0$
$O + HCO \rightarrow OCHO + 85.0$
$O + NOH \rightarrow HNO_2 + 145.0$
$O + HO_2 \rightarrow HO_3 + 41.0$
$O + CCO \rightarrow C_2O_2 + 200.0$
$O + NO_2 \rightarrow NO_3 + 50.0$
$O + CH_3 \rightarrow CH_3O + 85.0$
$O + CH_2C \rightarrow H_2CCO + 170.0$
$O + NH_2C \rightarrow NH_2CO + 170.0$
$O + CH_2N \rightarrow CH_2NO + 50.0$
$O + CHNH \rightarrow OCHNH + 80.0$
$O + CHOH \rightarrow HCO_2H + 170.0$
$O + NHOH \rightarrow ONHOH + 50.0$
$O + OCHO \rightarrow OOCHO + 35.0$
$O + CO_2H \rightarrow HCO_3 + 80.0$

NOTE.- REACTION EXOERGICITIES IN UNITS OF KILOCALORIES MOLE^{-1}.

TABLE I – Continued

$O + CH_2CH \rightarrow CH_2CH\text{-}O + 85.0$
$O + CHNH_2 \rightarrow NH_2CHO + 170.0$
$O + CH_3O \rightarrow CH_3OO + 35.0$
$O + CH_2OH \rightarrow OCH_2OH + 85.0$
$O + CHCHO \rightarrow (HCO)_2 + 170.0$
$O + CH_2CH \rightarrow CH_3CHO + 170.0$
$CH + CH \rightarrow C_2H_2 + 230.0$
$CH + NH \rightarrow CHNH + 140.0$
$CH + OH \rightarrow CHOH + 85.0$
$CH + C_2 \rightarrow C_3H + 100.0$
$CH + CN \rightarrow CHCN + 100.0$
$CH + NO \rightarrow HCNO + 100.0$
$CH + O_2 \rightarrow HCO + O + 85.0$
$CH + CH_2 \rightarrow CH_2CH + 120.0$
$CH + NH_2 \rightarrow CHNH_2 + 80.0$
$CH + C_2H \rightarrow CHC_2H + 100.0$
$CH + COH \rightarrow HC_2OH + 200.0$
$CH + HCO \rightarrow CHCHO + 80.0$
$CH + NOH \rightarrow CHNOH + 140.0$
$CH + HO_2 \rightarrow CHOOH + 50.0$
$CH + CCO \rightarrow HCCCO + 140.0$
$CH + NO_2 \rightarrow CHNO_2 + 80.0$
$CH + CH_3 \rightarrow CH_3CH + 80.0$
$CH + CH_2C \rightarrow CH_2CCH + 140.0$
$CH + NH_2C \rightarrow NH_2C_2H + 200.0$
$CH + CH_2N \rightarrow CH_2NCH + 70.0$
$CH + CHNH \rightarrow CHCHNH + 80.0$
$CH + CHOH \rightarrow CHCHOH + 140.0$
$CH + NHOH \rightarrow CHNHOH + 70.0$
$CH + CO_2H \rightarrow CHCO_2H + 80.0$
$CH + CH_2CH \rightarrow CH_2CHCH + 85.0$
$CH + CHNH_2 \rightarrow CHCHNH_2 + 140.0$
$CH + CH_3O \rightarrow CH_3OCH + 85.0$
$CH + CH_2OH \rightarrow CHCH_2OH + 85.0$
$CH + CHCHO \rightarrow CHCHCHO + 140.0$
$CH + CH_3CH \rightarrow CH_3CHCH + 140.0$
$NH + NH \rightarrow N_2H_2 + 120.0$
$NH + OH \rightarrow NHOH + 50.0$
$NH + C_2 \rightarrow NHC_2 + 90.0$
$NH + CN \rightarrow NHCN + 90.0$
$NH + NO \rightarrow NHNO + 40.0$
$NH + O_2 \rightarrow NHOO + 50.0$
$NH + CH_2 \rightarrow CH_2NH + 154.0$
$NH + NH_2 \rightarrow NH_2NH + 40.0$
$NH + C_2H \rightarrow NHC_2H + 90.0$
$NH + COH \rightarrow NHCOH + 140.0$
$NH + HCO \rightarrow NHCHO + 70.0$
$NH + NOH \rightarrow HN_2OH + 100.0$
$NH + HO_2 \rightarrow NHOOH + 50.0$
$NH + CCO \rightarrow HNCCO + 145.0$
$NH + NO_2 \rightarrow NHNO_2 + 40.0$
$NH + CH_3 \rightarrow CH_3NH + 70.0$
$NH + CH_2C \rightarrow CH_2CNH + 145.0$
$NH + NH_2C \rightarrow NH_2CNH + 145.0$
$NH + CH_2N \rightarrow CH_2NNH + 40.0$
$NH + CHNH \rightarrow NHCHNH + 70.0$
$NH + CHOH \rightarrow NHCHOH + 140.0$
$NH + NHOH \rightarrow NHNHOH + 40.0$
$NH + OCHO \rightarrow NHOCHO + 50.0$
$NH + CO_2H \rightarrow NHCO_2H + 70.0$
$NH + CH_2CH \rightarrow CH_2CHNH + 145.0$
$NH + CH_3CH \rightarrow CH_3CHNH + 145.0$
$OH + OH \rightarrow H_2O_2 + 50.0$
$OH + C_2 \rightarrow C_2OH + 90.0$
$OH + CN \rightarrow HOCN + 90.0$
$OH + NO \rightarrow HNO_2 + 50.0$
$OH + CH_2 \rightarrow CH_2OH + 85.0$
$OH + NH_2 \rightarrow NH_2OH + 50.0$
$OH + C_2H \rightarrow HC_2OH + 90.0$
$OH + COH \rightarrow C(OH)_2 + 85.0$
$OH + HCO \rightarrow HCO_2H + 96.0$
$OH + NOH \rightarrow N(OH)_2 + 50.0$
$OH + HO_2 \rightarrow H_2O_3 + 28.0$
$OH + CCO \rightarrow HOCCO + 85.0$
$OH + NO_2 \rightarrow HNO_3 + 50.0$
$OH + CH_3 \rightarrow CH_3OH + 92.0$
$OH + CH_2C \rightarrow CH_2COH + 85.0$
$OH + NH_2C \rightarrow NH_2COH + 85.0$
$OH + CH_2N \rightarrow CH_2NOH + 50.0$
$OH + CHNH \rightarrow HOCHNH + 85.0$
$OH + CHOH \rightarrow CH(OH)_2 + 85.0$
$OH + NHOH \rightarrow NH(OH)_2 + 50.0$
$OH + OCHO \rightarrow HOOCHO + 35.0$
$OH + CO_2H \rightarrow H_2CO_3 + 85.0$
$OH + CH_2CH \rightarrow CH_2CHOH + 85.0$
$OH + CHNH_2 \rightarrow NH_2CHOH + 85.0$
$OH + CH_3O \rightarrow CH_3OOH + 35.0$
$OH + CH_2OH \rightarrow CH_2(OH)_2 + 85.0$
$OH + CHCHO \rightarrow HOCHCHO + 85.0$
$OH + CH_3CH \rightarrow CH_3CHOH + 85.0$
$NO + C_2 \rightarrow C_2NO + 90.0$
$NO + CN \rightarrow NCNO + 90.0$
$NO + NO \rightarrow (NO)_2 + 40.0$
$NO + C_2H \rightarrow HC_2NO + 90.0$
$NO + COH \rightarrow HOCNO + 100.0$
$NO + NOH \rightarrow NOHNO + 40.0$
$NO + CCO \rightarrow ONCCO + 70.0$
$NO + CH_2C \rightarrow CH_2CNO + 70.0$
$NO + NH_2C \rightarrow NH_2CNO + 100.0$
$NO + CH_2N \rightarrow CH_2NNO + 40.0$
$NO + CHNH \rightarrow ONCHNH + 70.0$
$NO + CHOH \rightarrow CHOHNO + 70.0$
$NO + NHOH \rightarrow NHOHNO + 40.0$
$NO + OCHO \rightarrow HCONO_2 + 50.0$
$NO + CO_2H \rightarrow ONCO_2H + 70.0$
$NO + CH_2CH \rightarrow CH_2CHNO + 70.0$
$NO + CH_3O \rightarrow CH_3NO_2 + 50.0$
$NO + CH_2OH \rightarrow NHCO_2H + 70.0$
$NO + CHCHO \rightarrow ONCHCHO + 70.0$
$NO + CH_3CH \rightarrow CH_3CHNO + 70.0$
$O_2 + C_2 \rightarrow CCO + O + 70.0$
$O_2 + CN \rightarrow OOCN + 85.0$
$O_2 + NO \rightarrow OONO + 50.0$
$O_2 + O_2 \rightarrow O_4 + 35.0$
$O_2 + CH_2 \rightarrow H_2CO + O + 60.0$
$O_2 + NH_2 \rightarrow NH_2OO + 50.0$
$O_2 + C_2H \rightarrow HC_2OO + 85.0$
$O_2 + COH \rightarrow HCO_2 + O + 60.0$
$O_2 + HCO \rightarrow OOCHO + 85.0$
$O_2 + NOH \rightarrow HNO_2 + O + 50.0$
$O_2 + HO_2 \rightarrow HO_4 + 35.0$
$O_2 + CCO \rightarrow C_2O_2 + O + 80.0$
$O_2 + NO_2 \rightarrow OONO_2 + 50.0$
$O_2 + CH_3 \rightarrow CH_3OO + 85.0$
$O_2 + CH_2C \rightarrow H_2CCO + O + 80.0$
$O_2 + NH_2C \rightarrow NH_2CO + O + 80.0$
$O_2 + CH_2N \rightarrow CH_2NOO + 85.0$
$O_2 + CHNH \rightarrow OOCHNH + 85.0$
$O_2 + CHOH \rightarrow HCO_2H + O + 80.0$
$O_2 + NHOH \rightarrow OONHOH + 50.0$
$O_2 + OCHO \rightarrow OOOCHO + 35.0$
$O_2 + CO_2H \rightarrow OOCO_2H + 85.0$
$O_2 + CH_2CH \rightarrow CH_2CHOO + 85.0$
$O_2 + CHNH_2 \rightarrow NH_2CHO + O + 80.0$
$O_2 + CH_3O \rightarrow CH_3OOO + 35.0$
$O_2 + CH_2OH \rightarrow OOCH_2OH + 85.0$
$O_2 + CHCHO \rightarrow (HCO)_2 + O + 80.0$
$O_2 + CH_3CH \rightarrow CH_3CHO + O + 80.0$
$CH_2 + C_2 \rightarrow CH_2C_2 + 90.0$
$CH_2 + CN \rightarrow CH_2CN + 90.0$
$CH_2 + NO \rightarrow CH_2NO + 70.0$
$CH_2 + CH_2 \rightarrow C_2H_4 + 163.0$
$CH_2 + NH_2 \rightarrow CH_2NH_2 + 70.0$
$CH_2 + C_2H \rightarrow CH_2C_2H + 90.0$
$CH_2 + COH \rightarrow CH_2COH + 80.0$
$CH_2 + HCO \rightarrow CH_2CHO + 80.0$
$CH_2 + NOH \rightarrow CH_2NOH + 140.0$
$CH_2 + HO_2 \rightarrow CH_2OOH + 85.0$
$CH_2 + CCO \rightarrow H_2CCCO + 140.0$
$CH_2 + NO_2 \rightarrow CH_2NO_2 + 70.0$
$CH_2 + CH_3 \rightarrow CH_3CH_2 + 96.0$
$CH_2 + CH_2C \rightarrow CH_2CCH_2 + 145.0$
$CH_2 + NH_2C \rightarrow CH_2CNH_2 + 145.0$
$CH_2 + CH_2N \rightarrow CH_2NCH_2 + 70.0$
$CH_2 + CHNH \rightarrow CH_2CHNH + 80.0$
$CH_2 + CHOH \rightarrow CH_2CHOH + 140.0$
$CH_2 + NHOH \rightarrow CH_2NHOH + 70.0$
$CH_2 + OCHO \rightarrow CH_2OCHO + 85.0$
$CH_2 + CO_2H \rightarrow CH_2CO_2H + 80.0$
$CH_2 + CH_2CH \rightarrow CH_2CHCH_2 + 80.0$
$CH_2 + CHNH_2 \rightarrow CH_2CHNH_2 + 145.0$
$CH_2 + CH_3O \rightarrow CH_3OCH_2 + 85.0$
$CH_2 + CH_2OH \rightarrow CH_2CH_2OH + 80.0$
$CH_2 + CHCHO \rightarrow CH_2CHCHO + 145.0$
$CH_2 + CH_2CH \rightarrow CH_2CHCH_3 + 145.0$
$NH_2 + C_2 \rightarrow NH_2C_2 + 90.0$
$NH_2 + CN \rightarrow NH_2CN + 90.0$
$NH_2 + NO \rightarrow NH_2NO + 40.0$
$NH_2 + NH_2 \rightarrow N_2H_4 + 57.0$
$NH_2 + C_2H \rightarrow NH_2C_2H + 90.0$
$NH_2 + COH \rightarrow NH_2COH + 70.0$
$NH_2 + HCO \rightarrow NH_2CHO + 70.0$
$NH_2 + NOH \rightarrow NH_2NOH + 40.0$
$NH_2 + HO_2 \rightarrow NH_2OOH + 50.0$
$NH_2 + CCO \rightarrow NH_2CCO + 70.0$
$NH_2 + NO_2 \rightarrow NH_2NO_2 + 40.0$
$NH_2 + CH_3 \rightarrow CH_3NH_2 + 81.0$
$NH_2 + CH_2C \rightarrow CH_2CNH_2 + 70.0$
$NH_2 + NH_2C \rightarrow C(NH_2)_2 + 70.0$
$NH_2 + CH_2N \rightarrow CH_2NNH_2 + 40.0$
$NH_2 + CHNH \rightarrow NH_2CHNH + 70.0$
$NH_2 + CHOH \rightarrow NH_2CHOH + 70.0$
$NH_2 + NHOH \rightarrow NH_2NHOH + 40.0$
$NH_2 + OCHO \rightarrow NH_2OCHO + 50.0$
$NH_2 + CO_2H \rightarrow NH_2CO_2H + 70.0$
$NH_2 + CH_2CH \rightarrow CH_2CHNH_2 + 70.0$
$NH_2 + CHNH_2 \rightarrow CH(NH_2)_2 + 70.0$
$NH_2 + CH_3O \rightarrow CH_3ONH_2 + 50.0$
$NH_2 + CH_2OH \rightarrow NH_2CH_2OH + 70.0$
$NH_2 + CHCHO \rightarrow NH_2CHCHO + 70.0$
$NH_2 + CH_3CH \rightarrow CH_3CHNH_2 + 70.0$
$C_2H + C_2 \rightarrow HC_2C_2 + 90.0$
$C_2H + CN \rightarrow HC_2CN + 90.0$
$C_2H + C_2H \rightarrow (HC_2)_2 + 100.0$
$C_2H + COH \rightarrow HC_2COH + 90.0$
$C_2H + NOH \rightarrow HC_2NOH + 90.0$
$C_2H + CCO \rightarrow HC_2CCO + 90.0$
$C_2H + CH_2C \rightarrow CH_2CC_2H + 90.0$
$C_2H + NH_2C \rightarrow HC_2CNH_2 + 90.0$
$C_2H + CH_2N \rightarrow CH_2NC_2H + 90.0$
$C_2H + CHNH \rightarrow HC_2CHNH + 90.0$
$C_2H + NHOH \rightarrow HC_2NHOH + 90.0$
$C_2H + OCHO \rightarrow HC_2OCHO + 90.0$
$C_2H + CO_2H \rightarrow HC_2CO_2H + 90.0$
$C_2H + CH_2CH \rightarrow CH_2CHC_2H + 90.0$
$C_2H + CH_3O \rightarrow CH_3OC_2H + 90.0$
$C_2H + CH_2OH \rightarrow HC_2CH_2OH + 90.0$
$C_2H + CHCHO \rightarrow HC_2CHCHO + 90.0$
$C_2H + CH_3CH \rightarrow CH_2CHC_2H + 90.0$
$HCO + C_2 \rightarrow C_2CHO + 90.0$
$HCO + CN \rightarrow HCOCN + 90.0$
$HCO + NO \rightarrow HCONO + 70.0$
$HCO + C_2H \rightarrow HC_2CHO + 90.0$
$HCO + COH \rightarrow HCOCOH + 80.0$
$HCO + HCO \rightarrow (HCO)_2 + 85.0$
$HCO + NOH \rightarrow HCONOH + 70.0$
$HCO + HO_2 \rightarrow HOOCHO + 85.0$
$HCO + CCO \rightarrow HCOCCO + 80.0$
$HCO + NO_2 \rightarrow HCONO_2 + 70.0$
$HCO + CH_3 \rightarrow CH_3CHO + 77.0$
$HCO + CH_2C \rightarrow CH_2CCHO + 80.0$
$HCO + NH_2C \rightarrow NH_2CCHO + 80.0$
$HCO + CH_2N \rightarrow CH_2NCHO + 70.0$
$HCO + CHNH \rightarrow HCOCHNH + 80.0$
$HCO + CHOH \rightarrow HOCHCHO + 80.0$
$HCO + NHOH \rightarrow HCONHOH + 70.0$
$HCO + OCHO \rightarrow (HCO)_2O + 85.0$
$HCO + CO_2H \rightarrow HCOCO_2H + 80.0$
$HCO + CH_2CH \rightarrow CH_2CHCHO + 80.0$
$HCO + CHNH_2 \rightarrow NH_2CHCHO + 80.0$
$HCO + CH_3O \rightarrow CH_3OCHO + 85.0$
$HCO + CH_2OH \rightarrow HOCH_2CHO + 80.0$
$HCO + CHCHO \rightarrow CH(CHO)_2 + 80.0$
$HCO + CH_3CH \rightarrow CH_3CHCHO + 80.0$
$HO_2 + C_2 \rightarrow C_2OOH + 90.0$
$HO_2 + CN \rightarrow HOOCN + 90.0$
$HO_2 + NO \rightarrow HOONO + 50.0$
$HO_2 + C_2H \rightarrow HC_2OOH + 90.0$
$HO_2 + COH \rightarrow HOOCOH + 85.0$
$HO_2 + NOH \rightarrow HOONOH + 50.0$
$HO_2 + HO_2 \rightarrow (HO_2)_2 + 35.0$
$HO_2 + CCO \rightarrow HOOCCO + 85.0$
$HO_2 + CH_3 \rightarrow CH_3OOH + 85.0$
$HO_2 + CH_2C \rightarrow CH_2COOH + 85.0$
$HO_2 + NH_2C \rightarrow NH_2COOH + 85.0$
$HO_2 + CH_2N \rightarrow CH_2NOOH + 50.0$
$HO_2 + CHNH \rightarrow HOOCHNH + 85.0$
$HO_2 + NHOH \rightarrow HOONHOH + 50.0$
$HO_2 + OCHO \rightarrow HOOOCHO + 35.0$
$HO_2 + CO_2H \rightarrow HOOCO_2H + 85.0$
$HO_2 + CH_2CH \rightarrow CH_2CHOOH + 85.0$
$HO_2 + CH_3O \rightarrow CH_3OOOH + 35.0$
$HO_2 + CH_2OH \rightarrow HOOCH_2OH + 85.0$
$HO_2 + CHCHO \rightarrow HOOCHCHO + 85.0$
$HO_2 + CH_3CH \rightarrow CH_3CHOOH + 85.0$
$CH_3 + C_2 \rightarrow CH_3C_2 + 120.0$
$CH_3 + CN \rightarrow CH_3CN + 120.0$
$CH_3 + NO \rightarrow CH_3NO + 70.0$
$CH_3 + C_2H \rightarrow CH_3C_2H + 117.0$
$CH_3 + COH \rightarrow CH_3COH + 80.0$
$CH_3 + NOH \rightarrow CH_3NOH + 70.0$
$CH_3 + CCO \rightarrow CH_3CCO + 80.0$
$CH_3 + CH_2C \rightarrow CH_2CCH_3 + 80.0$
$CH_3 + NH_2C \rightarrow CH_3CNH_2 + 80.0$
$CH_3 + CH_2N \rightarrow CH_2NCH_3 + 70.0$
$CH_3 + CHNH \rightarrow CH_3CHNH + 80.0$
$CH_3 + NHOH \rightarrow CH_3NHOH + 70.0$
$CH_3 + OCHO \rightarrow CH_3OCHO + 85.0$
$CH_3 + CO_2H \rightarrow CH_3CO_2H + 80.0$
$CH_3 + CH_2CH \rightarrow CH_2CHCH_3 + 29.0$
$CH_3 + CH_3O \rightarrow CH_3OCH_3 + 80.0$
$CH_3 + CH_2OH \rightarrow CH_3CH_2OH + 83.0$
$CH_3 + CHCHO \rightarrow CH_3CHCHO + 80.0$
$CH_3 + CH_3CH \rightarrow CH_3CHCH_3 + 80.0$
$CH_2CH + C_2 \rightarrow CH_2CHC_2 + 120.0$
$CH_2CH + CN \rightarrow CH_2CHCN + 128.0$
$CH_2CH + COH \rightarrow CH_2CHCOH + 80.0$
$CH_2CH + CH_2N \rightarrow CH_2NCHCH_2 + 70.0$
$CH_2CH + OCHO \rightarrow CH_2CHOCHO + 85.0$
$CH_2CH + CO_2H \rightarrow CH_2CHCO_2H + 80.0$
$CH_2CH + CH_3O \rightarrow CH_2CHOCH_3 + 85.0$

notions of molecular recombination. Because dark clouds are so cold, it seemed reasonable to consider the possibility that many exotic compounds never produced nor even considered to exist in laboratory experiments might occur in interstellar space. In table 1 there are several families of structural isomers in which the individual members have widely varying free energies. Although internal rearrangements may be thermodynamically favorable, it will be presumed that such processes are kinetically hindered since internal rearrangements normally have measureable activation energies (March 1968). Even though it is true that the smallest grains might be heated sufficiently to enable thermodynamically allowed rearrangements and/or decomposition to occur in cases of some of the less stable species, it is not possible at present to estimate such fine details with any confidence. Two further simplifications have also been made in choosing the reactions: (1) If a number of possible product channels exist for a given recombination, the one that releases the most energy was chosen. (2) When several electronic resonance structures existed for a particular nuclear framework, the seemingly most stable configuration was picked. The errors introduced by these assumptions will be discussed in § III.

The reaction exoergicities, the actual physical parameter that affects the grain temperature, were derived in a number of ways. The reaction exoergicity E_{bond} is related to the reaction enthalpy change measured at 0° K and 0 atm, $\Delta H^{0,0}$ --

$$E_{bond} = -\Delta H^{0,0}. \qquad (3)$$

Since $\Delta H^{0,0} = \Delta H^{0,P}$ and $\Delta H^{0,P} \approx \Delta H^{T,P}$ to within a few percent when $T = 298°K$, heats of formation $\Delta H_f^{T,P}$ measured at the standard conditions of 298°K and 1 atm can be used to determine E_{bond},

$$\Delta H^{T,P} = \sum_{\text{products}} \Delta H_f^{T,P} - \sum_{\text{reactants}} \Delta H_f^{T,P} . \qquad (4)$$

In the case of a simple recombination of two free radicals, E_{bond} also equals the thermodynamic bond dissociation energy $BDE^{T,P}$ when $T = 0°K$ and $P = 0$ atm. Values for $\Delta H_f^{T,P}$ were obtained from Dean (1973) and the JANAF Thermochemical Tables (1971, 1974, 1975). Benson (1965), Tsuji (1964, 1973), Roberts and Caserio (1964), and Darwent (1970) were the sources of E_{bond} and/or $BDE^{T,P}$ values. Upon inspection of thermodynamic tables, one sees that the entropy contribution to the free energy of a species is very small at 10°K. Therefore all of the reactions in table 1 fulfill the requirement of spontaneity. Finally, although ΔH for a reaction in the gas phase is not necessarily equal to the ΔH for the reaction when occurring on a grain, the difference is probably minimal in the case of physically adsorbed species.

Another set of parameters that affect the reaction rates are the adsorption energies E_{ads} for the various species. For the purposes of the present calculations, the heats of physical adsorption of A on bare silicate grains ($E_{ads}^{A\text{-}SiO_2}$) and on grains with molecular hydrogen mantles ($E_{ads}^{A\text{-}H_2}$) are needed. Since the physical adsorption interaction is basically due to dispersion and electrostatic forces (Steele 1974), the energies of physical adsorption for any species A on two different

surfaces are approximately in a constant proportion to each other. Because calculations have shown that the H_2 physical adsorption energy on the basal plane of graphite is about equal to that on typical refractory surfaces (Augason 1970), adsorption energies on silicates can then be derived from the extensive literature existing on the subject of the physical adsorption of gases on graphite. Avgul and Kiselev (1970) have developed sophisticated techniques to calculate the adsorption energies of a wide range of species on basal graphite and their results agree quite well with experimentally determined values. Their methods utilize the idea that the adsorption energy of a whole molecule can be treated as the sum of the interaction energies between various parts of the molecule and the surface. By using this additivity principle and the values they calculate for a variety of species, values for $E_{ads}^{A\text{-}SiO_2}$ for the chemical species in the interstellar reaction set were determined and are listed in tables 2 and 3. Since the adsorption energy of H_2 on silicates is approximately five times the adsorption energy on solid H_2 (Augason 1970), the values for $E_{ads}^{A\text{-}H_2}$ were scaled from the $E_{ads}^{A\text{-}SiO_2}$ values by the same factor.

b) Reaction Efficiency

Since there is a high probability that a molecule resulting from a surface reaction may desorb from the surface and/or may be chemically inert, the surface reaction rates will be calculated using the statistical assumption that every second collision between a grain and a reactive species will result in a reaction occurring on the grain. Several factors affect the validity of this 100% reaction efficiency

assumption.

First, the accommodation coefficient a, the probability that an atom or molecule does not rebound from the surface after the initial collision and reaches thermal equilibrium with the surface, must be unity. This is a reasonable assumption for even the lightest species under the conditions of $T_{gr} \simeq T_k \simeq 10°K$ (Hobson 1967) and nonactivated adsorption, as physical adsorption generally is. At 10°K, the adsorbed lifetime of a species is generally greater than the grain-gas collision timescale, so the next time a reactive species collides with the grain, a reaction can occur. Although the accommodation coefficient of H on solid H_2 is probably unity at these temperatures, its adsorbed lifetime on an H_2 mantle is usually much less than the grain-gas collision time-scale (cf. figure 1 of Paper II). Therefore, as an exception to the 100% reaction efficiency assumption, reactions involving H atoms will not occur on H_2-mantled grains.

Second, the surface mobility of at least one member of the reaction pair must be high enough to allow it to locate its partner on the grain before another species that could react with one or both of the previously adsorbed reactive species collides with the grain. The time τ_N required for an atom or molecule to search an entire grain with N adsorption sites is a function of the time τ_D for the atom or molecule to diffuse between adjacent adsorption sites (Hollenbach and Salpeter 1970). At low temperatures, quantum mechanical factors dominate the diffusion rate. Then,

$$\tau_N = N\tau_D \tag{5}$$

with τ_D inversely proportional to the energy band width of the ground adsorption state. In the case of the H_2 migration on solid H_2O, Hollenbach and Salpeter (1970) find that $\tau_D \simeq 10^{-11}$ s (the value for silicate grains being probably quite similar). In the present reaction model, HO_2 is the heaviest, most strongly adsorbed species that needs to migrate to maintain 100% reaction efficiency. At 10°K, its de Broglie wavelength is ~ 3 Å, approximately the spacing between adsorption sites, therefore enabling τ_D to be calculated quantum mechanically. If analogy to trends in rare gas calculations (Steele 1974) is valid, the band width of the ground adsorption state of HO_2 on silicates is probably $\gtrsim 10^{-6}$ that of H_2 on silicates. Then $\tau_D^{HO_2\text{-}SiO_2} \lesssim 10^{-5}$ s. Similar arguments result in a value of $\tau_D^{HO_2\text{-}H_2} \lesssim 10^{-7}$ s. The largest bare silicate grains that need to be considered are ~ 400 Å in radius and have $\sim 2\times10^4$ adsorption sites (Paper II). Then $\tau_N^{HO_2\text{-}SiO_2}$ is $\sim .2$ s, much less than the timescale for successive collisions of H atoms, the most abundant reactive species, with the grain (cf. figure 1 of Paper II). The largest grains of any chemical relevance are ~ 3000 Å in radius and are coated with solid H_2. Then the important grain-gas collision timescale is ~ 10 s, still a little longer than the appropriate $\tau_N^{HO_2\text{-}H_2}$ of ~ 6 s. Thus surface migration seems to be rapid enough to maintain 100% reaction efficiency.

Third, reaction efficiency is affected by the relative reactivities of the free radicals. Under a common set of conditions, lifetimes for free radicals vary over 7 orders of magnitude, seemingly

dependent on structure--the more sterically bulky species having the longest lifetimes (Griller and Ingold 1976). Since all of the free radicals considered in this paper have basically simple structures, the presumption is that all reactions occur upon initial encounter.

c) Detailed Formation Rate Expressions

As is the case in the surface chemistry model of Watson and Salpeter (1972a), it will be assumed here that every reactive species colliding with a grain will eventually be involved in a reaction on the grain surface. Moreover, it will be further assumed that a new molecule will be formed upon every second collision of the grain with a reactive species (as discussed in the previous subsection). The surface reaction rates are calculated accordingly.

The total rate expression for a particular reaction can be factored into two parts. One part involves the abundances and velocities of the reactants and will be denoted $R_{A+B,}$ for the reaction of A with B. The other factor involves the surface area available for an effective reaction.

Associated with each reactive species A is a set of coreactants C_i^A. Now consider a grain free of reactants. After a reactive species A hits the grain (the initiating step of the reaction sequence), the probability that a particular one of its coreactants, say B, is the next to collide with the grain, with AB resulting, is $V_B[B] / \sum_i V_i^A [C_i^A]$. However, AB could also result if B were the first to collide and then, of all B's coreactants, A was the next. These alternative events

therefore need to be weighted by their probability of occurring to prevent an overestimation of the rate of formation of AB; the probability of A being the first to collide is $V_A[A]/(V_A[A] + V_B[B])$. Then, for the formation of AB from A and B,

$$R_{A+B} = \alpha_{AB} \left(V_A[A] \frac{V_B[B]}{\sum_i V_i^A [C_i^A]} \frac{V_A[A]}{V_A[A] + V_B[B]} + V_B[B] \frac{V_A[A]}{\sum_i V_i^B [C_i^B]} \frac{V_B[B]}{V_A[A] + V_B[B]} \right), \quad (6)$$

where the brackets indicate volume concentration, $\alpha_{AB} = 0.5$ if A = B and unity otherwise, and

$$V_X = (8 k T_k / \pi M_X)^{\frac{1}{2}} \quad (7)$$

in which case k is Boltzmann's constant and M_X is the mass of X.

For a grain to be an effective reaction site, i.e., contribute to a net increase of AB in the gas phase, the nascent molecule AB must desorb before (1) something collides with the grain that can react with AB (a problem if AB is a radical) or (2) before another AB molecule collides with that grain. This then depends on the concentrations of various species in the gas phase and the adsorbed lifetime of nascent AB. The adsorbed lifetime, in turn, is a function of the adsorption energy of the nascent molecule, the reaction exoergicity, and grain size. Nascent molecule adsorbed lifetimes are calculated as described in

Paper I with the following added assumption: (1) The recombination of molecules can be treated as a recombination of atoms. Internal molecular modes usually have high frequencies, allowing them to be excluded from the calculations. (2) The surface vibrational frequency ω_{gm} is $\sim 100\ cm^{-1}$ in all cases of physical adsorption. In reality, the surface frequency for the H atom is larger than the surface frequency for heavier species that may be equally tightly bound, the extra short lifetime for H atoms on H_2 mantles thus resulting.

Two types of grain surfaces exist in the present model. Grains with radii less than $r_{min}^{H_2}$ or greater than $r_{max}^{H_2}$ will be coated with an H_2 mantle (see Paper II) and the adsorbed lifetime appropriate to the A + B reaction on these grains ($L(r)^{A+B-H_2}$) depends on $E_{ads}^{AB-H_2}$. All other grains are relatively bare and $L(r)^{A+B-SiO_2}$ depends on $E_{ads}^{AB-SiO_2}$. Associated with each reaction and with each type of grain surface is the radius of the largest grain which can be an effective reaction site, $r_{max}^{A+B-H_2}$ or $r_{max}^{A+B-SiO_2}$. For $r \geq r_{max}^{A+B-H_2}$,

$$L(r)^{A+B-H_2} \geq 1/(V_{AB}[AB] + \sum_i V_i^{AB}[C_i^{AB-H_2}])\pi r^2; \qquad (8)$$

a similar relationship exists for $r_{max}^{A+B-SiO_2}$. It is obvious that in all cases $r_{max}^{A+B-SiO_2}$ is less than $r_{max}^{A+B-H_2}$. In the case of H + H reaction, the denominator of the right-hand expression in equation (8) also has a term for the rate of formation of H_2 since $r_{max}^{H+H-SiO_2} = r_{max}^{H_2}$ (cf. eq. [4] in Paper II). Since reactions involving H atoms have zero efficiency on H_2-coated grains, each reactive species has two coreactant sets, $C_i^{A-H_2}$ which excludes H atoms and is appropriate for reactions on

H_2-coated grains and $C_i^{A\text{-}SiO_2}$ which includes H atoms and is for reactions on bare silicate grains. (Similarly, for each reaction, there are two appropriate abundance and temperature dependent factors, $R_{A+B}^{H_2}$ and $R_{A+B}^{SiO_2}$).

Now assume that the concentrations of gas-phase species are such that

$$0 \leq r_{min}^{H_2} \leq r_{max}^{A+B\text{-}SiO_2} \leq r_{max}^{H_2} \leq r_{max}^{A+B\text{-}H_2} . \tag{9}$$

Then the effective rate of formation of gas phase AB via the reaction channel A + B is

$$\left.\frac{d[AB]}{dt}\right|_{+}^{A+B} = R_{A+B}^{H_2} \int_0^{r_{min}^{H_2}} \pi r^2 \beta n(r) dr$$

$$+ R_{A+B}^{SiO_2} \int_{r_{min}^{H_2}}^{r_{max}^{A+B\text{-}SiO_2}} \pi r^2 \beta n(r) dr + R_{A+B}^{H_2} \int_{r_{max}^{H_2}}^{r_{max}^{A+B\text{-}H_2}} \pi r^2 \beta n(r) dr. \tag{10}$$

The rate equation under other circumstances can be readily formulated in a similar manner. In the case of a reaction involving an H atom (or atoms),

$$\left.\frac{d[HE]}{dt}\right|_{+}^{H+E} = R_{H+E}^{SiO_2} \int_{r_{min}^{H_2}}^{r_{max}^{H_2}} \pi r^2 \beta n(r) dr \tag{11}$$

for the situation

$$0 \leq r_{min}^{H_2} \leq r_{max}^{H_2} \leq r_{max}^{H+E-SiO_2} \leq r_{max}^{H+E-H_2} . \qquad (12)$$

Other cases are similarly derivable. In equations (10) and (11), $\beta\, n(r)$ is the grain size distribution suggested in Paper II. For the reaction $H + H \rightarrow H_2$, equation (11) reduces to equation (5) of Paper II.

Finally, it should be noted that heavy molecules can and will adsorb onto other grains already covered with sufficient H_2 to suppress further H_2 depletion, since they interact more strongly with solid H_2 than does H_2 itself. However the only result will be that additional H_2 will adsorb locally (due to the enhancement of the H_2-surface interaction from the presence of the heavy molecule) until the adsorption energy again is reduced to the sublimation point. If large grain mantles were not basically solid H_2, all of the molecular hydrogen in a cloud would rapidly be depleted by the grains, which is contrary to observations. In the case of the smaller bare grains, adsorption of hea molecules does not change the surface energies to any significan extent.

III. THE DYNAMIC NATURE OF CHEMISTRY IN DENSE CLOUDS

A dense cloud physical model that serves as the setting for the time evolution of the cloud chemistry has been previously discussed in Paper II. Only the details from the paper essential for understanding the calculations of the present work will be mentioned here (without further attribution).

It will be assumed that a cold dark cloud can condense out of the diffuse interstellar medium relatively instantaneously, compared to the timescale for cloud chemistry. The cloud remains at a physical steady-state--constant temperature, constant mass density--for the duration of the calculation. The chemical elements have their "cosmic" (i.e., solar system) abundances; the H : He : C : N : O : Si ratio is $1 : 6.95\times10^{-2} : 3.71\times10^{-4} : 1.18\times10^{-4} : 6.67\times10^{-4} : 3.14\times10^{-5}$ (Cameron 1973). Initially, the gas-phase species are all atoms and the dusty cloud component consists of bare quartz grains with a size distribution of $\beta\, n(r)$. The particular normalized size distribution $n(r)$ used both here and in Paper II is one of many that have been proposed to fit the interstellar extinction curve and was chosen only because of its convenient feature of involving only highly refractory grains. The scaling factor β is determined by $n(r)$ and the assumption that all the silicon atoms are incorporated into the grains.

Early in the chemical evolution of the cloud, the high energy adsorption sites on the grains are quickly occupied by H atoms, a fact which at low cloud temperatures renders the grains chemically inert. Afterwards, all further grain-gas interactions are due to physical

adsorption forces. Bimolecular gas-phase reactions will be presumed not to occur. Instead gas-phase molecules will be formed via the surface reactions outlined in § II and possibly through photodegradation of larger species.

What also needs to be considered are the depletion channels for gas-phase species. For each molecule, there is a rate constant for radiative destruction k_{rad}^{A}, either due to dissociation or ionization, which depends on the local radiation density.

Atoms and molecules are also depleted through collisions on grains. The range of grain sizes which are effective depletion sites (i.e., molecules of a particular species adsorbing more rapidly than they are desorbing) depends on the nature of the species. Every free radical that becomes adsorbed on a grain will disappear through further reaction with other adsorbed species. However, in the case of H atoms, only grains without H_2 mantles will be effective depletion sites since H atoms will desorb from H_2-coated grains before reacting further. Unreactive species that become adsorbed onto a grain may later desorb if the grain is heated by some reaction. Associated with every molecule and each type of grain surface is an adsorbed lifetime $\Lambda(r)^{A-X}$, the residence time for an unreactive species A on a grain which has been heated by a reaction not involving A. The $\Lambda(r)^{A-X}$ can be computed for each species, independent of its formation path, with $E_{bond} = 75$ kcal mole^{-1} (an estimate of the average amount of energy released during a surface reaction) and the appropriate E_{ads}^{A-X}. Since the timescale for some kind of reaction to occur on a grain is generally much shorter than the timescale for successive collisions between a grain and a

particular gas-phase species, a grain will be an effective depletion site for species A if the adsorbed lifetime $\Lambda(r)^{A-X}$ is greater than the time for successive collisions of the grain with A molecules. For each type of grain surface, there exists a lower radius limit ($r_d^{A-H_2}$ or $r_d^{A-SiO_2}$) to the size of a grain on which A depletes effectively. For $r \geq r_d^{A-H_2}$,

$$\Lambda(r)^{A-H_2} \geq 1/V_A[A]\,\pi r^2, \tag{13}$$

and similarly for $r_d^{A-SiO_2}$ ($r_d^{A-H_2}$ is always greater than $r_d^{A-SiO_2}$). In the special case of H_2, no grain is a effective depletion site since bare grains (as calculated in this paper) do not accumulate H_2, and H_2 desorbs rapidly from the other grains which are coated with solid H_2. (When $\Lambda(r)^{A-X}$ is calculated, $\omega_{gm} = 100\ cm^{-1}$ is assumed since A is physically adsorbed in all cases. Due to its small mass, the frequency for H_2 is in reality much higher than the frequency for heavier species, resulting in the significantly shorter adsorbed lifetimes for H_2, compared to the heavier species, that have been postulated.)

The detailed rate equation for a species AB is the sum of the formation and depletion terms. For example, in the case of a heavy unreactive species AB for which

$$0 \leq r_{min}^{H_2} \leq r_d^{AB-SiO_2} \leq r_{max}^{H_2} \leq r_d^{AB-H_2}, \tag{14}$$

the total rate equation is

$$\frac{d[AB]}{dt} = \sum_{\substack{\text{reaction} \\ \text{channels}}} \left.\frac{d[AB]}{dt}\right|_{+} + k_{rad}^{ABC}[ABC] - k_{rad}^{AB}[AB]$$

$$- \left(\int_{r_d}^{r_{max}^{H_2}} {}_{AB\text{-}SiO_2} \pi r^2 \beta n(r) dr + \int_{r_d}^{\infty} {}_{AB\text{-}H_2} \pi r^2 \beta n(r) dr \right) V_{AB}[AB] . \quad (15)$$

For a reactive species, the depletion integral runs from 0 to ∞, except in the case of H for which the integral is only evaluated between $r_{min}^{H_2}$ and $r_{max}^{H_2}$. For H_2, the depletion integrals are zero. Paper II suggests that radiation may have a minimal effect on dense cloud chemistry. Therefore, in the present model, all radiative rate constants are zero unless otherwise specified.

The kinetic rate equations for the 372 species in the interstellar chemical model are obviously coupled and were solved numerically on a high-speed computer as a function of time using Runge-Kutta techniques. Since all the important radius limits for formation and depletion are time-dependent, much iterative recalculation is necessary. Each time step requires about one minute of actual computation time, even after much effort has been invested to maximize program efficiency.

To simulate dark cloud chemical evolution, calculations were performed at two initial hydrogen atom densities, $[H(0)] = 10^4$ and 10^5 cm^{-3}, in the temperature regime $T_{gr} = T_k = 10°$K. Unfortunately, of the observed interstellar molecules, those of highest complexity are

seen only in the giant molecular clouds, which are generally denser and hotter than the isolated dark clouds for which this reaction model is designed. However, to enable some comparison between the model and observations, a calculation was also performed under the conditions, $[H(0)] = 2\times10^6$ cm^{-3}, $T_{gr} = 10°$K, and $T_k = 70°$K. Since the grains actually are hotter in Sgr B2 ($\sim 20°$K; Righini et al. 1975) and in Ori A ($\sim 90°$K; Brandshaft, McLaren, and Werner 1975), the low T_{gr} of this calculation will result in an underestimate of the ejection probability for nascent molecules. On the other hand, the higher cloud temperatures probably reduce the reaction efficiency below the 100% assumed in the calculation, thus partially cancelling the previous effect. In an attempt to approximate the real situation, the accommodation coefficient was reduced by one-half by multiplying the grain-gas terms in the rate expressions by 0.5. Although the chemistry in the hotter, denser clouds may be modified by new reaction channels possibly becoming available and by a possible increase in the radiation field, H_2 mantles will still accumulate on the larger grains and the basic surface reactions described in § II will still occur. In the final analysis, the model seems to remain a plausible simulation of interstellar surface chemistry in these regions.

The results of the calculations are presented in figures 1-3 and tables 2 and 3. The abundances [X(t)] of a few chosen species are plotted as a function of time in the figures, with an emphasis on the time periods of astrophysical relevance. (The jaggedness of the lines is introduced by the discrete time steps in the calculations.) Since the

Fig. 1. - Time-dependent abundances of selected species. $[H(0)] = 10^4\ cm^{-3}$, $T_{gr} = T_k = 10°\,K$.

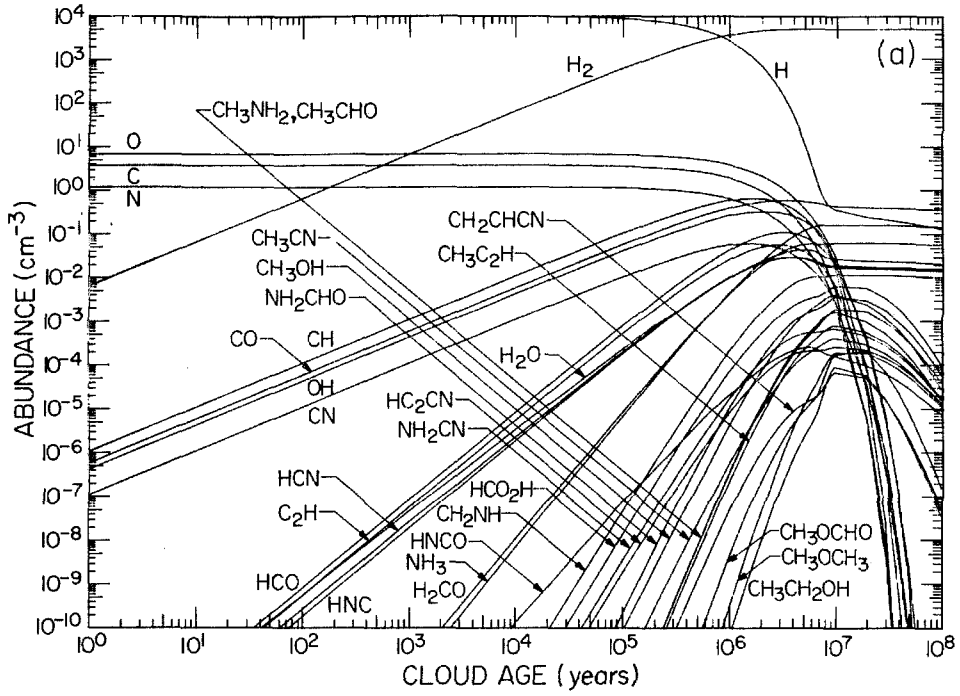
(a)
ABUNDANCE (cm^{-3})
CLOUD AGE (years)
H$_2$
H
CH$_3$NH$_2$,CH$_3$CHO
O
C
N
CH$_2$CHCN
CH$_3$CN
CH$_3$C$_2$H
CH$_3$OH
NH$_2$CHO
CO
CH
H$_2$O
OH
CN
HC$_2$CN
NH$_2$CN
HCN
HCO$_2$H
C$_2$H
CH$_2$NH
HNCO
CH$_3$OCHO
NH$_3$
CH$_3$OCH$_3$
HCO
H$_2$CO
CH$_3$CH$_2$OH
HNC

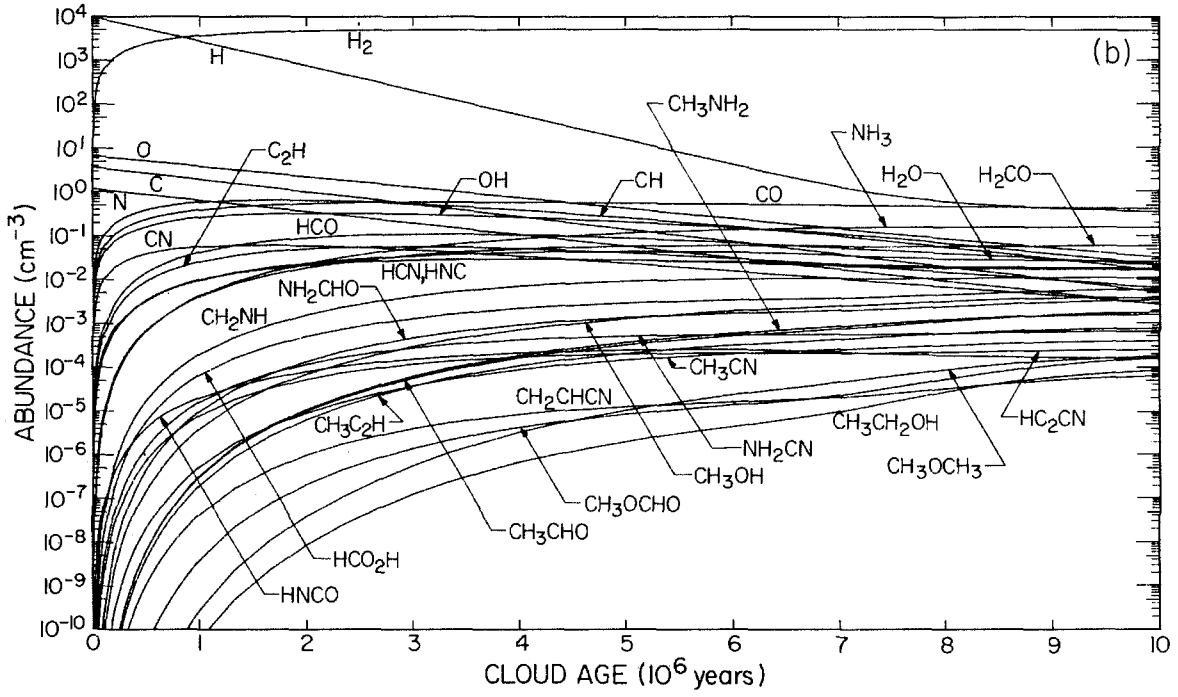
(b)
ABUNDANCE (cm^{-3})
CLOUD AGE (10^6 years)
H
H$_2$
CH$_3$NH$_2$
NH$_3$
O
C$_2$H
H$_2$O
H$_2$CO
OH
CH
CO
C
N
CN
HCO
HCN,HNC
NH$_2$CHO
CH$_2$NH
CH$_3$CN
CH$_2$CHCN
CH$_3$C$_2$H
CH$_3$CH$_2$OH
HC$_2$CN
NH$_2$CN
CH$_3$OH
CH$_3$OCH$_3$
CH$_3$OCHO
CH$_3$CHO
HCO$_2$H
HNCO

Fig. 2. - Time-dependent abundances of selected species. $[H(0)] = 10^5\ cm^{-3}$, $T_{gr} = T_k = 10°K$.

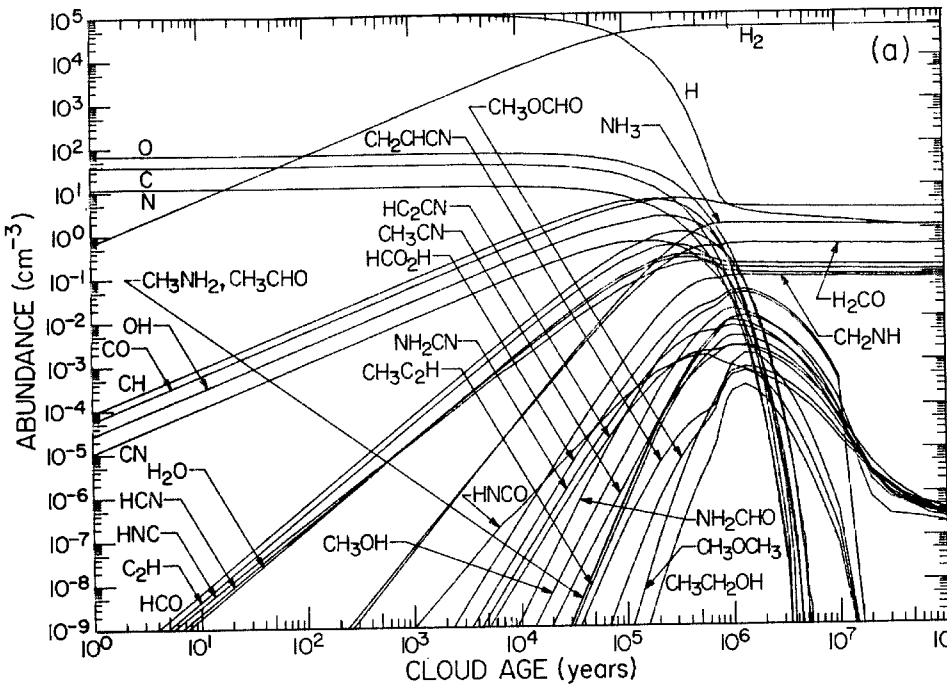
(a)
ABUNDANCE (cm^{-3})
CLOUD AGE (years)
H$_2$
H
CH$_3$OCHO
NH$_3$
CH$_2$CHCN
O
C
N
HC$_2$CN
CH$_3$CN
HCO$_2$H
CH$_3$NH$_2$, CH$_3$CHO
H$_2$CO
CH$_2$NH
OH
CO
CH
NH$_2$CN
CH$_3$C$_2$H
CN
H$_2$O
HCN
HNCO
NH$_2$CHO
HNC
CH$_3$OH
CH$_3$OCH$_3$
C$_2$H
CH$_3$CH$_2$OH
HCO

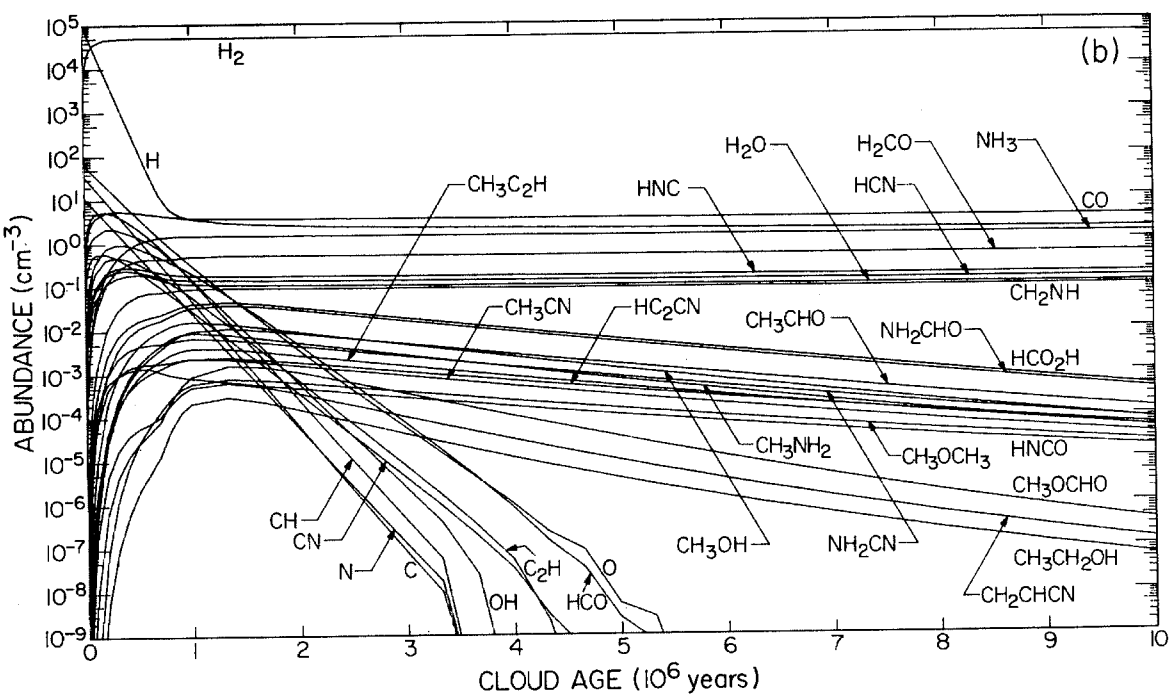
(b)
ABUNDANCE (cm^{-3})
CLOUD AGE (10^6 years)
H$_2$
H
H$_2$O
H$_2$CO
NH$_3$
CH$_3$C$_2$H
HNC
HCN
CO
CH$_2$NH
CH$_3$CN
HC$_2$CN
CH$_3$CHO
NH$_2$CHO
HCO$_2$H
CH$_3$NH$_2$
CH$_3$OCH$_3$
HNCO
CH$_3$OCHO
CH
CN
CH$_3$OH
NH$_2$CN
CH$_3$CH$_2$OH
N
C
C$_2$H
O
CH$_2$CHCN
OH
HCO

Fig. 3. - Time-dependent abundances of selected species. $[H(0)] = 2 \times 10^6$ cm^{-3}, $T_{gr} = 10°$K, $T_k = 70°$K.

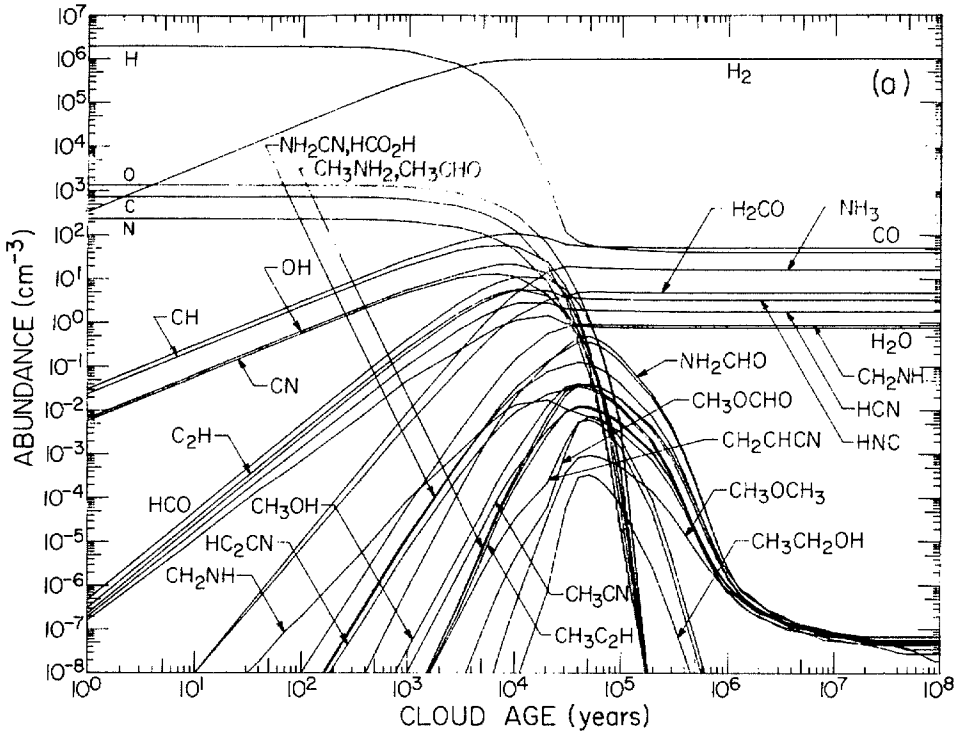
(a)
H
H2
NH2CN,HCO2H
CH3NH2,CH3CHO
O
C
N
H2CO
NH3
CO
OH
CH
CN
H2O
NH2CHO
CH2NH
CH3OCHO
HCN
HNC
CH2CHCN
C2H
CH3OCH3
HCO
CH3OH
CH3CH2OH
HC2CN
CH2NH
CH3CN
CH3C2H
ABUNDANCE (cm-3)
CLOUD AGE (years)

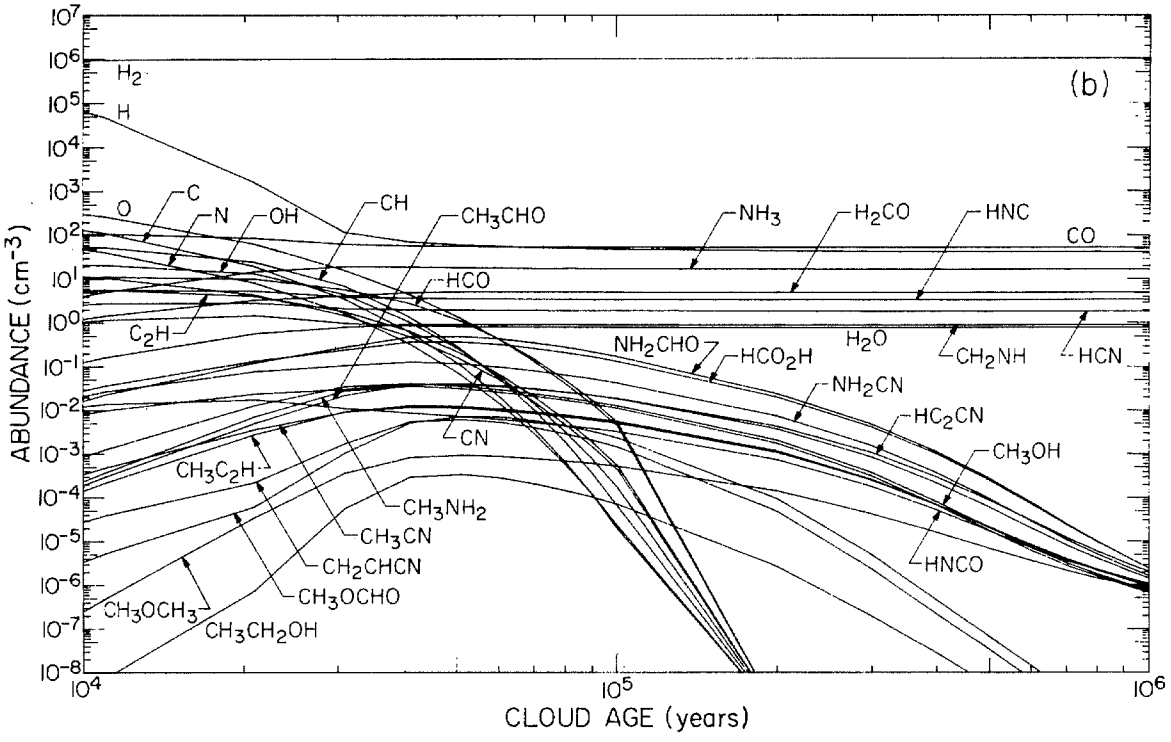
(b)
H2
H
O
C
N
OH
CH
CH3CHO
NH3
H2CO
HNC
CO
HCO
C2H
NH2CHO
HCO2H
H2O
CH2NH
HCN
NH2CN
HC2CN
CN
CH3OH
CH3C2H
CH3NH2
CH3CN
HNCO
CH2CHCN
CH3OCHO
CH3OCH3
CH3CH2OH
ABUNDANCE (cm-3)
CLOUD AGE (years)

TABLE 2
NORMALIZED ABUNDANCES $[X]/[H_2]$ - COMPARISON OF THEORETICAL INTERSTELLAR CHEMICAL MODELS WITH OBSERVATIONS

		Theoretical Models										Observations			
		This Paper				Watson and Salpeter 1972b	Iguchi 1975		Herbst and Klemperer 1973			Sgr E2	Ori A	Dark Clouds	
		$T_{gr} = T_k = 10°K$		$T_{gr} = T_k = 10°K$		$T_{gr} = 10°K$, $T_k = 70°K$	$T_k = 50°K$	$T_{gr} = 20°K$, $T_k = 100°K$	$T_{gr} = 50°K$, $T_k = 100°K$	$T_k = 30°K$	$T_k = 30°K$	$T \simeq 30°K$	$T \simeq 70°K$	$T \simeq 10°K$	
		$[E(0)] = 10^4 cm^{-3}$		$[E(0)] = 10^5 cm^{-3}$		$[H(0)] = 2 \times 10^6 cm^{-2}$	$[H + 2E_2] = 10^5 cm^{-3}$	$[H + 2E_2] = 10^4 cm^{-2}$	$[H + 2E_2] = 10^4 cm^{-2}$	$[E_2] = 10^4 cm^{-3}$, $\zeta = 10^{-17} s^{-1}$	$[E_2] = 10^5 cm^{-3}$, $\zeta = 10^{-17} s^{-1}$	$[E_2] \simeq 10^5 cm^{-3}$	$[E_2] \simeq 10^6 cm^{-3}$	$[E_2] \simeq 5 \times 10^2 cm^{-3}$	
Species	$E_{ads}^{X-SiO_2}$ (kcal mole^{-1})	$t = 10^6$ yr	$t = 10^7$ yr	$t = 10^6$ yr	$t = 10^7$ yr	$t = 10^5$ yr	$A_V = 4$ mag			$[O(0)]/[E(0)] = 4.4(-4)$ or $6.8(-4)$	$[O(0)]/[E(0)] = 4.4(-4)$ or $6.8(-4)$	$L \simeq 10^{19}$ cm	$L \simeq 10^{18}$ cm		Reference
H		7.5(-1)	7.3(-5)	7.3(-5)	3.4(-5)	4.7(-5)	2(-4)			1(-4)	1(-5)			1(-2)-1(-1)	Paper II*
E_2	1.0	1.0	1.0	1.0	1.0	1.0	1.0	1.0	1.0	1.0	1.0	1.0	1.0	1.0	
CE	1.3	1.6(-4)	3.2(-6)	3.0(-6)	0.0	6.5(-11)	1(-7)			8(-11)	1(-13)	4(-10)	< 4(-10)	~3(-9)-1(-8)	Zuckerman and Turner 1975*
OE	2.5	7.3(-5)	4.5(-6)	3.2(-6)	0.0	1.8(-10)				7(-9) or 1(-8)	7(-11) or 9(-11)	1(-7)		~1(-7)-1(-6)	Zuckerman and Turner 1975*
CN	3.0	1.5(-5)	5.7(-7)	6.0(-7)	0.0	4.1(-10)	4(-5)			5(-9) or 4(-8)	4(-10) or 4(-13)		~1(-8)	< 1(-9)	Turner and Gammon 1975*
CO	2.4	1.1(-4)	8.5(-5)	7.6(-5)	6.6(-5)	5.2(-5)	4(-4)	1(-12)	1(-1)	7.5(-4)	7.5(-4)	8(-5)	~1(-4)	9(-5)	Scoville, Solomon, and Penzias 1975*; Turner and Gammon 1975*; Dickman 1975*, respectively
NO	2.4	2.8(-5)	1.5(-6)	1.6(-6)	0.0	2.0(-9)			5(-6)	2(-6) or 4(-8)	2(-10) or 3(-10)	< 3(-7)			Solomon 1973*
C_2H	2.9	6.9(-8)	1.3(-6)	1.2(-6)	0.0	5.1(-10)							5(-10)-2(-9)		Tucker, Kutner, and Thaddeus 1974 ‡
HCN	3.5	2.7(-6)	3.4(-6)	2.9(-6)	2.6(-6)	1.9(-6)	4(-8)	5(-12)	9(-3)	8(-9) or 2(-8)	1(-10) or 4(-13)		~1(-9), 3(-8)-1(-5)		Gottlieb et al. 1975*; Kwan and Scoville 1975*, respectively
ENO	3.0	5.7(-6)	1.0(-5)	9.7(-6)	8.6(-6)	8.8(-6)		1(-15)	4(-6)			< 5(-5)			Fourikis et al. 1974a ||
CCO	4.0	8.4(-7)	4.5(-7)	4.4(-7)	3.9(-21)	3.1(-9)						< 1(-10)	< 1(-10)		Allen 1976 ‡
N_2O	4.0	2.1(-7)	2.3(-7)	2.2(-7)	2.0(-9)	5.2(-8)						< 1(-10)			Cheung et al. 1974 ||
NE_3	2.2	1.2(-5)	3.3(-5)	3.0(-5)	2.7(-5)	1.7(-5)		5(-5)	5(-3)	1(-5) or 8(-6)	4(-10) or 1(-9)	5(-9)	3(-9)	3(-9)	Zuckerman and Turner 1975*
E_2CO	3.5	1.1(-6)	1.2(-5)	1.0(-5)	9.6(-6)	5.0(-6)	4(-8)	1(-10)	4(-3)	1(-9) or 7(-9)	1(-10) or 1(-9)	6(-5)	2(-9)	5(-8)	Zuckerman and Turner 1975*
HNCO	4.5	5.4(-9)	3.2(-8)	1.7(-8)	3.5(-10)	3.1(-9)			7(-3)			8(-11)			Buhl et al. 1973*
ENO_2	4.5	5.7(-8)	8.6(-7)	4.6(-7)	5.2(-9)	8.3(-8)							< 1(-10)		Allen 1976 ‡
CH_2NE	3.7	5.3(-8)	2.3(-8)	1.8(-8)	1.7(-8)	6.9(-7)		1(-10)	8(-4)			~1(-9)			Godfrey et al. 1973 ‡
CE_2N_2	4.3	6.5(-10)	1.8(-8)	1.3(-8)	3.3(-10)	2.7(-6)							< 1(-10)		Allen 1976 ‡
NE_2CN	5.0	4.3(-9)	1.4(-7)	1.3(-7)	1.5(-9)	4.0(-8)						2(-11)-6(-10)			Turner et al. 1975 §
HCO_2H	5.1	1.8(-8)	1.3(-6)	6.4(-7)	8.5(-9)	1.3(-7)		1(-15)	9(-4)			5(-11)			Winnewisser and Churchwell 1975 §
EC_2CN	5.9	2.1(-9)	5.2(-8)	4.7(-8)	1.1(-9)	1.8(-8)			5(-5)			1(-11)-4(-10)	2(-10)	1(-10)-2(-10)	Morris et al. 1976*
ENO_3	7.5	9.1(-11)	1.5(-8)	6.8(-9)	4.9(-12)	2.2(-9)						< 1(-9)-3(-8)	< 6(-10)-2(-8)		Giguere et al. 1973 §
CE_3OE	4.1	1.1(-6)	8.0(-7)	3.3(-7)	1.5(-9)	1.2(-8)	4(-8)	8(-9)	7(-4)			~ 1(-7)	2.5(-8)-4(-7)		Peiling 1975 †
CE_2CN	5.2	1.4(-10)	8.2(-8)	4.6(-8)	6.8(-10)	4.9(-9)	4(-11)		7(-5)			~ 1(-8)			Solomon 1973*
NE_2CHO	4.7	2.6(-9)	7.1(-7)	6.9(-7)	7.3(-8)	1.6(-7)		6(-15)	8(-5)			~ 1(-9)			Gottlieb et al. 1973 §
CH_2NOE	4.9	4.3(-10)	1.7(-7)	1.0(-7)	1.5(-9)	1.4(-8)						< 1(-8)			Tigelaar 1973 ||
$(HCO)_2$	6.0	9.3(-10)	2.9(-7)	2.6(-7)	8.2(-9)	1.3(-7)						< 1(-10)			Clark and Johnson 1975 ||
CH_3NE_2	4.7	8.5(-11)	3.3(-7)	1.8(-7)	9.1(-10)	1.1(-8)		3(-9)	1(-5)			~ 4(-9)			Kaifu, Takagi, and Kojima 1975 §
CH_3C_2E	5.3	5.4(-11)	1.6(-7)	7.9(-8)	9.4(-10)	5.3(-9)		1(-14)	4(-5)			3(-9)			Snyder and Buhl 1973 §
CH_2CHO	5.4	8.6(-11)	3.8(-7)	2.0(-7)	2.6(-9)	1.8(-8)		8(-14)	1(-4)			~ 1(-8)			Fourikis et al. 1974b ‡
CH_2CHCN	5.5	1.2(-11)	1.3(-8)	1.0(-8)	2.7(-12)	1.4(-9)			6(-8)			~ 1(-8)			Gardner and Winnewisser 1975 ‡
CH_2CENE_2	5.2	2.4(-11)	2.7(-7)	2.1(-7)	2.5(-9)	3.3(-8)		2(-15)	2(-7)				< 1(-8)		Clark, Lovas, and Johnson 1975 ||
CE_2CECEO	6.5	7.5(-12)	8.0(-8)	5.6(-8)	1.0(-11)	8.3(-9)			7(-6)			< 1(-9)	< 1(-9)		Batchelor et al. 1973 ||
CH_3OCHO	6.5	1.0(-12)	3.4(-8)	1.8(-8)	7.5(-12)	2.2(-9)						~ 1(-6)			Churchwell and Winnewisser 1975 ‡
CE_3CO_2H	6.3	1.5(-13)	5.3(-9)	2.1(-9)	2.0(-13)	1.2(-10)							< 1(-8)		Allen 1976 ‡
CE_2CH_2OE	6.9	1.6(-14)	1.8(-8)	4.4(-9)	1.2(-12)	6.7(-11)		3(-13)	7(-7)			~1(-9)			Zuckerman et al. 1975 §
CE_3OCE_3	5.7	7.4(-14)	3.7(-8)	1.2(-8)	4.5(-10)	5.0(-10)							5(-10)-1.8(-9)		Snyder et al. 1974 §

NOTE. — $1.0(-4)$ means 1.0×10^{-4}.

* Reference gives normalized abundance. † Reference gives total molecular volume density. ‡ Reference gives one-state column density. § Reference gives total molecular column density. \|\| Reference gives upper limit to antenna temperature.

TABLE 3

NORMALIZED ABUNDANCES [X]/[H_2] - THEORETICAL PREDICTIONS

Species	E_{ads}	Cloud I $t=10^6$ yr	Cloud I $t=10^7$ yr	Cloud II $t=10^6$ yr	Cloud II $t=10^7$ yr	Cloud III $t=10^5$ yr
C		5.3(-4)	1.1(-6)	1.0(-6)	0.0	1.8(-11)
N		1.8(-4)	5.4(-7)	5.4(-7)	0.0	2.1(-11)
O		1.1(-3)	6.5(-6)	6.5(-6)	0.0	4.2(-9)
NH	1.2	6.2(-5)	1.6(-6)	1.6(-6)	0.0	9.1(-11)
C_2	2.4	2.5(-5)	7.6(-7)	7.9(-7)	0.0	3.9(-10)
N_2	2.4	2.9(-6)	3.1(-6)	2.8(-6)	2.4(-6)	1.7(-6)
O_2	2.4	7.1(-5)	5.1(-6)	5.4(-6)	1.2(-23)	1.1(-8)
CH_2	1.9	2.0(-5)	4.5(-6)	3.7(-6)	0.0	6.7(-11)
NH_2	1.7	9.4(-6)	2.2(-6)	2.2(-6)	0.0	1.5(-10)
H_2O	3.7	2.6(-6)	5.3(-6)	2.3(-6)	2.0(-6)	7.7(-7)
HNC	3.0	2.7(-8)	3.7(-6)	3.7(-6)	3.2(-6)	3.4(-6)
N_2H	3.0	7.3(-7)	1.9(-7)	2.0(-7)	0.0	2.5(-10)
HCO	3.0	1.2(-5)	4.4(-6)	4.3(-6)	0.0	5.1(-9)
COH	3.5	2.5(-8)	9.1(-7)	7.0(-7)	0.0	4.6(-10)
NOH	3.0	7.8(-7)	3.8(-7)	2.9(-7)	0.0	2.6(-10)
HO_2	3.0	4.4(-6)	3.2(-6)	2.4(-6)	0.0	3.2(-9)
C_3	4.0	7.7(-7)	5.2(-7)	4.9(-7)	2.4(-9)	6.9(-8)
CCN	4.0	6.3(-7)	1.7(-7)	1.7(-7)	2.1(-22)	5.5(-10)
NCN	4.0	1.3(-7)	4.3(-8)	4.3(-8)	1.7(-22)	1.7(-10)
NCO	4.0	6.5(-7)	2.9(-7)	3.0(-7)	5.2(-21)	2.1(-9)
CNO	4.0	5.3(-7)	1.9(-7)	2.0(-7)	2.1(-21)	8.7(-10)
NO_2	5.0	1.4(-7)	2.8(-7)	2.0(-7)	4.8(-20)	3.7(-9)
NOO	5.0	3.5(-7)	2.0(-7)	1.7(-7)	1.2(-20)	9.3(-10)
O_3	5.0	5.7(-11)	5.5(-7)	8.2(-7)	8.2(-9)	2.2(-7)
CH_3	2.3	5.0(-7)	1.7(-6)	8.7(-7)	0.0	9.5(-12)
CH_2C	3.0	4.9(-7)	7.5(-7)	6.3(-7)	0.0	2.4(-10)
C_2H_2	3.2	1.1(-6)	7.5(-6)	5.5(-6)	4.8(-6)	2.2(-6)
NH_2C	3.2	2.2(-7)	3.4(-7)	3.5(-7)	0.0	3.4(-10)
CH_2N	3.2	1.5(-7)	3.2(-7)	2.7(-7)	0.0	1.4(-10)
CHNH	2.5	4.4(-7)	7.3(-7)	7.2(-7)	0.0	8.0(-10)
N_2H_2	2.4	1.6(-7)	2.4(-6)	2.2(-6)	2.0(-6)	1.7(-6)
NH_2N	3.4	6.8(-8)	1.4(-7)	1.5(-7)	0.0	2.0(-10)
CHOH	3.8	5.6(-8)	7.1(-7)	3.8(-7)	0.0	2.6(-10)
NH_2O	2.9	3.8(-7)	1.1(-6)	1.2(-6)	0.0	2.7(-9)
NHOH	3.8	3.1(-9)	1.9(-7)	1.4(-7)	0.0	2.1(-10)
H_2O_2	5.0	6.0(-8)	1.0(-6)	4.9(-7)	2.3(-9)	2.9(-8)
C_3H	4.5	2.4(-7)	3.4(-7)	3.2(-7)	2.3(-22)	7.6(-10)
NHC_2	3.6	5.3(-8)	1.1(-7)	1.3(-7)	3.3(-22)	5.9(-10)
CHCN	4.5	7.3(-8)	1.4(-7)	1.4(-7)	3.6(-22)	4.3(-10)
NC_2H	4.0	3.3(-6)	5.1(-6)	4.8(-6)	1.3(-22)	1.3(-10)
CCHO	4.0	1.5(-7)	2.8(-7)	2.8(-7)	2.3(-21)	9.6(-10)
HCCO	4.5	1.5(-10)	1.3(-10)	1.2(-10)	6.1(-25)	1.3(-13)
NHCN	4.5	2.8(-8)	6.0(-8)	6.3(-8)	5.3(-22)	3.6(-10)
HC_2O	4.0	1.6(-7)	3.9(-7)	3.7(-7)	5.2(-21)	1.8(-9)
C_2OH	5.0	9.1(-8)	2.6(-7)	2.0(-7)	1.8(-21)	6.4(-10)
HCNC	5.5	1.4(-8)	8.7(-8)	4.8(-8)	7.3(-10)	1.0(-8)
HCNO	4.5	1.1(-7)	6.1(-7)	5.8(-7)	4.4(-9)	1.0(-7)
NCHO	4.2	4.8(-8)	1.2(-7)	1.2(-7)	2.8(-21)	5.8(-10)
HOCN	5.5	4.5(-8)	3.4(-7)	2.5(-7)	2.4(-9)	4.4(-8)
N_2OH	5.0	4.0(-9)	1.2(-8)	8.5(-9)	5.0(-22)	3.9(-11)
OCHO	4.2	4.1(-8)	5.7(-7)	4.6(-7)	1.9(-19)	8.0(-9)
CO_2H	4.6	4.5(-8)	2.4(-7)	1.9(-7)	3.3(-20)	2.0(-9)
COOH	4.0	5.5(-8)	1.6(-7)	1.3(-7)	6.8(-21)	5.3(-10)
NHNO	3.6	4.7(-8)	1.6(-7)	1.8(-7)	8.8(-21)	1.4(-9)
NHOO	3.8	1.3(-7)	5.1(-7)	5.9(-7)	6.6(-20)	5.8(-9)
NOOH	4.2	1.6(-8)	6.8(-8)	5.0(-8)	6.7(-21)	2.4(-10)
HO_3	4.0	8.0(-8)	5.1(-7)	3.5(-7)	2.9(-19)	4.3(-9)
CCCO	5.0	1.3(-8)	2.9(-8)	2.8(-8)	1.9(-20)	2.6(-10)
NCCO	5.0	4.1(-9)	1.2(-8)	1.2(-8)	1.8(-20)	1.6(-10)
C_2NO	4.8	1.5(-8)	4.5(-8)	4.9(-8)	7.4(-20)	9.7(-10)
C_2O_2	5.0	2.4(-8)	2.2(-7)	2.2(-7)	5.4(-9)	1.0(-7)
NCNO	5.4	9.2(-9)	6.1(-8)	6.4(-8)	1.5(-9)	3.8(-8)
CNO_2	6.0	1.8(-9)	8.5(-9)	4.8(-9)	3.3(-20)	1.8(-10)
OOCN	5.4	2.0(-8)	8.8(-8)	1.0(-7)	5.4(-19)	2.8(-9)
NNO_2	6.0	5.1(-10)	3.3(-9)	2.0(-9)	3.8(-20)	1.1(-10)
$(NO)_2$	4.8	5.3(-9)	4.9(-8)	5.4(-8)	1.7(-9)	3.0(-8)
OONO	4.8	2.5(-8)	1.7(-7)	1.8(-7)	3.5(-18)	6.9(-9)
NO_3	6.0	2.5(-9)	2.7(-8)	1.7(-8)	3.5(-18)	2.5(-9)
O_4	5.0	9.7(-11)	1.4(-7)	1.6(-7)	6.2(-9)	1.5(-7)
CH_4	2.7	4.4(-8)	8.6(-8)	3.9(-8)	3.2(-8)	4.9(-7)
CH_3C	3.4	8.6(-9)	1.9(-7)	1.1(-7)	0.0	2.5(-11)
CH_2CH	3.5	1.1(-7)	1.5(-6)	1.2(-6)	0.0	4.5(-10)
$CHNH_2$	3.7	4.7(-8)	6.8(-7)	6.8(-7)	0.0	6.2(-10)
CH_3N	3.6	2.6(-9)	8.2(-8)	4.8(-8)	0.0	1.5(-11)
NH_2NH	2.9	1.7(-8)	2.9(-7)	3.1(-7)	0.0	5.3(-10)
CH_3O	3.4	1.5(-8)	7.1(-7)	4.2(-7)	0.0	2.1(-10)
CH_2OH	4.3	4.7(-9)	7.8(-7)	3.9(-7)	0.0	2.1(-10)
NH_2OH	4.2	1.8(-8)	1.0(-6)	8.3(-7)	2.5(-9)	4.8(-8)
CH_2C_2	4.3	1.2(-8)	1.8(-7)	1.8(-7)	2.7(-22)	3.5(-10)
CHC_2H	4.2	2.7(-8)	2.4(-7)	2.1(-7)	3.4(-22)	4.5(-10)
CH_2CC	4.0	7.0(-9)	5.4(-8)	4.2(-8)	7.3(-23)	8.2(-11)
CH_2CN	5.0	9.1(-9)	1.5(-7)	1.3(-7)	7.2(-22)	3.5(-10)
CCHNH	3.5	6.1(-9)	5.3(-8)	5.6(-8)	2.9(-22)	2.3(-10)
NHC_2H	4.2	1.0(-8)	1.1(-7)	9.9(-8)	5.4(-22)	3.7(-10)
NH_2C_2	4.2	8.5(-9)	1.1(-7)	1.1(-7)	6.2(-22)	5.5(-10)
CH_2NC	4.2	1.9(-9)	1.7(-8)	1.4(-8)	7.8(-23)	3.6(-11)
CCHOH	4.8	7.0(-10)	2.6(-8)	1.1(-8)	3.1(-22)	4.0(-11)
H_2CCO	5.0	1.3(-8)	4.6(-7)	3.7(-7)	3.7(-9)	6.7(-8)
CHCHO	4.3	5.1(-9)	3.6(-7)	2.7(-7)	8.1(-21)	1.3(-9)
HC_2OH	5.3	2.1(-8)	7.6(-7)	5.1(-7)	4.0(-9)	5.8(-8)
NCHNH	3.5	1.9(-9)	2.2(-8)	2.4(-8)	3.9(-22)	1.3(-10)
CHOHN	4.8	2.2(-10)	1.2(-8)	5.3(-9)	4.4(-22)	2.6(-11)
CHNOH	4.3	2.9(-9)	5.8(-8)	4.1(-8)	1.8(-21)	1.3(-10)
NHCOH	4.7	3.4(-9)	8.6(-8)	5.0(-8)	2.2(-21)	2.4(-10)
NHCHO	4.2	1.3(-8)	2.4(-7)	2.5(-7)	1.1(-20)	1.6(-9)
CNHOH	4.8	3.6(-11)	4.0(-9)	2.7(-9)	2.2(-22)	2.5(-11)
OCHNH	3.5	1.0(-8)	1.8(-7)	2.0(-7)	1.5(-20)	2.1(-9)
CH_2NO	4.3	1.2(-8)	3.1(-7)	2.7(-7)	1.3(-20)	1.1(-9)
NH_2CO	3.9	5.4(-9)	1.1(-7)	1.2(-7)	1.3(-20)	1.9(-9)
HN_2OH	5.5	1.0(-9)	4.4(-8)	3.2(-8)	6.9(-10)	9.6(-9)
CHOOH	4.3	1.1(-8)	3.2(-7)	2.1(-7)	2.2(-20)	8.1(-10)
$C(OH)_2$	6.0	3.3(-9)	1.3(-7)	7.5(-8)	8.5(-21)	2.7(-10)
NH_2NO	4.1	4.4(-9)	2.1(-7)	2.0(-7)	2.5(-9)	5.4(-8)
NNHOH	4.8	1.1(-11)	1.7(-9)	1.2(-9)	2.6(-22)	1.5(-11)
ONHOH	4.8	6.0(-11)	1.5(-8)	1.1(-8)	1.4(-20)	3.2(-10)
NH_2OO	6.0	9.3(-9)	3.5(-7)	3.3(-7)	7.6(-20)	3.1(-9)
NHOOH	4.2	4.1(-9)	1.4(-7)	1.1(-7)	2.0(-20)	6.9(-10)
$N(OH)_2$	6.0	8.7(-10)	4.7(-8)	2.8(-8)	6.9(-21)	1.1(-10)
HC_2C_2	5.3	3.5(-9)	3.9(-8)	3.7(-8)	1.2(-20)	3.8(-10)
H_2O_3	6.0	7.3(-11)	2.2(-7)	1.3(-7)	2.6(-9)	2.4(-8)
C_2CHO	5.4	5.2(-9)	3.9(-8)	9.1(-8)	1.4(-19)	1.8(-9)
HCCCO	5.4	2.8(-9)	5.4(-8)	5.0(-8)	6.0(-20)	5.3(-10)
HC_2NO	5.3	3.2(-9)	1.0(-7)	9.3(-8)	2.1(-9)	3.8(-8)
HCOCN	6.0	3.1(-9)	1.1(-7)	1.1(-7)	2.5(-9)	5.3(-8)
HNCCO	5.2	1.0(-9)	4.3(-8)	4.2(-8)	1.2(-9)	1.7(-8)
C_2OOH	5.4	1.9(-9)	5.8(-8)	4.5(-8)	2.5(-19)	9.2(-10)
HOCCO	6.5	4.4(-10)	2.4(-8)	1.7(-8)	1.3(-19)	3.6(-10)
HC_2OO	6.0	7.3(-9)	1.8(-7)	1.7(-7)	8.1(-19)	3.5(-9)
CCO_2H	5.6	4.9(-10)	7.3(-9)	5.3(-9)	2.6(-20)	8.4(-11)
COCHO	5.2	4.3(-10)	1.3(-8)	8.0(-9)	6.8(-20)	3.0(-10)
NCO_2H	5.6	1.5(-10)	3.2(-9)	2.3(-9)	2.6(-20)	5.5(-11)
NOCHO	5.2	1.3(-10)	5.2(-9)	3.4(-9)	9.7(-20)	1.9(-10)
HOCNO	6.5	4.8(-10)	2.0(-8)	1.5(-8)	4.7(-12)	3.3(-9)
HCONO	5.4	4.4(-9)	2.0(-7)	2.1(-7)	5.3(-9)	9.9(-8)
$CHNO_2$	6.3	1.9(-10)	9.7(-9)	5.9(-9)	9.5(-20)	2.7(-10)
HOOCN	6.0	1.1(-9)	6.7(-8)	5.1(-8)	1.8(-9)	2.5(-8)
$HNNO_2$	6.2	1.4(-10)	7.2(-9)	4.9(-9)	1.4(-19)	3.9(-10)
OOCHO	5.4	1.1(-8)	4.1(-7)	4.6(-7)	1.4(-17)	2.1(-8)
HCO_3	5.0	8.2(-10)	2.8(-8)	2.0(-8)	2.5(-15)	1.5(-9)
NOHNO	5.4	2.7(-10)	9.7(-9)	8.4(-9)	1.5(-19)	2.3(-10)
HOONO	5.4	1.4(-9)	1.1(-7)	9.1(-8)	3.4(-9)	4.3(-8)
HO_4	6.0	7.1(-11)	1.1(-7)	9.1(-8)	7.4(-18)	4.7(-9)
ONCCO	6.4	1.5(-10)	5.4(-9)	5.4(-9)	2.1(-18)	9.2(-10)
$OONO_2$	7.4	8.7(-11)	8.4(-9)	5.9(-9)	3.2(-17)	3.4(-9)
CH_2CH_2	4.0	8.4(-9)	1.5(-8)	9.8(-7)	2.2(-9)	3.7(-8)
CH_3CH	3.9	2.4(-10)	2.4(-7)	1.0(-7)	0.0	2.1(-11)
CH_2NH_2	4.2	3.9(-9)	5.2(-7)	4.4(-7)	0.0	3.1(-10)
CH_3NH	4.2	6.9(-10)	1.5(-7)	9.8(-8)	0.0	3.2(-11)
N_2H_4	3.4	1.4(-9)	4.3(-7)	4.2(-7)	4.1(-7)	3.5(-7)
CH_2CCH	4.4	1.6(-9)	1.1(-7)	8.6(-8)	3.1(-22)	1.7(-10)
CH_2CHC	4.8	1.1(-9)	8.2(-8)	4.9(-8)	1.9(-22)	1.1(-10)
CH_2C_2H	4.8	2.7(-9)	2.5(-7)	1.9(-7)	8.5(-22)	3.3(-10)
CH_2C_2	4.7	2.4(-10)	1.2(-7)	9.8(-8)	7.8(-10)	8.5(-9)
CH_2CHN	4.5	3.4(-10)	2.8(-8)	2.3(-8)	2.8(-22)	8.4(-11)
CH_2CNH	4.2	5.9(-10)	9.8(-8)	7.8(-8)	9.8(-10)	1.4(-8)
CH_2NCH	4.5	4.8(-10)	3.7(-8)	2.9(-8)	3.2(-22)	7.5(-11)
$CCHNH_2$	4.7	5.0(-10)	3.4(-8)	3.2(-8)	3.8(-22)	1.5(-10)
NH_2C_2H	4.6	2.0(-9)	3.1(-7)	2.7(-7)	2.4(-9)	5.3(-8)
CHCHNH	3.8	1.3(-9)	8.7(-8)	6.3(-8)	9.2(-22)	3.3(-10)
NHCHNH	4.4	4.8(-10)	3.9(-8)	3.9(-8)	1.3(-21)	2.8(-10)
CH_3OC	4.4	1.4(-10)	2.2(-8)	1.3(-8)	4.7(-22)	3.1(-11)
CH_2CH-O	4.5	1.8(-9)	2.3(-7)	1.9(-7)	1.3(-20)	1.2(-9)
NH_2CHN	4.0	1.8(-10)	3.0(-9)	2.7(-8)	5.7(-10)	8.4(-9)
CH_2NNH	4.4	1.5(-10)	1.5(-8)	1.3(-8)	4.3(-22)	5.5(-11)
CHCHOH	5.4	1.8(-10)	5.2(-9)	2.7(-8)	1.3(-21)	8.5(-11)
NH_2CNH	4.4	2.5(-10)	2.2(-8)	2.3(-8)	3.9(-22)	1.7(-10)
CCH_2OH	5.4	4.5(-11)	1.2(-8)	9.2(-9)	4.2(-22)	2.7(-11)
CH_2CHO	4.9	3.6(-9)	5.8(-7)	5.0(-7)	1.8(-20)	1.5(-9)
CH_2COH	5.4	1.4(-8)	2.3(-7)	1.5(-7)	4.8(-21)	3.7(-10)
CHNHOH	5.1	8.3(-12)	1.0(-8)	6.8(-9)	9.3(-22)	5.8(-11)
HOCHNH	5.0	8.0(-10)	2.0(-7)	1.4(-7)	2.0(-8)	2.7(-8)
CH_3NO	4.8	2.2(-10)	1.4(-7)	9.2(-8)	1.3(-8)	9.9(-9)
CH_3ON	4.4	4.3(-11)	9.2(-8)	5.8(-9)	5.7(-20)	1.9(-11)
NCH_2OH	5.3	1.4(-11)	8.8(-8)	3.9(-9)	5.9(-22)	1.7(-11)
NH_2COH	5.2	8.5(-10)	1.0(-7)	9.1(-8)	8.5(-21)	4.5(-10)
NHNHOH	5.0	3.0(-12)	4.3(-8)	3.1(-9)	1.1(-21)	4.8(-11)
OCH_2OH	5.4	7.7(-11)	7.4(-8)	3.5(-8)	3.0(-20)	3.7(-10)
NH_2NOH	5.2	1.1(-10)	2.1(-8)	1.7(-8)	3.1(-21)	1.1(-10)
CH_3OO	4.7	5.7(-10)	3.1(-7)	1.9(-7)	4.0(-20)	5.8(-10)
$CH(OH)_2$	6.5	3.5(-11)	3.8(-8)	1.3(-8)	4.9(-21)	6.5(-11)
CH_2OOH	4.9	1.4(-9)	3.7(-7)	2.5(-7)	4.2(-20)	8.2(-10)
$NH(OH)_2$	6.5	2.2(-12)	1.0(-8)	5.0(-9)	1.8(-12)	5.7(-10)
NH_2OOH	4.7	5.7(-10)	2.8(-7)	1.9(-7)	3.1(-9)	4.0(-8)
$(HC_2)_2$	5.8	3.8(-10)	4.8(-8)	3.8(-8)	9.3(-10)	1.1(-8)
CCHCHO	5.3	4.6(-11)	9.8(-8)	5.8(-9)	1.3(-20)	9.7(-11)
HC_2CHO	5.9	1.1(-9)	2.6(-7)	1.8(-7)	3.3(-9)	5.7(-8)
HC_2COH	6.4	1.3(-10)	1.5(-8)	1.6(-8)	3.2(-20)	1.4(-10)
H_2CCCO	5.9	2.8(-10)	9.4(-8)	7.6(-8)	1.9(-9)	1.7(-8)
HCOCHN	5.3	1.4(-11)	3.9(-9)	2.8(-9)	1.7(-20)	6.4(-11)
HC_2NOH	5.9	7.1(-11)	1.1(-8)	9.0(-9)	3.7(-20)	1.1(-10)
NH_2CCO	5.7	1.1(-10)	2.1(-8)	2.2(-8)	9.7(-20)	5.4(-10)
CH_2CNO	5.4	1.7(-10)	2.2(-8)	2.0(-8)	9.5(-20)	3.5(-10)
HCOCOH	6.5	1.8(-10)	3.4(-8)	2.8(-8)	3.4(-19)	7.0(-10)
HC_2OOH	5.9	4.1(-10)	1.2(-7)	9.8(-8)	2.7(-9)	2.8(-8)
HOCHCO	7.0	4.3(-14)	1.0(-12)	4.3(-13)	4.8(-15)	1.7(-14)
$CHCO_2H$	5.9	1.1(-10)	1.8(-8)	1.2(-8)	9.3(-20)	1.9(-10)
NH_2CNO	5.7	7.6(-11)	1.9(-8)	1.9(-8)	8.6(-10)	1.4(-8)
CH_2NNO	5.9	5.0(-11)	1.3(-8)	1.1(-8)	6.5(-10)	5.1(-9)
ONCHNH	4.9	1.5(-10)	3.4(-8)	3.4(-8)	1.3(-9)	2.3(-8)
CH_2NO_2	6.9	2.2(-11)	1.2(-8)	6.6(-9)	1.8(-19)	2.3(-10)
HCONOH	6.6	1.1(-10)	2.8(-8)	1.9(-8)	3.6(-19)	5.4(-10)
$NHCO_2H$	5.8	4.0(-11)	7.2(-9)	5.5(-9)	9.8(-20)	1.7(-10)
NHOCHO	5.4	3.5(-11)	1.2(-8)	9.8(-9)	2.7(-19)	5.8(-10)
CH_2NOO	5.3	1.3(-10)	2.9(-8)	2.5(-8)	4.2(-19)	6.9(-10)
OOCHNH	4.8	3.9(-10)	8.7(-8)	7.2(-8)	1.1(-18)	2.2(-9)
CHOHNO	6.2	1.7(-11)	2.0(-8)	2.2(-9)	5.3(-10)	5.1(-9)
OOOCHO	6.6	1.1(-11)	1.2(-8)	1.0(-8)	4.6(-20)	5.5(-9)
NH_2NO_2	6.7	1.1(-11)	7.2(-9)	4.4(-9)	3.7(-12)	2.3(-9)
HOOCHO	6.0	6.1(-10)	2.9(-7)	2.2(-7)	5.1(-9)	9.5(-8)
H_2CO_3	6.1	4.5(-11)	2.9(-8)	1.5(-8)	9.9(-10)	5.1(-9)
NHOHNO	6.2	9.3(-13)	3.4(-8)	2.4(-9)	4.3(-10)	3.0(-8)
HOOCOH	6.5	5.9(-11)	2.3(-8)	1.4(-8)	5.7(-19)	4.0(-10)
OONHOH	5.2	2.4(-12)	5.5(-9)	6.4(-9)	7.3(-19)	5.9(-10)
HOONOH	6.0	3.0(-11)	1.5(-8)	9.3(-9)	5.5(-19)	2.6(-10)
HC_2CO	6.9	4.0(-11)	5.5(-8)	4.9(-9)	5.0(-19)	3.7(-10)
$(HO_2)_2$	6.0	4.6(-11)	3.7(-8)	2.3(-8)	1.9(-9)	1.2(-8)
HCOCCO	7.0	5.8(-11)	1.3(-8)	1.3(-8)	4.8(-18)	2.0(-9)
ONCHCO	6.9	1.3(-14)	3.3(-13)	2.0(-13)	3.7(-15)	1.8(-14)
HOOCCO	7.0	2.2(-11)	3.8(-8)	8.7(-9)	7.8(-18)	1.1(-9)
$ONCO_2H$	7.0	7.3(-12)	2.9(-8)	2.2(-9)	6.1(-18)	1.8(-9)
$HCONO_2$	8.0	1.6(-11)	1.3(-8)	8.7(-9)	1.8(-11)	1.5(-8)
$OOCO_2H$	7.0	1.9(-11)	7.5(-8)	5.8(-9)	5.8(-18)	1.7(-9)
$HOONO_2$	7.2	5.2(-15)	2.3(-13)	8.9(-14)	1.8(-15)	4.3(-15)
CH_2CH_2	4.2	1.9(-10)	4.1(-7)	1.9(-7)	0.0-	3.1(-11)
CH_2CCH_2	4.2	1.6(-10)	2.2(-7)	1.4(-7)	1.5(-9)	1.4(-8)
CH_2CHCH	4.8	2.7(-10)	1.5(-7)	1.1(-7)	8.5(-22)	2.3(-10)
CH_2CHC	5.0	2.0(-12)	8.5(-9)	2.8(-9)	2.7(-23)	3.7(-12)
CH_2CHNH	4.7	2.3(-10)	1.8(-7)	1.4(-7)	2.9(-21)	4.5(-10)
$CHCHNH_2$	4.7	1.2(-10)	7.7(-8)	7.0(-8)	1.5(-21)	3.1(-10)
CH_2NCH_2	5.0	4.5(-11)	4.1(-8)	2.3(-8)	5.1(-22)	8.0(-11)
CH_2CHN	4.3	6.0(-13)	3.0(-8)	1.2(-9)	4.1(-23)	2.3(-12)
CH_2CNH_2	4.7	1.4(-10)	1.0(-7)	9.8(-8)	1.8(-21)	3.1(-10)
CH_2NNH_2	4.9	2.0(-11)	3.0(-8)	2.4(-8)	5.8(-10)	5.5(-9)
CH_2CHOH	5.7	1.2(-10)	3.9(-7)	2.0(-7)	2.7(-9)	2.1(-8)
CH_3COH	5.7	1.8(-11)	4.6(-8)	2.0(-8)	1.0(-21)	2.6(-11)

NOTE. – E_{ads} is for bare silicate grains and is in units of kcal mole^{-1}. 1.0(-4) means 1.0×10^{-4}. Cloud I: [H(0)] = 10^4 cm^{-3}, $T_{gr} = T_k = 10°K$.
Cloud II: [H(0)] = 10^5 cm^{-3}, $T_{gr} = T_k = 10°K$. Cloud III: [H(0)] = 2×10^6 cm^{-3}, $T_{gr} = 10°K$, $T_k = 70°K$.

TABLE 3 – Continued

Species	E_{ads}	Cloud I $t=10^6$ yr	Cloud I $t=10^7$ yr	Cloud II $t=10^6$ yr	Cloud II $t=10^7$ yr	Cloud III $t=10^5$ yr
NH_2CHNH	4.9	1.0(-10)	1.3(-7)	1.3(-7)	1.8(-9)	4.0(-8)
CH_3OCH	4.7	4.3(-11)	5.4(-8)	3.2(-8)	2.0(-21)	6.8(-11)
$C(NH_2)_2$	4.4	3.0(-11)	2.1(-8)	2.2(-8)	1.2(-21)	1.9(-10)
$CHCH_2OH$	5.9	1.1(-11)	4.8(-8)	2.1(-8)	1.8(-21)	6.2(-11)
$NHCH_2OH$	5.5	3.9(-12)	2.2(-8)	1.0(-8)	2.4(-21)	5.3(-11)
NH_2CHOH	5.5	5.3(-11)	1.0(-7)	6.7(-8)	1.2(-20)	4.0(-10)
CH_2NHOH	5.6	8.2(-13)	1.3(-8)	7.7(-9)	1.7(-21)	4.8(-11)
CH_3NOH	5.3	5.1(-12)	1.8(-8)	7.7(-9)	9.1(-22)	1.2(-11)
CH_3ONH	4.6	1.2(-11)	2.3(-8)	1.4(-8)	2.4(-21)	5.3(-11)
NH_2NHOH	5.7	3.8(-13)	7.8(-9)	5.3(-9)	3.6(-10)	2.9(-9)
$CH_2(OH)_2$	7.0	2.7(-12)	4.3(-8)	1.5(-8)	2.8(-12)	6.3(-10)
CH_3OOH	5.2	3.6(-11)	2.5(-7)	1.1(-7)	2.0(-9)	5.8(-9)
CH_2CHC_2	5.9	3.2(-11)	2.8(-8)	2.3(-8)	2.5(-20)	2.3(-10)
CH_2CC_2H	5.9	4.2(-11)	2.3(-8)	1.8(-8)	1.8(-20)	1.5(-10)
HC_2CHNH	5.4	3.7(-11)	3.6(-8)	3.1(-8)	1.0(-9)	1.3(-8)
HC_2CNH_2	5.6	1.8(-11)	1.0(-8)	9.7(-9)	1.9(-20)	1.7(-10)
CH_2NC_2H	6.1	1.3(-11)	1.5(-8)	1.1(-8)	5.4(-10)	3.0(-9)
HC_2CHOH	6.7	4.1(-15)	2.4(-13)	5.3(-14)	4.0(-25)	1.6(-17)
CH_2CCHO	6.0	6.3(-11)	5.2(-8)	4.4(-8)	2.1(-19)	7.4(-10)
$CHCHCHO$	6.0	1.1(-11)	2.2(-8)	1.4(-8)	6.0(-20)	2.2(-10)
CH_3CCO	6.3	3.1(-12)	9.3(-9)	5.1(-9)	1.9(-20)	3.3(-11)
HC_2NHOH	6.7	1.5(-13)	2.3(-9)	1.4(-9)	1.7(-12)	3.6(-10)
$HCOCHNH$	6.2	6.0(-11)	8.8(-8)	8.0(-8)	2.8(-9)	4.5(-8)
CH_2NCHO	6.2	1.9(-11)	3.2(-8)	2.6(-8)	1.2(-9)	1.0(-8)
CH_2CHNO	6.1	2.9(-11)	5.5(-8)	4.5(-8)	1.7(-9)	1.7(-8)
NH_2CCHO	6.2	2.8(-11)	2.3(-8)	2.4(-8)	2.0(-19)	8.8(-10)
NH_2CHCO	6.2	1.4(-14)	1.5(-12)	1.2(-12)	1.1(-12)	2.9(-13)
CH_2CHOO	5.9	7.8(-11)	1.2(-7)	1.0(-17)	1.5(-18)	2.2(-9)
CH_2COOH	6.0	2.3(-11)	3.4(-8)	2.2(-8)	3.8(-19)	3.9(-10)
CH_2CO_2H	6.4	6.6(-12)	1.1(-8)	6.8(-9)	1.1(-19)	1.1(-10)
CH_2OCHO	6.1	9.7(-12)	5.2(-8)	2.6(-8)	1.8(-9)	1.4(-8)
$HOCHCHO$	7.0	6.4(-12)	3.3(-8)	1.6(-8)	4.7(-19)	5.0(-10)
$HCONHOH$	6.5	2.3(-13)	5.6(-9)	3.8(-9)	4.0(-12)	1.6(-9)
CH_3NO_2	7.4	2.3(-12)	1.1(-8)	6.4(-9)	4.1(-12)	8.9(-10)
$HOOCHNH$	5.5	2.0(-11)	4.7(-8)	3.6(-8)	1.8(-9)	1.9(-8)
CH_2NOOH	6.2	6.8(-12)	1.8(-8)	1.2(-8)	8.8(-10)	4.2(-9)
$HOCH_2NO$	6.8	7.3(-13)	9.6(-9)	4.6(-9)	3.9(-12)	8.5(-10)
NH_2CO_2H	5.6	4.9(-12)	1.3(-8)	9.3(-9)	7.1(-10)	5.1(-9)
NH_2OCHO	5.9	4.3(-12)	2.2(-8)	1.4(-8)	1.3(-9)	1.4(-8)
NH_2COOH	6.2	9.9(-12)	1.5(-8)	1.2(-8)	3.4(-19)	4.6(-10)
CH_3OOO	5.8	7.4(-12)	2.2(-8)	1.5(-8)	1.0(-18)	3.8(-10)
$HOOCHOH$	6.8	2.1(-15)	1.3(-13)	8.4(-15)	4.4(-26)	1.2(-17)
$OOCH_2OH$	6.7	1.9(-12)	2.6(-8)	1.3(-8)	1.2(-18)	4.8(-10)
$HOONHOH$	6.8	8.7(-14)	3.9(-9)	2.0(-9)	3.8(-12)	7.7(-10)
HC_2CHCO	7.4	3.0(-15)	2.3(-13)	1.3(-13)	2.2(-15)	7.4(-15)
$HCOCHCO$	7.5	4.2(-15)	3.3(-13)	1.8(-13)	3.3(-15)	9.6(-15)
HC_2OCHO	7.1	1.7(-12)	5.8(-9)	3.6(-9)	7.6(-12)	9.1(-9)
HC_2CO_2H	6.5	1.9(-12)	3.0(-9)	2.0(-9)	4.2(-12)	8.2(-10)
$ONCHCHO$	6.7	7.1(-13)	3.1(-9)	2.2(-9)	2.1(-18)	4.0(-10)
$(HCO)_2O$	7.2	2.5(-12)	1.4(-8)	9.6(-9)	2.1(-11)	1.5(-8)

Species	E_{ads}	Cloud I $t=10^6$ yr	Cloud I $t=10^7$ yr	Cloud II $t=10^6$ yr	Cloud II $t=10^7$ yr	Cloud III $t=10^5$ yr
$HOOCHCO$	7.5	1.6(-15)	1.8(-13)	7.7(-14)	1.7(-15)	4.4(-15)
$HCOCO_2H$	7.6	2.8(-12)	7.0(-9)	5.1(-9)	1.1(-11)	4.0(-9)
$HOOCO_2H$	7.6	1.0(-12)	4.7(-9)	2.7(-9)	1.0(-11)	2.0(-9)
$HOOOCHO$	7.2	8.2(-13)	7.3(-9)	4.6(-9)	1.9(-11)	7.5(-9)
CH_3CH_3	4.6	2.1(-12)	1.3(-7)	4.6(-8)	3.4(-10)	7.2(-10)
CH_3CHCH	5.3	4.9(-13)	1.7(-8)	6.7(-9)	1.3(-22)	8.5(-12)
CH_2CHCH_2	5.3	2.7(-11)	1.7(-7)	1.2(-7)	1.7(-21)	1.9(-10)
CH_2CCH_3	5.3	3.1(-12)	3.8(-8)	1.7(-8)	2.3(-22)	1.5(-11)
CH_2CHCH_3	5.8	6.3(-13)	7.6(-8)	3.0(-8)	6.9(-10)	1.6(-9)
CH_3CHNH	4.8	2.9(-12)	6.8(-8)	3.5(-8)	7.2(-10)	3.7(-9)
CH_2NCH_3	5.5	9.4(-13)	2.5(-8)	1.1(-8)	3.5(-10)	7.1(-10)
CH_3CNH_2	5.1	1.4(-12)	1.6(-8)	9.5(-9)	3.3(-22)	1.9(-11)
CH_3CHOH	6.1	1.9(-13)	1.8(-8)	5.5(-9)	5.4(-22)	9.2(-12)
$CH(NH_2)_2$	4.7	5.2(-12)	3.5(-8)	3.4(-8)	3.8(-21)	3.1(-10)
CH_3OCH_2	5.2	3.4(-12)	6.5(-8)	3.4(-8)	3.6(-21)	5.6(-11)
CH_2CH_2OH	6.4	6.9(-13)	3.6(-8)	1.4(-8)	2.3(-21)	3.5(-11)
CH_3ONH_2	5.1	1.6(-12)	4.2(-8)	2.6(-8)	7.8(-10)	4.0(-9)
CH_3NHOH	6.1	1.8(-14)	7.1(-9)	2.8(-9)	2.3(-10)	3.5(-10)
NH_2CH_2OH	6.0	5.0(-13)	4.0(-8)	1.7(-8)	7.0(-10)	3.5(-9)
CH_2CHC_2H	6.4	4.6(-12)	2.5(-8)	1.8(-8)	3.8(-12)	1.6(-9)
HC_2CHNH_2	6.6	4.9(-16)	1.7(-13)	7.7(-14)	4.5(-26)	3.1(-17)
HC_2CH_2OH	7.2	1.9(-13)	9.8(-9)	4.1(-9)	2.7(-12)	4.9(-10)
CH_2CHCOH	7.0	1.5(-12)	1.3(-8)	7.7(-9)	8.7(-20)	1.0(-10)
CH_3OC_2H	6.3	6.0(-13)	1.1(-8)	5.7(-9)	2.7(-12)	4.3(-10)
CH_3CHCO	6.8	3.2(-16)	9.6(-14)	3.5(-14)	5.1(-15)	7.5(-15)
NH_2CHCHO	6.0	5.3(-12)	4.8(-8)	4.5(-8)	6.7(-19)	1.7(-9)
CH_3CHNO	6.3	3.5(-14)	2.6(-8)	1.1(-9)	2.1(-20)	1.5(-11)
$HOCH_2CHO$	7.4	2.9(-13)	2.4(-8)	1.1(-8)	6.6(-12)	1.8(-9)
CH_2CHOOH	6.5	2.5(-12)	4.2(-8)	2.5(-8)	8.6(-12)	3.3(-9)
NH_2CHOOH	6.0	5.9(-16)	1.3(-13)	5.4(-14)	3.8(-25)	2.1(-17)
CH_3OOOH	6.4	3.1(-13)	1.4(-8)	7.0(-9)	6.0(-12)	8.5(-10)
$HOOCH_2OH$	7.3	1.1(-13)	1.0(-8)	5.5(-9)	6.3(-12)	8.0(-10)
HC_2CHCHO	7.4	1.9(-13)	3.1(-9)	2.0(-9)	5.3(-19)	1.6(-10)
$CH(CHO)_2$	7.3	2.8(-13)	7.7(-9)	5.3(-9)	4.9(-18)	9.1(-10)
$ONCH_2CHO$	7.3	6.5(-17)	2.2(-14)	6.3(-15)	2.0(-16)	2.0(-16)
$HOOCHCHO$	7.3	1.0(-13)	5.3(-9)	2.8(-9)	7.8(-18)	5.0(-10)
CH_3CHNH_2	5.2	2.2(-14)	8.8(-9)	3.5(-9)	3.5(-22)	8.5(-12)
$CH_2(NH_2)_2$	5.3	5.2(-16)	7.9(-13)	5.8(-13)	5.0(-13)	1.4(-13)
CH_3CHC_2H	6.5	9.6(-15)	2.7(-9)	1.0(-9)	4.1(-21)	5.8(-12)
CH_2NCHCH_2	6.7	8.7(-14)	5.6(-9)	3.5(-9)	2.1(-12)	3.1(-10)
$HC_2CH_2NH_2$	6.5	4.6(-20)	2.8(-15)	7.6(-17)	5.8(-18)	3.6(-16)
$CH_2CHCHOH$	7.2	3.4(-17)	3.1(-14)	1.2(-15)	1.5(-27)	5.9(-19)
CH_3CHCHO	6.6	2.9(-14)	1.2(-8)	4.6(-9)	7.0(-20)	4.7(-11)
NH_2CH_2CHO	6.6	4.7(-18)	5.0(-13)	3.3(-13)	4.0(-15)	2.4(-14)
CH_3CH_2NO	6.5	3.1(-18)	7.0(-15)	1.1(-15)	3.7(-17)	1.3(-17)
CH_3CHOOH	6.6	5.4(-15)	4.5(-9)	1.5(-9)	8.5(-20)	1.7(-11)
NH_2CH_2OOH	6.6	4.9(-20)	1.8(-16)	9.6(-17)	7.9(-18)	3.1(-15)
HC_2CH_2CHO	7.8	1.5(-17)	1.7(-14)	4.2(-15)	1.3(-16)	8.3(-17)
$CH_2(CHO)_2$	7.9	2.3(-17)	2.7(-14)	6.7(-15)	2.1(-16)	1.3(-16)
$CH_2CHOCHO$	7.7	1.9(-14)	5.3(-9)	3.0(-9)	9.5(-12)	2.1(-8)

Species	E_{ads}	Cloud I $t=10^6$ yr	Cloud I $t=10^7$ yr	Cloud II $t=10^6$ yr	Cloud II $t=10^7$ yr	Cloud III $t=10^5$ yr
CH_2CHCO_2H	8.1	2.2(-14)	2.7(-9)	1.3(-9)	5.2(-12)	5.0(-10)
$HOOCH_2CHO$	7.9	8.1(-15)	1.3(-14)	2.3(-15)	1.1(-16)	5.1(-17)
CH_3CHCH_3	5.9	1.1(-15)	7.2(-9)	1.8(-9)	9.4(-23)	7.9(-13)
$CH_3CH_2NH_2$	5.8	1.9(-16)	4.1(-14)	5.4(-15)	4.9(-15)	8.9(-17)
$CH_3CH_2C_2H$	7.0	7.9(-16)	4.4(-15)	7.6(-16)	2.4(-17)	4.8(-18)
CH_2CHCH_2OH	6.1	2.7(-21)	1.7(-17)	2.1(-18)	7.0(-12)	7.2(-20)
CH_3CH_2CHO	7.1	2.3(-16)	1.5(-14)	2.3(-15)	8.4(-17)	1.5(-17)
CH_2CHOCH_3	6.9	7.5(-15)	9.8(-8)	4.5(-9)	3.3(-12)	2.8(-10)
CH_3CH_2OOH	7.1	4.1(-17)	3.5(-15)	4.8(-15)	2.2(-17)	3.2(-18)
$CH_3CH_2CH_3$	6.4	8.2(-23)	5.1(-15)	5.8(-16)	1.5(-17)	2.4(-16)

ages of dark clouds seem to be between 10^6 and 10^7 years (Paper II), the normalized abundances $[X(t)]/[H_2(t)]$ of all of the species at these two cloud ages are listed in tables 2 and 3 for the two low temperature ($T_k = 10°K$) calculations. (Molecules are ordered by the number of constituent atoms, and then by mass). The ages of the very dense giant clouds are probably significantly shorter than those of dark clouds; one estimate for the Orion optical nebula is $\lesssim 10^6$ yr (Balick, Gammon, and Hjellming 1974). Likewise the chemistry timescales are much shorter than before, so the data for 10^5 yr is reported in tables 2 and 3 for the $T_k = 70°K$ calculation.

To facilitate comparison between the results of the surface reaction model proposed in this paper and the results of other theoretical interstellar chemical models, data from these other studies are reported in table 2. Every model is labelled with the appropriate physical parameters so that intercomparison between data for basically the same type of region can be made. (A_V is the visual extinction through the whole cloud and ζ is the ionization rate.) Observational results are listed in the last few columns of table 2 to provide a basic test of all the theories. Since all observational reports are not in the normalized abundance form directly compatible with the table, any data or analyses of data that were already in such a form were used directly. Otherwise the astronomical data were modified accordingly, using the necessary physical parameters. The physical parameters for each region were adopted as a consensus of the various literature values and listed at the top of each column.

In addition to all the errors that may have been introduced into the calculation by the assumptions incorporated into the chemical model, the uncertainties in the numbers reported in tables 2 and 3 cannot be safely said to be less than a factor of five, just because of the numerical simplifications adopted to expedite the execution of the computer program. If the electronic configuration of certain species or the products of certain reaction channels were inaccurately estimated, species may have been included in the reaction model which should not be there. This does not introduce much error since elimination of particular species only results in the abundance being distributed over related molecules. Furthermore, because H atoms are the most abundant reactive species, the reaction rate of a complicated free radical is relatively insensitive to the concentrations of other complicated molecules.

One systematic factor that might affect the theoretical rates involves the growth of grain mantles and the resulting change in grain-gas collision rates. Such an effect has been ignored and Paper II presents a rationale for why it seems reasonable to do so. More important is another assumption--that the surface formation rates reflect only the gas-phase abundances. The formation and retention of reactive species on grains larger than the maximum effective formation radius has been ignored up to now. How this might affect the reaction rates is unclear. Another reactive species could come along, react with the trapped molecule, and add to the gas-phase abundance of the product at an enhanced rate. On the other hand, the product could also be trapped on the surface, reducing the probability that the second reactant could

be involved in some other more "successful" reaction. It should also be noted that the results are relatively insensitive to the grain size distribution as long as the fractional grain area function F(r),

$$F(r) = \int_0^r n(r)\, r^2\, dr \Big/ \int_0^\infty n(r)\, r^2\, dr \,, \qquad (16)$$

remains relatively constant (Paper II).

The most significant factor that could appreciably alter the calculated abundances involves the assumed radiation density in the bulk of the cloud. Because of the photodissociation calculations of Stief et al. (1972), it has been generally thought that throughout the cloud interior the lifetimes of complicated molecules against photodegradation is about equal to the lifetime of the cloud (in the case of sturdy molecules like CO, the photodegradation lifetime is even longer). Recently, Whitworth (1975) has suggested that a consequence of the measured high albedo and forward scattering nature of interstellar grains at ultraviolet wavelengths (Witt and Lillie 1973) is a significant increase in UV radiation density in dark cloud interiors, possibly by more than a factor of 100 over what previously had been assumed. Then the molecular lifetimes against photodegradation are fairly short (Sandell and Mattila 1975), less than the lifetimes of Stief et al. by factors of 10^3 to 10^5. As a test, the Sandell and Mattila lifetimes for high extinction (A_V = 8 mag) and isotropic scattering (forward scattering decreases the lifetimes further) were included in the calculations. As expected, the abundances were generally suppressed by many orders of magnitude; in essence the molecules were being destroyed almost

faster than they could be formed. In fact, all the theoretical chemical models would suffer this fate. Since complex molecules are seen in interstellar clouds, one might conclude that the theoretical models presented to date are not as efficient as the actual chemical processes. On the other hand, the real UV radiation field in cloud interiors may be more like that used by Stief et al. due to an incorrect interpretation of interstellar grain properties or to significant self-shielding by gas-phase species, something not considered by Sandell and Mattila.

IV. DISCUSSION

Several general conclusions may be drawn from an initial examination of figures 1-3 and tables 2 and 3. First, there exist a sufficient number of small grains to furnish enough effective reaction area to result in reasonable formation rates. Second, no external energy inputs (radiation, cloud-cloud collisions, etc.) are needed to trigger molecule production. Third, the results clearly suggest that, on astrophysically reasonable timescales, interstellar chemistry is not at steady-state; abundances are functions of cloud age, density, and temperature. Fourth, contributing to the dynamic nature of cloud chemistry is depletion of gas-phase species on grains, something that cannot be ignored by theories attempting to model reasonably old clouds. Fifth, dark clouds are predicted to be rich in complex molecules, detection being limited by the column density and excitation conditions.

a) Comparison Between the Various Theoretical Models and Observations

Before making a detailed comparison between predicted and observed abundances, one should note that the reported abundances derived from observations may have large errors if the excitation of interstellar molecules is determined inaccurately. For example, consider how one set of spectra lines has given rise to estimates of the normalized abundance of HCN in Ori A ranging over several orders of magnitude (1×10^{-9} [Gottlieb et al. 1975] versus 3×10^{-8} - 1×10^{-5} [Kwan and Scoville 1975]).

Although the chemical model was designed for dark clouds, the physical conditions of Sgr B2 seem to be reasonably matched by the conditions of the $[H(0)] = 10^5$ cm^{-3} calculation. Likewise the Ori A conditions can be well fitted by the $[H(0)] = 2 \times 10^6$ cm^{-3} calculation. If one makes a molecule-by-molecule comparison between the theoretical results of this paper and observations and allows age to be a relatively free parameter, one finds that the predictions of the ab initio surface reaction model match observation surprisingly well. In the case of some of the lighter unreactive molecules, the predicted abundances appear to be systematically too high, which can be easily attributed to an underestimate of their grain interaction energies which would result in an overestimate of their effective formation rate and an underestimate of their effective depletion rate. There are many other variables associated with the efficiency of every reaction which could be rationally modified to enhance agreement between theory and observations when the situation warrants it--when abundances can be derived more accurately from observations.

One molecule that should be considered in particular is carbon monoxide, the second most abundant interstellar molecule that has been observed. The CO predictions of the reaction model of this paper provide an important test of the general validity of the model. Until recently, it has been thought that almost all of the carbon in a given region is in CO. This has been adopted as a boundary condition in several chemical models, including that of Herbst and Klemperer (1973). However, upon further observation and analysis, several investigators have suggested that only a tenth of the carbon may be in CO (e.g.,

Scoville, Solomon, and Penzias 1975 and Dickman 1975). In good agreement with these recent ideas is the ab initio model prediction that only 20-30 percent of the carbon is in CO under widely varying conditions (cf. table 2).

It is also interesting to compare the results of this model with some of the abundance ratios of complex molecules reported in the literature and thought to be unexplainable in terms of theoretical models. Among other reasons, ratios might be more valid than the raw normalized abundances of both theory and observations since systematic effects may cancel out. The theoretical values of the [CH]/[OH] ratio decrease from low density clouds ($\sim$ .75-2) to higher density clouds ($\sim$ .3-1) in agreement with the general trends reported by Rydbeck et al. (1975). In fact, the theoretical ratio is sensitive to cloud age, giving some support to their suggestion that the scatter in their data (greatest for the less dense regions) results from varying cloud age. Turner and Gammon (1975) find CN anomalously underabundant compare to HCN and CH_3CN. Again this situation occurs naturally in the present model and the relative CN depletion increases with cloud age. In the context of simple chemical models, the observed $[NH_2CHO]$ / $[NH_2CN]$ ratio of $\sim$10 surprises Turner et al. (1975). But again the present model is in good agreement with his observations, predicting a relatively time-insensitive value of $\sim$5 for $[H_2] \simeq 10^5$ cm^{-3} (approximately the density of Sgr B2).

It is valuable at this point to compare the predictions of other chemical models with the observational data in order to determine the relative merit of the different approaches. The abundances derived by

Iguchi (1975) generally do bracket the observations of regions for which his model is relevant--the hotter molecular clouds of Sgr B2 and Ori A. At low temperatures of dark clouds, the chemisorption model would suppress all reactions. On the other hand, the Watson and Salpeter (1972b) calculations are limited to regions with moderately high UV radiation densities, basically applicable only to the lower density dark clouds and the peripheral regions of the giant molecule clouds. However, if the UV radiation penetrates as deeply into the cloud as Whitworth (1975) suggests, their model will have wider utility. Their results do not compare as favorably with observations as the other surface models, but many of the parameters they needed had to be so roughly estimated that their predictions could err by several orders of magnitude. Lastly, the applicability of the gas-phase model of Herbst and Klemperer (1973) is limited to regions of moderately high ionization--which may include everywhere. Within the uncertainties of their calculations, their results for the simpler molecules agree with the observational data. Unfortunately, processes leading to the most complicated molecules are not included in their model, preventing a more extensive comparison.

Since interstellar molecular ions have been observed in certain regions, it is clear that ion-molecule reactions are important elements of the chemistry in those regions. However, all indications are that molecular hydrogen is the most abundant species in these areas, indicating that surface reactions are occurring concurrently. Because all of the theoretical models are in general agreement with observations, one cannot easily distinguish between the various proposals when it

comes to formation of neutral molecules. In fact, what is probably the case is that many of the different processes are occurring simultaneously. With better knowledge of the physical conditions of interstellar regions and with more extensive observations, the differences among the models will become significant.

There are several consequences of the surface formation model proposed in this paper that may be used in the future to distinguish it from other chemical models. The predicted presence of a large number of exotic radical and non-radical molecules and the time dependence of the abundances eventually should be able to be verified observationally. This will prove to be especially valuable when the other proposed interstellar chemical models are extended to include more molecules in a time-dependent framework. A further result that could clarify the relative importance of the surface processes of this paper is the need for reactive surface area to be provided by small grains, especially in the case of large molecule synthesis. If this were true, there should be an observable inverse relationship between R_V (the ratio of total to selective extinction) and the abundances of large molecules, because an increase in R_V means a decrease in the fraction of the total grain surface area contributed by small grains. Due to uncertainties about the correct values of R_V for different regions, it is not yet possible to discover any correlation.

b) Various Chemical Processes and Their Effects on Abundances

The molecules whose time-varying abundances are displayed in figures 1-3 seem to be grouped into three categories, the characteristic

trend of each category reflecting the net effect of the special processes particularly affecting the member molecules. In Group 1 are the lighter nonreactive species whose abundances peak early at relatively high values due to the high concentrations of their precursors. Furthermore, as the cloud ages and all the grains become coated with H_2, Group 1 molecules are less able to be effectively depleted onto the grains due to their low adsorption energy on solid H_2. As a result, their abundances remain relatively constant at high levels. In Group 2 are the heavier nonreactive species that peak in abundance at later times than those of Group 1 (their precursors are less abundant). Also, Group 2 molecules eventually become significantly, if not totally, depleted onto the grains because their adsorption energy on solid H_2 is appreciable. Finally, Group 3 is composed of the reactive species, whose abundances and timescales for reaching peak abundances vary according to the concentrations of their precursors. Since it has been assumed that every reactive species colliding with a grain is involved in a further reaction, Group 3 molecules ultimately become totally depleted in old clouds. In the cases of Groups 2 and 3, the time-varying abundances rise and then decline because the development of each species reaches a point at which the molecules are being depleted faster than they are being formed and ejected to the gas phase. The time-dependent abundance patterns of the molecules not in figures 1-3 also fall into one of these general categories.

Another way of reviewing the physics and chemistry determining the molecular abundance results of this paper is by considering the factors that affect the concentration of CO relative to OH. Indeed,

a recurring theme in Papers I and II is the nature of the possible processes that could result in the observed overabundance of CO relative to OH, with respect to the cosmic abundances of the constituent atoms. Since the general surface reaction model of this paper does result in approximately the same overabundance as observed, some, or all, of the physical and chemical processes incorporated into the model may be fundamentally important for interstellar chemistry.

Since CO is a Group 1 molecule and OH belongs to Group 2, the CO/OH abundance ratio should increase with time in old clouds. Interestingly, Winnewisser, Mezger, and Breuer (1974) and others have commented upon the observed underabundance of free radicals and suggest that this is due to their high reactivity. Moreover, Rank, Townes, and Welch (1971) suggest the need for reemission from grains as a way of maintaining high abundances over the cloud lifetime.

The higher adsorption energy of OH versus CO and the larger heat of formation of CO, since it has a triple bond, result in a significantly larger effective formation surface area for CO. It is interesting that Turner (1974b) suggests that the high abundances of unsaturated molecules reflects chemistry occurring at high temperatures, for indeed, the formation of multiple bonds results in hotter grains (and larger desorption rates) in the present model.

The [CO]/[OH] ratio is also enhanced by the rapid conversion of hydrogen atoms to hydrogen molecules, thus reducing the [H]/[C] ratio and allowing C to compete for O more effectively [somewhat akin to an idea of Duley (1970)]. The probable presence of mainly H_2-mantles on the larger grains presents the possibility not considered by

others that reactions with hydrogen atoms cannot occur over a significant fraction of the total grain surface area, further reducing the OH formation rate relative to the CO rate. Lastly, it has been suggested by many authors (for example, Turner 1974b) that presence of UV radiation will result in the selective destruction of weakly bonded molecules. This effect has not been included in the calculations, but would also result in increasing the [CO]/[OH] ratio since the CO bond strength is over twice that of OH.

Although many of the empirical deductions about interstellar chemistry that are in the literature find theoretical support in this model, several suggestions are contradicted. (1) The inability to detect molecules with nitrogen-oxygen bonds (for example, NO, HNO, HNO_2, HNO_3, N_2O) has led to the suggestion that something special is occurring to hinder their formation (Solomon 1973; Iguchi 1975). However, table 2 shows that the detection problem simply may be due to low observational sensitivity since the predicted abundances of molecules containing NO bonds are not inconsistent with the upper limits derived from astronomical data. (2) Fertel and Turner (1975) suggest that their inability to detect several cyclic compounds reflects on the type of interstellar chemistry that is important. They conclude that surface chemistry is not. Unfortunately their observational limits are not very sensitive. Many of the more complex molecules have predicted abundances less than their upper limits for the rather large ring molecules. Moreover, although cyclic molecules were not included in the reaction set of this paper, the products of certain reactions might have as easily been chosen to be ring compounds. Actually, cyclization in the gas-

phase is not impossible, so judgement ought to be reserved on this question. (3) The proposal that families of unreactive molecules, one such being HC_2CN, CH_2CHCN, and CH_3CH_2CN (for other examples, see table 9.5 of Turner 1974b), result from successive reactions (e.g., Morris et al. 1976) is not consistent with possible neutral-neutral reactions at low temperatures. The observations are well fit by the present surface reaction model which has related molecules being formed in parallel reaction sequences rather than being produced directly from each other.

c) Grain Mantle Composition

An integral part of any surface chemistry model is the nature of the grains on which the reactions are occurring. In the model proposed in this paper, the grains were divided into two groups: bare silicate and silicate with H_2 mantles. Even though other molecules will accumulate on the grains as the cloud ages, it was shown that the surface adsorption energies will remain relatively unchanged and the chemistry will be unaffected.

However, the exact nature of the grain mantles will affect the optical transmission properties of the dust cloud. To fit the interstellar extinction curve, Greenberg and Hong (1974) derive a bimodal grain distribution which consists of silicate cores with ice mantles, total radius ~ 800Å, to account for the visible extinction and bare silicate grains with radii of ~ 100Å to account for the UV extinction. The icy nature of the mantle composition seems to be an obvious consequence of the depletion of cosmically abundant elements onto grains and is

supported by the observation of a 3 μ absorption band in the infrared spectra of the BN object in Orion (Gillett and Forrest 1973) and other sources (Cohen 1975, 1976; Merrill, Russell, and Soifer 1975). This band matches to a limited degree the predictions of Mie scattering calculations using water ice constants (Cohen 1975, 1976).

It is interesting to compare this picture of interstellar grains to that derived from the surface reaction model under consideration. Table 4 shows the radius-dependent grain composition for a three million year-old dark cloud with $[H + 2H_2] \simeq 10^4$ cm^{-3} and $T_{gr} = T_k =$ 10° K. The variation of composition with radius results from the variation of the effective formation radius limits and the effective depletion radius limits for the different species on the two different basic types of surfaces. Notice that the grain composition suggested here is more complex than that proposed in Papers I and II. In this model, the grain composition is strongly time-dependent. If the 3 μ band is due to mantle absorption, wide variation in the 3 μ band should be seen among sources with different ages. Moreover, 3 μ absorption variation associated with $\mathcal{R}_V$ should also be observable. Tarafdar and Wickramasinghe (1975) have raised the possibility that the astronomical 3 μ band might be due to absorption by simple hydrocarbons which have strong vibrational bands in this region. Also table 4 indicates that many grains are covered with a variety of large organic molecules, many of which also have vibrational bands at 3 μ (Silverstein and Bassler 1967), but are not covered with lighter molecules like H_2O. This all suggests that the observed 3 μ band might have contributions

TABLE 4

SIZE DEPENDENCE OF GRAIN COMPOSITION IN A DARK CLOUD*

Approximate Radius Range (Å)	Composition
0 - 40	Bare silicate grains
40 - 100	Silicate grains with very thin mantles composed of large molecules
100 - 380	Silicate grains with mantles composed of large and small molecules
380 - 700	Silicate grains with pure H_2 mantles
700 - 3000	Silicate grains with mantles composed of large molecules in an H_2 matrix
3000 - ∞	Silicate grains with mantles composed of large and small molecules in an H_2 matrix

* Cloud age = 3×10^6 yr, $[H + 2H_2] \simeq 10^4 cm^{-3}$, $T_{gr} = 10°K$

from many different species, thus possibly explaining why analyses with Mie theory using H_2O ice constants do not match observed 3 μ bands well (Merrill, Russell, and Soifer 1975). Low temperature laboratory spectroscopy studies of condensed phases of different composition are needed to clarify this point.

Finally, the preponderance of molecular hydrogen in grain mantles is a conclusion unique to the present model and is very important to the chemical development of a cloud as outlined in this paper. In addition to the other consequences that have been discussed previously, a result of H_2 mantles on large grains is the increase in effective surface area for the formation of complex molecules due to their shorter adsorbed lifetimes on solid H_2. The calculated abundances would be significantly lower if the basic mantle composition were predominantly ice.

V. CONCLUSIONS

A time-dependent ab initio interstellar chemical model incorporating grain surface reactions is shown to produce molecular abundances consistent with observations of a variety of astronomical environments. Unlike other published chemical models, the heat released upon molecule bond formation is utilized to enable efficient molecule synthesis even under conditions of low temperatures and a negligible radiation field. As a result, dark clouds are predicted to be rich in complex molecules. The computations of other chemical models were performed assuming the clouds are in a steady-state. However, the present time-dependent analysis suggests that this is not true, for depletion on grains is important in old clouds. Thus the observed abundances reflect cloud age, density, and temperature. The surface reaction timescales are astrophysically relevant and are similar to those for gas-phase ion-molecule reactions, suggesting a coupling between the two reaction schemes. When the amount and accuracy of observational results increase and when the various gas-grain interactions and surface reaction rates are better known, it will be worth doing a full-scale dynamic interstellar reaction model, which includes both gas-phase and surface reactions.

A unique result of the surface reaction model is the suggestion that grain mantles are predominantly molecular hydrogen. The chemical consequences of a mantle composition of this nature are significant. On the other hand, the other molecular constituents of the mantles will affect the optical properties of the grains. Since large

molecules, some of which having vibrational bands around 3 μ, are an important fraction of many grain mantles, it is possible that the observed astronomical 3 μ band may have contributions from species other than H_2O. The exact mantle composition is suggested to be a strong function of grain size and cloud age, suggesting variations in the infrared absorption that may be observed and providing possible explanations for those that have been seen.

We thank J. Berg, S. Cunningham, W. Goddard III, T. Kuiper, M. Morris, W. Weinberg, and M. Werner for their help during the preparation of this paper. This work was supported by a National Science Foundation grant (MPS73-05140).

REFERENCES

Aannestad, P. A. 1973a, Ap. J. Suppl., 25, 205.

_____. 1973b, Ap. J. Suppl., 25, 223.

Allen, M. A. 1976, unpublished Ph.D. thesis, California Institute of Technology, Pasadena (Chapter 4).

Allen, M., and Robinson, G. W. 1975, Ap. J., 195, 81 (Paper I; also Chapter 1 of this thesis).

_____. 1976, Ap. J., in press (Paper II; also Chapter 2 of this thesis).

Augason, G. C. 1970, Ap. J., 162, 463.

Avgul, N. N., and Kiselev, A. V. 1970, in Chemistry and Physics of Carbon, Vol. 6, ed. P. L. Walker (New York: Marcel Dekker), p. 1.

Balick, B., Gammon, R. H., and Hjellming, R. M. 1974, Pub. Astron. Soc. Pacific, 86, 616.

Batchelor, R. A., Brooks, J. W., Godfrey, P. D., and Brown, R. D. 1973, Aust. J. Phys., 26, 557.

Benson, S. W. 1965, J. Chem. Ed., 42, 502.

Brandshaft, D., McLaren, R. A., and Werner, M. W. 1975, Ap. J. (Letters), 199, L115.

Brown, R. D. 1974, in IAU Symposium, No. 60, Galactic Radio Astronomy, ed. F. J. Kerr and S. C. Simonson (Dordrecht: Reidel), p. 155.

Buhl, D., Snyder, L. E., Schwartz, P. R., and Edrich, J. 1973, Nature, 243, 513.

Cameron, A. G. W. 1973, Space Sci. Rev., 15, 121.

Cheung, A. C., Chui, M. F., Matsakis, D., and Townes, C. H. 1974, Quarterly Summary of Radio Telescope Observations, January 1974, 26.

Churchwell, E., and Winnewisser, G. 1975, Astr. and Ap., 45, 229.

Clark, F. O., and Johnson, D. R. 1975, Quarterly Summary of Radio Telescope Observations, January 1975, 5.

Clark, F. O., Lovas, F. J., and Johnson, D. R. 1975, Quarterly Summary of Radio Telescope Observations, January 1975, 11.

Cohen, M. 1975, M.N.R.A.S., 173, 279.

_____. 1976, Ap. J., 203, 169.

Darwent, B. de B. 1970, NSRDS-NBS 31 (Washington: U.S. Government Printing Office).

Dean, J. A., ed. 1973, Lange's Handbook of Chemistry (11th ed.; New York: McGraw-Hill).

Dickman, R. L. 1975, Ap. J., 202, 50.

Duley, W. W. 1970, R.A.S.C. Jour., 64, 331.

Fertel, J. H., and Turner, B. E. 1975, Ap. Lett., 16, 61.

Fourikis, N., Sinclair, M. W., Brown, R. D., Crofts, J. G., and Godfrey, P. D. 1974a, Ap. J., 194, 41.

Fourikis, N., Sinclair, M. W., Robinson, B. J., Godfrey, P. D., and Brown, R. D. 1974b, Aust. J. Phys., 27, 425.

Gardner, F. F., and Winnewisser, G. 1975, Ap. J. (Letters), 195, L127.

Giguere, P. T., Clark, F. O., Snyder, L. E., Buhl, D., Johnson, D. R., and Lovas F. J. 1973, Ap. J., 182, 477.

Gillett, F. C., and Forrest, W. J. 1973, Ap. J., 179, 483.

Godfrey, P. D., Brown, R. D., Robinson, B. J., and Sinclair, M. W. 1973, Ap. Lett., 13, 119.

Gottlieb, C. A., Lada, C. J., Gottlieb, E. W., Lilley, A. E., and Litvak, M. M. 1975, Ap. J., 202, 655.

Gottlieb, C. A., Palmer, P., Rickard, L. J., and Zuckerman, B. 1973, Ap. J., 182, 699.

Greenberg, J. M., and Hong, S. S. 1974, in IAU Symposium, No. 60, Galactic Radio Astronomy, ed. F. J. Kerr and S. C. Simonson (Dordrecht: D. Reidel), p. 155.

Griller, D., and Ingold, K. U. 1976, Accts. Chem. Res., 9, 13.

Herbst, E., and Klemperer, W. 1973, Ap. J., 185, 505.

Hobson, J. P. 1967, in The Solid-Gas Interface, Vol. 1, ed. E. A. Flood (New York: Marcel Dekker), p. 447.

Hollenbach, D., and Salpeter, E. E. 1970, J. Chem. Phys., 53, 79.

Iguchi, T. 1975, Publ. Astron. Soc. Japan, 27, 515.

JANAF Thermochemical Tables. 1971, NSRDS-NBS-37 (Washington: U.S. Government Printing Office).

_____. 1974, J. Phys. Chem. Ref. Data, 3, 311.

_____. 1975, J. Phys. Chem. Ref. Data, 4, 1.

Kaifu, N., Takagi, K., and Kojima, T. 1975, Ap. J. (Letters), 198, L85.

Kerr, J. A. 1973, in Free Radicals, Vol. 1, ed. J. K. Kochi (New York: Wiley-Interscience), p. 1.

Kwan, J., and Scoville, N. 1975, Ap. J. (Letters), 195, L85.

Langer, W. D., and Glassgold, A. E. 1976, Astr. and Ap., in press.

March, J. 1968, Advanced Organic Chemistry: Reactions, Mechanisms, and Structure (New York: McGraw-Hill).

Merrill, K. M., Russell, R. W., and Soifer, B. T. 1975, Bull. AAS, 7, 429.

Metz, W. D. 1973, Science, 182, 467.

Millar, T. J., and Williams, D. A. 1975, M.N.R.A.S., 173, 527.

Morris, M., Turner, B. E., Palmer, P., and Zuckerman, B. 1976, Ap. J., in press.

Pelling, M. 1975, M.N.R.A.S., 172, 41.

Rank, D. M., Townes, C. H., and Welch, W. J. 1971, Science, 174, 1083.

Reiter, E. R., Bauer, E., and Coroniti, S. C., ed. 1975, The Natural Stratosphere of 1974, CIAP Monograph 1 (Washington: U.S. Department of Transportation).

Righini, G., Simon, M., Joyce, R. R., and Gezari, D. Y. 1975, Ap. J. (Letters), 195, L77.

Roberts, J. D., and Caserio, M. C. 1964, Basic Principles of Organic Chemistry (New York: W. A. Benjamin).

Rydbeck, O. E. H., Kollberg, E., Hjalmarson, Å., Sume, A., Elldér, J., and Irvine, W. M. 1975, Res. Rept. No. 120, Res. Lab. of Electronics and Onsala Space Observatory, Chalmers University of Technology, Gothenburg.

Sandell, G., and Mattila, K. 1975, Astr. and Ap., 42, 357.

Scoville, N. Z., Solomon, P. M., and Penzias, A. A. 1975, Ap. J., 201, 352.

Silverstein, R. M., and Bassler, G. C. 1967, Spectrometric Identification of Organic Compounds (2d ed.; New York: John Wiley and Sons).

Snyder, L. E., and Buhl, D. 1973, Nature Phys. Sci., 243, 45.

Snyder, L. E., Buhl, D., Schwartz, P. R., Clark, F. O., Johnson, D. R., Lovas, F. J., and Giguere, P. T. 1974, Ap. J. (Letters), 191, L79.

Solomon, P. M. 1973, Phys. Today, 26, 32.

Steele, W. A. 1974, The Interaction of Gases with Solid Surfaces (Oxford: Pergamon Press).

Stief, L. J., Donn, B., Glicker, S., Gentieu, E. P., and Mentall, J. E. 1972, Ap. J., 171, 21.

Tarafdar, S. P., and Wickramasinghe, N. C. 1975, Ap. and Space Sci., 35, L41.

Tsuji, T. 1964, Ann. Tokyo. Astron. Obs., 2d. ser. 9, 1.

_____. 1973, Astr. and Ap., 23, 411.

Turner, B. E. 1974a, R.A.S.C. Jour., 68, 55.

_____. 1974b, in Galactic and Extra-Galactic Radio Astronomy, ed. G. L. Verschuur and K. I. Kellerman (New York: Springer-Verlag), p. 199.

Turner, B. E., and Gammon, R. H. 1975, Ap. J., 198, 71.

Turner, B. E., Kislyakov, A. G., Liszt, H. S., and Kaifu, N. 1975, Ap. J. (Letters), 201, L149.

Turner, B. E., and Thaddeus, P. 1976, in preparation.

Watson, W. D. 1975, in Atomic and Molecular Physics and the Interstellar Matter, ed. R. Balian, P. Encrenaz, and J. Lequeux (Amsterdam: North-Holland), p. 177.

Watson, W. D., Crutcher, R. M., and Dickel, J. R. 1975, Ap. J., 201, 102.

Watson, W. D., and Salpeter, E. E. 1972a, Ap. J., 174, 321.

_____. 1972b, Ap. J., 175, 659.

Whitworth, A. P. 1975, Ap. and Space Sci., 34, 155.

Winnewisser, G., and Churchwell, E. 1975, Ap. J. (Letters), 200, L33.

Winnewisser, G., Mezger, P. G., and Breuer, H.-D. 1974, Topics in Current Chemistry, 44, 1.

Witt, A. N., and Lillie, C. F. 1973, Astr. and Ap., 25, 397.

Zuckerman, B., and Turner, B. E. 1975, Ap. J., 197, 123.

Zuckermann, B., Turner, B. E., Johnson, D. R., Clark, F. O., Lovas, F. J., Fourikis, N., Palmer, P., Morris, M., Lilley, A. E., Ball, J. A., Gottlieb, C. A., Litvak, M. M., and Penfield, H. 1975, Ap. J. (Letters), 196, L99.

PART II

RADIO ASTRONOMY OBSERVATIONS

Chapter 4

REPORT ON NEGATIVE RESULTS

To further the analysis of the chemical composition of interstellar molecule clouds, a number of searches for previously undetected microwave molecular transitions were conducted. The radio telescopes used in these projects are listed in table 1 and all except the Haystack telescope are pictured in figures 1-4. To enhance detection of weak signals, several different observing procedures were employed to subtract out sky and system noise and monitor system gain fluctuations. Beam switching involves the receiver input being switched between two horns, one "on" and one "off" the source, several times a second; no overall antenna motion is involved except for regular tracking movement. When the receiver is at the Cassegrain focus, the same effect can be produced by a wobbling secondary mirror at the prime focus. In position switching, the whole antenna is switched between two sky positions, one "source" and the other "reference", several times a minute. Total power measurements involve observing the "source" for several minutes and then the reference position for an equal amount of time, with the data being combined during later processing. This last technique is useful only when the receiver is extremely stable, with only long term changes in the gain occurring.

The observations yielded no definite detections. Reports of the completed projects are included at the end of this chapter,

TABLE 1

RADIO TELESCOPES USED IN OBSERVING PROJECTS

Observatory	Telescope Diameter	Spectrometer
Owens Valley Radio Observatory (OVRO)*, California Institute of Technology, Big Pine, California	130 feet (40 meters)	100-channel autocorrelator with bandwidth = 2.5 MHz, 625 kHz, 250 kHz, or 62.5 kHz.
NASA/JPL Deep Space Network †, Goldstone, California	210 feet (64 meters)	64-channel autocorrelator with maximum bandwidth = 4.8 MHz.
The Aerospace Corporation ‡, El Segundo, California	15 feet (4.6 meters)	2 64-channel filter banks with bandwidths of 16 and 64 MHz, respectively.
National Radio Astronomy Observatory (NRAO) §, Kitt Peak, Arizona	36 feet (11 meters)	4 256-channel filter banks with bandwidths of 25.6, 64, 128, and 256 MHz, respectively.
Haystack Observatory ‖, Northeast Radio Observatory Corporation, Westford, Massachusetts	120 feet (37 meters)	100-channel autocorrelator with bandwidth = 20 MHz, 6.67 MHz, 2.0 MHz, 667 kHz, 66.7 kHz, 20 kHz, 6.67 kHz, or 2.0 kHz.

* Research at the Owens Valley Radio Observatory is supported by the National Science Foundation under grant GP 30400-X1, and by the Office of Naval Research under contract number N00014-67-A-0094-0019.

† The NASA/JPL Deep Space Network is operated by the Jet Propulsion Laboratory, California Institute of Technology, under contract NAS7-100 sponsored by the National Aeronautics and Space Administration.

‡ The Aerospace spectral line radio astronomy program is supported jointly by National Science Foundation Grant MPS 73-04554 and the Aerospace Company Programs for Research and Investigation.

§ The National Radio Astronomy Observatory is operated by Associated Universities, Inc. under contract with the National Science Foundation.

‖ The Haystack Observatory is operated by the Northeast Radio Observatory Corporation with support from the National Science Foundation.

Fig. 1.-130-foot radio telescope, Owens Valley Radio Observatory.

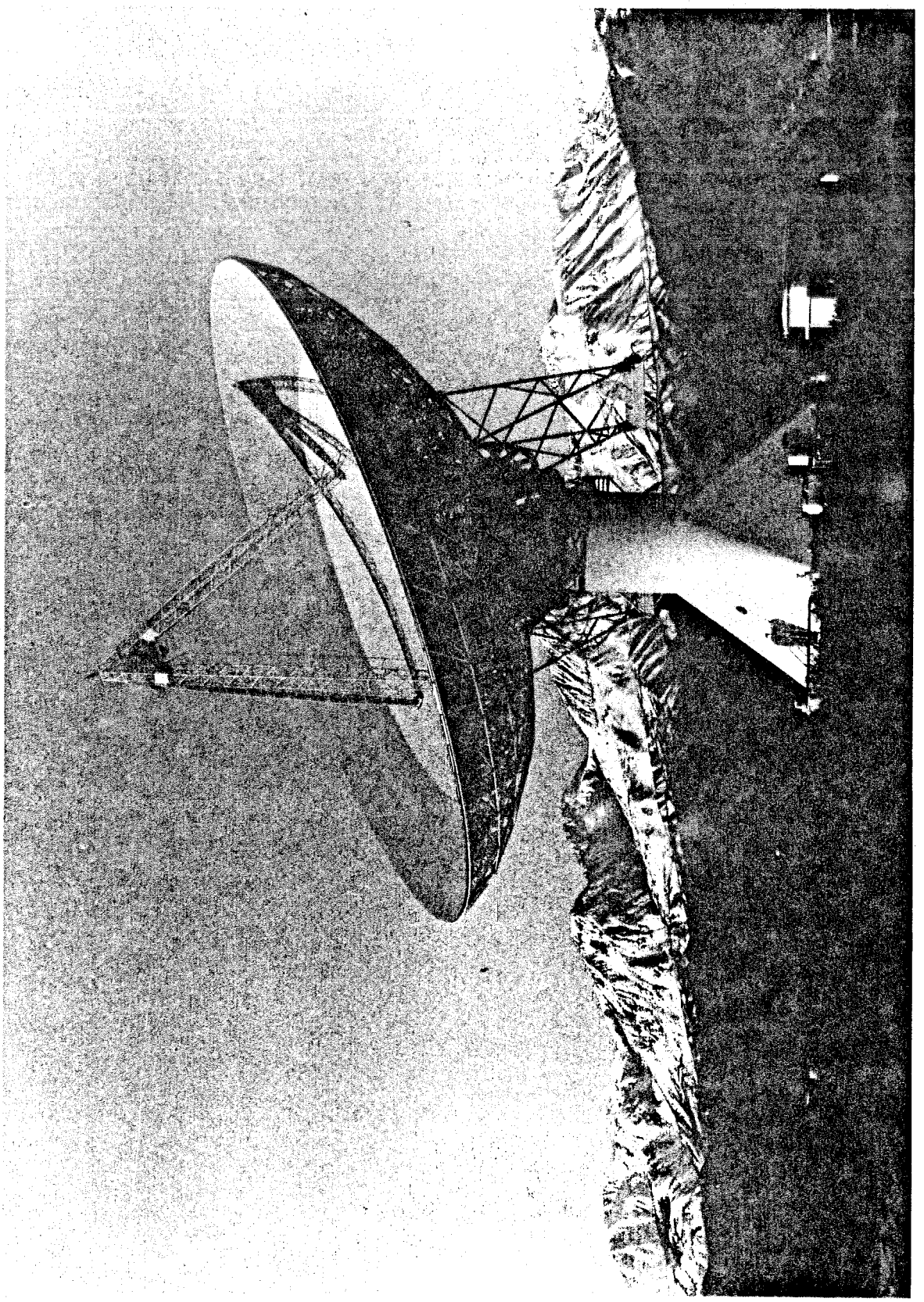

Fig. 2. - 210-foot antenna, Mars Station, Goldstone Deep Space Communications Complex.

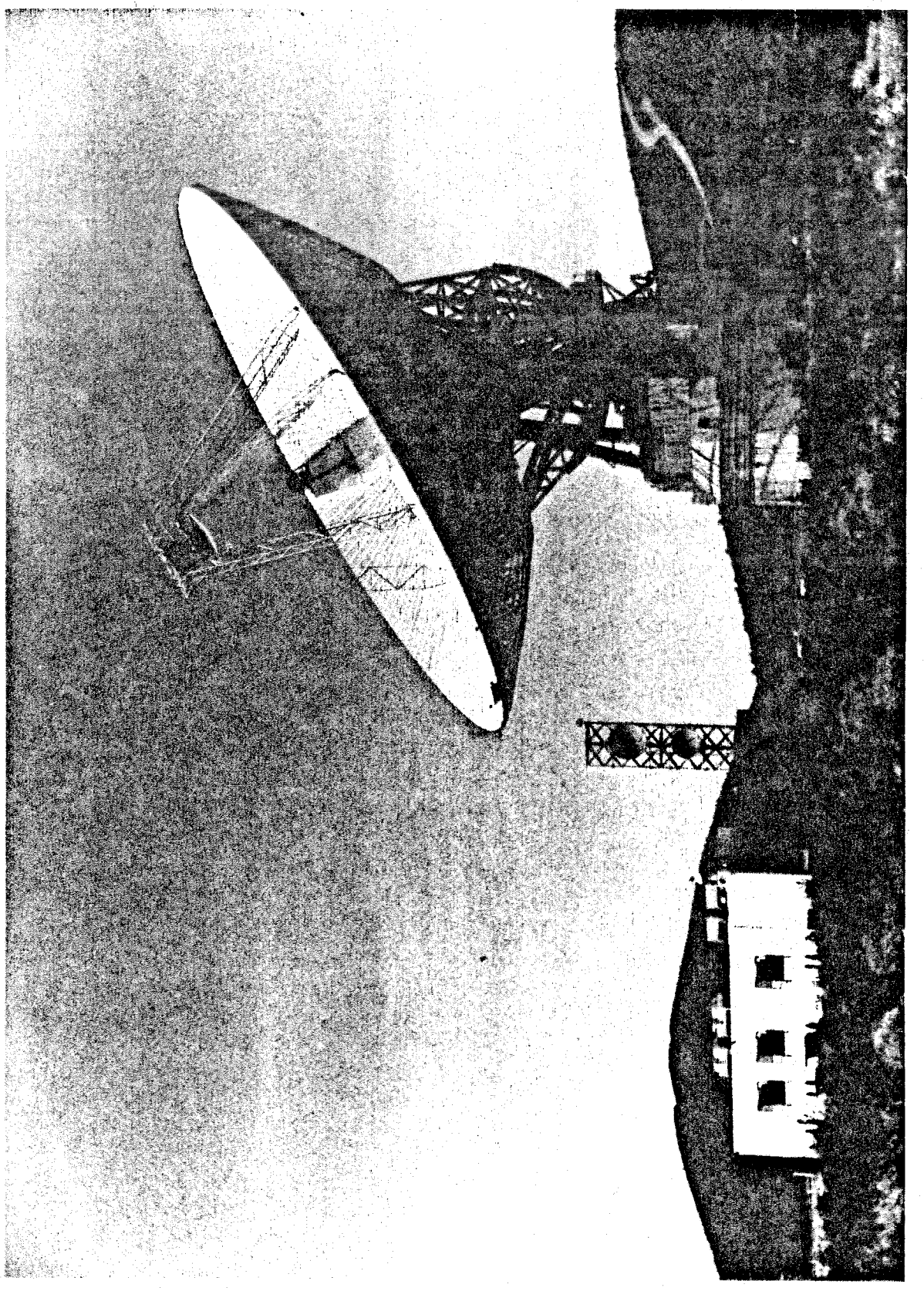

Fig. 3. - The Aerospace 15-foot millimeter radio telescope.

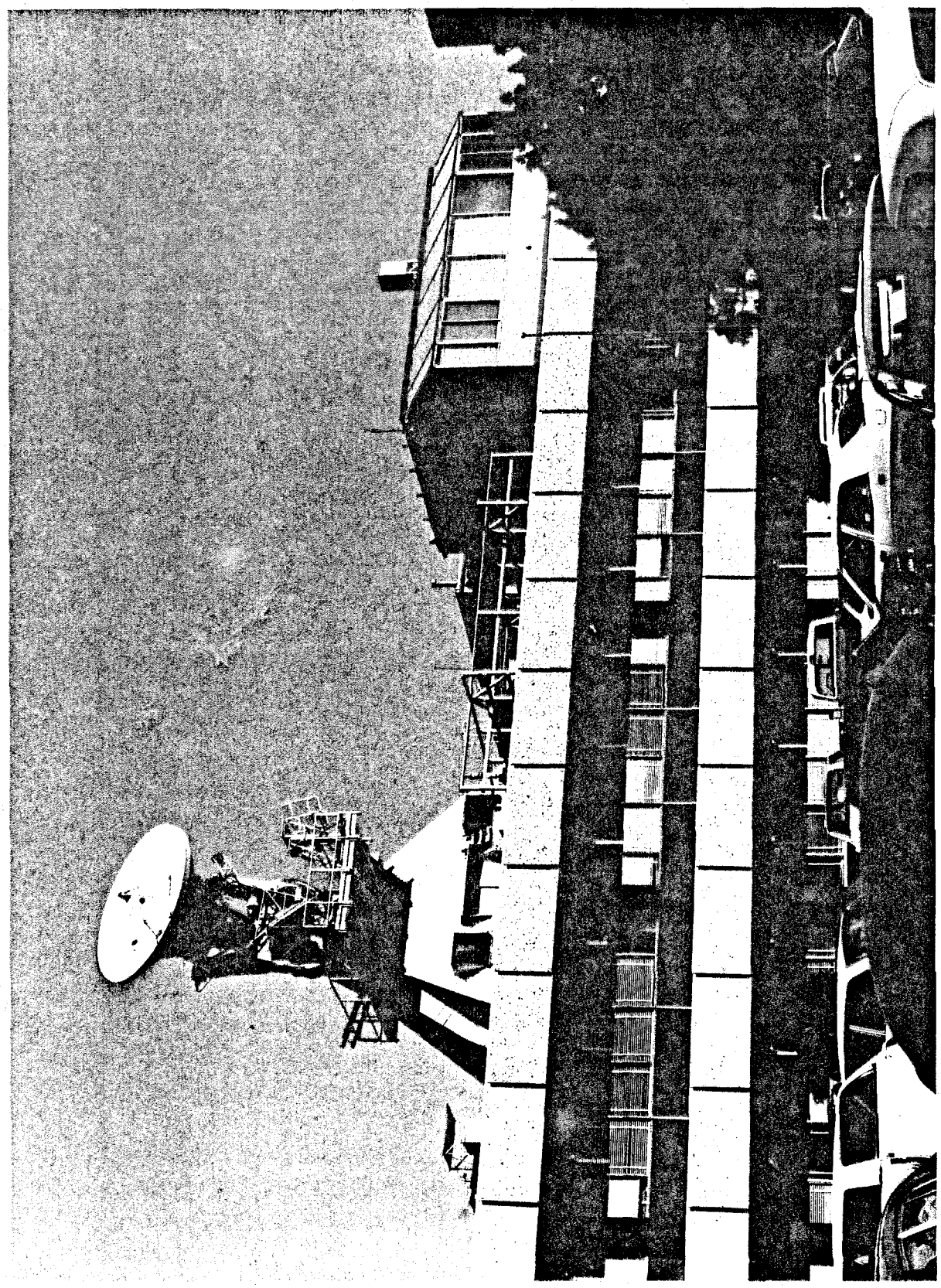

Fig. 4.-NRAO 36-foot radio telescope.

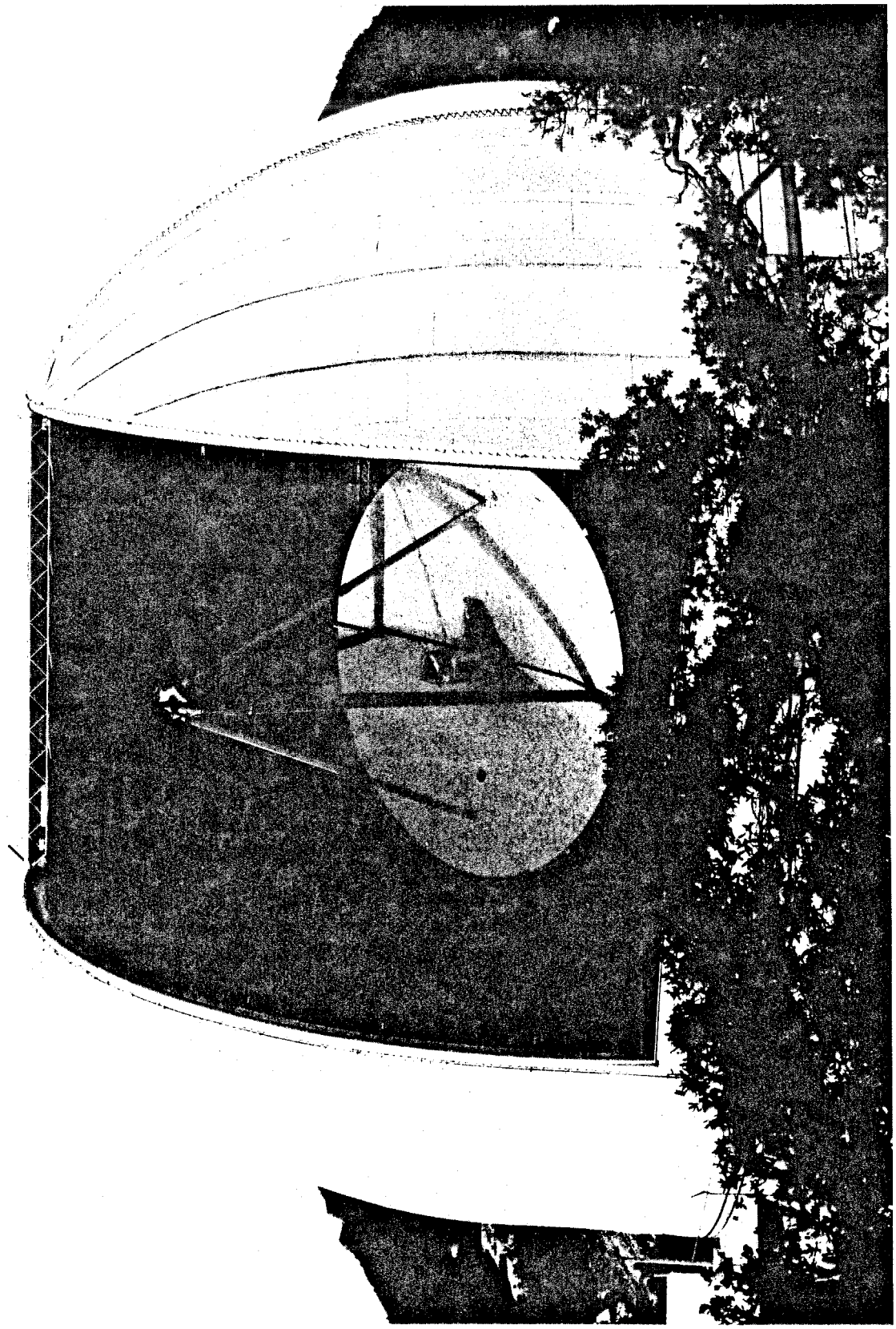

except for the OD project, which is described in Chapter 5 of this thesis. Order-of-magnitude upper limits to the abundances of the molecules in the observed states can, however, be determined from the data. Before presenting these results, a quick review of the theory of radio spectral lines is given to enable the reader to understand the uncertainties in the derived abundances.

In radio astronomy, the radiation intensity I_ν observed at a given frequency ν is often reported in units of temperature where, from the Planck function, T is the temperature of a black-body that would emit I_ν per unit solid angle per unit area (Penzias 1975):

$$I_\nu = 2h\nu^3/c^2 [\exp(h\nu/kT) - 1] , \qquad (1)$$

where h is Planck's constant, k is Boltzmann's constant, and c is the speed of light. In the Rayleigh-Jeans limit,

$$h\nu \ll kT \qquad (2)$$

and

$$T = c^2 I_\nu / 2k\nu^2 . \qquad (3)$$

This approximation is accurate to within $\sim 30\%$ when $(h\nu/kT) = 0.5$, so that even at the highest frequencies at which we observed (~ 100 GHz) the relationship of equation (3) can be employed for temperatures as low as 10°K.

The same transition in different celestial objects along the line of sight is observed on earth at slightly different frequencies due to the variation in the velocity of the different objects relative to earth. The observed frequency shift $\Delta\nu$ relative to the laboratory

frequency measurement ν can be related to the velocity of the object relative to earth (Δv) by the Doppler shift formula:

$$\Delta\nu/\nu = \Delta v/c \ . \qquad (4)$$

The velocity of every celestial object relative to a "local standard of rest" defined for the neighborhood of the Solar System is usually relatively constant and unique for a given direction. However, the velocity relative to a terrestial observer is constantly changing due to the motion of the earth rotating on its axis and revolving around the sun. To clarify the origin of the spectral lines seen, the abscissa of a reported astronomical spectrum is usually in units of velocity relative to the local standard of rest for a given reference frequency. Often the center frequency of the spectral bandwidth being observed (ν_{sky}) is the laboratory-measured frequency ν_o shifted accordingly for local motions and the motion of the object. Because of the heterodyne detection techniques used, one, two, or more frequency ranges can be observed simultaneously, depending on the nature of the receiver. In the "double sideband" case, the central frequencies of the two ranges being observed are separated by twice the intermediate frequency (IF) of the system. The data from both sidebands are superimposed in the output with the frequency (and velocity scales) of the two ranges being inverted with respect to each other.

In order to calculate the upper limits to the abundances, it will be assumed that the astronomical sources observed are congruent

with background continuum radiation sources. The magnitude of a detected spectral line after the continuum is subtracted can be reported in terms of an antenna temperature T_A (Penzias 1975):

$$T_A(v) = \eta(T_{ex} - T_{bg} - 2.7)\{1 - \exp[-\tau(v)]\} , \qquad (5)$$

where τ is the optical depth of the line and both T_A and τ are functions of velocity (i.e., sky frequency). The excitation temperature T_{ex} reflects the relative populations of the two states involved in the transition. The background continuum is contributed by localized celestial sources (T_{bg}) and the isotropic 2.7°K background, a possible remnant of the universe-forming big bang. The η factor is due to effects in the detection process that diminish the signal. If the solid angle of the source Ω_s is less than the solid angle of the main beam of the telescope Ω_{MB},

$$\eta = \frac{\Omega_s}{\Omega_{MB}} \eta_A , \qquad (6)$$

where η_A is the aperture efficiency of the telescope, the efficiency in detecting radiation from a point source. If $\Omega_s \geq \Omega_{MB}$,

$$\eta = \eta_B = \frac{\Omega_{MB}}{\Omega_B} , \qquad (7)$$

where η_B is the beam efficiency of the telescope, i.e., the fraction of the total beam Ω_B contained in the main beam. At $\lambda \lesssim 1$ cm, atmospheric attenuation also decreases the signal $T_A(v)$. However,

the system response of a telescope operating at millimeter wavelengths is generally calibrated with atmospheric and antenna losses included, the reported signal being denoted T_A^*. A line is seen in emission if $T_A(v)$ is positive.

In the absence of a detected spectral line, an upper limit to the column density of molecules in the direction being observed can be determined from the magnitude of the baseline noise level. Since non-detectability can often mean that any line that is there is optically thin, $\tau \ll 1$, equation (5) reduces to

$$T_A(v) = \eta(T_{ex} - T_{bg} - 2.7)\,\tau(v) \,. \qquad (8)$$

Because the antenna losses are often included in the system calibration and spectral lines observed above 5 GHz are usually seen in emission, a good order-of-magnitude upper limit estimate of the optical depth in the transition can be determined from

$$T_A^{\text{upper limit}}(v) = T_{ex}\,\tau^{\text{upper limit}}(v) \,. \qquad (9)$$

For a transition between two levels m and n (n being higher in energy) with degeneracies g_m and g_n, respectively, the column density of molecules in state m (N_m) is related to the optical depth integrated over the whole line profile (Penzias 1975):

$$\int \tau(\nu)\,d\nu = \frac{8\pi^3\nu^2}{3ckT_{ex}} \frac{g_n}{g_m} \mu^2_{n\to m} N_m \,, \qquad (10)$$

where $\mu_{n\rightarrow m}$ is the dipole moment matrix element for the transition from n to m. In the case of symmetric-top molecules (Townes and Schawlow 1955):

$$\mu^2_{n\rightarrow m} = \frac{(J+1)^2 - K^2}{(J+1)(2J+3)} \mu^2 \qquad (11)$$

for the transition $J+1, K\rightarrow J, K$. The factor μ^2 is the square of the permanent dipole moment of the molecule. For the special case of linear molecules, $K = 0$. The squared dipole moment matrix element for asymmetric-top molecules is

$$\mu^2_{n\rightarrow m} = \frac{{}^{x}S_{nm}}{(2J+3)} \mu^2_x \qquad (12)$$

for a transition $J+1\rightarrow J$ (the states actually having a more complicated notation). The factors ${}^{x}S_{nm}$ and μ^2_x depend on which of the components of the permanent dipole moment of the molecule (x = a, b, or c) is responsible for the transition. The line strength ${}^{x}S_{nm}$ is complicated to calculate, but has been tabulated in many places, including Appendix V of Townes and Schawlow (1955).

Now, from equations (9) and (10),

$$\left(\int T_A(\nu) d\nu \right)^{\text{upper limit}} = \frac{8\pi^3\nu^2}{3ck} \frac{g_n}{g_m} \mu^2_{n\rightarrow m} N_m^{\text{upper limit}} . \qquad (13)$$

The upper limit to the integrated line magnitude can be approximated:

$$\left(\int T_A(\nu) d\nu \right)^{\text{upper limit}} = T_A^{\text{upper limit}} \Delta v \left(\frac{\nu}{c} \right) , \quad (14)$$

where $T_A^{\text{upper limit}}$ is the upper limit to the peak line magnitude and Δv is the full line width at half power in velocity space (converted from frequency space by eq. [4]). The velocity line width is often characteristic of the source, independent of the transition or molecule being observed. To set an upper limit to N_m, $T_A^{\text{upper limit}}$ can be equated to the peak-to-peak noise level and Δv estimated from other spectral lines observed in the same source. Then equations (13) and (14) can be combined to calculate $N_m^{\text{upper limit}}$ from the non-detection result.

The reports of the unsuccessful molecule searches are presented on the following pages. They are ordered by the date of the observing run. For a given observing period, the reports are in order of increasing rest frequency.

MOLECULE: 1-Cyanopropyne (methylcyanoacetylene)(CH_3C_2CN)

TRANSITION: $1_0 - 2_0$* REST FREQUENCY (ν_0): 8263.01 MHz (F=2 - 3) DIPOLE MOMENT: 5.09 D

REFERENCE: Sheridan and Thomas 1954 (ν_0); Heeks 1958 (μ)

COLLABORATORS: N. Evans, Owens Valley Radio Observatory, California Institute of Technology

N. Scoville, Owens Valley Radio Observatory, California Institute of Technology

DATE OF SEARCH: March 24-30, 1974 TELESCOPE: OVRO 130-foot

RECEIVER: Nondegenerate paramp (4 sidebands) I. F.: 30 MHz SYSTEM TEMPERATURE: ~ 500°(SSB)

BEAM WIDTH: 4′ EFFICIENCY: $\eta_A \sim 45\%$, $\eta_B \sim 65\%$ OPERATING MODE: Total power

SEARCH REGION	SOURCE COORDINATES RA(1950) h m s	DEC(1950) ° ′ ″	AVERAGE SOURCE PARAMETERS VELOCITY (km s^{-1})	LINE WIDTH (km s^{-1})	FREQUENCY RANGE AROUND ν_{sky}§ (MHz)	FREQUENCY RESOLUTION (kHz)	TIME ON SOURCE† (hr)	UPPER LIMITS T_A‡ (°K)	N_m (cm^{-2})
Sgr B2	17 44 08	-28 22 06	60	20	± 1.05	50	10.84	0.21	10^{13}

* Another almost equally strong, transition in the bandpass is the $1_1 - 2_1$ transition at 8263.11 MHz (F=2-3).

† Equal time spent off source.

‡ Four times root mean square noise level.

§ ν_{sky} is in upper sideband: equivalent frequency ranges in lower sideband and in two mirror image sidebands below 8085 MHz simultaneously observed, no line detected.

MOLECULE: 1,3-Pentadiyne (methyldiacetylene)($CH_3C_2C_2H$)

TRANSITION: $1_0 - 2_0$* REST FREQUENCY (ν_0): 8142.96 MHz DIPOLE MOMENT: 1.207 D

REFERENCE: Heath et al. 1955 (ν_0); Heeks 1958 (μ)

COLLABORATORS: N. Evans, Owens Valley Radio Observatory, California Institute of Technology

N. Scoville, Owens Valley Radio Observatory, California Institute of Technology

DATE OF SEARCH: April 24-26 and 28, 1974 TELESCOPE: OVRO 130-foot

RECEIVER: Degenerate paramp (double sideband) I. F.: 30 MHz SYSTEM TEMPERATURE: ~300°K (SSB)

BEAM WIDTH: 4′ EFFICIENCY: $\eta_A \sim 45\%$, $\eta_B \sim 65\%$ OPERATING MODE: Total power

SEARCH REGION	SOURCE COORDINATES RA (1950) h m s	DEC (1950) ° ′ ″	AVERAGE SOURCE PARAMETERS VELOCITY (km s^{-1})	LINE WIDTH (km s^{-1})	FREQUENCY RANGE AROUND ν_{sky} § (MHz)	FREQUENCY RESOLUTION (kHz)	TIME ON SOURCE† (hr)	UPPER LIMITS T_A‡ (°K)	N_m (cm^{-2})
Sgr B2	17 44 08	-28 22 06	60	20	±0.95	50	9.71	0.076	10^{13}

* Another, almost equally strong, transition in the bandpass is the $1_1 - 2_1$ transition at 8142.88 MHz.

† Equal time spent off source.

‡ Four times root mean square noise level.

§ ν_{sky} is in upper sideband; equivalent frequency range in lower sideband simultaneously observed, no line detected.

MOLECULE: Thioacetaldehyde (CH_3CHS)

TRANSITION: $1_{01} - 2_{02}$ (A) REST FREQUENCY (ν_0): 22113.62 MHz DIPOLE MOMENT: 1 D (μ_a) (assumed)

REFERENCE: Kroto et al. 1974 (rotational constants)

COLLABORATOR: M. Morris, Owens Valley Radio Observatory, California Institute of Technology

DATE OF SEARCH: April 15-21, 1975 TELESCOPE: OVRO 130-foot

RECEIVER: NRAO 1.3 cm degenerate paramp (double sideband) I. F.: 30 MHz SYSTEM TEMPERATURE: ~600 °K (SSB)

BEAM WIDTH: 1'.5 EFFICIENCY: $\eta_A \sim 25\%$, $\eta_B \sim 33\%$ OPERATING MODE: Total power

SEARCH REGION	SOURCE COORDINATES RA (1950) h m s	DEC(1950) ° ′ ″	AVERAGE SOURCE PARAMETERS VELOCITY (km s^{-1})	LINE WIDTH (km s^{-1})	FREQUENCY RANGE AROUND ν_{sky}‡ (MHz)	FREQUENCY RESOLUTION (kHz)	TIME ON SOURCE* (hr)	UPPER LIMITS† T_A (°K)	N_{m_2} (cm^{-2})
Orion A	05 32 47	-05 24 21	8.5	4	± 1	80	0.76	0.41	10^{13}

* Equal time spent off source.

† Five times root mean square noise level.

‡ ν_{sky} is in lower sideband; equivalent frequency range in upper sideband simultaneously observed, no line detected.

MOLECULE: Diazomethane (CH_2N_2)

TRANSITION: $0_{00} - 1_{01}$ REST FREQUENCY (ν_0): 22150.88 MHz DIPOLE MOMENT: 1.50 D (μ_a)

REFERENCE: Sheridan 1962 (rotational constants and μ_a)

COLLABORATOR: M. Morris, Owens Valley Radio Observatory, California Institute of Technology

DATE OF SEARCH: April 15-21, 1975 TELESCOPE: OVRO 130-foot

RECEIVER: NRAO 1.3 cm degenerate paramp (double sideband) I. F.: 30 MHz SYSTEM TEMPERATURE: ~ 560 °K (SSB)

BEAM WIDTH: 1'.5 EFFICIENCY: $\eta_A \sim 25\%$, $\eta_B \sim 33\%$ OPERATING MODE: Total power

SEARCH REGION	SOURCE COORDINATES RA(1950) h m s	DEC(1950) ° ′ ″	AVERAGE SOURCE PARAMETERS VELOCITY (km s^{-1})	LINE WIDTH (km s^{-1})	FREQUENCY RANGE AROUND ν_{sky}‡ (MHz)	FREQUENCY RESOLUTION (kHz)	TIME ON SOURCE* (hr)	UPPER LIMITS T_A† (°K)	N_m (cm^{-2})
Orion A	05 32 47	-05 24 21	8.5	4	± 1	80	0.68	0.34	10^{13}

* Equal time spent off source.

† Five times root mean square noise level.

‡ ν_{sky} is in upper sideband; equivalent frequency range in lower sideband simultaneously observed, no line detected.

MOLECULE: Formic Acid (HCO_2H)

TRANSITION: $0_{00} - 1_{01}$ REST FREQUENCY (ν_0): 22471.0 MHz DIPOLE MOMENT: 1.391 D (μ_a)

REFERENCE: Lerner, Dailey, and Friend 1957 (ν_0); Kim, Keller, and Gwinn 1962 (μ_a)

COLLABORATOR: M. Morris, Owens Valley Radio Observatory, California Institute of Technology

DATE OF SEARCH: April 15-21, 1975 TELESCOPE: OVRO 130-foot

RECEIVER: NRAO 1.3 cm degenerate paramp (double sideband) I. F.: 30 MHz SYSTEM TEMPERATURE: 564 °K (SSB)

BEAM WIDTH: 1'.5 EFFICIENCY: $\eta_A \sim 25\%$, $\eta_B \sim 33\%$ OPERATING MODE: Total power

SEARCH REGION	SOURCE COORDINATES RA(1950) h m s	DEC(1950) ° ′ ″	AVERAGE SOURCE PARAMETERS VELOCITY (km s^{-1})	LINE WIDTH (km s^{-1})	FREQUENCY RANGE AROUND ν_{sky}‡ (MHz)	FREQUENCY RESOLUTION (kHz)	TIME ON SOURCE* (hr)	UPPER LIMITS T_A† (°K)	N_m (cm^{-2})
Orion A	05 32 47	-05 24 21	8.5	4	± 1	80	0.46	0.34	10^{13}

* Equal time spent off source.

† Five times root mean square noise level.

‡ ν_{sky} is in upper sideband; equivalent frequency range in lower sideband simultaneously observed, no line detected.

MOLECULE: Formimide $(HCO)_2NH$

TRANSITION: $3_{03} - 4_{04}$ REST FREQUENCY (ν_0): 22686.61 MHz DIPOLE MOMENT: 2.20 D (μ_a)

REFERENCE: Steinmetz 1973 (ν_0 and μ_a)

COLLABORATOR: M. Morris, Owens Valley Radio Observatory, California Institute of Technology

DATE OF SEARCH: April 15-21, 1975 TELESCOPE: OVRO 130-foot

RECEIVER: NRAO 1.3 cm degenerate paramp (double sideband) I. F.: 30 MHz SYSTEM TEMPERATURE: ~ 590°K (SSB)

BEAM WIDTH: 1.'5 EFFICIENCY: $\eta_A \sim 25\%$, $\eta_B \sim 33\%$ OPERATING MODE: Total power

SEARCH REGION	SOURCE COORDINATES RA (1950) h m s	DEC (1950) ° ′ ″	AVERAGE SOURCE PARAMETERS VELOCITY (km s^{-1})	LINE WIDTH (km s^{-1})	FREQUENCY RANGE AROUND ν_{sky}‡ (MHz)	FREQUENCY RESOLUTION (kHz)	TIME ON SOURCE * (hr)	UPPER LIMITS T_A† (°K)	N_m (cm^{-2})
Orion A	05 32 47	-05 24 21	8.5	4	±1	80	0.97	0.35	10^{12}

* Equal time spent off source.

† Five times root mean square noise level.

‡ ν_{sky} is in upper sideband; equivalent frequency range in lower sideband simultaneously observed, no line detected.

MOLECULE: cis-Glyoxal $(HCO)_2$

TRANSITION: $2_{02} - 2_{11}$ REST FREQUENCY (ν_0): 22886.86 MHz DIPOLE MOMENT: 4.8 D (μ_b)

REFERENCE: Durig, Tong, and Li 1972 (ν_0 and μ_b)

COLLABORATOR: M. Morris, Owens Valley Radio Observatory, California Institute of Technology

DATE OF SEARCH: April 15-21, 1975 TELESCOPE: OVRO 130-foot

RECEIVER: NRAO 1.3 cm degenerate paramp (double sideband) I. F.: 30 MHz SYSTEM TEMPERATURE: ~ 490°K(SSB)

BEAM WIDTH: 1'.5 EFFICIENCY: $\eta_A \sim 25\%$, $\eta_B \sim 33\%$ OPERATING MODE: Total power

SEARCH REGION	SOURCE COORDINATES RA (1950) h m s	DEC (1950) ° ′ ″	AVERAGE SOURCE PARAMETERS VELOCITY (km s^{-1})	LINE WIDTH (km s^{-1})	FREQUENCY RANGE AROUND ν_{sky}‡ (MHz)	FREQUENCY RESOLUTION (kHz)	TIME ON SOURCE* (hr)	UPPER LIMITS T_A† (°K)	N_m (cm^{-2})
Orion A	05 32 47	-05 24 21	8.5	4	± 1	80	0.97	0.28	10^{12}

* Equal time spent off source.

† Five times root mean square noise level.

‡ ν_{sky} is in upper sideband; equivalent frequency range in lower sideband simultaneously observed, no line detected.

MOLECULE: Formamide (NH_2CHO)

TRANSITION: $5_{15} - 5_{14}$ REST FREQUENCY (ν_0): 23081.762 MHz (F=6 - 6) DIPOLE MOMENT: 3.616 D (μ_a)

REFERENCE: Johnson, Lovas, and Kirchhoff 1972 (ν_0 and μ_a)

COLLABORATOR: M. Morris, Owens Valley Radio Observatory, California Institute of Technology

DATE OF SEARCH: April 15-21, 1975 TELESCOPE: OVRO 130-foot

RECEIVER: NRAO 1.3 cm degenerate paramp (double sideband) I. F.: 30 MHz SYSTEM TEMPERATURE: ~ 530°K (SSB)

BEAM WIDTH: 1'.5 EFFICIENCY: $\eta_A \sim 25\%$, $\eta_B \sim 33\%$ OPERATING MODE: Total power

SEARCH REGION	SOURCE COORDINATES RA (1950) h m s	DEC (1950) ° ′ ″	AVERAGE SOURCE PARAMETERS VELOCITY (km s^{-1})	LINE WIDTH (km s^{-1})	FREQUENCY RANGE AROUND ν_{sky}‡ (MHz)	FREQUENCY RESOLUTION (kHz)	TIME ON SOURCE* (hr)	UPPER LIMITS T_A† (°K)	N_m (cm^{-2})
W3(OH)	02 23 17	61 38 54	-47.4	6.8	± 1	80	0.65	0.39	10^{14}
Orion A	05 32 47	-05 24 21	8.5	4	± 1	80	1.20	0.25	10^{13}

* Equal time spent off source.

† Five times root mean square noise level.

‡ ν_{sky} is in upper sideband; equivalent frequency range in lower sideband simultaneously observed, no line detected.

MOLECULE: Sulfur dioxide (SO_2)

TRANSITION: $6_{15} - 5_{24}$ REST FREQUENCY (ν_o): 23414.30 MHz DIPOLE MOMENT: 1.59 D (μ_b)

REFERENCE: Kivelson 1954 (ν_o); Crable and Smith 1951 (μ_b)

COLLABORATOR: M. Morris, Owens Valley Radio Observatory, California Institute of Technology

DATE OF SEARCH: April 15-21, 1975 TELESCOPE: OVRO 130-foot

RECEIVER: NRAO 1.3 cm degenerate paramp (double sideband) I. F.: 30 MHz SYSTEM TEMPERATURE: ~ 490 °K (SSB)

BEAM WIDTH: 1'.5 EFFICIENCY: $\eta_A \sim 25\%$, $\eta_B \sim 33\%$ OPERATING MODE: Total power

SEARCH REGION	SOURCE COORDINATES RA (1950) h	m	s	DEC (1950) °	′	″	AVERAGE SOURCE PARAMETERS VELOCITY (km s^{-1})	LINE WIDTH (km s^{-1})	FREQUENCY RANGE AROUND ν_{sky}‡ (MHz)	FREQUENCY RESOLUTION (kHz)	TIME ON SOURCE* (hr)	UPPER LIMITS T_A† (°K)	N_m (cm^{-2})
W3(OH)	02	21	47	61	52	54	-47.4	6.8	± 1	80	1.29	0.24	10^{14}
Orion A	05	32	47	-05	24	21	8.5	4	± 1	80	3.13	0.15	10^{13}
NGC 2264	06	38	24	09	32	06	8.3	4	± 1	80	0.52	0.41	10^{14}
DR-21(OH)	20	37	14	42	12	00	-4	3	± 1	80	0.99	0.30	10^{14}

* Equal time spent off source.

† Five times root mean square noise level.

‡ ν_{sky} is in upper sideband; equivalent frequency range in lower sideband simultaneously observed, no line detected.

MOLECULE: Dimethylamine[$(CH_3)_2NH$]

TRANSITION: $3^{+}_{03} - 3^{-}_{13}$ REST FREQUENCY (ν_o): 23595.51 MHz (Wollrab 1968) DIPOLE MOMENT: 0.967 D (μ_c)

REFERENCE: Wollrab and Laurie 1968 (ν_o and μ_c)

COLLABORATOR: M. Morris, Owens Valley Radio Observatory, California Institute of Technology

DATE OF SEARCH: April 15-21, 1975 TELESCOPE: OVRO 130-foot

RECEIVER: NRAO 1.3 cm degenerate paramp (double sideband) I. F.: 30 MHz SYSTEM TEMPERATURE: 530°K (SSB)

BEAM WIDTH: 1.'5 EFFICIENCY: $\eta_A \sim 25\%$, $\eta_B \sim 33\%$ OPERATING MODE: Total power

SEARCH REGION	SOURCE COORDINATES RA (1950) h m s	DEC (1950) ° ′ ″	AVERAGE SOURCE PARAMETERS VELOCITY (km s^{-1})	LINE WIDTH (km s^{-1})	FREQUENCY RANGE AROUND ν_{sky}‡ (MHz)	FREQUENCY RESOLUTION (kHz)	TIME ON SOURCE* (hr)	UPPER LIMITS T_A† (°K)	N_m (cm^{-2})
Orion A	05 32 47	-05 24 21	8.5	4	± 1	80	0.66	0.41	10^{13}

* Equal time spent off source.

† Five times root mean square noise level.

‡ ν_{sky} is in upper sideband; equivalent frequency range in lower sideband simultaneously observed, no line detected.

MOLECULE: Hydrazoic acid (HN_3)

TRANSITION: $0_{00} - 1_{01}$ REST FREQUENCY (ν_o): 23815.58 (F=1 - 2) DIPOLE MOMENT: 0.837 D (μ_a)

REFERENCE: Kewley, Sastry, and Winnewisser 1964 (μ_b); White and Cook 1967 (μ_a)

COLLABORATOR: M. Morris, Owens Valley Radio Observatory, California Institute of Technology

DATE OF SEARCH: April 15-21, 1975 TELESCOPE: OVRO 130-foot

RECEIVER: NRAO 1.3 cm degenerate paramp (double sideband) I. F.: 30 MHz SYSTEM TEMPERATURE: ~ 550°K (SSB)

BEAM WIDTH: 1.'5 EFFICIENCY: $\eta_A \sim 25\%$, $\eta_B \sim 33\%$ OPERATING MODE: Total power

SEARCH REGION	SOURCE COORDINATES RA (1950) h m s	DEC (1950) ° ′ ″	AVERAGE SOURCE PARAMETERS VELOCITY (km s^{-1})	LINE WIDTH (km s^{-1})	FREQUENCY RANGE AROUND ν_{sky}‡ (MHz)	FREQUENCY RESOLUTION (kHz)	TIME ON SOURCE* (hr)	UPPER LIMITS T_A† (°K)	N_m (cm^{-2})
Orion A	05 32 47	-05 24 21	8.5	4	1	80	1.02	0.38	10^{14}

* Equal time spent off source.

† Five times root mean square noise level.

‡ ν_{sky} is in lower sideband; equivalent frequency range in upper sideband simultaneously observed, no line detected.

MOLECULE: CCO

TRANSITION: $1_0 - 2_1$ REST FREQUENCY (ν_0): 22253.6 MHz DIPOLE MOMENT: 1 D (assumed)

REFERENCE: Devilliers and Ramsay 1971 (rotational constants)

COLLABORATORS: A. G. Cardiasmenos, Department of Physics and Astronomy, University of Massachusetts at Amherst

N. Z. Scoville, Department of Physics and Astronomy, University of Massachusetts at Amherst

DATE OF SEARCH: Nov. 24-27, 1975 TELESCOPE: Haystack 120-foot

RECEIVER: Maser (single sideband) I. F.: 137.5 MHz SYSTEM TEMPERATURE: ~ 200°K

BEAM WIDTH: 1.'5 EFFICIENCY: $\eta_A \sim 20\%$, $\eta_B \sim 30\%$ OPERATING MODE: Beam switching (alternate scans off source)

SEARCH REGION	SOURCE COORDINATES, RA (1950) h m s	DEC (1950) ° ′ ″	AVERAGE SOURCE PARAMETERS VELOCITY (km s^{-1})	LINE WIDTH (km s^{-1})	FREQUENCY RANGE AROUND ν_{sky} (MHz)	FREQUENCY RESOLUTION (kHz)	ACTUAL TIME ON SOURCE (hr)	UPPER LIMITS T_A† (°K)	N_m (cm^{-2})
Orion A	05 32 47.0	-05 24 30	8.5	4	±1	50	0.4	0.05	10^{12}
Sgr B2(OH)	17 44 11.0	-28 22 30	60	20	±3.33	170	1	0.05	10^{13}
W51	19 21 23.0	14 24 29	57.1	12.5	±3.33	170	0.33	0.05	10^{13}

† Peak-to-peak noise level.

MOLECULE: Acetic acid (CH_3CO_2H)

TRANSITION: $3_{03} - 3_{12}$ (E) REST FREQUENCY (ν_o): 23494.55 MHz DIPOLE MOMENT: 1.47 D (μ_b)

REFERENCE: Krisher and Saegebarth 1971 (ν_o and μ_b)

COLLABORATORS: A. G. Cardiasmenos, Department of Physics and Astronomy, University of Massachusetts at Amherst

N. Z. Scoville, Department of Physics and Astronomy, University of Massachusetts at Amherst

DATE OF SEARCH: Nov. 24-27, 1975 TELESCOPE: Haystack 120-foot

RECEIVER: Maser (single sideband) I. F.: 137.5 MHz SYSTEM TEMPERATURE: ~ 150 - 180°K

BEAM WIDTH: 1'.5 EFFICIENCY: $\eta_A \sim 20\%$, $\eta_B \sim 30\%$ OPERATING MODE: Beam switching (alternate scans off source)

SEARCH REGION	SOURCE COORDINATES RA (1950) h m s	DEC (1950) ° ′ ″	AVERAGE SOURCE PARAMETERS VELOCITY (km s^{-1})	LINE WIDTH (km s^{-1})	FREQUENCY RANGE AROUND ν_{sky} (MHz)	FREQUENCY RESOLUTION (kHz)	ACTUAL TIME ON SOURCE (hr)	UPPER LIMITS T_A† (°K)	N_m (cm^{-2})
Orion A	05 32 47.0	-05 24 30	8.5	4	±1	50	1.0	0.10	10^{13}
IRC+10216	09 45 14.8	13 30 40	-26	26.7	±3.33	170	0.33	0.05	10^{13}
W51	19 21 23.0	14 24 29	57.1	12.5	±3.33	170	0.25	0.05	10^{13}
DR-21(OH)	20 37 14.0	42 12 00	-4	3	±3.33	170	0.33	0.06	10^{13}

† Peak-to-peak noise level.

MOLECULE: Malononitrile [$CH_2(CN)_2$]

TRANSITION: $0_{00} - 1_{11}$ REST FREQUENCY (ν_o): 23498.82 MHz DIPOLE MOMENT: 3.735 D (μ_b)

REFERENCE: Cook, Walden, and Jones 1974 (μ_b); Hirota and Morino 1960 (μ_b)

COLLABORATORS: A. G. Cardiasmenos, Department of Physics and Astronomy, University of Massachusetts at Amherst

N. Z. Scoville, Department of Physics and Astronomy, University of Massachusetts at Amherst

DATE OF SEARCH: Nov. 24-27, 1975 TELESCOPE: Haystack 120-foot

RECEIVER: Maser (single sideband) I. F.: 137.5 MHz SYSTEM TEMPERATURE: ~ 150°K

BEAM WIDTH: 1.'5 EFFICIENCY: η_A ~ 20%, η_B ~ 30% OPERATING MODE: Beam swtiching (alternate scans off source)

SEARCH REGION	SOURCE COORDINATES RA (1950) h m s	DEC (1950) ° ′ ″	AVERAGE SOURCE PARAMETERS VELOCITY (km s^{-1})	LINE WIDTH (km s^{-1})	FREQUENCY RANGE AROUND ν_{sky} (MHz)	FREQUENCY RESOLUTION (kHz)	ACTUAL TIME ON SOURCE (hr)	UPPER LIMITS T_A† (°K)	N_m (cm^{-2})
W51	19 21 23.0	14 24 29	57.1	12.5	±3.33	170	0.25	0.06	10^{11}
DR-21(OH)	20 37 14.0	42 12 00	-4	3	±3.33	170	0.33	0.04	10^{11}

† Peak-to-peak noise level.

MOLECULE: trans-Nitrous acid (HNO_2)

TRANSITION: $0_{00} - 1_{01}$ REST FREQUENCY (ν_0): 23541.5 MHz (F=1 - 2) DIPOLE MOMENT: 1.378 D (μ_a)

REFERENCE: Cox, Brittain, and Finigan 1971 (ν_0 and μ_a)

COLLABORATORS: A. G. Cardiasmenos, Department of Physics and Astronomy, University of Massachusetts at Amherst

N. Z. Scoville, Department of Physics and Astronomy, University of Massachusetts at Amherst

DATE OF SEARCH: Nov. 24-27, 1975 TELESCOPE: Haystack 120-foot

RECEIVER: Maser (single sideband) I. F.: 137.5 MHz SYSTEM TEMPERATURE: 150 - 300°K

BEAM WIDTH: 1.'5 EFFICIENCY: $\eta_A \sim 20\%$, $\eta_B \sim 30\%$ OPERATING MODE: Beam switching (alternate scans off source)

SEARCH REGION	SOURCE COORDINATES RA (1950) h m s	DEC (1950) ° ′ ″	AVERAGE SOURCE PARAMETERS VELOCITY (km s^{-1})	LINE WIDTH (km s^{-1})	FREQUENCY RANGE AROUND ν_{sky} (MHz)	FREQUENCY RESOLUTION (kHz)	ACTUAL TIME ON SOURCE (hr)	UPPER LIMITS T_A† (°K)	N_m (cm^{-2})
Orion A	05 32 47.0	-05 24 30	8.5	4	±1	50	0.5	0.05*	10^{12}
IRC+10216	09 45 14.8	13 30 40	-26	26.7	± 3.33	170	0.5	0.07*	10^{13}
W51	19 21 23.0	14 24 29	57.1	12.5	±3.33	170	0.33	0.33	10^{12}

* Unadjusted for attenuation due to rain.

† Peak-to-peak noise level.

MOLECULE: 1-Cyanopropyne (methylcyanoacetylene) (CH_3C_2CN)

TRANSITION: $5_0 - 6_0$ REST FREQUENCY (ν_0): 24788.64 MHz DIPOLE MOMENT: 5.09 D

REFERENCE: Sheridan and Thomas 1954 (ν_0); Heeks 1958 (μ)

COLLABORATORS: A. G. Cardiasmenos, Department of Physics and Astronomy, University of Massachusetts at Amherst

N. Z. Scoville, Department of Physics and Astronomy, University of Massachusetts at Amherst

DATE OF SEARCH: Nov. 24-27, 1975 TELESCOPE: Haystack 120-foot

RECEIVER: Maser (single sideband) I. F.: 137.5 MHz SYSTEM TEMPERATURE: 200 - 300 °K

BEAM WIDTH: 1.'5 EFFICIENCY: $\eta_A \sim 20\%$, $\eta_B \sim 30\%$ OPERATING MODE: Beam switching (alternate scans off source)

SEARCH REGION	SOURCE COORDINATES RA (1950) h m s	DEC (1950) ° ′ ″	AVERAGE SOURCE PARAMETERS VELOCITY (km s^{-1})	LINE WIDTH (km s^{-1})	FREQUENCY RANGE AROUND ν_{sky} (MHz)	FREQUENCY RESOLUTION (kHz)	ACTUAL TIME ON SOURCE (hr)	UPPER LIMITS T_A† (°K)	N_m (cm^{-2})
Orion A	05 32 37.0	-05 24 30	8.5	4	±1	50	0.8	0.07*	10^{11}
Sgr B2(OH)	17 44 11.0	-28 22 30	60	20	± 3.33	170	0.7	0.05	10^{12}
W51	19 21 23.0	14 24 29	57.1	12.5	± 3.33	170	0.8	0.05*	10^{11}
DR-21(OH)	20 37 14.0	42 12 00	-4	3	±3.33	170	0.2	0.15*	10^{11}

* Unadjusted for attenuation due to heavy clouds or rain.

† Peak-to-peak noise level.

MOLECULE: Acetone [$(CH_3)_2CO$]

TRANSITION: $1_{01} - 2_{12}$ (Q) REST FREQUENCY (μ_b): 24899.44 MHz DIPOLE MOMENT: 2.90 D (μ_b)

REFERENCE: Swalen and Costain 1959 (μ_b and μ_b)

COLLABORATORS: A. G. Cardiasmenos, Department of Physics and Astronomy, University of Massachusetts at Amherst

N. Z. Scoville, Department of Physics and Astronomy, University of Massachusetts at Amherst

DATE OF SEARCH: Nov. 24-27, 1975 TELESCOPE: Haystack 120-foot

RECEIVER: Maser (single sideband) I. F.: 137.5 MHz SYSTEM TEMPERATURE: ~ 200°K

BEAM WIDTH: 1.'5 *EFFICIENCY:* $\eta_A \sim 20\%$, $\eta_B \sim 30\%$ *OPERATING MODE:* Beam switching (alternate scans off source)

SEARCH REGION	SOURCE COORDINATES RA (1950) h m s	DEC(1950) ° ′ ″	AVERAGE SOURCE PARAMETERS VELOCITY (km s^{-1})	LINE WIDTH (km s^{-1})	FREQUENCY RANGE AROUND ν_{sky} (MHz)	FREQUENCY RESOLUTION (kHz)	ACTUAL TIME ON SOURCE (hr)	UPPER LIMITS T_A† (°K)	N_m (cm^{-2})
Orion A	05 32 47.0	-05 24 30	8.5	4	± 1	50	0.5	0.09*	10^{12}
IRC+10216	09 45 14.8	13 30 40	-26	26.7	± 3.33	170	0.5	0.06	10^{12}
Sgr B2(OH)	17 44 11.0	-28 22 30	60	20	± 3.33	170	0.5	0.05	10^{12}

* Unadjusted for attenuation due to rain.

† Peak-to-peak noise level.

MOLECULE: Isothiocyanic acid (HNCS)

TRANSITION: $8_{08} - 9_{09}$ REST FREQUENCY (ν_0): 105558.08 MHz DIPOLE MOMENT: 1 D (μ_a) (assumed)

REFERENCE: Kewley, Sastry, and Winnewisser 1963 (4)

COLLABORATOR: T. Kuiper, Jet Propulsion Laboratory, California Institute of Technology

DATE OF SEARCH: Feb. 10-12, 1976 TELESCOPE: NRAO 36-foot

RECEIVER: 80-120 GHz cooled mixer (double sideband) I. F.: 4.75 GHz SYSTEM TEMPERATURE: ~ 500°K (SSB)

BEAM WIDTH: 1.'2 EFFICIENCY: $\eta_A \sim 37\%$, $\eta_B \sim 67\%$ OPERATING MODE: Position switching

SEARCH REGION	SOURCE COORDINATES RA (1950) h m s	DEC (1950) ° ′ ″	AVERAGE SOURCE PARAMETERS VELOCITY (km s^{-1})	LINE WIDTH (km s^{-1})	FREQUENCY RANGE AROUND ν_{sky} (MHz)	FREQUENCY RESOLUTION (MHz)	TIME ON SOURCE* (hr)	UPPER LIMITS T_A† (°K)	N_m (cm^{-2})
W3(OH)	02 23 16.7	61 38 54	-47.4	6.8	-35, +75	1	1.2	0.1‡	10^{12}
Orion A	05 32 47.0	-05 24 21	9.0	4	-35, +75	0.5	2.3	0.2	10^{12}
IRC+10216	09 45 14.8	13 30 40	-26.0	26.7	-35, +75	1	2.8	0.08‡	10^{13}
Sgr B2(OH)	17 44 11.0	-28 22 30	70.0	20	-35, +75	1	2.3	0.13‡	10^{13}
DR-21(OH)	20 37 14.0	42 12 00	-3.3	3	-35, +75	0.5	0.5	0.3	10^{12}

* Reference position observed one-half of the time.

† Actually T_A^*, peak-to-peak noise level.

‡ Two polarizations observed simultaneously and added together.

REFERENCES

Cook, R. L., Walden, R. T., and Jones, G. E. 1974, J. Mol. Spect., 53, 370.

Cox, A. P., Brittain, A. H., and Finnigan, D. J. 1971, Trans. Faraday Soc., 67, 2179.

Crable, G. F., and Smith, W. V. 1951, J. Chem. Phys., 19, 502.

Devillers, C., and Ramsay, D. A. 1971, Can. J. Phys., 49, 2839.

Durig, J. R., Tong, C. C., and Li, Y. S. 1972, J. Chem. Phys., 57, 4425.

Heath, G. A., Thomas, L. F., Sherrard, E. I., and Sheridan, J. 1955, Disc. Faraday Soc., 19, 38.

Heeks, J. S. 1958, unpublished Ph.D. thesis, University of Birmingham, Birmingham (England).

Hirota, E., and Morino, Y. 1960, Bull. Chem. Soc. Japan, 33, 158.

Johnson, D. R., Lovas, F. J., and Kirchhoff, W. H. 1972, J. Phys. Chem. Ref. Data, 1, 1011.

Kewley, R., Sastry, K. V. L. N., and Winnewisser M. 1963, J. Mol. Spect., 10, 418.

_____. 1964, J. Mol. Spect., 12, 387.

Kim, H., Keller, R., and Gwinn, W. D. 1962, J. Chem. Phys., 37, 2748.

Kivelson, D. 1954, J. Chem. Phys., 22, 904.

Krisher, L. C., and Saegebarth, E. 1971, J. Chem. Phys., 54, 4553.

Kroto, H. W., Landsberg, B. M., Suffolk, R. J., and Vodden, A. 1974, Chem. Phys. Lett., 29, 265.

Lerner, R. G., Dailey, R. G., and Friend, J. P. 1957, J. Chem. Phys., 26, 680.

Penzias, A. A. 1975, in Atomic and Molecular Physics and the Interstellar Matter, ed. R. Balian, P. Encrenaz, and L. Lequeux (Amsterdam: North-Holland), p. 373.

Sheridan, J. 1962, Adv. Mol. Spect., 1, 139.

Sheridan, J., and Thomas, L. F. 1954, Nature, 174, 798.

Steinmetz, W. E. 1973, J. Amer. Chem. Soc., 95, 2777.

Swalen, J. D., and Costain, C. C. 1959, J. Chem. Phys., 31, 1562.

Townes, C. H., and Schawlow, A. L. 1955, Microwave Spectroscopy (New York: McGraw-Hill).

White, K. J., and Cook, R. L. 1967, J. Chem. Phys., 46, 143.

Wollrab, J. E., and Laurie, V. W. 1968, J. Chem. Phys., 48, 5058.

Chapter 5

A SEARCH FOR OD IN THE GALACTIC CENTER*

MARK ALLEN

Arthur Amos Noyes Laboratory of Chemical Physics,†

California Institute of Technology

and

DIEGO A. CESARSKY AND RICHARD M. CRUTCHER

Owens Valley Radio Observatory,

California Institute of Technology

* The Astrophysical Journal, 188, 33 (1974).

† Contribution No. 4747.

I. INTRODUCTION

Deuterium recently has been detected in the interstellar medium in the molecules DCN (Wilson et al. 1973) and HD (Spitzer et al. 1973) and possibly in atomic form (Cesarsky et al. 1973). The DCN/HCN ratio is 40 times larger than the terrestial D/H ratio, while the HD/H_2 ratio is about two orders of magnitude less than the D/H ratio on earth. However, consideration of the greater ultraviolet destruction of HD leads to a probable HD/H_2 formation rate ratio of 5×10^{-3}, an enhancement similar to the DCN case. Observations of the galactic center at the 327 MHz frequency of the atomic deuterium hyperfine transition give a possible detection, but in any case set an upper limit of about 4×10^{-4} to the D/H ratio in the 0 km s^{-1} feature in Sgr A. The enhanced deuterium abundance in DCN is attributed to chemical fractionation (Solomon and Woolf 1973). If such is the case, observations of deuterated molecules may furnish revealing information about the processes of chemical synthesis in interstellar regions. Also, the D/H ratio is an important parameter in big-bang cosmologies. The results and their consequences summarized above led us to search for the $\Delta F = 0$ Λ-doublet transitions of the $^2\Pi_{3/2}$, $J = 3/2$ state of OD which occur at about 310 MHz, these being analogous to the 1665/1667 MHz transitions of OH.

A previous search for OD at this frequency was unsuccessful (Pasachoff et al. 1970), but the sensitivity was significantly less than ours.

II. OBSERVATIONS

The 130-foot (40-m) radio telescope and 100-channel autocorrelator at the Owens Valley Radio Observatory were used for the two one-week observing periods in 1973 June. The receiver was the same as that of the atomic deuterium search (Cesarsky et al. 1973); observing and data reduction procedures of the two experiments were very similar and will not be described again here.

Sgr A was chosen for observation because of the large optical depth in the OH absorption in this direction and because there is a strong background continuum source at low frequencies. It was expected that the +40 km s^{-1} feature would be the most prominent line of OD since this is by far the strongest feature in the OH spectrum. The +60 km s^{-1} feature in Sgr B2 could also have been seen since that source was at about the 60 percent sensitivity level of the main beam. The bandwidth of the autocorrelator was 625 kHz centered at a rest frequency of 310.2122 MHz, which allowed the three $\Delta F = 0$ hyperfine components to be observed simultaneously. These transitions are listed in table 1, together with their rest frequencies (Meerts and Dymanus 1973) and Einstein A-factors computed by the method outlined by Lide (1967) using a value of 5.66×10^{-13} s^{-1} for A_Λ (Poynter 1973).

The spectrum resulting from ~ 24.4 hours of integration on source was smoothed to an 18 km s^{-1} resolution (which is somewhat

TABLE 1

OBSERVED Λ- DOUBLET TRANSITIONS OF THE $^2\Pi_{3/2}$, J = 3/2 STATE OF OD

Transition	Rest frequency (MHz)	A-factor $(s^{-1})(\times 10^{-13})$
F = 5/2-5/2	310.3627 (± 0.001)	4.75
F = 3/2-3/2	310.2147 (± 0.0005)	3.04
F = 1/2-1/2	310.1445 (± 0.0005)	3.16

less than the halfwidth of the +40 km s^{-1} OH feature) and folded so that the three OD hyperfine components were averaged together. No feature was detected to an rms noise limit of about 0.04°K.

In order to compute an upper limit to the OD/OH ratio it is necessary to know what fraction of the continuum sources in the telescope beam is covered by the absorbing OH clouds. This filling factor is not easily estimated for the 1.°8 beam at 310 MHz. Cesarsky et al. (1973) discussed the procedures involved in making this estimate for their atomic deuterium search. Data about the spatial distribution of OH in the region of the galactic center is available from maps by Robinson and McGee (1970). In addition, Bieging (1973) has produced interferometric synthesis maps of the OH line in Sgr A. From these data, we estimate a filling factor of ~ 1/4 for the +40 km s^{-1} Sgr A feature; with $T_C = 1200$°K and $T_L < 0.12$°K (~ 3 times rms noise level), we find $\tau_{OD} < 4 \times 10^{-4}$ (for exact formula, see Cesarsky et al. 1973). The τ_{OD} limit for the +60 km s^{-1} Sgr B2 feature is considerably larger than this due to a small but uncertain filling factor. From Weinreb et al. (1963) and a value of $7.71 \times 10^{-11} s^{-1}$ for the A-factor of the 1667 MHz transition of OH (Poynter and Beaudet 1968), the OD/OH column density calculated with the parameters for the strongest OD transition is

$$OD/OH = 5.62\ \tau_{OD}/\tau_{OH}\ , \qquad (1)$$

assuming that the excitation temperature and velocity line width are the same in both cases. Robinson et al. (1964) calculate an average

$\tau_{OH} = 0.9$ for the +40 km s^{-1} feature in Sgr A. Thus our observations show that

$$OD/OH < 2.5 \times 10^{-3} \simeq 1/400. \qquad (2)$$

Hence, the OD/OH ratio in the +40 km s^{-1} Sgr A feature is at least a factor of two less than the DCN/HCN number ratio and the HD/H_2 formation-rate ratio found in other parts of the interstellar medium.

III. DISCUSSION

Several theories have been presented in the literature to account for the deuterium enrichment in deuterated molecules. Solomon and Woolf (1973) suggest that the enrichment results from exchange reactions occurring on interstellar grains or in the gas phase. Under the same conditions (i.e., the same D/H ratio and the same dust temperature of 80°K) which produce a DCN/HCN ratio of 1/170, the expected OD/OH ratio is 1/850 since the zero-point vibrational energy difference between OH and OD is 507 cm^{-1} (Herzberg 1950) or 730°K. This is a factor of two smaller than the upper limit established by our observations. An expected ratio derived this way is very uncertain; a lower equilibrium temperature in the OH cloud would significantly enhance the OD/OH ratio. Also, if OD and OH are derived from the dissociation of larger molecules, the OD/OH ratio would reflect the enrichment of deuterium in the parent molecules, resulting in a different predicted OD/OH ratio.

On the other hand, Watson (1973) proposes that the gas phase in a very dense interstellar cloud has a D/H free-atom ratio larger than the cosmic ratio. Depending on the value chosen for the cosmic ratio (10^{-4} - 4×10^{-4}), Watson predicts an enrichment factor of 100-200 in the depths of very dense clouds (and greater enrichment in regions closer to the cloud edge). This, he suggests, accounts for the enriched DCN/HCN abundance ratio and the increased HD/H_2 formation rate ratio. His theory predicts that at chemical

equilibrium any deuterated molecule would show an enrichment factor of 100-200 if its formation-and destruction-rate constants and the intensity of destroying radiation are the same as for the protonated molecule. Our observations show that OD is apparently underabundant by at least a factor of two if the physical conditions in the Orion and Sgr A clouds are the same.

Research in radio astronomy at the Owens Valley Radio Observatory is supported by the National Science Foundation under grant GP 30400-Xl and by the Office of Naval Research under contract N00014-67-A-0094-0019. M.A. was partially supported by a California State Graduate Fellowship and a DuPont Summer Fellowship.

REFERENCES

Bieging, J. 1973, private communication.

Cesarsky, D. A., Moffet, A. J., and Pasachoff, J. M. 1973, Ap. J. (Letters), 180, L1.

Herzberg, G. 1950, Molecular Spectra and Molecular Structure. I. Spectra of Diatomic Molecules (2d ed.; New York: Van Nostrand Reinhold).

Lide, D. R. 1967, Nature, 213, 694.

Meerts, W. L., and Dymanus, A. 1973, Ap. J. (Letters), 180, L93.

Pasachoff, J. M., Gottlieb, C. A., Snyder, L. E., Buhl, D., Palmer, P., Zuckerman, B., and Dickinson, D. F. 1970, Bull. AAS, 2, 213.

Poynter, R. L. 1973, private communication.

Poynter, R. L., and Beaudet, R. A. 1968, Phys. Rev. Letters, 21, 305.

Robinson, B. J., Gardner, F. F., van Damme, K. J., and Bolton, J. G. 1964, Nature, 202, 989.

Robinson, B. J., and McGee, R. X. 1970, Australian J. Phys., 23, 405.

Spitzer, L., Drake, J. F., Jenkins, E. B., Morton, D. C., Rogerson, J. B., and York, D. G. 1973, Ap. J. (Letters), 181, L116.

Solomon, P. M., and Woolf, N. J. 1973, Ap. J. (Letters), 180, L98.

Watson, W. D. 1973, Ap. J. (Letters), 181, L129.

Weinreb, S., Barrett, A. H., Meeks, M. L., and Henry, J. C. 1963, Nature, 200, 829.

Wilson, R. W., Penzias, A. A., Jefferts, K. B., and Solomon, P. M. 1973, Ap. J. (Letters), 179, L107.

PROPOSITIONS

Proposition 1

ATOM-MOLECULE CHARGE TRANSFER SPECTRA AND THE DIFFUSE INTERSTELLAR ABSORPTION BANDS

I. INTRODUCTION

Over forty years have passed since diffuse absorption bands in stellar visible spectra have been identified as interstellar features. Yet no general agreement on the nature of the species producing the bands has been reached. There is a wide range of suggested identifications for one or more of the bands, with much effort being concentrated on the 4430 Å feature since it is the most intense band. It has been proposed that the bands are due to electronic transitions of atoms trapped in a frozen gas matrix, in particular, Ca in an inert gas (Duley 1968) or hydrocarbon (Duley 1969a) matrix and Na in a hydrocarbon matrix (Duley 1969b). On the other hand, similarities have been shown to exist between some of the diffuse interstellar bands and visible absorption spectra of certain terrestial minerals which contain metal ions in metal oxide crystal lattices (for example, Huffman 1970 and Manning 1972). A unique approach is that of Johnson (1972) who finds that many of the interstellar bands match absorption bands of porphyrin molecules. As can be seen, suggestions for the origins of the bands involve refractory grains or "icy" grain mantles. On the other hand, Herzberg (1971) suggests that the bands may be due to predissociation-broadened absorption of an interstellar gas-phase radical or molecular ion.

One possibility involving the grains that has not yet been mentioned in the literature is that the diffuse interstellar absorption lines

may be charge transfer bands involving metal atoms or atomic ions embedded in the grain mantle. [Although Snow and Cohen (1975) interpret their observational data as showing that the diffuse interstellar absorption bands could not result from grain mantles, the situation is far from being conclusive and the aforementioned suggestion warrants study.] This proposition suggests a laboratory investigation of one possible astrophysical situation, a Mg^+ - NH_3 complex, that might produce an absorption line in the visible region which corresponds to one of the interstellar lines. However, before discussing this system in particular, a general approach to estimating the energies of charge transfer bands will be presented.

The lowest energy charge transfer band of a complex can be approximated using the approach of Mulliken and Person (1969). The nature of the complex must be postulated to enable a simplification of the calculations. In the case of an atom A simply embedded in a host matrix and interacting only weakly with its neighbors M, the result shall be assumed to be a loose 1:1 complex. Two electronic configurations, one a no-bond (AM) structure with a wavefunction ψ_0 and the other a "dative" (A^-M^+) structure with a wavefunction ψ_1, are in resonance. However, in the case of a loose complex, the ground state is basically ψ_0 and the excited state ψ_1. The fact that the AM and A^-M^+ configurations are in resonance requires that the ground and excited states of the complex belong to the same spatial symmetry group.

For a weak 1:1 complex between an impurity atom A with an electron affinity EA(A) and a matrix molecule M with an ionization

potential IP(M), the estimated energy E_{ct} and frequency ν_{ct} of the lowest energy charge transfer band can be estimated:

$$E_{ct} = h\nu_{ct} = IP(M) - EA(A) + G_1 - G_0 + X_1 - X_0 \qquad (1)$$

where

$$X_0 = \beta_0^2/\Delta \quad \text{and} \quad X_1 = \beta_1^2/\Delta \ , \qquad (2)$$

$$\beta_0 = W_{01} - W_0 S_{01} \quad \text{and} \quad \beta_1 = W_{01} - W_1 S_{01} \ , \qquad (3)$$

$$\Delta = W_1 - W_0 \ , \qquad (4)$$

$$W_{01} = \int \psi_0^* \mathcal{H} \psi_1 dv \ , \quad W_0 = \int \psi_0^* \mathcal{H} \psi_0 dv, \text{ and } W_1 = \int \psi_1^* \mathcal{H} \psi_1 dv, \qquad (5)$$

and

$$S_{01} = \int \psi_0^* \psi_1 dv \ . \qquad (6)$$

The integrals are over all space. $\mathcal{H}$ is the Hamiltonian operator for the system. S_{01} is the overlap integral between ψ_0 and ψ_1. W_0 and W_1 are the energies of ψ_0 and ψ_1, respectively, and Δ is their energy difference. G_0 and G_1 are the energy changes that occur when A and M and A^- and M^+, respectively, are brought together from infinite separations, the most important contributions coming from the

resulting Coulombic interactions. X_0 and X_1 are the resonance energies resulting from the fact that the complex states are linear combinations of ψ_0 and ψ_1.

The intensity of the charge transfer band is partly a function of the proximity of A to M. The transition moment decreases as A is removed from M.

II. THE $Mg^+ - NH_3$ COMPLEX

The $Mg^+ - NH_3$ solid-state complex probably occurs in interstellar regions. Magnesium is the seventh "cosmically" most abundant non-noble gas element (Aller 1961). The ionization potential of Mg^0 is 7.65 eV (Herzberg 1944). Since this is much less than the 13.6 eV high energy cutoff for optical radiation in HI regions,most of the observed interstellar magnesium exists in the gas-phase as Mg^+ (Rogerson et al. 1973). Ammonia is one of the most abundant interstellar molecules detected by radio astronomy (Rank, Townes, and Welch 1971) and has been suggested to be one of the components of icy grain mantles (Wickramasinghe and Nandy 1972). Therefore, a $Mg^+ - NH_3$ complex should not be as astrophysically rare as some of the other situations advanced to explain the interstellar absorption bands.

The frequency of the lowest energy charge transfer band in a $Mg^+ - NH_3$ complex may be estimated from equation (1), guided by the suggestions of Mulliken and Person (1969). The ground state of the complex is basically $(Mg^+)NH_3$, the first excited state $Mg(NH_3^+)$. The ionization potential of NH_3[IP(M)] is 10.15 eV (Mulliken and Person 1969). The electron affinity of Mg^+[EA(A)] is equal to the ionization potential of Mg^0 (7.65 eV). Then, the zero interaction energy difference Δ is ~ 2.50 eV [$= IP(NH_3) - EA(Mg^+)$]. To a first approximation,

$$G_1 - G_0 = 0 \qquad (7)$$

since the Coulombic terms are relatively small because one member of the complex is always essentially electrically neutral. S_{01} and β_0 will be estimated to be 0.1 and -0.5 eV, respectively, since a weak complex is assumed. Then, the following values for the remaining variables can be derived:

$$X_0 = 0.1 \text{ eV}, \quad \beta_1 = -0.75 \text{ eV}, \text{ and } X_1 = 0.22 \text{ eV}. \tag{8}$$

Thus,

$$E_{ct} = 2.62 \text{ eV and } \lambda_{ct} = 4732 \text{ Å}. \tag{9}$$

It is interesting to note that Ogg (1946) observed continuous absorption bands peaking toward the red in liquid ammonia solutions of Mg. However, he ascribed these features to single electrons and electron pairs trapped in NH_3 bubbles.

The value of ν_{ct} calculated above is strongly dependent on the variable values chosen. But it does demonstrate the fact that the complex might absorb at a wavelength corresponding to one of the diffuse interstellar bands. Moreover, the laboratory bands will be broadened by the wide variation in the nature of the Mg^+- NH_3 complex (degree of overlap, etc.) in a given NH_3 matrix, also paralleling the interstellar situation.

Preparing and maintaining a solid NH_3 matrix impregnated with Mg^+ is the major experimental problem. One apparatus appropriate for this experiment, based on a design of Linevsky (1961), is shown in figure 1. An arc-discharge ion source and an

Fig. 1.- Apparatus for preparing Mg^{+}- NH_3 complex and observing its charge transfer spectra.

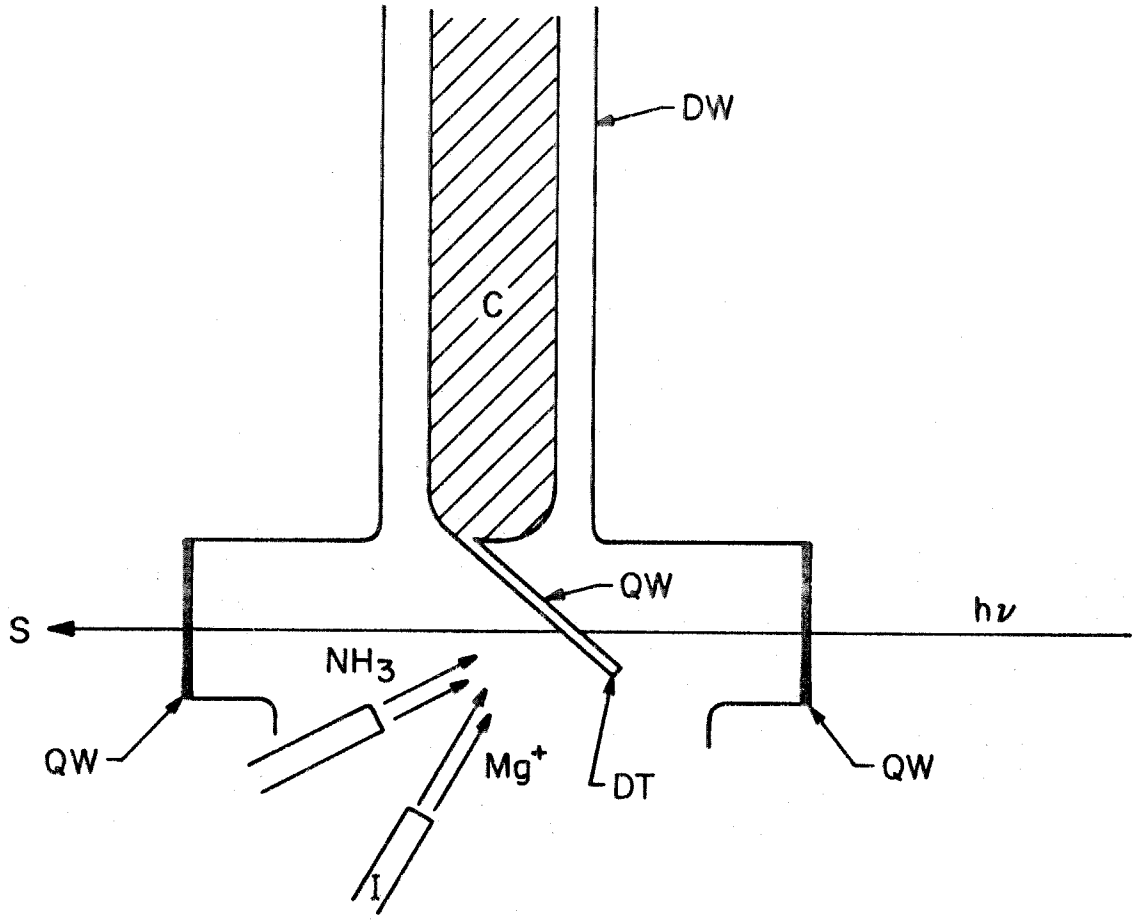

C - cold finger cooled by liquid helium
DT - doughnut
DW - dewar
I - ion source + ion beam focusing system
QW - quartz window
S - spectrometer

ion-optical system to extract and focus the ions (Panev et al. 1974) can produce the necessary Mg^+ beam, which is merged with the NH_3 beam and condensed onto a quartz window. The window is cooled to ~ 3°K by a hollow metal "doughnut" cooled with liquid helium (in the doughnut hole sits the quartz window on which the molecular beams are condensed and through which the light beam passes). The NH_3 matrix is stable since the melting point of solid ammonia is 195°K. The whole assembly is in an evacuated Dewar flask which has two exterior quartz windows to allow the passage of a light beam for absorption spectroscopy.

One problem to be considered is the neutralization of embedded Mg^+ through the scavenging of stray electrons. Whether or not this should be a significant factor is uncertain considering that the spectra of matrix-isolated cations have been observed (Milligan and Jacox 1972). If an absorption band is seen, its attribution to an Mg^+-NH_3 or Mg-NH_3 complex may be easily checked by replacing the ion source and focusing system with an effusion-type source and collimating slits (Panev et al. 1974) to produce an Mg^0 beam and repeating the experiment. Another control experiment is to take the spectrum of an undoped solid NH_3 matrix to certify that any absorption bands are not due to trace impurities in the NH_3 beam.

Thus, ion (or atom)- molecule charge transfer bands may exist in the visible spectrum that could account for the diffuse interstellar absorption lines. The Mg^+- NH_3 complex probably exists in interstellar space and would be a good start for a systematic laboratory study of such systems.

REFERENCES

Aller, L. H. 1961, The Abundance of the Elements (New York: Interscience).

Duley, W. W. 1968, Nature, 218, 153.

_____. 1969a, Nature, 224, 785.

_____. 1969b, Physica, 41, 134.

Herzberg, G. 1944, Atomic Spectra and Atomic Structure (New York: Dover).

_____. 1971, Quart. Rev., XXV, 201.

Huffman, D. R. 1970, Ap. J., 161, 1157.

Johnson, F. M. 1972, Mem. Soc. Roy. des Sci. de Liège, 6 Ser., III, 391.

Linevsky, M. 1961, J. Chem. Phys., 34, 587.

Manning, P. G. 1972, Nature, 240, 547.

Milligan, D. E., and Jacox, M. E. 1972, in Molecular Spectroscopy: Modern Research, ed. K. N. Rao and C. W. Mathews (New York: Academic Press), p. 259.

Mulliken, R. S., and Person, W. B. 1969, Molecular Complexes, (New York: Wiley-Interscience).

Ogg, R. A. 1946, J. Chem. Phys., 14, 114.

Panev, G. S., Zavilopulo, A. N., Zapesochnyi, I. P., and Shpenik, O. B. 1974, Zh. Eksp. Teor. Fiz, 67, 47.

Rank, D. M., Townes, C. H., and Welch, W. J. 1971, Science, 174, 1083.

Rogerson, J. B., York, D. G., Drake, J. F., Jenkins, E. B., Morton, D. C., and Spitzer, L. 1973, Ap. J. (Letters), 181, L110.

Snow, F. P., and Cohen, J. G. 1975, Ap. and Space Sci., 34, 33.

Wickramasinghe, N. C., and Nandy, K. 1972, Rep. Prog. Phys., 35, 157.

Proposition 2

OBSERVATION OF MICROWAVE SPECTRAL LINES OF INTERSTELLAR "METASTABLE" MOLECULAR HYDROGEN

Hydrogen is the cosmically most abundant element. In dense dust clouds, hydrogen is predicted to exist mainly in the form of H_2 (Hollenbach, Werner, and Salpeter 1971). Although not observable in the dense clouds, H_2 ultraviolet transitions detected by the Orbiting Astronomical Observatory 3 (Copernicus) in low density dust clouds indicate that the fraction of hydrogen in molecular form does increase with the column density of dust in the cloud (Spitzer et al. 1973). Further evidence for the predominance of H_2 in dense clouds comes from observations of the 21-cm atomic hydrogen line that indicate an underabundance of atomic hydrogen relative to the dust column density (as determined from interstellar extinction measurements), assuming that proportionality is as valid for dense clouds as it is for the general interstellar medium (Heiles 1971). Moreover, the excitation of other molecules observed in these clouds indicates gas densities that can be accounted for only if the missing atomic hydrogen is in the form of H_2 (Zuckerman and Palmer 1974).

Direct observation of H_2 in dense dust clouds (often called "dark" or "black" clouds [Winnewisser, Mezger, and Breuer 1974]) is nearly impossible because (1) electric dipole-allowed electronic transitions from the ground state of H_2 occur in the ultraviolet and (2) weaker electric quadrupole vibrational transitions within the ground electronic state are in the visible, dark clouds being opaque in both spectral regions. Although infrared radiation can penetrate

dark clouds, rotational transitions within the ground vibrational and electronic state are very weak since H_2 has no permanent dipole moment. However, due to the large H_2 column densities expected, the rotational transitions may be detectable and the technological capability (frequency resolution and sensitivity) to successfully observe these lines may be just now becoming available (Bussoletti and Stasinska 1975). Radio frequency waves can also penetrate dark clouds and the $c\ ^3\Pi_u$ state of H_2 ("metastable" H_2) has microwave fine and hyperfine transitions that could be detected by present techniques if the lines are of sufficient strength. Since information about H_2 densities are of great importance to theories of interstellar molecule formation and excitation and to theories of cloud collapse and star formation, it is proposed that a high sensitivity search for the microwave transitions be conducted.

The v=0 level of the $c\ ^3\Pi_u$ state of H_2 is its only metastable vibronic state (Johnson 1972). The fine structure results from the nonzero electronic orbital and electron spin angular momenta coupling to the orbital angular momentum due to nuclear motion and is best fitted by the Hund's case b coupling pattern (Lichten 1960). The projection of the electronic orbital angular momentum onto the internuclear axis (Λ, where $\Lambda = 1$ for a Π state) is coupled to the nuclear motion angular momentum ($\hat{O}$) to define rotational levels N,

$$N = \Lambda + O,\ O = 0,1,2,3,\ldots \qquad (1)$$

The electron spin angular momentum $\hat{S}$ (S = 1 for triplet state) is

coupled to the total orbital angular momentum $\hat{N}$ to form fine structure levels J,

$$J = N + S,\ N + S - 1,\ \ldots,\ |N - S|, \tag{2}$$

where $\hat{J}$ is the total angular momentum exclusive of nuclear spin. Since the nuclear spin of the hydrogen atom is 1/2, the hydrogen molecule has two possible nuclear spin configurations, ortho (I=1) and para (I=0). For para-H_2, $\hat{J}$ is the total angular momentum of the molecule. In the case of ortho-H_2, the nuclear spin angular momentum $\hat{I}$ is coupled to $\hat{J}$ to form hyperfine levels F,

$$F = J + I,\ J + I - 1,\ \ldots,\ |J - I|, \tag{3}$$

where now $\hat{F}$ is the total angular momentum.

Only the odd-N levels of ortho-H_2 and the even-N levels of para-H_2 are metastable (Johnson 1972). Since $S \neq 0$, the $c^3\Pi_u$ state has a magnetic dipole moment. The transitions, $\Delta N = 0$ and $\Delta J = \pm 1$, are the possible magnetic dipole-allowed microwave transitions for this state. Figure 1 shows the fine and/or hyperfine splittings of the lowest rotational level in each spin ladder (the spacing between ortho N=1 and para N=2 is not to scale). The magnetic dipole transition frequencies are derived from Brooks, Lichten, and Reno (1971) for the N=1 level and from Lichten (1962) for the N=2 level.

Interstellar metastable H_2 could be formed in several ways, in

Fig. 1.- Fine structure, hyperfine structure, and magnetic dipole transition frequencies for the lowest rotational levels of the c $^3\Pi_u$, v=0 state of H_2. Separation between N=1 and N=2 is not to scale.

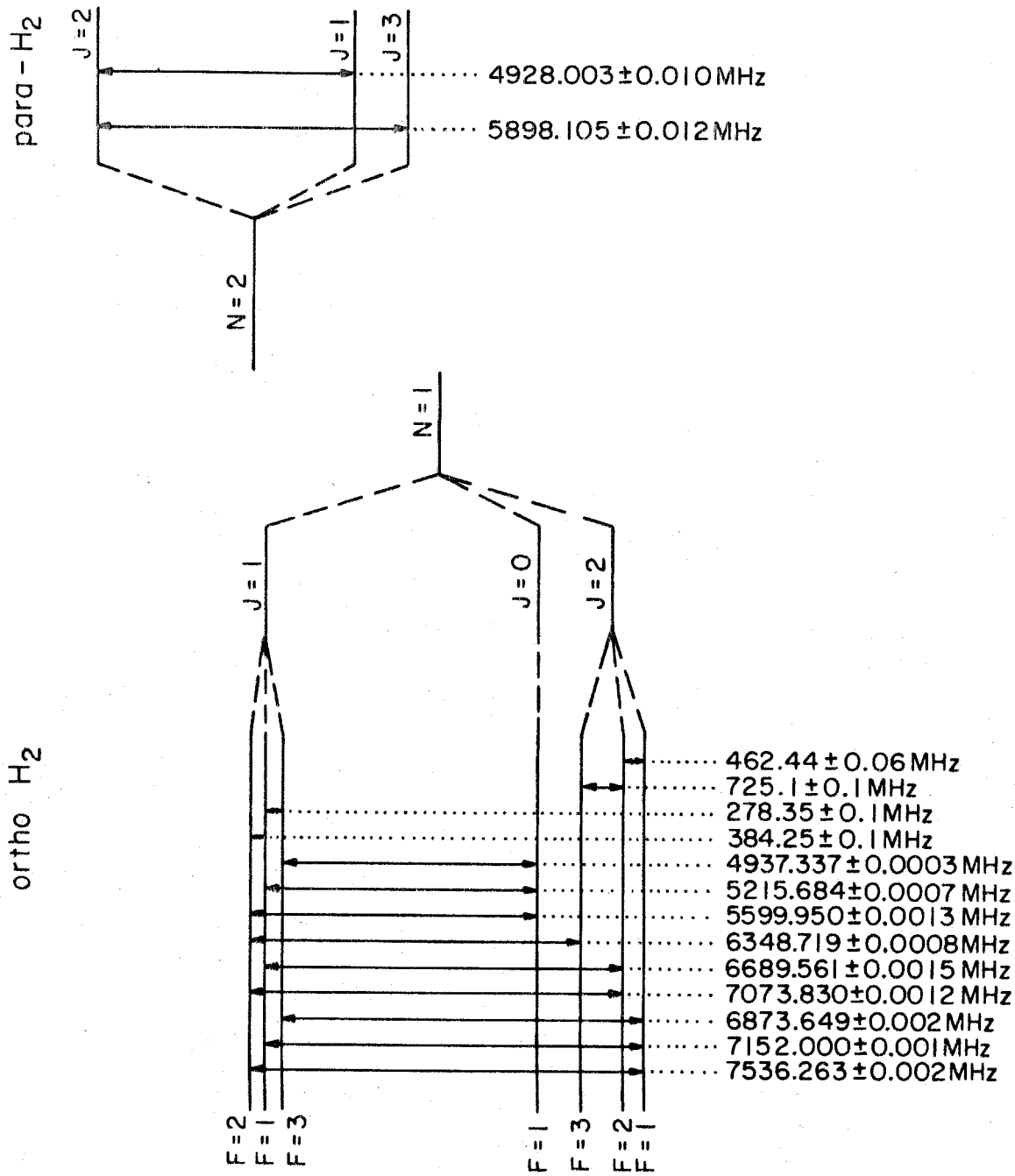
para - H_2
J=2
J=1
J=3
4928.003±0.010MHz
5898.105±0.012MHz
N=2
ortho H_2
N=1
J=1
J=0
J=2
462.44±0.06MHz
725.1±0.1MHz
278.35±0.1MHz
384.25±0.1MHz
4937.337±0.0003MHz
5215.684±0.0007MHz
5599.950±0.0013MHz
6348.719±0.0008MHz
6689.561±0.0015MHz
7073.830±0.0012MHz
6873.649±0.002MHz
7152.000±0.001MHz
7536.263±0.002MHz
F=2
F=1
F=3
F=1
F=3
F=2
F=1

particular, electron recombination with H_2^+ (Malville 1964) and electron impact excitation from the H_2 ground electronic state (threshold energy is ~ 11.9 eV [Lichten 1960]). The later process is probably the most efficient and the rate constants are most easily calculable. Since the $b\ ^3\Sigma_u^+ - c\ ^3\Pi_u$ transition is electric dipole-forbidden, the $c\ ^3\Pi_u$ state is metastable, although its lifetime of 1 ms (Johnson 1972) is still very short compared to normal interstellar collision timescales. Therefore, the optimum region for a substantial metastable H_2 presence (and towards which the observations should be directed) is one in which the formation rate is significant, high concentrations of H_2 and high energy (≥ 12 eV) electrons being required. If the present picture of dense molecule clouds is correct, the interface of a dense cloud (in which an abundance of H_2 exists) and an HII region (where sufficiently energetic electrons may be plentiful) is suggested to be the optimum search area.

The best place for an initial detection of metastable H_2 transitions may be the Orion Nebula. Indeed, Zuckerman (1973) suggests that the visible HII region is in physical contact with the dense molecule cloud behind it. Since the estimated transition probabilities for these magnetic dipole transitions are approximately 100 times greater than the 21-cm atomic hydrogen line (Malville 1964) but still 100 times less than typical electric dipole transitions (Pacholczyk 1970), detection will only be possible for a very large column density. The dark bay northeast of the Trapezium region of the Orion nebula might be the best place to concentrate the search, because it is thought that this may be a region where the background dense

molecular cloud is curling around the optical nebula (Zuckerman 1973). The possible column density might be enhanced in this direction since one would be observing along the edge of the H_2-HII interface, and not across as would be the case if one looked towards the center of the molecule cloud (the KL nebula). Indeed, only in the area of the dark bay was there a detection of a faint emission feature in the visible spectrum, which corresponds to an H_2 vibrational-rotational transition (Werner and Harwit 1968).

Gammon, Brown, and Gordon (1973) have searched previously for the N=2, J=1-2 line of para-H_2, but they were only able to set an upper limit to the column density an order of magnitude higher than their predicted value. The sensitivity of the search for metastable H_2 lines can be easily increased by an order of magnitude by optimizing some of the observational parameters. First, as was discussed earlier, the choice of observing region can make a big difference. The earlier observations were performed with a 140-foot diameter telescope whose beam width at 5 GHz is ~4 arcminutes. Since the telescope was pointed at the KL nebula, only a fraction of the beam was filled by the dark bay and the antenna response would be reduced proportionally, assuming that most of the signal would be coming from the dark bay as suggested above. So, filling the telescope beam with the dark bay should increase significantly the chances of detection. Second, Copernicus observations of H_2 in low density clouds in the direction of Orion show that the ortho to para abundance ratio is ~ 3 (Spitzer, Cochran, and Hirshfeld 1974), which is to be expected if the populations of the states are weighted

in proportion to their spin statistics. If this also were to be true in dense clouds, the population of the N=1 level may be three times that of the N=2 level and it would be better to observe ortho $\Delta J=1$ transitions. However, any one of the N=1, $\Delta J=1$ transitions are approximately only as strong as the corresponding N=2 transition since the hyperfine splitting basically results in three transitions in N=1 for every one in N=2. A three-fold enhancement of sensitivity may still be obtainable if the data for each of the transitions corresponding to the three hyperfine components were to be added together by velocity (all components having the same Doppler shift since they all probably originate in the same region) as was done for OD by Allen, Cesarsky, and Crutcher (1974).

Thus, another observing attempt with sensitivity enhanced as suggested may have a good chance of detecting metastable H_2 if the theoretical predictions of Gammon, Brown, and Gordon (1973) are correct. If detection were achieved, direct measurement of the density of the molecule cloud nearest the HII region would be possible. Moreover, the detection raises the possibility that metastable H_2 lines could serve as tracers for delineating the boundaries of H_2-HII regions. Many of the largest molecule clouds observed seem to be associated with HII regions (Zuckerman and Palmer 1974) and the ability to map the boundary would add to our knowledge of the dynamics of these complex regions.

REFERENCES

Allen, M., Cesarsky, D. A., and Crutcher, R. M. 1974, Ap. J., 188, 33 (also Chapter 5 of this thesis).

Brooks, P. R., Lichten, W., and Reno, R. 1971, Phys. Rev. A, 4, 2217.

Bussoletti, E., and Stasinska, G. 1975, Astr. and Ap., 39, 177.

Gammon, R. H., Brown, R. L., and Gordon, M. A. 1973, Bull. AAS, 5, 23.

Heiles, C. 1971, Ann. Rev. Astr. and Ap., 9, 293.

Hollenbach, D., Werner, M. W., and Salpeter, E. E. 1971, Ap. J., 163, 165.

Johnson, C. E. 1972, Phys. Rev. A, 5, 1026.

Lichten, W. 1960, Phys. Rev., 120, 848.

_____. 1962, Phys. Rev., 126, 1020.

Malville, J. M. 1964, Ap. J., 139, 198.

Pacholcyzk, A. G. 1970, Radio Astrophysics (San Francisco: W. H. Freeman).

Spitzer, L., Cochran, W. D., and Hirshfeld, A. 1974, Ap. J. Suppl., 28, 373.

Spitzer, L., Drake, J. F., Jenkins, E. B., Morton, D. C., Rogerson, J. B., and York, D. G. 1973, Ap. J. (Letters), 181, L116.

Werner, M. W., and Harwit, M. 1968, Ap. J., 154, 881.

Winnewisser, G., Mezger, P. G., and Breuer, H.-D. 1974, Topics in Current Chemistry, 44, 1.

Zuckerman, B., and Palmer, P. 1974, Ann. Rev. Astr. and Ap., 12, 279.

Proposition 3

THE EFFECT OF THE METAL-LIQUID INTERFACE ON THE MEASURED PHOTOELECTRIC WORK FUNCTION

I. INTRODUCTION

In a manner similar to the approaches of other investigators ... the field, Holroyd and Allen (1971) calculate the energy V_0 of the bottom of the conduction band of a liquid (relative to the vacuum) as the difference $\Delta\Phi$ between the photoelectric work functions of a metal in a vacuum (Φ_{vac}) and of the metal immersed in the liquid of interest (Φ_{liq}):

$$V_0 = \Delta\Phi = \Phi_{liq} - \Phi_{vac} \cdot \qquad (1)$$

The nature of the metal-liquid interface is not considered to affect the results. However, the spread in the measured values of $\Delta\Phi$ for a given liquid (see table 1) does not seem to be random. Some correlation with the composition of the metal surface is suggested. Indeed, Gomer (1972) indicates that the metal-liquid interface can affect the measurement of $\Delta\Phi$ in field emission studies. In this proposition, the nature of interfacial effects will be considered and experiments to measure the effects will be outlined.

Before the possible changes in the work function due to the metal-liquid interface are considered, the basic theory of the photoelectric ejection technique and known surface effects from vacuum studies will be discussed. Figure 1 shows the relative potential energies of the various states involved in electron emission. On the average, the Fermi level is the highest occupied energy level in a

TABLE 1

EXPERIMENTALLY DETERMINED VALUES OF $\Delta\Phi$*

Liquid	Metal Surface		
	Ba	Zn	Mg
n-Hexane	+0.09 ± 0.03	-0.02 ± 0.06	-0.07 ± 0.03
n-Pentane	+0.06 ± 0.03	-0.08 ± 0.06	-0.19 ± 0.04
Cyclopentane	-0.26 ± 0.03	-0.29 ± 0.05	-0.46 ± 0.04
2,2,4-Trimethyl pentane	-0.17 ± 0.03	-0.18 ± 0.04	†
Neopentane	-0.37 ± 0.03	-0.48 ± 0.06	†
Tetramethylsilane	-0.58 ± 0.04	-0.65 ± 0.06	-0.64 ± 0.03

NOTE. - Units are eV.

* Holroyd and Allen 1971.

† Data not available.

Fig. 1.- Potential-energy levels involved in photoelectric emission from a metal into a vacuum or liquid when no external electric field is applied (solid lines) and when one is applied with the metal as the cathode (dashed lines).

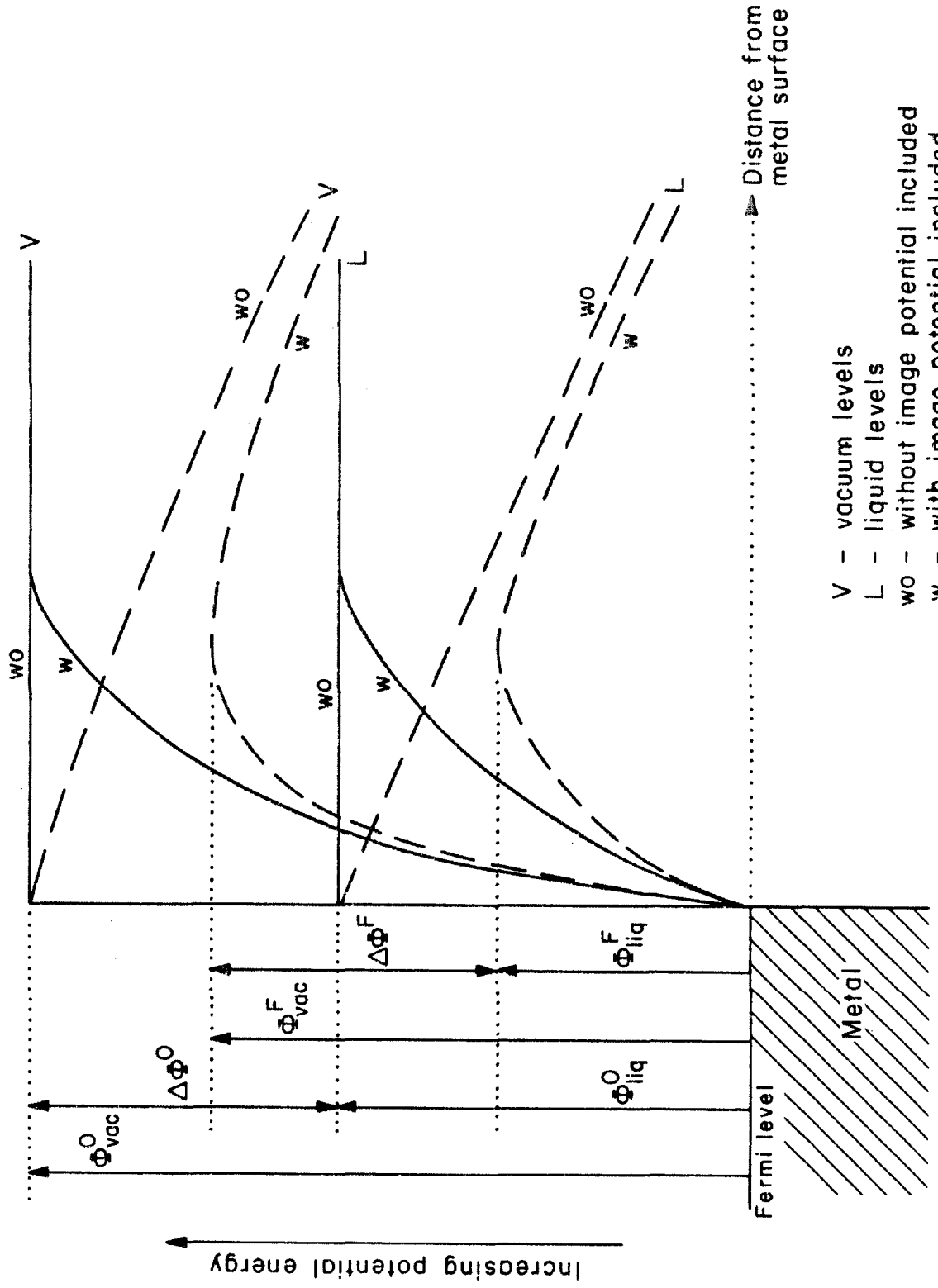
V - vacuum levels
L - liquid levels
wo - without image potential included
w - with image potential included
Distance from metal surface
Increasing potential energy
Fermi level
Metal
Φ^O_{vac}
$\Delta\Phi^O$
Φ^O_{liq}
Φ^F_{vac}
$\Delta\Phi^F$
Φ^F_{liq}
V
L
wo
w

metal. In the absence of an external electric field, the work function Φ^0_{vac} is the minimum energy needed to eject an electron from the metal surface into the vacuum. An electron will be emitted upon absorption of a photon of light whose energy is equal to or greater than Φ^0_{vac}, thus the photoelectric effect discovered by Hertz and Hallwachs and explained by Einstein (Mauerer 1958). When one includes for completeness the contribution of the image potential, the energy barrier at the surface is not abrupt (Gomer 1961; see also fig. 1). In the zero field case, the image potential term does not change the value of the work function. However, when an external electric field F is applied and the metal is the cathode, the inclusion of the image potential results in a decrease in the work function (Gomer 1961):

$$\Phi^F_{vac} = \Phi^0_{vac} - 3.8\sqrt{F} \qquad (2)$$

where F is in volts per angstrom. The top of the resulting curved barrier (fig. 1) is called the Schottky saddle.

Besides decreasing the work function, the application of an external field warps the vacuum energy level and thus permits quantum mechanical tunneling out of the metal into the vacuum at energies lower than that of the top of the barrier (Adamson 1967). This results in a reduced effective work function. However, in the experiment to be described later, the field is applied only to enhance the collection of photoelectrons. At the field strengths used ($\sim$10 kV cm^{-1} or $\sim 10^{-4}$ V Å^{-1}), the work function reduction is only

$\sim$0.04 eV ($\sim$ 1-2 % of Φ_{vac}) and it will be assumed that $\Phi^{0}_{vac} \approx \Phi^{F}_{vac}$. Moreover, the warped barrier is so wide that quantum mechanical tunneling is negligible.

When the metal is immersed in a liquid, the new barrier to electron escape from the metal is Φ_{liq} (Gomer 1972; see also fig. 1). Depending on the particular nature of the liquid, Φ_{liq} may be less than, equal to, or greater than Φ_{vac}. As in the vacuum situation, an exact description of the energy levels in the liquid includes the image potential term and, therefore, the measured Φ_{liq} is field-dependent, although again $\Phi^{o}_{liq} \approx \Phi^{F}_{liq}$ at low field strengths. As defined in equation (1), $\Delta\Phi$ can be thought of as the energy of the bottom of the conduction band of the liquid (Holroyd and Allen 1971) and also as the solvation energy of the electron relative to the vacuum (Gomer 1972).

In vacuum studies, the experimentally measured value of Φ_{vac} has been shown to be very sensitive to the exact nature of the surface, a phenomena very easily seen in field emission studies. Theory shows that a redistribution of electron density at the metal surface will change the observed work function. This redistribution may be caused by the surface adsorption of molecules, surface impurities in the metal, or simply a variation in the structure of the metal lattice at the surface.

In the case of chemisorption resulting in electron transfer from the metal to the adsorbate, Φ_{vac} increases since the photo-ejected electrons are coming from lower energy levels in the metal (Somorjai 1972). If the reverse electron transfer occurs, the

adsorbate becomes positively charged and Φ_{vac} decreases. In either case, a bipolar surface straddles the interface.

The change in work function due to the polarization of physically adsorbed molecules can be treated in a more quantitative fashion (Thompkins 1967). The adsorbate layer can be bipolar if the adsorbed molecules have dipole moments which are all oriented in the same direction. These dipole moments may be permanent or induced by the local electrical environment of the adsorption sites (an externally applied electric field is not necessary). In tunneling through this layer to escape the surface, the ejected electron, in effect, has to cross the potential gap between the plates of a capacitor. The potential drop per unit charge across the adsorbed layer, χ, is

$$\chi = \pm 4\pi M_T , \tag{3}$$

where

$$M_T = \sigma_s \Theta M , \tag{4}$$

and

$$M = |q|d \text{ (or } = aE \text{ for nonpolar adsorbates)} . \tag{5}$$

The total dipole moment per unit surface area is M_T, the number density of available adsorption sites, σ_s, the fraction of sites occupied, Θ, and the dipole moment of an adsorbed molecule, M. If M is a permanent dipole moment, $\underline{d}$ is the separation between the centers of positive and negative charge of magnitude $|q|$. If M is an induced dipole moment, $\underline{a}$ is the polarizability of the adsorbed

molecule and E is the local electric field strength. Then, the measured work function Φ'_{vac} can be estimated:

$$\Phi'_{vac} = \Phi_{vac} + e\chi , \qquad (6)$$

where $\underline{e}$ is the charge on an electron. χ is positive when the positively charged side of the bipolar adsorbed layer is adjacent to the metal surface and vice versa.

II. THE METAL-LIQUID INTERFACE

Analogous to the vacuum effects described in the previous section, the metal-liquid interface can affect the measured value Φ'_{liq}, and therefore the measured $\Delta\Phi'$, in two ways: (1) through charge transfer between the metal and a chemisorbed layer of liquid molecules and (2) through polarization of physically adsorbed molecules and/or of molecules in the liquid near the metal surface. In all cases, there is probably some shift in Φ'_{liq} due to the induced polarization effect. If the liquid molecules are nonpolar (as is the case for the experiments to be described later),

$$\Phi'_{liq} = \Phi_{liq} + e\chi(E), \tag{7}$$

where χ is a function of the local field. Any electron transfer across the interface will modify the bilayer effect.

According to this model,

$$\Delta\Phi' = \Phi'_{liq} - \Phi_{vac} = \Phi_{liq} - \Phi_{vac} + e\chi(E), \tag{8}$$

differing from the true $\Delta\Phi(=V_0)$ by the interface term. As long as the metal surface is stable throughout the course of the experiment, the actual value of the measured vacuum work function is unimportant (and therefore enters eq. [8] as an unprimed term).

Previous groups evaluated the magnitude of interfacial effects

on the measured work function in several different ways. If Φ'_{vac} is the same before and after immersion, it is concluded that no permanent changes in the surface have occurred during immersion (Holroyd and Allen 1971). Although it has been generally assumed that this proves the relative unimportance of interfacial effects, effects due to the temporary metal-liquid interface would not be revealed. Since measurements with different phototubes immersed in liquid He resulted in the same $\Delta\Phi'$ (which is not surprising if the cathode material is always the same), Woolf and Rayfield (1965) concluded that surface effects were not important. However, they did suggest that the measured work function in the liquid might be shifted by 5% due to the polarizability of He. Thus, the effect of the metal-liquid interface on the measurement of $\Delta\Phi$ has not been conclusively disproved. Indeed, Delahay (comments in Holroyd, Tames, and Kennedy 1975) suggested recently that dipoles induced at the interface may affect the V_0 measurements.

It is proposed that a series of experiments might elucidate factors affecting $\Delta\Phi'$ and might provide insight into the nature of the metal-liquid interface. The apparatus, metal surfaces, nonpolar liquids, and technique for photoelectrically-determining $\Delta\Phi$ would be basically those employed by Holroyd and Allen (1971). One improvement in the experimental procedure would be to mount the phototube on a vacuum line, enabling Φ_{vac} to be repeatedly measured under high vacuum conditions and thereby allowing more accurate monitoring of any permanent surface changes during the course of the experiment.

Variations in precisely measured values of $\Delta\Phi'$ for a given

liquid, but with different metal cathodes, would reveal the reality of interfacial effects since $\Delta\Phi'$ ideally is only a function of the liquid. A metal-to-metal spread in $\Delta\Phi'$ values could result from variation in adsorption site density in the case of physical adsorption and additionally through different degrees of electron transfer in the case of chemisorption. If the formation of a bipolar layer via physical adsorption is important, $\Delta\Phi'$ for nonpolar liquids will show a field dependence (after correction for the Schottky saddle) and the variation with E will be different for different metals, reflecting σ_s. Charge transfer in chemisorption will not result in a field-dependent value of a $\Delta\Phi'$, but the differences in $\Delta\Phi'$ for different metals might show a correlation with Φ_{vac} (nothing like this is readily seen in the data reported by Holroyd and Allen 1971). Another approach would involve some of the field emission techniques of Gomer (1972). If the vapor pressure of the liquid in the phototube is increased slowly so that first a submonolayer, then a monolayer, and gradually additional layers of the liquid molecules are adsorbed onto the metal surface, changes in the "vacuum" work function will clearly reveal interfacial effects. The changes should correlate with the degree of coverage. Differences in the shifts of the vacuum work function as a function of the fractional coverage for different metals may reflect the metal-to-metal variation in σ_s. Also the metal-to-metal variation in the vacuum work function shift for one or two layers of adsorbed molecules should correlate with the spread of values for $\Delta\Phi'$.

Possibly $\Delta\Phi'$ will vary with F, but not with the nature of the

metal surface. Such results might indicate that the bipolar layer is not an adsorbed layer, but simply the region in the liquid nearest to the surface being polarized by the high charge density.

The variation of $\Delta\Phi'$ with F (and thus E) for a given metal/liquid combination may not be easily seen. Holroyd and Allen (1971) report that Φ'_{liq} is the same for a Zn electrode in n-hexane when either 500 V or 1000 V were applied. Therefore, the polarizability of the liquid molecule is clearly important. Nonpolar liquids with large polarizabilities must be chosen to enhance the magnitude of the effect being studied.

Thus, high precision measurements of $\Delta\Phi'$ for different combinations of metal surfaces and liquids and performed under different conditions can determine the accuracy of the values of V_0 derived by previous investigators. Variations in $\Delta\Phi'$ for a given liquid should reveal details of the character of the metal-liquid interface.

REFERENCES

Adamson, A. W. 1967, Physical Chemistry of Surfaces (New York: Interscience).

Gomer, R. 1961, Field Emission and Field Ionization (Cambridge: Harvard University Press).

_____. 1972, Accts. Chem. Res., 5, 41.

Holroyd, R. A.,and Allen, M. 1971, J. Chem. Phys., 54, 5014.

Holroyd, R. A., Tames, S., and Kennedy, A. 1975, J. Phys. Chem., 79, 2857.

Mauerer, R. J. 1958, in Handbook of Physics, ed. E. U. Condon and H. Odishaw (New York: McGraw-Hill), p. 8-60.

Somorjai, G. A. 1972, Principles of Surface Chemistry (Englewood Cliffs: Prentice-Hall).

Thompkins, F. C. 1967, in The Solid-Gas Interface, Vol. 2, ed. E. A. Flood (New York: Marcel Dekker), p. 765.

Woolf, M.,and Rayfield, G. W. 1965, Phys. Rev. Lett., 15, 235.

Proposition 4

WAVELENGTH DEPENDENCE OF THE QUANTUM YIELD FOR PHOTODISSOCIATION OF NITRIC OXIDE BETWEEN 1800 AND 2300 Å

The injection of trace chemical species into the stratosphere from human-related sources is suggested to result in the depletion of atmospheric ozone (Johnston 1975). The ensuing increase in solar ultraviolet radiation reaching the earth's surface could have deleterious biological consequences. Nitric oxide, derived from airplane exhausts, nuclear explosions, and various natural sources (e.g., solar cosmic ray bursts), is involved in the following catalytic cycle in the stratosphere (Johnston 1975):

$$NO + O_3 \rightarrow NO_2 + O_2 \qquad (1)$$

$$NO_2 + O \rightarrow NO + O_2 \ , \qquad (2)$$

the net effect being the conversion of $O_3 + O$ to $2O_2$. In the atmospheric spectral window between 1840 and 2250 Å, the range important for the photodissociation of chlorofluoromethanes (Rowland and Molina 1975), it is known that NO photodissociates, but the quantum yield is unknown and the process has not been quantitatively included in atmospheric models (Reiter, Bauer, and Coroniti 1975). If the photodestruction of NO is competitive with its reactions with other species, the depletion of O_3 by the NO_x cycle (eq. [1] and [2]) would be less severe than presently calculated.

It is proposed that a high resolution wavelength-dependent study

of the NO absorption cross section and photodissociation quantum yield be performed for the wavelength range 1840 - 2250 Å. Mandelman, Carrington, and Young (1973) have conclusively shown that, upon absorption from the ground state of NO at 1910 Å ($X\,^2\Pi$, $v'' = 0 \rightarrow C\,^2\Pi$, $v' = 0$), predissociation occurs part of the time. Therefore, an examination of the whole spectral region may provide relevant data.

A schematic of an appropriate apparatus for this experiment is presented in figure 1. Since the scanning range is basically in the vacuum ultraviolet, the optics have to be specially chosen for transparency and the light paths have to be under vacuum. Because a high resolution study is proposed, the ultraviolet light source must be continuous and of sufficient intensity that the output of the monochromator will be strong enough to allow a measureable amount of photoinduced decomposition to quickly occur at each wavelength. Synchrotrons are radiation sources suitable for these purposes (Perlman, Rowe, and Watson 1974). The transmission characteristics $T_i(\lambda)$ of the beam splitters are easily determined and included in later processing for scaling the data to unit light intensity.

The monochromator output at a particular wavelength is $I_0(\lambda)$. The magnitude of $I_0(\lambda)$ can be determined from the characteristics of the synchrotron radiation source if the efficiency of the monochromator is known (Perlman, Rowe, and Watson 1974) or can be measured directly using gaseous HBr actinometry (Calvert and Pitts 1966). Although a synchrotron is a very stable light source, the time variations in $I_0(\lambda)$ can be monitored by signal S3(t).

Fig. 1.- Apparatus for measuring wavelength dependence of NO absorption cross section and photodissociation quantum yield.

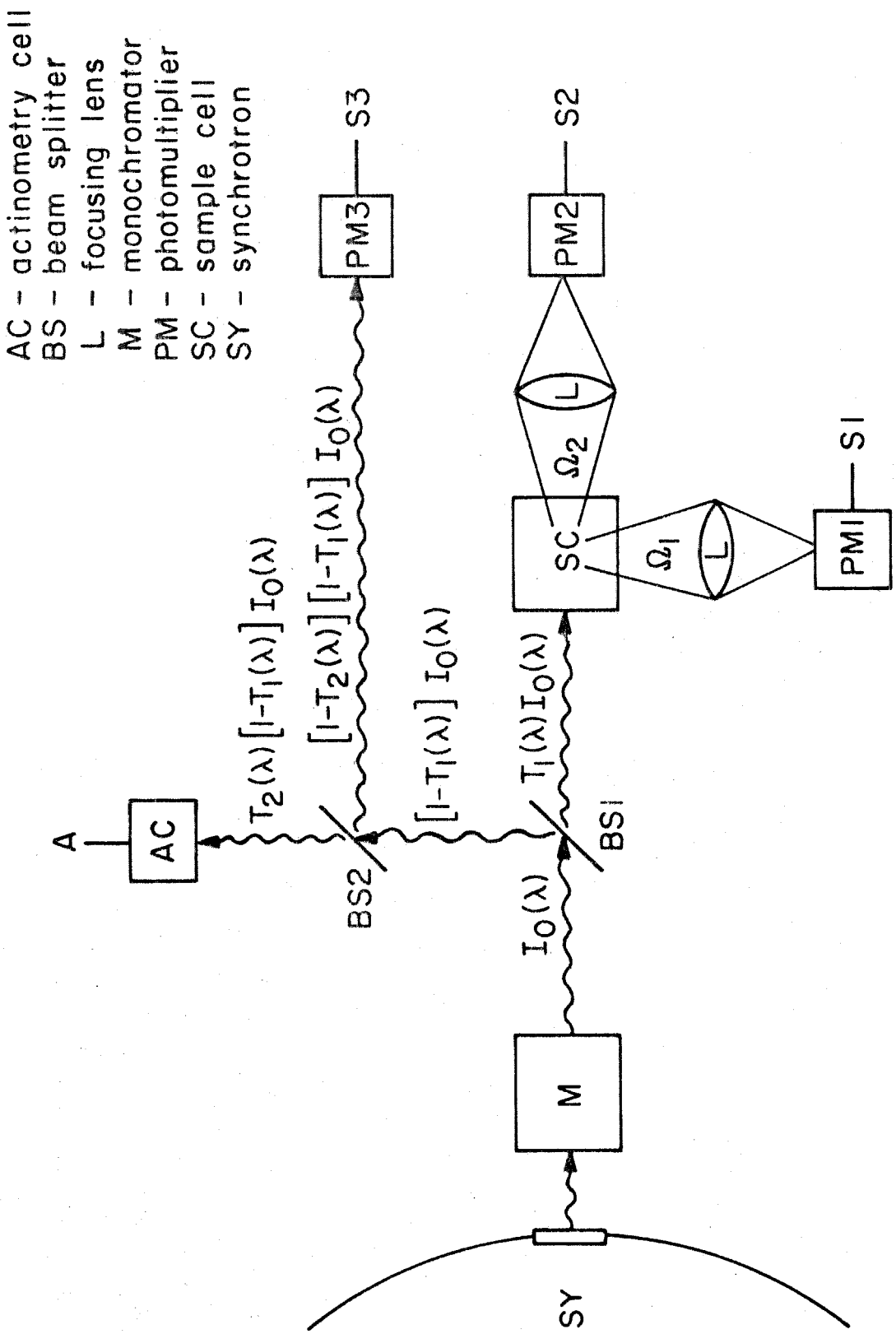
AC - actinometry cell
BS - beam splitter
L - focusing lens
M - monochromator
PM - photomultiplier
SC - sample cell
SY - synchrotron
A
AC
$T_2(\lambda)[1-T_1(\lambda)]I_0(\lambda)$
BS2
$[1-T_2(\lambda)][1-T_1(\lambda)]I_0(\lambda)$
PM3
S3
$[1-T_1(\lambda)]I_0(\lambda)$
$T_1(\lambda)I_0(\lambda)$
BS1
$I_0(\lambda)$
M
SY
SC
Ω_2
L
PM2
S2
Ω_1
L
PM1
S1

At any given point in time, the signal S2(t) reflects the number of photons passing through the cell. If NO did not fluoresce in this frequency range, S2(t)/S3(t) would be proportional to the fractional absorption of light by the system. Since NO does fluoresce from the states being pumped (Herzberg 1950), S2(t)/S3(t) will be an underestimate of the absorption and has to be corrected by the fluorescence signal S1(t) detected at right angles to the incident light beam. By taking into account the relative solid angles Ω_1 and Ω_2 subtended by PM1 and PM2, respectively, the total number of photons absorbed by the sample cell over the course of the photolysis, $I_\lambda(t')$, can be determined:

$$I_\lambda(t') = \int_0^{t'} \frac{\left[S2(t) - \frac{\Omega_2}{\Omega_1} S1(t)\right] / T_1(\lambda)}{S3(t)/[1-T_2(\lambda)][1-T_1(\lambda)]} \left\{ A_\lambda / T_2(\lambda)[1-T_1(\lambda)] \right\} \left\{ \frac{S3(t)}{S3(0)} \right\} dt. \quad (3)$$

Reactions subsequent to the dissociation of NO are used to monitor the total amount of dissociation during the course of a photolysis of duration t' (Mandelman, Carrington, and Young 1973). For every NO dissociated, one molecule of N_2 results because the reaction

$$N + NO \rightarrow N_2 + O \quad (4)$$

is very rapid at high NO concentrations. The oxygen atom can react further with other oxygen atoms to form O_2 or with a NO molecule to form NO_2, which in turn can photodissociate. Any O_2 formed disappears through further reactions. Since every dissociation of a NO molecule results in the formation of a N_2 molecule and since N_2

is inert under the conditions of this experiment, the amount of N_2 present at the end of the experiment is a measure of the amount of dissociation, assuming an initially pure NO sample. If the contents of the gas cell are condensed out at 77°K, the residual pressure will only be due to N_2 (very little of which condenses out). The number of molecules of nitric oxide dissociated in the time t′ at wavelength λ, $n_\lambda(t')$, is directly proportional to the N_2 residual pressure P_{N_2},

$$n_\lambda(t') = P_{N_2} V/kT \ , \tag{5}$$

where k is Boltzmann's constant, T temperature, and V the total volume of the sample cell.

Since N_2 and O_2 absorb only very weakly in the spectral range of interest and other species that do, like NO_2, are present only in trace amounts, light absorption by the cell can be directly attributed to absorption by NO. As the degree of NO dissociation increases, the fractional light absorption decreases. Thus S1(t), S2(t), and S3(t) must be continuously recorded so that eq. (3) can be accurately integrated over time. Then the quantum yield for NO decomposition at a given wavelength $\phi(\lambda)$,

$$\phi(\lambda) = \frac{\text{number of NO molecules dissociated per unit time}}{\text{number of photons absorbed per unit time}} \ , \tag{6}$$

can be calculated:

$$\phi(\lambda) = n_\lambda(t')/I_\lambda(t') \ . \tag{7}$$

Photodissociation in the 1840 to 2250 Å range may occur in several different ways since that spectral range includes transitions

to four different electronic excited states -- β bands ($X\,^2\Pi \rightarrow B\,^2\Pi$), γ bands ($X\,^2\Pi \rightarrow A\,^2\Sigma^+$), δ bands ($X\,^2\Pi \rightarrow C\,^2\Pi$), and ϵ bands ($X\,^2\Pi \rightarrow D\,^2\Sigma^+$). Mandelman, Carrington, and Young (1973) have shown that the $C\,^2\Pi$ levels partially predissociate. Predissociation may also occur upon absorption into $B\,^2\Pi (v' > 7)$ and $A\,^2\Sigma^+$ $(v' > 4)$ as indicated by the breaking off of the emission bands at these points (Calvert and Pitts 1966). Moreover the $D\,^2\Sigma^+$ may emit into levels of lower excited states that could predissociate. Lastly, collisional processes involving the $C\,^2\Pi$ state can result in dissociation (Mandelman, Carrington, and Young 1973). Variation of the photodissociation quantum yield with wavelength therefore would not be surprising.

The applicability of results derived from experiments starting with pure NO samples to models of upper atmosphere chemistry is not straightforward. At gas pressures above 20 torr, besides leading to dissociation of $C\,^2\Pi$ states, collisions between $A\,^2\Sigma^+$, $B\,^2\Pi$, or $C\,^2\Pi$ NO and $X\,^2\Pi$ NO can result in the direct formation of N_2 and O_2 (Mandelman, Carrington, and Young 1973). The photodissociation quantum yields would, in turn, be overestimated for an atmospheric system at the same pressure, which is mainly composed of N_2 with a trace amount of NO. Therefore it would be best to make the measurements on samples at stratospheric pressures with the appropriate ratio of N_2 to NO. Then the photo-induced processes leading to dissociation can still occur (in nonreactive collisions, N_2 acts very much like NO), but spurious processes that would affect the N_2 measurement are suppressed.

Two side results from the wavelength-dependent photodissociation quantum yield measurements are the measurement of the wavelength dependence of the absolute and net absorption cross sections of NO. With a knowledge of the pathlength of the cell, ℓ, and the initial concentration of NO, the absolute absorption cross section $\sigma(\lambda)$ can be determined from Beer's Law,

$$\sigma(\lambda) = -\frac{1}{[NO]\ell}\left\{\ln\frac{[1-T_1(\lambda)][1-T_2(\lambda)]}{T_1(\lambda)} + \ln\frac{S2(0) - \frac{\Omega_2}{\Omega_1}S1(0)}{S3(0)}\right\}, \quad (8)$$

where [NO] is in units of molecules cm^{-3}. At present, high resolution absorption cross sections are only known for the 1100 - 1500 Å range (Calvert and Pitts 1966). Flourescence from the excited states reduces the overall opacity due to NO, although the frequency of the emitted light is scrambled to some extent. Therefore the wavelength dependence of S1 could be used in atmospheric radiative transfer calculations to estimate the actual attenuation over a given wavelength region due to NO.

Many studies of the physical and chemical processes in the atmosphere are presently being pursued throughout the world. The NO quantum yields and cross sections that could be derived from the proposed experiment might be of significant importance to these endeavors.

REFERENCES

Calvert, J. G., and Pitts, J. N. 1966, Photochemistry (New York: Wiley).

Herzberg, G. 1950, Molecular Spectra and Molecular Structure. I. Spectra of Diatomic Molecules (2d ed.; New York: Van Nostrand Reinhold).

Johnston, H. S. 1975, Ann. Rev. Phys. Chem., 26, 315.

Mandelman, M., Carrington, T., and Young, R. A. 1973, J. Chem. Phys., 58, 84.

Perlman, M. L., Rowe, E. M., and Watson, R. E. 1974, Phys. Today, 27, 30.

Reiter, E. R., Bauer, E., and Coroniti, S. C. 1975, The Natural Stratosphere of 1974, CIAP Mon. 1 (Washington: U.S. Dept. of Transportation).

Rowland, F. S., and Molina, M. J. 1975, Rev. Geophys. and Space Phys., 13, 1.

Proposition 5

DATING OF GEOLOGICAL AND ARCHEOLOGICAL SAMPLES BY PHOTOINDUCED LUMINESCENCE

The phenomena of thermoluminescence can be used to accurately date geological and archeological samples over a wider age range [up to a million years] than radiocarbon techniques [under 50,000 years] (Wagner 1976). In the simplest model, high-energy ionizing radiation (α, β, or γ-rays) passing through an object containing minerals with a wide band gap can excite electrons from the valence band to the conduction band. A fraction of the mobile electrons thus produced may become trapped in lattice imperfections, called electron traps, with energies only a few electron volts below the bottom of the conduction band, the deexcitation occurring through phonon emission (fig. 1a). The traps are only weakly coupled to lower energy levels, so that at room temperature they may remain occupied over long periods of time, depending on their distance from the conduction band. When the sample is heated to a few hundred degrees Centigrade (either naturally or in the laboratory), the trapped electrons can be thermally excited to the conduction band and return to the ground state through nonradiative or radiative processes, the latter being thermoluminescence (fig. 1b).

Again, in the simplest case, the number of occupied electron traps is linear with the total radiation exposure of the sample. Then the age of the sample can be derived from (1) the total amount of thermoluminescence, (2) a determination of the radiation dose rate during the history of the object, and (3) a laboratory measurement of

Fig. 1.- Transitions involved in (a) occupation of electron traps, (b) thermoluminescence, and (c) photoinduced luminescence.

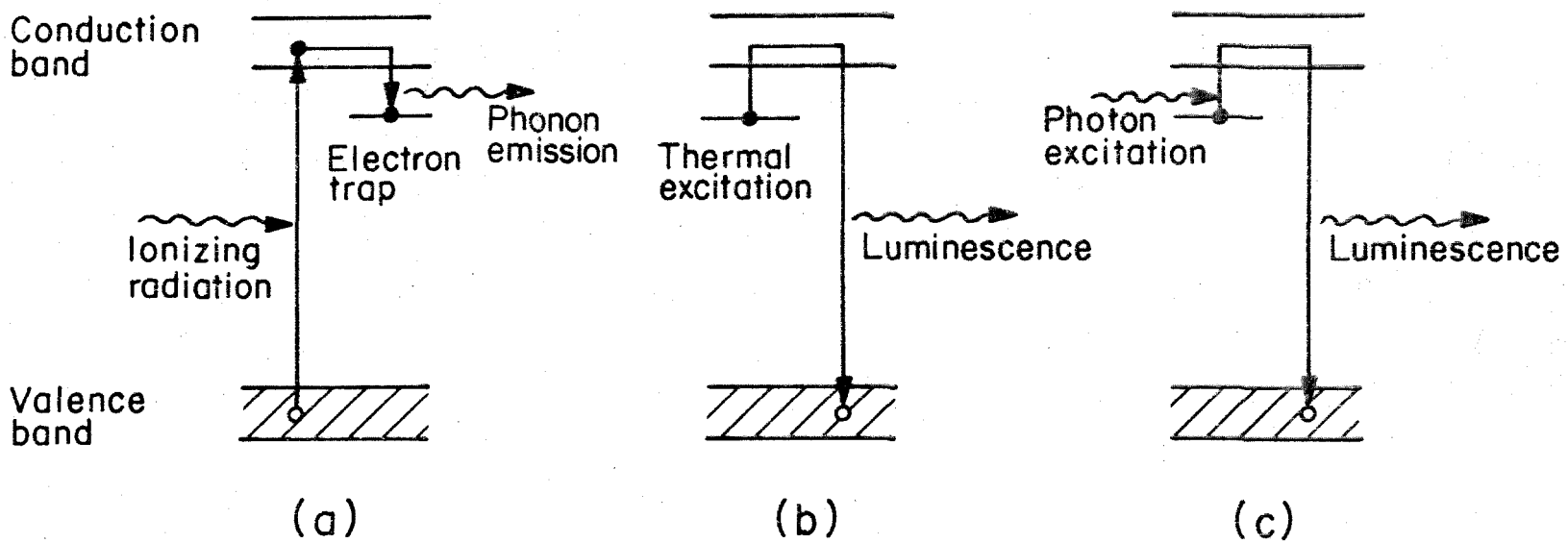
Conduction band
Phonon emission
Electron trap
Ionizing radiation
Valence band
(a)
Thermal excitation
Luminescence
(b)
Photon excitation
Luminescence
(c)

the efficiency of producing trapped electrons. Actually, the zero point for the age is the last time the sample was heated sufficiently to deexcite all the trapped electrons. In the case of a volcanic rock, this is the point at which it cooled to a temperature below ~ 100°C. For archeological artifacts such as pottery, this is when the object was last fired. In many situations, especially for unearthed samples, the source of ionizing radiation is indigenous to the object, coming from radioactive isotopes naturally occurring in trace amounts in many minerals. An analysis of the radioactive content of a sample furnishes the average dose rate over its history.

It is suggested in this proposition that the trapped electrons also could be excited to the conduction band by absorbing light of the proper energy (fig. 1c) and the total amount of luminescence could again be used to determine the age of the object. The nature of the electron traps is uncertain for many minerals and the question of whether radiative transitions between the trap levels and the conduction band exist is not clear in all cases. However, photodetrapping has been used to study the energy depths of electron traps in alkali halide crystals (Fieschi and Scaramelli 1968), thus showing that photoinduced luminescence is possible in at least certain situations. Moreover, photoinduced luminescence has been suggested to be a general technique for determining trap energies in wide-gap semiconductors (Fok 1970).

Several problems are associated with thermoluminescent measurements that result from the need to heat the samples (Wagner 1976). Because temperatures of up to ~ 500°C are reached before

all the trapped electrons are excited to the conduction band, the resulting thermal glow can contaminate the light intensity measurement. Also, the elevated temperatures can trigger chemical reactions in the sample that may result in chemiluminescence, again resulting in spurious light signals. As envisioned in this proposition, the light source would be a laser and, by controlling the radiation intensity and by external cooling of the sample, no overall heating should occur, thus avoiding the problems just mentioned.

The long-lived traps which are valuable for dating old objects usually have depths of $\sim$ 1-2 eV (Fieschi and Scaramelli 1968). Tunable lasers that operate in this range, 0.6-1.2 μ, are available (Demtröder 1973). The special characteristics of tunable lasers compared to the average incoherent light source may be used to alleviate some other experimental difficulties associated with the thermoluminescent dating technique. The necessary heating discussed before often results in the destruction of the object or requires at least some defacement to obtain a sample for the measurement, neither case being a desireable prospect for a rare and valuable artifact. Moreover, very delicate preparative work prior to the heating is necessary to separate the sample into its constituents, in the case of a pottery shard, fine grain clay versus quartz inclusions. The need for separate analyses results from the fact that different minerals have different radiation sensitivities. Thermoluminescent ages derived for heterogeneous objects have been shown to be highly inaccurate (Wagner 1976).

The intensity of the laser light should result in a significant amount of detrapping while still avoiding an overall heat rise. The use of lasers should minimize the need for the tedious preparative decomposition in several ways. First, the tunability should allow specific interaction with the traps of a particular mineral constituent, since the trap depths for different minerals are at different energies. Second, because the laser output can be easily focussed to a spot size less than the size of a grain inclusion or the average separation between grain inclusions, the various components of the sample matrix can be spatially excited separately, but in situ. Analogous to this, although involving different transitions, is the present use of laser-induced luminescence to probe at high spatial resolution the variation in composition across a semiconductor heterojunction (Daniels and Steinvall 1973). These points show that the employment of lasers in dating should minimize the defacement of the precious objects being studied.

However, before photoinduced luminescence could become a general tool in dating geological and archeological objects, experiments would have to be performed on a wide range of minerals to ascertain whether the cross section for photodetrapping was sufficiently large for this technique to efficiently produce luminescence. In addition, the trap depths would have to be better determined. Interestingly, the accumulation of such information might lead to a method of easily qualitatively analyzing the mineral composition of an object. The development of photoinduced luminescence into an accurate, nondestructive dating technique might encourage the

analysis of highly precious objects which are unavailable for study at present.

REFERENCES

Daniels, E., and Steinvall, O. 1973, J. Appl. Phys., 44, 5526.

Demtröder, W. 1973, Topics in Current Chemistry, 17, 1.

Fieschi, R., and Scaramelli, P. 1968, in Thermoluminescence of Geological Materials, ed. D. J. McDougall (London: Academic Press), p. 291.

Fok, M. V. 1970, Fiz. Tekh. Pol., 4, 1009.

Wagner, G. A. 1976, Endeavour, 35, 3.